

Copyright is owned by the Author of the thesis. Permission is given for a copy to be downloaded by an individual for the purpose of research and private study only. The thesis may not be reproduced elsewhere without the permission of the Author.

Development and applications of filamentous phage-derived particles in immunotherapy and diagnostics

A dissertation presented in partial fulfilment of the
requirements for the degree of

Doctor of Philosophy
in
Biochemistry

at Massey University (Manawatū),
New Zealand.

Marina I. Rajič

2020

Copyright is owned by the Author of the thesis. Permission is given for a copy to be downloaded by an individual for research and private study only. The thesis may not be reproduced elsewhere without the permission of the Author.

Dedicated to my parents, Gordana and Irica Rajić

Abstract

Most vaccines that are currently in clinical use induce antibody-mediated responses. However, for many infectious diseases, T cells are an essential part of naturally acquired protective immune responses. T cell-inducing vaccines, such as the one developed in this research, could additionally be used for treatments in cancer or chronic viral infections. One way to target the immune cells and stimulate their responses is to use filamentous phage particles.

Filamentous phages (Ff) are ssDNA viruses that infect *Escherichia coli*, which have been adapted and used extensively in phage display technology and nanotechnology. In this research, a filamentous phage (Ff)-based vaccine carrier was constructed to allow the tuneable display of non-protein immune adjuvant molecules (BODIPY- α -GalCer) and antigenic peptides (OVA; MHC I + MHC II) on the same particle. For the first time, azide groups were incorporated into the recombinant pVIII phage coat proteins that expressed recombinant peptides. Azide groups were subsequently used to attach fluorescently labelled adjuvant molecules, which were successfully presented to NKT cells *in vivo*. Additionally, high induction of *in vitro* proliferation of OVA-specific CD8⁺ T-cells was achieved.

Abstract

However, the Ff-derived particle use outside the laboratory is hindered because they are genetically modified viruses, which in addition, carry antibiotic resistance genes that can be horizontally transferred to gut bacteria. These limitations were overcome by developing a system for efficient production of non-replicating, controllable-length protein-DNA nanorods, derived from Ff, named BSFnano (~100 × 6 nm). In this research, functionalised BSFnano particles were constructed, and their application in diagnostics was tested in a proof of concept dipstick assay for detection of a soluble analyte (fibronectin). For the first time, an ultrasensitive dipstick assay was achieved with Ff-derived nanorods, detecting the test-analyte at a concentration of as low as 0.04 pg/μL, equivalent to only 100,000 molecules/μL.

Overall, while the phage-based vaccine produced in this research elicited CD8⁺ T-cell responses *in vitro*, but not *in vivo*, the Ff-derived nanorods were successfully functionalised and tested in lateral flow immunoassay, with promising implications for use in point of care diagnostics.

Acknowledgements

The Author would like to thank all the people that actively contributed to her research thesis. Special thanks go to her primary supervisor, A/Prof Jasna Rakonjac, for all her contributions in developing research questions, giving thoughtful guidance and supportively helping craft the writing skills. Thanks to the co-supervisors, Prof Kathryn Stowell (Massey University) and Prof Ian Hermans (Malaghan Institute for Medical Research, MIMR) for contributing in fields of biochemistry and immunology and providing a helping hand in data interpretation. Further acknowledgements go to Prof Gavin Painter and Dr Benjamin Compton from Ferrier Research Institute, for providing the adjuvant needed for the vaccine. Finally, a great deal of thanks goes to Kathryn Farrand from the MIMR for handling the animals for *in vivo* experiments and her help in flow cytometry.

Without the funding, this research would not be possible; therefore the Author also wishes to acknowledge and thank the providers: Massey University School of Fundamental Sciences Doctoral Scholarship, Massey University Alumni Fund, Maurice Wilkins Centre for Molecular Biodiscovery, Anonymous Donor, Palmerston North Medical Research Foundation, and Massey Ventures Ltd. Approval for the research in this thesis has been obtained from the Massey University Ethics Committee for work on GMOs (*E. coli* and Ff phage), and from the MIMR Ethics Committee for the *in*

Abstract

vivo experiments on murine models. Finally, thanks to Rakonjac and Hermans laboratories for hosting this research over the past four years. The professional editor was not used in preparation of this thesis.

Table of Contents

LIST OF FIGURES	XI
LIST OF TABLES	XVI
ABBREVIATIONS	XVII
CHAPTER 1. INTRODUCTION.....	1
1.1 FILAMENTOUS PHAGE.....	1
1.1.1 <i>Ff infection and replication</i>	6
1.1.2 <i>Phage display technology</i>	9
1.2 FF-DERIVED NANORODS.....	11
1.2.1 <i>Development of BSFnano production system</i>	13
1.3 IMMUNODIAGNOSTICS	18
1.3.1 <i>Lateral flow assays (LFA)</i>	19
1.3.2 <i>Ff phage applications in immunodiagnostics</i>	21
1.4 COMPONENTS AND ACTIVATION OF CELLULAR ADAPTIVE IMMUNE RESPONSES	23
1.4.1 <i>Dendritic cells</i>	23
1.4.1.1 Antigen processing and presentation.....	24
1.4.1.2 <i>Activation of DCs</i>	25
1.4.2 <i>T cells and anti-tumour responses</i>	30
1.4.2.1 CD8 ⁺ T cells.....	30
1.4.2.2 CD4 ⁺ T cells.....	31
1.4.2.3 Invariant natural killer T cells (iNKT).....	32
1.5 CANCER IMMUNOTHERAPY.....	37
1.5.1 <i>T cell vaccines targeting cancer cells</i>	38
1.5.2 <i>Carriers used in cancer vaccines</i>	40
1.6 PHAGE-INDUCED IMMUNE RESPONSES.....	41
1.7 HYPOTHESIS AND AIMS OF THE RESEARCH.....	44
CHAPTER 2. MATERIAL AND METHODS	46

Table of Contents

2.1	CHEMICALS, BUFFERS AND MEDIA.....	46
2.2	ESCHERICHIA COLI STRAINS.....	56
2.2.1	<i>P1 Transduction</i>	57
2.3	MURINE MODELS.....	59
2.3.1	<i>Maintenance and ethical approval</i>	59
2.3.2	<i>Murine strains</i>	60
2.4	GENERAL METHODS.....	60
2.4.1	<i>Cloning</i>	60
2.4.1.1	Plasmids and oligonucleotides	60
2.4.1.2	Preparation of chemically competent cells	63
2.4.1.3	Preparation of electro-competent cells.....	64
2.4.1.4	Polymerase Chain Reactions (PCR)	64
2.4.1.5	Restriction endonuclease reactions	65
2.4.1.6	Ligation.....	65
2.4.1.7	Transformation by heat shock.....	65
2.4.1.8	Transformation by electroporation	66
2.4.1.9	Plasmid purification	67
2.4.1.10	DNA sequencing	67
2.4.2	<i>Electrophoresis</i>	67
2.4.2.1	Agarose gel DNA electrophoresis	67
2.4.2.2	SDS-PAGE and western blot.....	68
2.4.2.1	Native phage agarose gels.....	69
2.4.2.2	Agarose gel electrophoresis of disassembled phages and phage-derived nanorods	70
2.5	PHAGE AND NANOROD PURIFICATION AND QUANTIFICATION.....	70
2.5.1	<i>CsCl gradient ultracentrifugation</i>	70
2.5.2	<i>LPS removal and LAL test</i>	71
2.5.3	<i>Quantification of phages and phage-derived nanorods by densitometry</i>	72
2.5.4	<i>Fluorescent labelling</i>	73
2.5.5	<i>Microscopy of Ff phages and nanorods</i>	74
2.5.5.1	Negative Staining Grid Preparation for TEM	74

2.5.5.2	On-grid gold labelling of Ff phage	75
2.6	IMMUNOLOGY METHODS AND VACCINE TRIALS.....	75
2.6.1	<i>Vaccination and tissue processing</i>	76
2.6.1.1	Intravenous vaccination	76
2.6.1.2	Blood	76
2.6.1.3	Spleen.....	77
2.6.1.4	Liver.....	77
2.6.1.5	Viable cell count	78
2.6.2	<i>Flow cytometry data acquisition and analysis</i>	78
2.6.2.1	CD8 ⁺ T cell responses ex vivo	79
2.6.2.2	NKT markers surface staining.....	79
2.6.3	<i>Software used for data analysis</i>	80
2.6.3.1	Statistical analysis	81
2.7	DIAGNOSTIC ASSAYS USING FF-DERIVED PARTICLES.....	81
2.7.1	<i>Dot blot</i>	81
2.7.2	<i>ELISA</i>	82
2.7.2.1	Qualitative ELISA for detection of fibronectin-binding peptide displayed on BSF nanorods	82
2.7.2.2	ELISA assay for OVA-pVIII quantification.....	83
2.7.3	<i>Fibronectin dipstick assay</i>	85
CHAPTER 3. DESIGN OF FILAMENTOUS PHAGE-BASED VACCINE FOR IMMUNOTHERAPY		87
3.1	INTRODUCTION	87
3.1.1	<i>Aim and objectives</i>	88
3.2	RESULTS	89
3.2.1	<i>Design and construction of a new system for production of an improved Ff-based vaccine</i>	89
3.2.1.1	Construction of an Ff phage mutant for azide display on the coat proteins	90
3.2.1.2	Plasmid design for expression of OVA-pVIII fusion	94
3.2.1.3	E. coli host strain for production of Ff-based vaccine	97
3.2.1.4	Optimising the conditions for azidohomoalanine incorporation into the phage	101
3.2.2	<i>Production of azide- and antigen-displaying phage particles</i>	103

Table of Contents

3.2.2.1	Long antigen peptide is displayed as protein fusion on phage coat protein	108
3.2.3	<i>Cycloaddition allows controlled modifications of phage coat proteins</i>	<i>111</i>
3.2.3.1	Modified phages are covalently labelled with the fluorescent dye DIBAC-TAMRA.....	113
3.2.3.2	Gold nanoparticles are attached to modified phages via click chemistry	116
3.2.4	<i>Fluorescently labelled glycolipid adjuvant BODIPY-α-GalCer chemically attached to phage particles</i>	<i>118</i>
3.3	DISCUSSION	124
 CHAPTER 4. ASSESSING THE PHAGE-BASED VACCINE-INDUCED IMMUNE RESPONSES IN MURINE MODELS 135		
4.1	INTRODUCTION.....	135
4.1.1	<i>Aim and objectives.....</i>	<i>137</i>
4.2	RESULTS.....	137
4.2.1	<i>Early iNKT (3 days) cell activation by a phage-displayed BODIPY-α-GalCer conjugate</i>	<i>138</i>
4.2.2	<i>Ff-derived OVA vaccine testing at a low antigen to BODIPY-α-GalCer ratio.....</i>	<i>147</i>
4.2.2.1	OVA-specific CD8 ⁺ T cell responses	150
4.2.2.2	iNKT cell activation after nine days	154
4.2.3	<i>Ff-derived OVA vaccine testing at a high antigen to BODIPY-α-GalCer ratio</i>	<i>158</i>
4.2.3.1	OVA-specific CD8 ⁺ T cell responses on day 7	158
4.2.3.2	iNKT cell activation after eight days	162
4.2.4	<i>In vitro T cell proliferation.....</i>	<i>165</i>
4.3	DISCUSSION	169
 CHAPTER 5. NOVEL FUNCTIONALISED BIOLOGICAL NANORODS FOR DIAGNOSTIC APPLICATIONS...182		
5.1	INTRODUCTION.....	182
5.1.1	<i>Aim and objectives.....</i>	<i>184</i>
5.2	RESULTS.....	184
5.2.1	<i>Helper plasmids for site-directed functionalising BSFnano via specific chemical handles... 184</i>	<i>184</i>
5.2.1.1	Helper plasmids for site-specific chemical conjugations	185
5.2.2	<i>Optimised production and purification generate high yields of nanorods</i>	<i>189</i>

5.2.4	<i>BSF-nanorods for fibronectin detection</i>	197
5.2.4.1	Construction of FnBP-pIII-fusion-expressing helper plasmid	197
5.2.4.2	Characterisation of the BSF719.Gly ₄ .FnBP and BSF719.Gly ₄ nanorods	198
5.2.4.3	Confirmation of FnBP-pIII fusion in the nanorods	201
5.2.4.4	Fluorescent labelling of nanorods via NHS-ester chemistry	204
5.2.5	<i>BSFnano-based lateral flow assay for the detection of fibronectin</i>	205
5.3	DISCUSSION	209
CHAPTER 6. CONCLUSIONS AND FUTURE DIRECTIONS		216
6.1	CONCLUSIONS	216
6.2	FUTURE DIRECTIONS	217
6.2.1	<i>Future developments of the Ff-based vaccine</i>	217
6.2.2	<i>Adaptation of BSFnano purification and concentration protocols for vaccine applications</i>	220
6.2.3	<i>Future developments of the BSFnano-based technology</i>	220
CHAPTER 7. APPENDICES		223
7.1	MPI APPROVAL FOR TRANSFER OF PHAGES	223
7.2	CHEMICAL STRUCTURES	225
7.2.1	<i>BODIPY-α-GalCer adjuvant molecule (CI270A)</i>	225
7.2.2	<i>Conjugate vaccine molecule (CI038)</i>	226
7.3	QUANTIFICATION AND MOLECULE ANALYSIS	227
7.3.1	<i>BSFnano particle quantification</i>	227
7.3.2	<i>Endotoxin quantification via LAL assay</i>	228
7.3.3	<i>TAMRA fluorescence quantification</i>	229
7.3.4	<i>BODIPY-α-GalCer quantification via fluorescence</i>	230
7.3.6	<i>Example of OVA-pVIII fusion quantification</i>	231
7.4	STATISTICAL ANALYSES	232
7.4.1	<i>iNKT cell activation in spleen and liver (Section 4.2.1)</i>	232
7.4.2	<i>OVA-specific T cell responses (Section 4.2.2)</i>	242
7.4.3	<i>iNKT cell activation after nine days (Section 4.2.2)</i>	246

Table of Contents

7.4.4 OVA-specific T cell responses (Section 4.2.3)	256
7.4.5 iNKT cell activation after eight days (Section 4.2.3)	260
REFERENCES	271

LIST OF FIGURES

Figure 1.1. The Ff genome and virion.....	3
Figure 1.2. Schematic presentation of Ff virion.....	5
Figure 1.3. Model of the Ff phage infection.....	7
Figure 1.4. The Ff phage cycle.....	8
Figure 1.5. Comparison of helper phage and helper plasmid assisted systems for the production of Ff-derived particles.	13
Figure 1.6. Map of a pBSFnano nanorod template plasmid..	15
Figure 1.7. Replication and packaging cassettes.....	16
Figure 1.8. Pathways of antigen cross-presentation in dendritic cells.....	25
Figure 1.9. iNKT cell-DC interactions after stimulation with α -GalCer.....	29
Figure 1.10. Antigen recognition by the type I NKT TCR..	34
Figure 1.11. Invariant NKT cells and their role in immunity.	36
Figure 1.12. Interaction of bacteriophages with mammalian immune cells.....	43
Figure 3.1. Schematic presentation of the vaccine particle design.....	90
Figure 3.2. Molecular structure of major coat protein pVIII.	92

List of Figures

Figure 3.3. Construction of R783 phage strain.....	93
Figure 3.4. Schematic presentation of OVA peptide and FLAG-tag fusions.....	96
Figure 3.5. Agarose gel analysis of the cloning steps of the pVIII fusion constructs.....	97
Figure 3.6. Structural formulas of methionine and azidohomoalanine.....	98
Figure 3.7. Methionine biosynthesis pathway in <i>E. coli</i> ..	99
Figure 3.8. Methionine-dependent growth of <i>E. coli</i> strain K2449.....	102
Figure 3.9. Flow-diagram of the optimised production and purification of Ff-vaccine carrying long peptide antigens and the click-chemistry-attached glycolipid adjuvants..	104
Figure 3.10. Agarose gel electrophoresis of phage fractions	106
Figure 3.11. Efficacy of Triton X-114 treatments for removal of residual LPS from R783.OVA vaccine samples.....	107
Figure 3.12. Immuno-detection and quantification of OVA peptide displayed along the phage filaments.....	110
Figure 3.13. Schematic presentation of alkyne cycloaddition to azide-displaying phage.....	112
Figure 3.14. Fluorescent labelling of Ff phages via pVIII-displayed azide handles.....	114
Figure 3.15. Quantification of fluorescent dye on phages labelled via click chemistry.....	115

Figure 3.16. Electron micrograph of gold-coated phages.	118
Figure 3.17. Fluorescent labelling of R783 phages with the BODIPY- α -GalCer adjuvant via pVIII-displayed azide handles.	121
Figure 3.18. Quantification of chemically attached adjuvant molecules on phage particles displaying antigenic peptides.	123
Figure 4.1. Schematic presentation of vaccine trials...	139
Figure 4.2. Gating strategy for iNKT cell analyses by flow cytometry.....	141
Figure 4.3. Total cell count comparison and iNKT composition in the liver and spleen three days after BODIPY- α -GalCer stimulation.....	143
Figure 4.4. iNKT cells analysed for the presence of the NK1.1 and CD69 markers.....	145
Figure 4.5. Mice groups for immunisation with phage vaccines.....	149
Figure 4.6. Representative plots for gating strategy from OVA- α -GalCer vaccinated group for analysis of vaccine-induced CD8 ⁺ T cell by fluorescence-activated cell sorting.	151
Figure 4.7. Detection of OVA-specific CD44 ^{hi} CD8 ⁺ T cells in blood seven days post-immunisation.....	153
Figure 4.8. Analysis of iNKT cells in spleen nine days after vaccination.....	156

List of Figures

Figure 4.9. iNKT cells from spleen analysed for the presence of the NK1.1 and CD69 markers.....	157
Figure 4.10. Detection of OVA-specific CD44 ^{hi} CD8 ⁺ T cells in blood seven days post-immunisation.....	161
Figure 4.11. Total cell count comparison and iNKT composition in the spleen eight days after the phage-based vaccine stimulation.....	163
Figure 4.12. iNKT cells from spleen analysed for the presence of the NK1.1 and CD69 markers.....	164
Figure 4.13. <i>In vitro</i> proliferation assay.....	168
Figure 5.1. Construction of helper plasmids pHAS8 and pRnano38.....	186
Figure 5.2. BSFnano functionalised for chemical modifications.....	187
Figure 5.3. Flow diagram of optimised production and purification of BSFnano particles.....	191
Figure 5.4. BSF529 nanorod purification monitored by agarose gel electrophoresis.....	193
Figure 5.5. Characterisation of BSF719.Gly ₄ .FnB and BSF.Gly ₄ nanorods.....	200
Figure 5.6. Detection of FnBP-pIII fusion in BSFnano particles functionalized for fibronectin detection.....	201
Figure 5.7. ELISA assay monitoring binding of the FnB-displaying nanorods to immobilised Fn.....	203
Figure 5.8. Lateral flow dipstick assay.....	206

Figure 5.9. Fibronectin detection using FnBP-displaying nanorods in the lateral-flow dipstick assay.....	208
--	-----

LIST OF TABLES

Table 1. Antibodies used in murine models.....	48
Table 2. E. coli strains.....	57
Table 3. Oligonucleotides.....	61
Table 4. Plasmids.....	62
Table 5. Amino acid sequences of phage pVIII fusions....	95
Table 6. Characterisations of vaccine samples for experiments in murine models.....	138
Table 7. Comparison of the i.v. vaccine results with the published similar experiment.....	175
Table 8. Nanorods constructs.....	196

ABBREVIATIONS

α -GalCer - α -galactosylceramide

AA - amino acid

AAC - azide-alkyne cycloaddition

Amp - ampicillin

ANOVA - analysis of variance

AP - alkaline phosphatase

APC - antigen-presenting cell

BCIP - 5-bromo-4-chloro-3'-indolyphosphate

BODIPY - boron-dipyrromethene

bp - base pairs

BPB - bromophenol blue (3',3'',5',5''- tetrabromo-phenol-sulphonphthalein)

BSA - bovine serum albumin

BSFnano - biological scalable Ff-derived nanorods

BUV - BD Horizon Brilliant™ Ultraviolet

Cm - chloramphenicol

CTL - cytotoxic T lymphocytes

DAMPs - danger associated molecular patterns

DAPI - 4,6-diamidino-2-phenylindole dihydrochloride

DBCO - dibenzyl-cyclooctyne

Abbreviations

DC - dendritic cell

DIBAC - dibenzo-azacyclooctyne

DMF - dimethylformamide

DMSO - dimethyl sulfoxide

dsDNA - double-stranded DNA

EDTA - ethylenediaminetetraacetic acid

ECL - enhanced chemiluminescence

ELISA - enzyme-linked immunosorbent assay

ER - endoplasmic reticulum

EtBr - ethidium bromide

EU - endotoxin units

FACS - fluorescence-activated cell sorting

FCS - flow cytometry standard

FDA - US Food and Drug Administration

Ff - filamentous phage

FITC - fluorescein isothiocyanate

FLAG - tag peptide DYKDDDDK

FMO - fluorescence minus one

Fn - fibronectin

FnBP - fibronectin-binding protein

HRP - horseradish peroxidase

IG - intergenic region

IL - interleukin

IFN - interferon

IMDM - Iscove's modified Dulbecco's medium

iNKT - invariant natural killer cells

IPTG - isopropyl β -d-1-thiogalactopyranoside

kb - kilobase

Km - kanamycin

LAL - Limulus Amebocyte lysate

LFA - lateral flow assay

LN - lymph nodes

LPS - lipopolysaccharide

mAb - monoclonal antibody

MCS - multiple cloning site

MHC - major histocompatibility complex

Mw - molecular weight

MWCO - molecular weight cut-off

NBT - nitro-blue tetrazolium

NKT - natural killer T cell

nt - nucleotides

ORF - open reading frame

ori - origin of replication

OVA - ovalbumin peptide (ISQAVHAAHAEINEAGRESIINEFKLTEWT)

Abbreviations

PAGE - polyacrylamide gel electrophoresis

PAMPs - pathogen-associated molecular patterns

PBS - phosphate-buffered saline

PCR - polymerase chain reaction

PE - phycoerythrin

PEG - polyethylene glycol

pfu - plaque-forming units

PRRs - pathogen recognition receptors

PS - packaging signal

RBC - red blood cells

RIA - radioimmuno assay

RF - replicative form

rpm - revolutions per minute

SAuNP - Streptavidin-conjugated gold nanoparticles

scFv - single-chain variable fragment

SDS - sodium dodecyl sulphate

SOC - super-optimal broth with catabolite repression

SOF - serum opacity factor

SrtA - sortase A

SS - signal sequence

ssDNA - single-stranded DNA

TAE - tris base, acetic acid, EDTA buffer

TAMRA - 5-carboxy-tetramethyl-rhodamine

TBS - tris-buffered saline

TBSTM - TBS buffer, Tween20, Milk

TCR - T cell receptor

TE - transformation efficiency

TEM - transmission electron microscopy

Tet - tetracycline

Th - helper T cell

TLR - Toll-like receptor

VLPs - virus-like particles

wt - wild-type

YT - yeast extract tryptone

Chapter 1. INTRODUCTION

1.1 FILAMENTOUS PHAGE

Filamentous bacteriophages (Ff) (genus: *Inovirus*, family: *Inoviridae*) belong to one of the two rod-like and filament-like genera of bacterial viruses that contain circular single-stranded DNA. Members of *Inovirus* mainly infect Gram-negative bacteria such as *Escherichia*, *Pseudomonas*, *Yersinia*, *Salmonella* (Bradley et al., 1981; Lawn et al., 1967), *Neisseria*, *Xanthomonas*, *Vibrio* and *Thermus* (Marvin and Hohn, 1969; Rakonjac et al., 2011; Russel and Model, 2006). Only two Gram-positive bacteria, *Propionibacterium freudenreichii* (Chopin et al., 2002) and *Clostridium acetobutylicum* (Kim and Blaschek, 1991) can be infected by inoviruses.

The most extensively studied filamentous bacteriophages are M13, f1 and fd. They are collectively called Ff and infect *Escherichia coli* that carry the F episome. With a genome sequence identity of 98%, the three Ff phages are used and studied interchangeably. The length of filamentous phage virions depends on the size of their genome. Interestingly, the circular ssDNA genome of Ff phage is arranged in a Watson-Crick-like right-handed helix inside the filamentous virion, even though there is weak complementarity between the two strands derived from two different halves of the genome (Day et al., 1988). The virion of wild type Ff phage is approximately 880 nm long and 6 - 7 nm in diameter (Model

and Russel, 1988). The flexible length of the virions allows insertion of foreign DNA; hence, Ff have been used for the past forty years as cloning vectors (Webster, 2001).

The main difference between Ff and other types of bacteriophages (e.g., λ phage) is that a secretion-like process is assembling the progeny virions and the host cell survives (Rakonjac et al., 1999). This means that their production can yield significant titres by continuous replication of phages without killing the cells. Genes of f1 are tightly packed in the 6,407 nt genome (Figure 1.1). There is an intergenic region (IG) between gIV and gII, which contains positive (+) and negative (-) origins of replication (*ori*) and a hairpin loop that targets the ssDNA genome to the assembly machinery (packaging signal or PS). Genes (and their products) can be grouped into three categories based on the function of the encoded proteins (Model and Russel, 1988): (1) those that comprise the virion (VIII, III, VI, VII and IX); (2) those that are required for DNA synthesis (II, V and X); (3) those that serve a morphogenic (phage secretion-assembly) function (I, IV and XI).

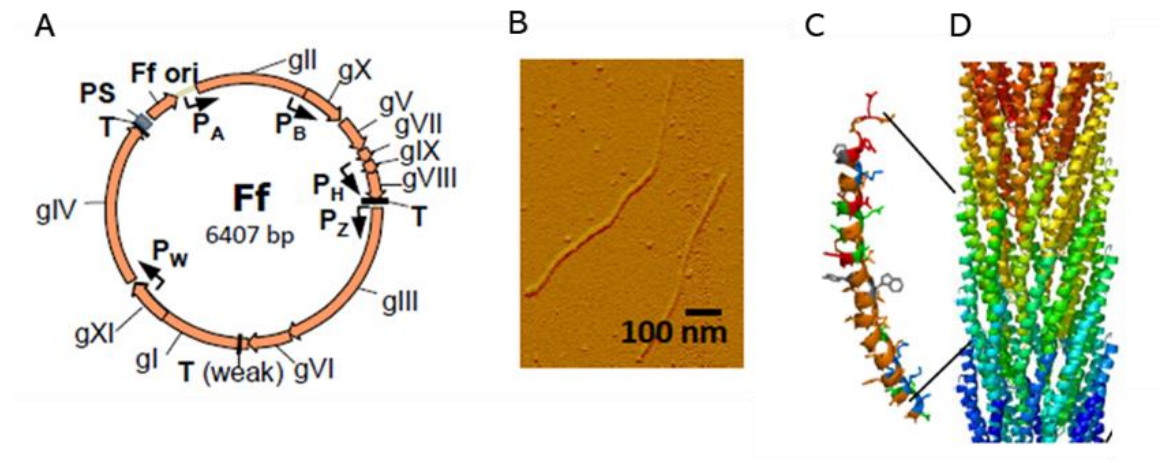


Figure 1.1. The Ff genome and virion.

A, The Ff genome; gI to gXI, genes (orange block arrows); PS, packaging signal; Ff ori; the origin of replication; P_A , P_B , P_H , P_W , P_Z ; promoters; T, terminators. **B**, Atomic force microscope image of two Ff virions, one (longer) that has encapsidated the helper phage R408 genome, and the smaller that contains a phagemid vector whose genome is smaller (J. Rakonjac, M. Russel and P. Model, unpublished). **C**, Structure of a pVIII (major coat protein) monomer. **D**, pVIII arrangement within the filamentous phage capsid. Figure adapted from (Rakonjac et al., 2011) with permission.

The virion is composed of a major coat protein (thousands of copies) along the filament shaft, and minor coat proteins (each present in five copies at the ends of virion). Major coat protein pVIII has only 50 amino acids and is helically arranged around the ssDNA (Figure 1.1D). There are 2,700 copies of pVIII in the Ff wild type, which makes a suitable candidate for displaying a high-copy number of fusion proteins. The N-terminal four to five amino acids are disordered, and this segment has an overall negative charge (Rakonjac et al., 2011). The α helix is amphipathic between the 5th and 20th residues and then hydrophobic to residue 39, ending with a 10-residue positively charged helix that interacts with encapsulated DNA (Marvin et al., 2006).

Multiple hydrophobic interactions of adjacent pVIII subunits hold the capsid together. The ratio of pVIII subunit per nucleotide in Ff was calculated to be 0.42 ± 0.01 (Newman et al., 1977).

Minor proteins form the endcaps of the filamentous virion directionally. Protein pIII is located within the distal cap, in five copies (Figure 1.2). This is the largest protein of the virion with 406 amino acid residues in length (Beck et al., 1978). Protein pIII mediates infection and entry of the phage into the cell (N-terminal domains N1 and N2; in conjunction with C domain), as well as the release of progeny virions from the cell (C-domain) (Bennett and Rakonjac, 2006; Rakonjac et al., 1999; Rakonjac and Model, 1998). Five copies of pIII make a complex with five copies of another minor protein, pVI. The structure of the cap complex is unknown (Boeke and Model, 1982; Endemann and Model, 1995). Together with pIII, pVI is required for termination of filament assembly and release of phages from the cells.

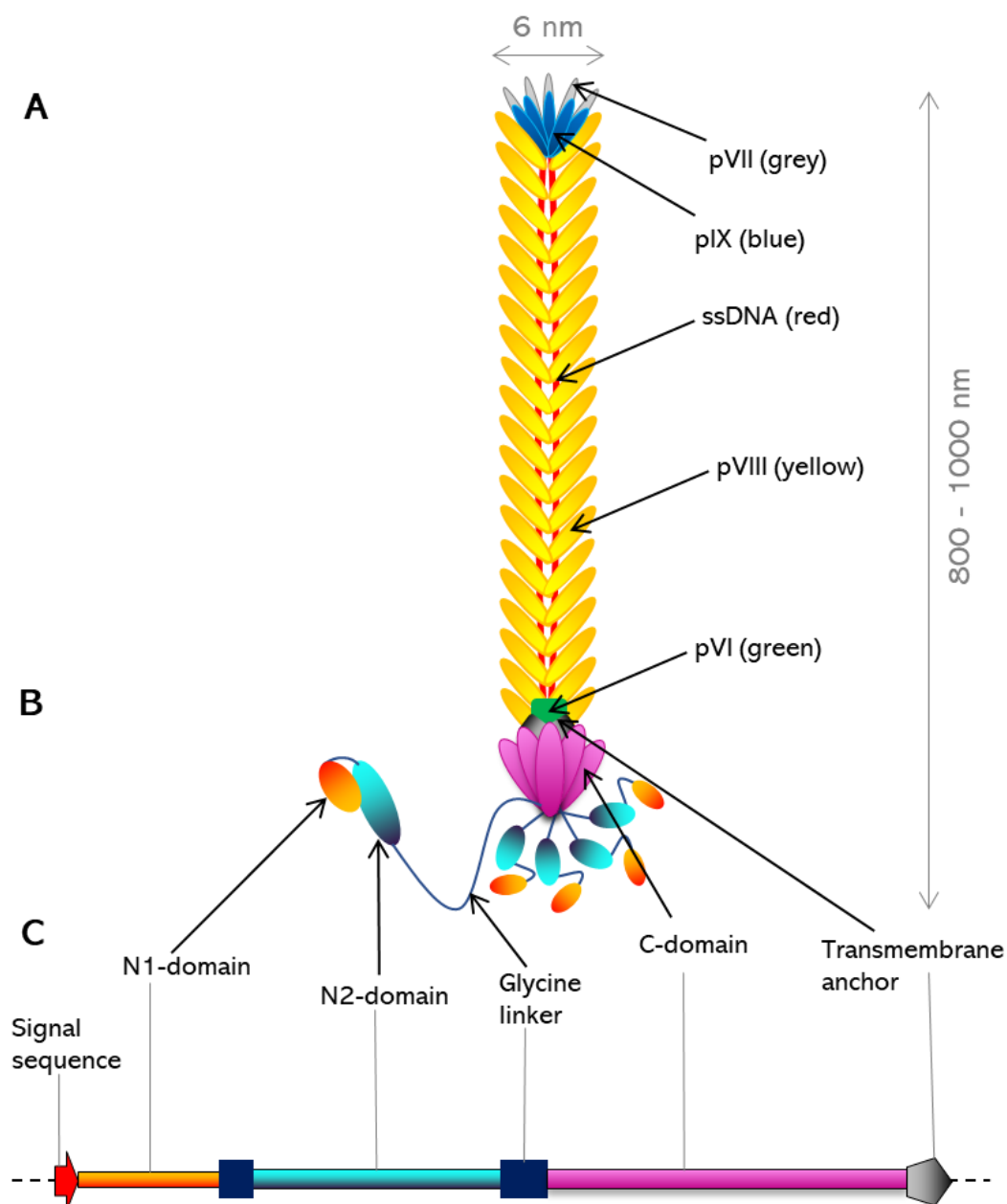


Figure 1.2. Schematic presentation of Ff virion.

A, Ff virion particle. **B**, pIII coat protein. **C**, domain organisation of pIII. Figure adapted from (Rakonjac et al., 2011) with permission.

Proteins pVII and pIX are small and hydrophobic; their lengths are 32 and 33 residues, respectively. These two proteins are incorporated into the virion at the initiation step of assembly (Figure 1.3) (Endemann and Model, 1995; Grant et al., 1980). Similarly to the distal cap (pIII/pVI),

the structure of the proximal cap (pVII/pIX) has not been determined at high resolution (Rakonjac et al., 2011). Phage “lifecycle” begins by attaching to the *E. coli* F-pilus.

1.1.1 Ff infection and replication

Most bacteriophages are temperate, they can integrate their DNA into the host chromosome, and many can be replicated as episomes, altering the phenotype of the host bacteria via lysogenic conversion (Brussow et al., 2004; Minot et al., 2011). While in this thesis, only Ff phages will be mentioned, for a detailed review of other phages, please refer to (Mai-Prochnow et al., 2015).

The initial binding of Ff to *E. coli* is to F-pilus tip via the pIII N2 domain. Retraction of the pilus (Boeke et al., 1982; Lin et al., 2011) brings the N1-domain of pIII to the TolQRA complex (Figure 1.3), which represents a secondary receptor for Ff and several related phages (Click and Webster, 1998; Heilpern and Waldor, 2000).

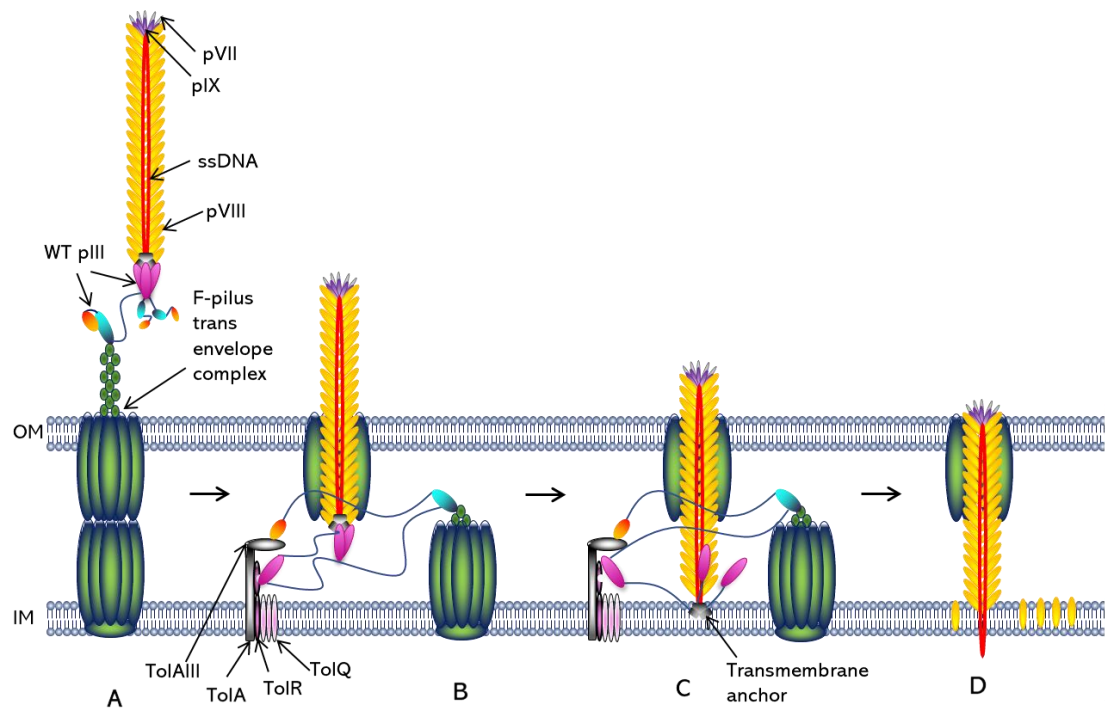


Figure 1.3. Model of the Ff phage infection.

A, Binding of N2 domain (aquamarine oval) to the tip of the F-pilus (dark-green circles) and pilus retraction. **B**, Binding of N1 domain (yellow-orange oval) to TolAIII domain (grey oval). **C**, "Opening" of the pIII C-domain and insertion of the C-terminal hydrophobic helix into the inner membrane. **D**, Entry of phage DNA into the cytoplasm and integration of the major coat protein pVIII into the inner membrane. Steps (A) and (D) are based on published findings, whereas steps (B) and (C) are speculative. **Symbols**: OM, outer membrane; IM, inner membrane. pIII N1 domain, yellow oval; pIII N2 domain, aquamarine oval; pIII C-domain, yellow-orange oval; pIII C-terminal hydrophobic helix (membrane anchor), grey rectangle; pIII glycine linkers, dark-blue lines; major coat protein pVIII, yellow ovals; pVII, white ovals, pIX, purple ovals; TolA and TolRQ, bright-pink shapes; F-pilus, and the trans-envelope pilus assembly/retraction system, dark-green ovals. The phage contains five copies of pIII, but for simplicity, only one full-length pIII is shown. This is consistent with experimental data: N1N2 and C domain operate "in cis" and fewer than five functional copies are sufficient for infection (Bennett and Rakonjac, 2006). Figure and legend adapted from (Rakonjac et. al., 2011) with permission.

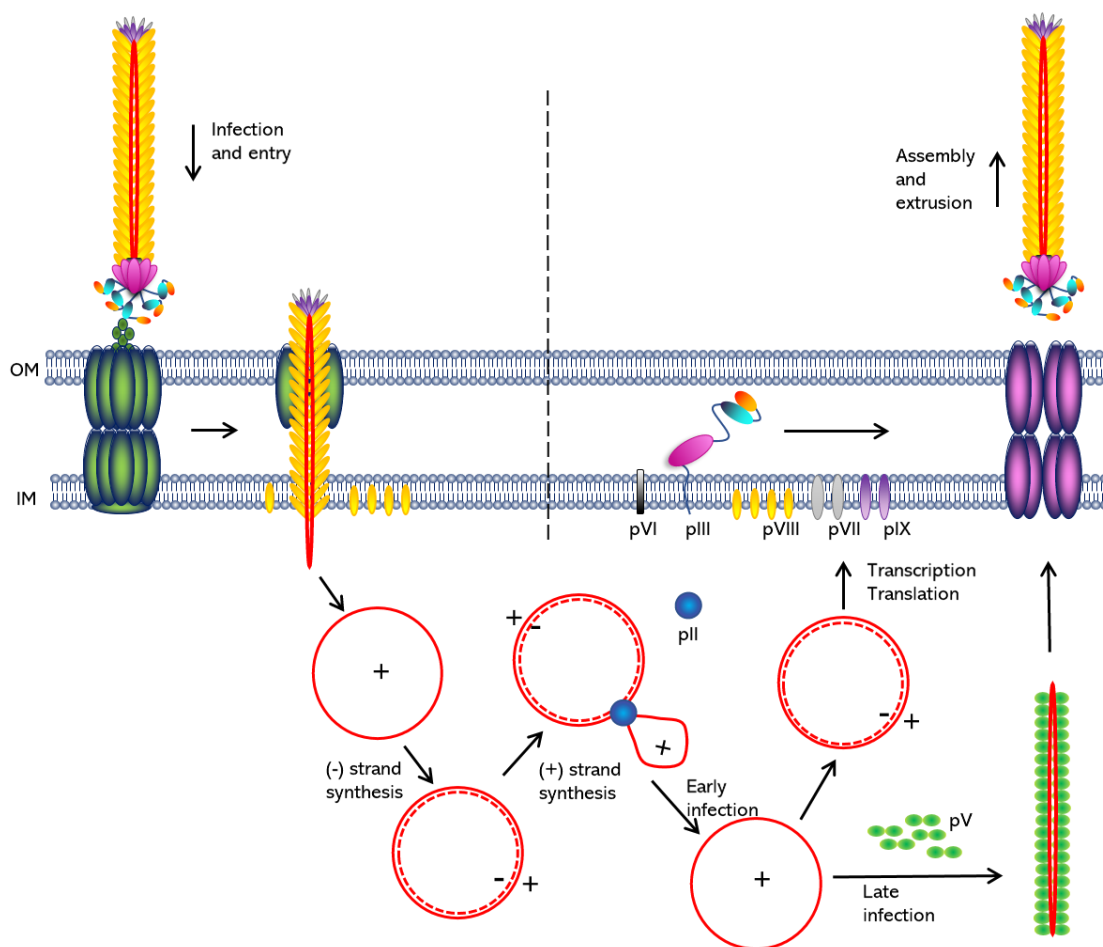


Figure 1.4. The Ff phage cycle.

Upon infection, the ssDNA (the + strand) enters the cytoplasm, while the pVIII major coat protein integrates into the inner membrane. Synthesis of the negative (-) strand is initiated at the negative strand origin of replication by RNA polymerase, which generates an RNA primer and is then released from the template (Zenkin et al., 2006). Host DNA polymerase III uses this primer to replicate the complete negative strand. Positive strand synthesis is initiated by pII (blue circle) which creates a nick in the (+) strand of the dsDNA replicative form at the positive origin of replication. Supercoiling and formation of a stem-loop structure of (+) ori are required for this step (not shown in this figure). Rolling circle replication then ensues one strand at the time. During the initial period of viral infection, new positive strands are used as templates for synthesis of negative strands, increasing the copy number of the dsDNA replicative form (RF). The RF serves as a template to produce phage proteins. Phage proteins II, V and X remain in cytoplasm and mediate genome replication and formation of the packaging substrate. Proteins pI, pIV and pXI form a transport complex spanning the inner and outer membrane (purple ovals). Virion proteins pVII, pIX, pVIII, pVI, pIII are inserted into the membrane before their assembly into phage particles. Later in the infection, positive strands

are coated by dimers of the phage-encoded single-stranded DNA binding protein pV to form the packaging substrate and brought to the cell membrane assembly/export complex (pI/pXI and pIV) for assembly and export. Figure and legend adapted from (Rakonjac et al., 2011) with permission.

Once Ff inserts the (+) ssDNA strand into the host (Figure 1.4), it can replicate in a rolling-circle mechanism from plasmid-like extra-chromosomal replicons (episomes) (Model and Russel, 1988). Inside the cell, a secondary structure is formed, that functions as a promoter, priming a short RNA synthesis by the host RNA polymerase. This primer is then extended by DNA polymerase III to complete the (-) strand, resulting in dsDNA, called the replicative form (RF) (Figure 1.4) (Russel and Model, 2006). Replication protein pII forms a nick in the (+) strand *ori* (initiator) within the RF and starts replication of the (+) strand. Replication finishes once pII reaches the terminator site of the (+) *ori*, joining the two ends into a newly formed (+) strand (Figure 1.4) and releasing the parental (+) strand. Positive strands bind to dimers of pV protein and form a complex for packaging. This complex is then transported to the inner membrane, where pIV, pI and pIX form a transmembrane secretion channel, in which coat proteins are assembled along the ssDNA and a new phage particle is released.

1.1.2 Phage display technology

Although other phages can be used to create phage display libraries (e.g., T4, T7, PH1, λ), the Ff filamentous phages of *E. coli* (f1, fd and M13) represent the leading platform

for this purpose (Henry et al., 2015). Ff phage have the significant advantage over the tailed bacteriophage, including variable length and resistance to a broad range of pH and temperatures (Karimi et al., 2016). The physical link between gene sequences and assembled coat proteins allows affinity screening of large libraries of many billions of variants. George Smith's work on phage display of peptides pioneered phage display technology (Smith, 1985). After this publication, the first phage display libraries of peptides (Scott and Smith, 1990) and antibodies were introduced (Barbas, 1993; Barbas et al., 1991; Clackson et al., 1991; Cwirla et al., 1990; Devlin et al., 1990; Marks et al., 1991). Since then, phages are mainly used for affinity screening to find a desired rare variant from large libraries (Abdolalizadeh et al., 2013; Hoogenboom et al., 1998; Schirrmann et al., 2011; Winter et al., 1994). In research laboratories, Ff phages are often used to create antibody libraries and screen for antibodies specific to certain pathogens (Moreland et al., 2012; Raynes et al., 2020) that can be used in immunoassays (e.g., ELISA) (Wu et al., 2014).

Phage display of a known protein or antibody can be used for therapeutic or diagnostic (detection) purposes (Deutscher, 2010; Fagbohun et al., 2013; Nagano and Tsutsumi, 2016). A foreign DNA sequence can be inserted into a gene encoding a phage coat protein, resulting in a fusion peptide in which the coat protein now "displays" the peptide product of the inserted sequence on the surface of the virion (Russel and Model, 2006). Most commonly used display-platform proteins

are pVIII and pIII (Figure 1.2), followed by pVII and pIX and occasionally pVI.

Adding a reporter molecule to a phage displaying a peptide or antibody enables the use of phage for imaging or diagnostics. For example, fluorescently labelled Ff displaying cell-targeting moieties have been used in cancer cell imaging (Li et al., 2010a). Additionally, Ff-based biosensors for bacteria and biomolecules have been reported that use various signal-detection methods, including linear dichroism (Lee et al., 2013; Oh et al., 2014; Zhu et al., 2008).

1.2 FF-DERIVED NANORODS

A multitude of applications using Ff phages have been published (Guo and Cai, 2006; Tikunova and Morozova, 2009); however, they are limited to laboratory containment. This is because Ff phages are live viruses that infect bacteria in the environment and within human hosts (Meaden and Koskella, 2013). Furthermore, Ff vectors used in diagnostics and other applications contain engineered antibiotic resistance genes that are easy to spread in the environment once introduced into host bacteria. Therefore, their applications may not be approved by environment protection or other regulatory agencies. Secondly, Ff phages and phagemids are long filaments rather than nanorods, under most conditions. The high length-to-diameter ratio interferes with applications that rely on diffusion, such as lateral flow detection devices in diagnostics, tissue

targeting and vaccines (Bertrand et al., 2014; Garg, 2019; Sattar, 2013).

To overcome these drawbacks, short Ff-derived particles were constructed, functionalised and applied for diagnostic assays (Sattar et al., 2015). These particles (named Ff-nano) were 50 nm in length and contained a 221 nt ssDNA without any coding sequences, so are therefore unable to replicate in bacteria (Sattar et al., 2015). The system for production of the Ff-nano particles was composed of a short template for rolling circle replication (Figure 1.4) that results in the circular 221-nt ssDNA, inserted into a plasmid. This replication template contains only the positive Ff origin of replication. The Ff-nano particles were functionalised and used for quantitative dipstick assays for detection of fibronectin (Sattar et al., 2015). However, this system had some drawbacks as replication of Ff-nano 221 nt ssDNA and packaging into the short nanorods was mediated by a helper phage (infectious virus). Consequently, the helper phage was produced in parallel with the Ff-nano and had to be separated from the short nanoparticles (

Figure 1.5A).

As a result, in a typical purified nanorod sample, the contamination with undesirable phage-derived viral particles was at a frequency of $1:10^6$. Given that the number of particles used (e.g., in vaccination is 10^{12} pfu/mouse), this was not a tolerable number as it would result in 10^6 infectious particles per injection (Sattar et al., 2015).

Furthermore, the replication cassette for the 221 nt Ff-nano genome lacked the negative Ff origin of replication, resulting in relatively poor production of the Ff-nano particles.

1.2.1 Development of BSFnano production system

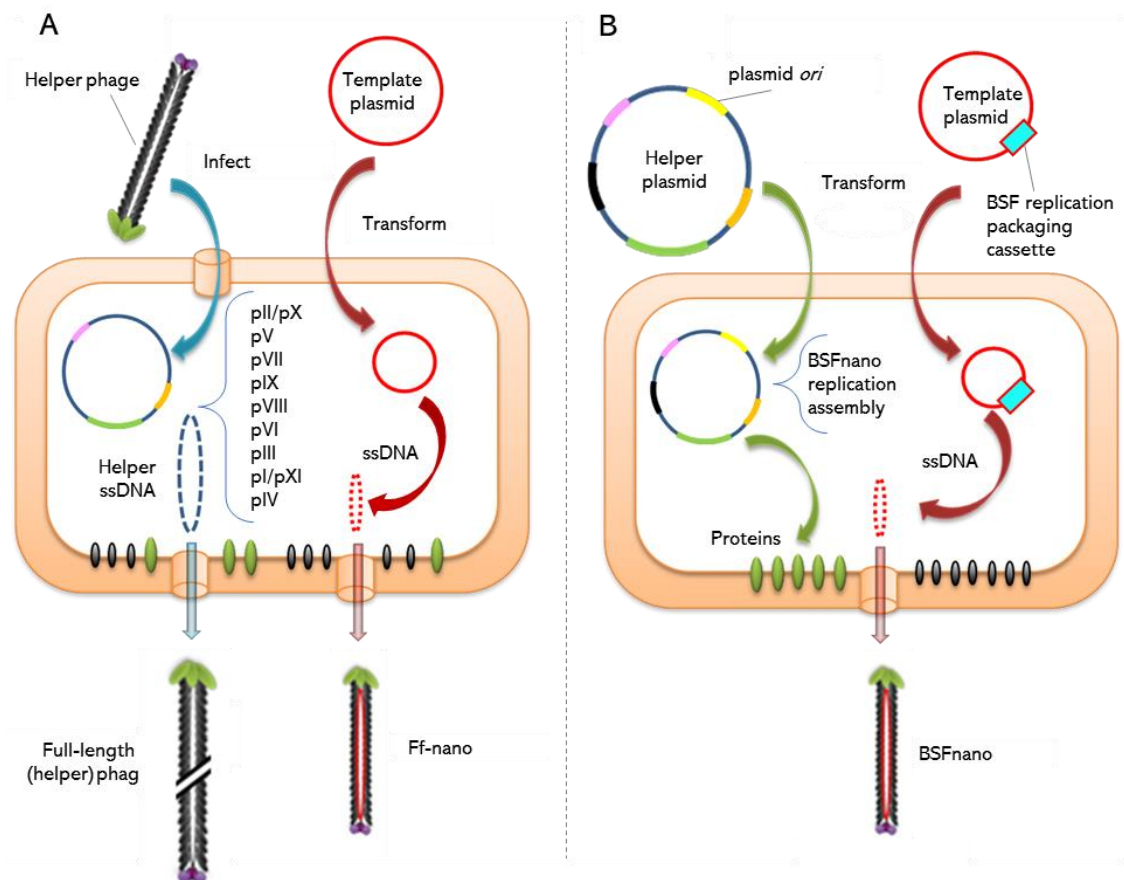


Figure 1.5. Comparison of helper phage and helper plasmid assisted systems for the production of Ff-derived particles.

A, Conventional method for producing Ff-derived particles using helper phage, which serves as a source of phage proteins required for replication of from F1 ori and assembly into the Ff-like particles. Presence of a helper phage, however, results in the production of full-length phage virions along with particles derived from a second replicon that contains F1 ori. **B**, Two-plasmid system. If helper plasmid is used instead of helper phage, only particles derived from the second episome (phagemid, Ff-nano or pBSFnano template) are produced. Helper plasmid is identical to the helper phage, apart from the deletion of intergenic

sequence, including the origin of replication and packaging signal (Rakonjac, Zhou and Bisset, unpublished).

To overcome the drawbacks of low yield of Ff-nano, and to eliminate the use of helper phage in a short nanorod production system described above, a new nanorod production system was designed. The system was composed of a novel template plasmid and a helper plasmid instead of a helper phage (

Figure 1.5B). The new template plasmid (pBSFnano) contained a replication cassette comprising both a positive and negative origins of replication (Figure 1.6), and helper plasmid was used instead of helper phage (Bisset, Zhou and Rakonjac, unpublished) (

Figure 1.5B). The rolling circle replication from the template, a BSF replication assembly cassette composed of the complete Ff origin of replication followed by the terminator (a truncated positive origin *ori* Δ 29; Figure 1.7B), that gives rise to a short circular ssDNA. These short DNA "genomes" further serve as a backbone for the assembly of nanoparticles. The name "BSFnano" comes from Biological Scalable Ff-derived Nanorods (patent in preparation).

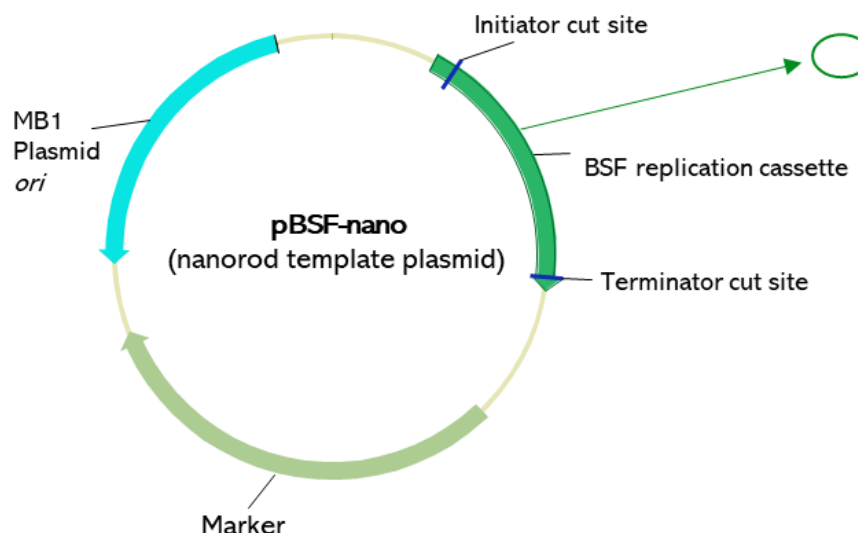


Figure 1.6. Map of a pBSFnano nanorod template plasmid. The scheme contains two functional blocks, Amp^R marker (light green) and BSF-nano replication cassette (dark green). BSFpn replication cassette (529; 719; 736). The green arrow pointing to green circle denotes that product of BSF replication cassette in the presence of pII/pX is circular ssDNA (BSFnano). This circular ssDNA is assembled into the BSF nanorods in the presence of the assembly/secretion and virion proteins (Rakonjac, Bisset, Zhou, unpublished).

The initiator in the 221 nt replication template contained only the essential (A) portion of the (+) *ori* (Figure 1.7A), further decreasing the replication efficacy and requiring a specific *gII* mutation in the helper phage. In the presence of pII replication protein from the helper plasmid, the section between the two (+) origins of the BSFpn replication cassette (736 nt) was excised. Both (+) and (-) strands get replicated independently of the pBSFnano plasmid (Figure 1.6), resulting in increased nanoparticle production, in comparison to the Ff-nano 221 nt cassette (Rakonjac, Bisset, Zhou, unpublished). The particles can be made shorter or longer by shortening or lengthening the sequence between the

initiator and terminator “arms” of the cassette which mark the start and the end of the BSFpn replicon (Figure 1.7B).

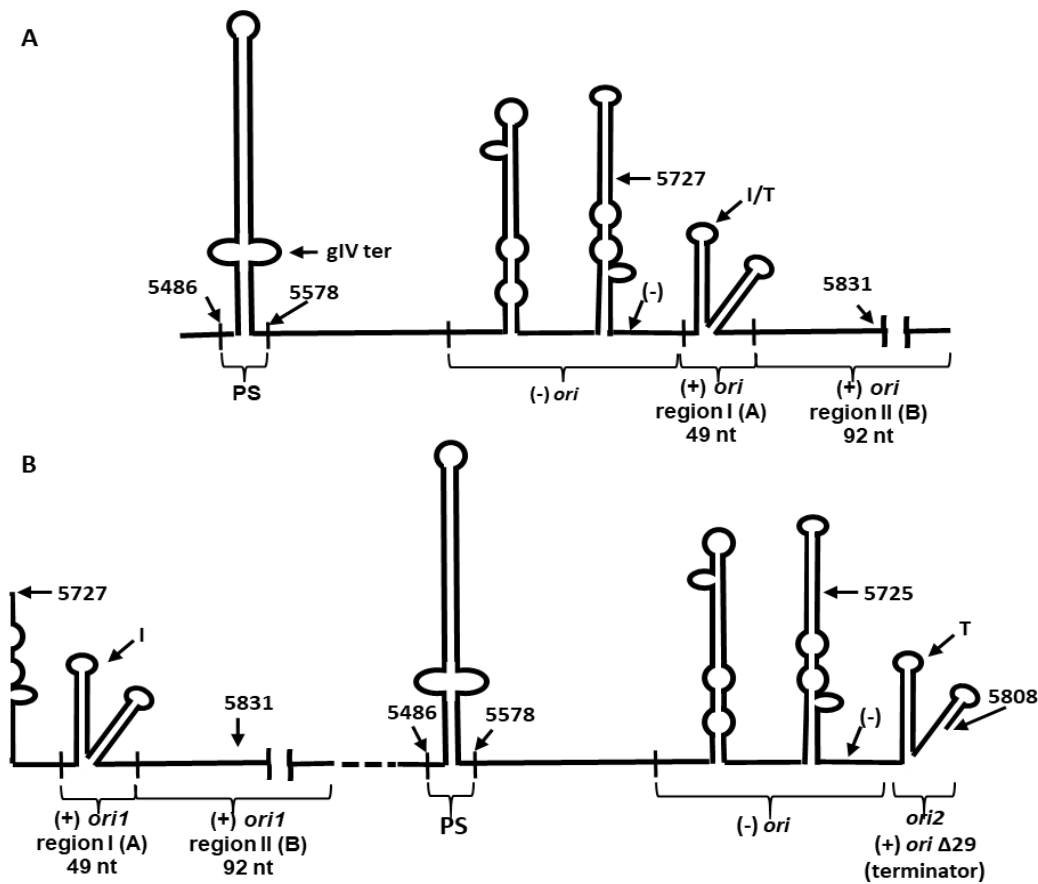


Figure 1.7. Replication and packaging cassettes.

A, A complete intergenic region of Ff phage (f1, M13 or fd) corresponding to the packaging signal, negative and complete positive origin of replication. **B**, BSFpn cassette. PS, packaging signal; I, initiator; T, terminator; *ori*, the origin of replication. Figure adapted from (Bisset, Rakonjac, unpublished).

Each cassette contains:

- Initiator (*ori1*), a positive-strand origin of replication. Protein pII (DNA-strand-transferase) binds to *ori1* and forms a nick in (+) DNA, forming primers for replication;

- Packaging signal (PS), required for transferring the ssDNA (+) strand to the trans-envelope assembly machinery, where BSFnano genome is packaged into nanoparticles with coat proteins.
- Negative origin of replication, (-) *ori* that allows replication of ssDNA by using the (+) DNA strand as a template. This increases the copy number of produced BSFnano genomes.
- Terminator (*ori2*), which consists of a mutant (+) origin of replication (*oriΔ29*), that allows the ligation of two DNA ends into a circular ssDNA genome.

Interestingly, comparison of the lengths of the particles vs the size of packaged ssDNA between 221 nt and 736 nt backbones (forming 45 nm and 100 nm particles), was in agreement with the proposed length of the particle cap at 17 nm and gave a length per nucleotide ratio of ~7.6 (S. Bisset and J. Rakonjac, unpublished). In the future, this will help to gauge the length of ssDNA to obtain particles of the desired length.

The second improvement of the nanorods production system was achieved by converting the helper phage into helper plasmid, by inserting a plasmid (pA15) *ori* of replication from helper phage VCSM13 to replace the *f1 ori* of the helper phage Rnano3 used in the Ff-nano system. Helper plasmid produces the Ff-encoded proteins required for replication of the BSFpn replication cassette, and packaging of the resulting ssDNA into the BSF nanorods, however, it does not assemble into the particles (

Figure 1.5). Only the short BSF nanorods are produced in this system, eliminating the need for separation from the full-length helper phages. In this study, BSFnano particles were functionalised and tested in a proof of concept lateral flow diagnostic assay, for detection of fibronectin.

1.3 IMMUNODIAGNOSTICS

Diagnostics play a crucial role in the prevention and monitoring of chronic and infectious diseases in a population. Immunoassays rely on the interaction between an antigen (analyte) and an antibody, to provide a specific and sensitive detection and quantification (Darwish, 2006). The first time this term was used was in 1959 for a test that measured serum insulin using polyclonal guinea-pig anti-bovine insulin antibodies (Yalow and Berson, 1959). Following this discovery, in the 1970s another immunodiagnostic test emerged for thyroid-stimulating hormone (TSH), firstly as a competitive test, then as a non-competitive assay (Chopra, 1972; Chopra et al., 1972). In 1977 Rosalyn Yalow was awarded the Nobel Prize in Medicine *"for the development of radioimmunoassay of peptide hormones"*. In 1980s colourimetric Enzyme-Linked Immuno-Sorbent Assay (ELISA) allowed a level of automation, but still required sophisticated equipment and laboratory staff. Finally in 1990s chemiluminescence immunoassays (CLIA) emerged, and are still being modified for a variety of instruments and products (Cinquanta et al., 2017). CLIA method increased the performance of diagnostic tests.

Today, specific antibodies can be labelled by conjugation of radionuclide, fluorescent dye, or a chromogenic molecule. Labelled antibodies can be used to rapidly detect parasites, microbes, hormones, illegal drugs, toxins, and environmental pollutants.

Overall, ELISA tests are still predominantly used immunoassays, with the detection limits between 0.01 pg/mL and 100 ng/mL (Zhang et al., 2014). When compared to RIA and CLIA assays (Warnken et al., 2016), all three tests gave different values for the same sample, with RIA and ELISA giving more similar results for the concentrations of the same analyte than a CLIA assay. While laboratory-based assays provide high sensitivity and specificity, diagnostic tests for use in the field additionally require flexibility and simplicity, speed, cost-effectiveness, and accuracy. One of the well-known such technologies is lateral-flow assay, also known as a dipstick test.

1.3.1 Lateral flow assays (LFA)

Initially immunoassays were performed manually by trained professionals and they required laboratory equipment. In contrast, immunodetection and quantification of analytes in a rapid way can be achieved with lateral flow assays (LFA). There are two main types of LFA, based on the elements of the assay: (1) the lateral flow immunoassay (LFIA), which uses antibodies as detector molecules, and (2) the nucleic acid lateral flow assay (NALFA) (Koczula and Gallotta, 2016). The later ones are usually used during PCR

amplification for the detection of amplicons (Connelly et al., 2008).

LFIA can be designed to detect circulating antigens as targets (e.g., parasites, viruses, proteins, hormones, etc.) (Boisen et al., 2015), or to detect serum antibodies against a specific antigen (Nielsen et al., 2008). Samples that are used for LFIA tests must be liquid and able to migrate along the dipstick membrane due to capillary forces. For medical purposes, most commonly tested are serum, blood, urine, and saliva (Carrio et al., 2015; Magambo et al., 2014; Moreno et al., 2017). However, there are many other applications in various industries, including food production (Ching et al., 2015), quality control (van Dam et al., 2013), veterinary medicine (Nielsen et al., 2009), and environment (Mei et al., 2013). While LFIA is widely spread for use in point of care (POC) in hospitals and general practitioner offices, regulatory bodies still require independent verification for the dipstick tests used in hospitals. The key advantages of dipstick assays are that they are simple one-step assays of low cost, that require minimal sample volume, and can be used in the point of care settings. Dipstick assays give rapid results, have long shelf-life and do not require refrigeration. Furthermore, they can detect proteins, amplicons or haptens in a qualitative or semi-quantitative way. However, these assays also have some disadvantages when compared to lab-based assays: reduced precision, restriction of a total assay volume, requirement for pre-treatment of non-liquid samples is needed, and high-affinity and highly purified antibodies. Nevertheless, these

tests are beneficial as a first screen for diseases (Kim et al., 2015), toxins (Shyu et al., 2002), pathogens (Morales-Narvaez et al., 2015) and environmental pollutants (Lopez Marzo et al., 2013).

In particular, the longevity of shelf life and independence from refrigeration during distribution and storage makes the LFIA ideal candidates for use in remote places, battlefields, developing countries for control and monitoring of diseases in cases of pandemic outbreaks. Recently there is an increased need for POC multiplex assays where simultaneous detection is allowed on multiple test lines that can detect several different analytes from a complex mixture (Koczula and Gallotta, 2016).

1.3.2 Ff phage applications in immunodiagnostics

Modifications of filamentous phages allow their use in a variety of diagnostics applications (Hairul Bahara et al., 2013). Unlike the functionalisation of antibodies, where reporter molecules (probes) are directly attached to the detector molecule, the use of Ff allows an increase in the number of labeled molecules due to hundreds to thousands attachment sites along the length of the phage filament. In Ff-phage-based immunoassays, the antibodies (e.g., mAb or scFv) are displayed at the tip of the phage filament (e.g., pIII). At the same time, a fluorescent dye, enzyme probe, or radioactive label can be conjugated in hundreds of copies to the major phage coat protein pVIII along the filament. Such design and combination of a small number of detector

molecules (e.g., scFv displayed on pIII) with multiple reporter molecules attached to pVIII allows amplification of the signal.

Multiple methods of chemical conjugation to the phage coat proteins have been developed to date: modifications of the primary amines (N-termini of peptides or the lysine side chains) with NHS-esters, tyrosine modifications, carboxylate modification (aspartic acid, glutamic acid, C-terminus), N-terminal transamination with pyridoxal phosphate (Bernard and Francis, 2014). The scFv-displaying phages can be combined in this way with, for example, gold nanoparticles (Liu et al., 2016a), offering highly selective and rapid bifunctional nanoprobe, which can be designed for colourimetric detection of pathogens. Labels commonly used in LFIA tests include: paramagnetic beads (Liu et al., 2011; Wang et al., 2015), carbon nanoparticles (Qiu et al., 2015), enzymes (Mirasoli et al., 2012) or fluorescent dyes (Song et al., 2015; Wang et al., 2015). Potentially, BSFnano particles could be functionalised with either one of these labels, depending on the specific application. Furthermore, functionalised full-length Ff phages have been reported as suitable nanoparticles for high sensitivity devices, such as piezoelectric bio detectors for pathogens with a sensor limit of 100 cells/mL (Olsen et al., 2006). Choice of detectors depends on the label used. While gold is detected by visual observation, other labels require equipment for reading the signal, including: electrochemical readers (Lin et al., 2008b), camera readers (Liu et al., 2011), chemiluminescent readers (Joung et al., 2014), optical

readers (Xu et al., 2009), and fluorescent readers (Li et al., 2010b).

Ff-nano particles were reported to show improved properties for LFIA tests when compared to the full-length filamentous phages in that they do not smear along the dipstick Sattar et al. (2015). However, these nanorods were produced at a low level and they required lengthy purification protocols, as stated in Section 1.2.

1.4 COMPONENTS AND ACTIVATION OF CELLULAR ADAPTIVE IMMUNE RESPONSES

Besides the development of Ff-nanorod-based technology and optimisation for use in immunodiagnostics, another major theme of this thesis was to test Ff-phage-based vaccines for applications in immunotherapy of cancer. Ff phages displaying antigen in conjunction with adjuvanting molecule α -galactosylceramide (α -GalCer) were examined for eliciting of the antigen-specific CTL responses (Chapter 4). It is therefore essential to introduce the components of immune system that play vital roles in vaccine-induced cellular immunity using α -GalCer as adjuvanting molecule.

1.4.1 Dendritic cells

Dendritic cells (DCs) are professional antigen-presenting cells (APCs) that are the key to development of antigen-specific (adaptive) immune responses.

1.4.1.1 Antigen processing and presentation

Once the DCs take up a pathogen or a vaccine, the internalised antigens are proteolytically cleaved into shorter peptides. Depending on the compartment in DCs from which they are derived, antigens will be proteolytically processed and presented on the MHC class I (Goldberg et al., 2002; Rock et al., 2002) (Figure 1.9), or the MHC class II molecules (Bryant and Ploegh, 2004; Honey and Rudensky, 2003; Watts, 2001).

Dendritic cells that had taken up antigens 1) upregulate expression of MHC, which presents the antigenic fragments (peptides) to the TCR of T cells, causing crosslinking of TCRs and signal transduction; 2) upregulate expression of co-stimulatory molecules that interact with CD28 on T cells to help convey stimulatory signals that drive T cell activation and proliferation (mainly through increased autocrine IL-2); 3) release of cytokines such as IL-12 p70 that helps drive differentiation programmes (e.g., differentiation of activated CD8⁺ T cells into CTL).

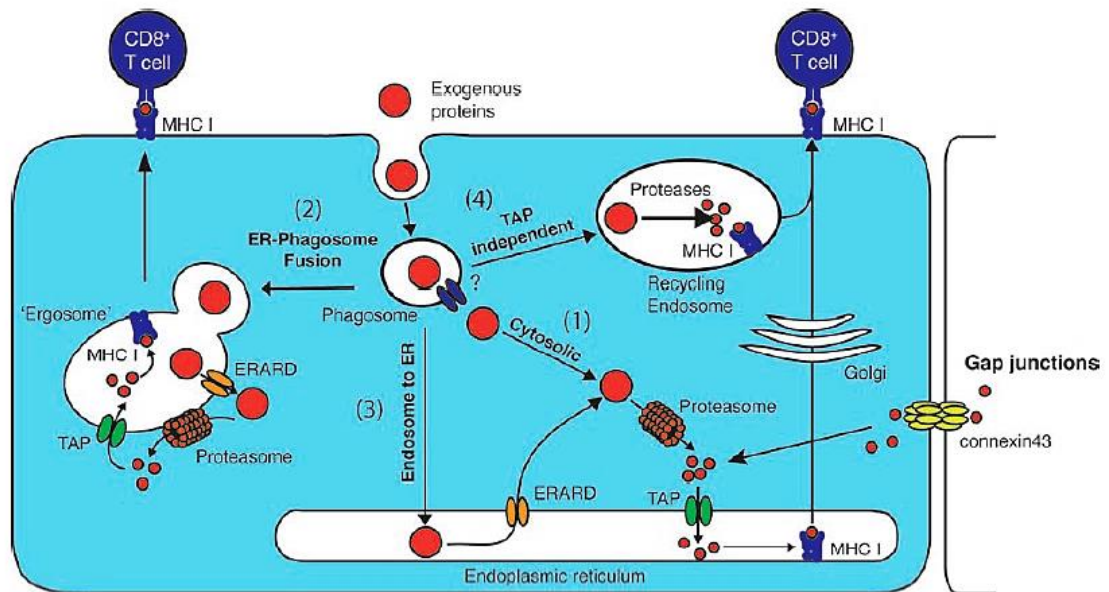


Figure 1.8. Pathways of antigen cross-presentation in dendritic cells. **1**, The endosome to cytosol pathway involves the exogenous protein leaving the endosome and entering the cytosol, where it is degraded by the proteasome. The antigens then enter the ER via the TAP complex and are loaded onto MHC class I. The MHC I/antigen complex is transported via the Golgi to the cell surface. **2**, The ER-phagosome fusion pathway involves the formation of an ergosome by fusion of the endosome and part of the ER. The proteins exit the ergosome and enter the cytosol via the ERAD system to be cleaved by the proteasome. The cleaved antigens then re-enter the ergosome via the TAP complex and are loaded onto MHC I molecules. The MHC I/antigen complex then transits to the cell surface. **3**, In the endosome to the ER pathway, the acquired exogenous proteins within the endosome enter the cytosol and directly enter the ER. The proteins then enter the ERAD pathway and leave the ER for cleavage by the proteasome. The antigens then re-enter the ER via the TAP complex, are loaded onto MHC I and then the MHC I/antigen complex transits to the cell surface. **4**, The proteasome and TAP independent pathway involves the exogenous proteins being cleaved within the endosome and loaded onto MHC I molecules that are recycled from the cell surface. The MHC I/antigen complex then transits to the cell surface. Figure and legend sourced from (Petersen et al., 2010) with permission.

1.4.1.2 Activation of DCs

Specific immune responses can be either initiated or prevented, depending on the activation state of DCs upon their interaction with T cells (Hernandez et al., 2001;

Kurts et al., 1997). Presence of pathogen-specific or danger-reporting molecules (e.g., DAMPs, PAMPs) triggers activation of DCs (Bennett et al., 1997; Smith et al., 2004). Once DCs sense these danger signals, phenotypic changes take place (Dhodapkar et al., 2001; McLellan et al., 2000; Tan and O'Neill, 2005).

These changes occur in three stages: maturation, activation and licensing. "Maturation" is characterised by upregulation of co-stimulatory molecules on the cell surface, essential for T cell activation, while "activation" is characterised by upregulation of co-stimulatory molecules and cytokines (e.g., IL-12) to stimulate naïve T cells to proliferate and differentiate into effector T cells (Tan and O'Neill, 2005). The term "licencing" was first introduced by Lanzavecchia (Lanzavecchia, 1998), and here it will be used to describe the process in which iNKT cells or CD4⁺ cells activate DCs through cytokine production and receptor binding (Figure 1.9) (Hermans et al., 2003; Ridge et al., 1998).

Naïve DCs are characterised by the low levels of expression of surface molecules (e.g., MHC I, MHC II, CD80, CD86, CD40). These naïve DCs are scattered throughout the body and are very efficient in acquiring the antigens from tissues (Inaba et al., 2000). Once activated, DCs upregulate the MHC I and MHC II expression on their cell surface, increase cytokine production and migrate to lymphoid tissues where they can activate T cells (Dieu et al., 1998; Koch et al., 1996; Sallusto et al., 1998). T cells that have been activated by DCs can in turn, depending on the cell type, induce or

mediate adaptive immune responses against the presented antigen.

To stimulate anti-tumour CD8⁺ T cell responses, neoantigens (tumour-specific antigens) first need to access DCs to induce neoantigen-specific CD8⁺ T cell responses. Indeed, cytotoxic T cell responses can be activated against the tumour antigens (McDonnell et al., 2010; Nowak et al., 2003). In this case, antigen-presenting cells, specifically DCs, need to acquire exogenous antigens from infectious agents or tissue and present it via MHC molecules (Bevan, 1976). The mechanical process of such antigen presentation is called cross-presentation. The whole process of stimulating T cells is called cross-priming (Bevan, 1976), while stimulated CD8⁺ T cells are referred to as "cross-primed" T cells.

The first time cross-presentation was demonstrated in 1976 when chicken ovalbumin (OVA) was found present in the cytosol of DCs after the cells were cultured with OVA (Rodriguez et al., 1999). In this study, it was also demonstrated that the macrophages, unlike DCs, were unable to present exogenous OVA on MHC I molecules. This suggests that antigens can leave the endosome after their uptake by DCs, and stimulate the CD8⁺ cells, while macrophages could not. Similarly, when macrophages were infected with influenza virus, they could not activate the CD8⁺ T cells. On the other hand, when DCs that were cultured with the infected macrophages a significant antigen cross-presentation was demonstrated by the induced CD8⁺ T cell responses. Furthermore, in another study (Jung et al.,

2002), all other APCs were excluded from cross-presentation, emphasising the importance of DCs in CD8⁺ T cell activation. There are several theories of different pathways for cross-presentation: (1) endosome to cytosol pathway (Lin et al., 2008a; Rodriguez et al., 1999), (2) ER phagosome fusion pathway (Guermónprez et al., 2003; Imai et al., 2005), (3) endosome to ER pathway (Ackerman et al., 2005), and (4) proteasome and TAP independent pathway (Shen et al., 2004) (Figure 1.8). However, the exact mechanism of how this happens is unknown (Lin et al., 2008a; Petersen et al., 2010).

It has been reported that, to sufficiently activate DCs to cross-present the acquired antigens to CD8⁺ T cells, licensing is needed (Schulz et al., 2000). Licensing involves an activating signal that is ultimately derived from an immune-alarm-triggering molecule, be it from a pathogen or tissue injury, and it could be a specific molecule on its own, or a molecule complexed with a cognate cell involved in the innate immune response (see below).

Various non-conventional T cells, some of which are capable of DC licensing, cannot be described as CD4⁺ or CD8⁺ T cells. The most studied type among those are invariant natural killer T (iNKT) cells that, in the presence of specific small molecules, can upregulate cytokine production and expression of their own and DCs' costimulatory markers to enhance the CD8⁺ T-cell activation (Fujii et al., 2003; Hermans et al., 2007; Hermans et al., 2003). For example, upregulation of CD40 molecule on the mature DCs enables

their binding to CD40L expressed by the licensing cells (Figure 1.9) (Schulz et al., 2000). Additionally, iNKT cells produce $\text{TNF-}\alpha$ and $\text{INF-}\gamma$ that provide CD40L-independent stimulation of DCs (Figure 1.11) (Fujii et al., 2004; Silk et al., 2004).

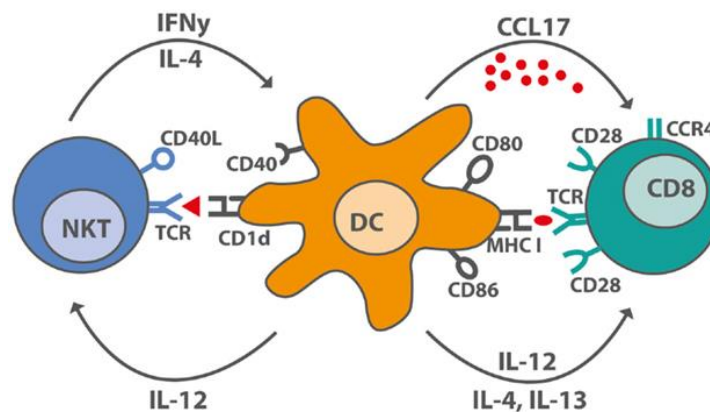


Figure 1.9. iNKT cell-DC interactions after stimulation with α -GalCer. Under optimal stimulatory conditions, iNKT cells produce IL-4, large amounts of IFN γ and upregulate CD40L, thereby inducing maturation in DC. DC maturation leads to increased costimulatory capacity through upregulation of CD80 and CD86, of MHC molecules, and by producing the pro-inflammatory cytokine, IL-12, and the chemokine, CCL17. CCL17 attracts CCR4⁺ cells, including CD8⁺ T cells, which can be activated by the licensed DC. Figure and legend sourced from (Gottschalk et al., 2015) with permission.

Importantly, CD4⁺ T cells also contribute to the activation of DCs, which, as a result, amplify the stimulation of CD8⁺ T cells. Of notice, cytokine IL-2 has been proved to be the key to the CD8⁺ priming; its absence was reported to cause generation of “helpless CD8⁺ T cells” (Feau et al., 2011; Williams et al., 2006; Wilson and Livingstone, 2008). Interestingly, this cytokine is produced by the CD8⁺ T cells themselves, and not the CD4⁺ T cells or the licensed DCs (Feau et al., 2011).

Cancer cells come from the host itself and derived antigens usually do not activate DCs. Moreover, tumour-associated antigens presented by DCs often inhibit tumour-specific T cells, rather than activating them, due to the lack of the PAMP- or DAMP-induced co-stimulation. Another challenge in developing a cancer therapeutic vaccine is to achieve targeting of antigen-presenting DCs to the lymphoid tissues in order to induce T cells to differentiate into CTL effector cells (Palucka and Banchereau, 2012). It has been proposed that the combination of iNKT and CD4⁺ T cell licensing of DCs would be beneficial for inducing a robust CD8⁺ T cell responses in vaccine-mediated cancer immunotherapy (Gibbins, 2014).

1.4.2 T cells and anti-tumour responses

1.4.2.1 CD8⁺ T cells

Cytotoxic CD8⁺ T cells (CTLs), the key effectors of immune response against target cancer cells, are derived from naïve T cells activated by DCs presenting specific antigenic peptides and expressing co-stimulatory surface molecules and cytokines (e.g., IL-12) (Ingulli et al., 1997; Mescher et al., 2006; van Stipdonk et al., 2001). The stimulation between DCs and CD8⁺ T cells is bidirectional, with activated T cells further enhancing the activation of DCs. TCR-MHCI interaction as a primary signal has to be accompanied by the T cell CD40 binding to DC CD40L and subsequently T-cell CD28 to DC molecules CD80 or CD86 (Cella et al., 1996; Fujii et

al., 2004; Larsen et al., 1992). Proliferation of CD8⁺ T cells is strongly driven by IL-2, therefore activated T cells also upregulate the receptor CD25 that binds the IL-2 with high affinity (Oehen and Brduscha-Riem, 1998).

Activated CD8⁺ T cells proliferate and differentiate into CTLs, then migrate to the target tissue where they kill cells displaying the cognate antigen (Belz and Kallies, 2010; Oehen and Brduscha-Riem, 1998; Weninger et al., 2001). Interaction of CTL's TCR with the cognate antigen-MHC I complex on the target cell triggers the release of cytolytic proteins (Balaji et al., 2002; Chavez-Galan et al., 2009; Kurschus et al., 2008; Metkar et al., 2003; Pinkoski et al., 2001). Notably, uncontrolled and massive release of cytotoxic proteins by CTLs can cause damage to healthy cells and tissues. Effector CTLs eventually undergo a programmed reduction in numbers (Arens and Schoenberger, 2010; Prlic and Bevan, 2008). Approximately 95% of effector T cells will undergo apoptosis in "contraction phase", while the remaining 5% become memory T cells (De Boer et al., 2001).

1.4.2.2 CD4⁺ T cells

CD4⁺ (helper) T cells, alongside the iNKT cells, play a crucial role in licensing of DCs, resulting in activation and differentiation of CTLs. Furthermore, recent studies show that CD4⁺ T cells play a critical role in anti-tumour immune responses (Tay et al., 2020). Additionally, some CD4⁺ T helper cells can produce cytotoxic chemicals, such as granzyme B (Akhmetzyanova et al., 2013; Hirschhorn-Cymerman

et al., 2012; Quezada et al., 2010), that become released upon binding of their TCR to a cognate peptide-MHC II complex. However, the importance of the cytotoxic function in CD4⁺ T cells is still poorly understood. During the CD4⁺ T cell priming, their environment dictates the class of helper T cell that is generated (Zhou et al., 2009). For example, when IL-12 is present during the activation of naïve CD4⁺ T cells, they are stimulated to differentiate into Th1 cells (Seder et al., 1993) that primarily stimulate CTL responses.

Interestingly, it had been reported that some Th1 cells could enter the tumour tissue and release IFN- γ , which in turn stimulates the tumour cells to express more MHC I molecules, enhancing their visibility to the CD8⁺ T cells (Propper et al., 2003). Other subsets of helper T cells (Th) include Th2, Th9, Th17, Th22, follicular helper T cells and T_{reg}. However, the detailed functions of individual Th cells are beyond the scope of this thesis and therefore, will not be mentioned further.

1.4.2.3 Invariant natural killer T cells (iNKT)

NKT cells were initially defined by the expression of NK cell-associated markers (such as NK1.1 in C57BL/6 mice) together with a TCR. However, it has been reported that some NKT cells do not carry NK markers (Benlagha et al., 2000). There are two different types of NKT cells: (1) type I NKT cells, also known as invariant NKT (iNKT), and (2) type II NKT cells. This classification was based on the type of TCR,

where iNKT cells have an invariant TCR α -chain combined with a limited repertoire of TCR β -chains in their TCRs (Arase et al., 1993), while type II NKT cells have a wide range of both TCR α - and TCR β -chains. For this research, iNKT cells were of primary interest and therefore, will be addressed in this section.

Like conventional T cells, iNKT cells undergo selection in the thymus, with the positive selection being driven by the MHC-like molecule CD1d (Bendelac et al., 1995). The selected iNKT cells that leave the thymus in murine models can be either CD4⁺ CD8⁻ or CD4⁻CD8⁻, with TCR variants V α 14-J α 18/V β 8, V β 7, or V β 2 TCR (Kawano et al., 1997; Lantz and Bendelac, 1994; Masuda et al., 1997). In humans, NKT cells can also be CD8⁺ and have V α 24-J α 14/V β 11 rearrangement (Bendelac et al., 2007). iNKT cells can be found in abundance in spleen, liver and bone marrow (MacDonald, 1995).

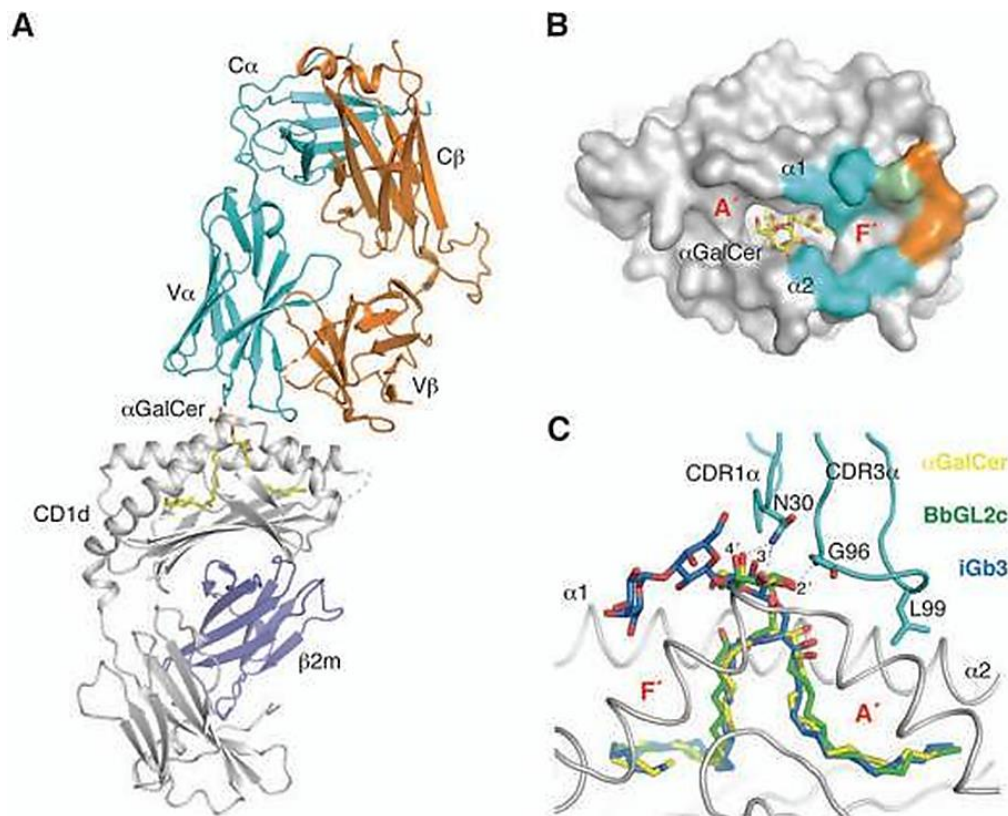


Figure 1.10. Antigen recognition by the type I NKT TCR.

A, Ternary complex (PDB ID 3HE6) between CD1d/b2m (grey and blue), α -GalCer (yellow), and the type I NKT TCR (α chain in cyan, β chain in orange). **B**, Footprint of the type I NKT TCR on CD1d. Residues on the CD1d surface contacting the α chain are shown in cyan, residues contacting the β chain are shown in orange, shared residues are in green. **C**, Details of the antigen-binding groove showing the superposition of the bound conformations of α -GalCer (yellow), BbGL2c (green, PDB ID 3O9W), and iGb3 (blue, PDB ID 3RZC), after being flattened by the TCR. The CDR loops (cyan) contact the antigens exclusively through Asn30 α and Gly96 α . Polar contacts are shown as dashed lines. Note how all the bound ligands adopt similar conformation for their first sugar upon TCR binding. Figure and legend adapted from (Girardi and Zajonc, 2012) with permission.

Invariant TCR provides iNKT cells with a unique ability to recognise and respond to glycolipid antigens presented on an MHC-I-like molecule CD1d (Figure 1.10), which is expressed by DCs (Mattner et al., 2005; Wu et al., 2005). Studies of iNKT cell functions and activity were

significantly accelerated after discovery that they interact with α -GalCer-loaded CD1d molecule and are experimentally tracked by staining with fluorescently labelled soluble α -GalCer-loaded CD1d tetramers (Benlagha et al., 2000; Kawano et al., 1997). One of the critical roles of these cells is in licensing DCs which, as mentioned earlier, stimulate effector CD8⁺ T cell responses. Furthermore, it has been reported that iNKT cells receive stronger signals from their TCRs than do conventional T cells (Moran et al., 2011). This suggests that CD1d-binding molecules, such as α -GalCer, can be used as very potent adjuvants in vaccine-mediated cancer immunotherapy.

Within the iNKT cell population, there are three different categories, depending on their developmental stages (iNK1, iNK2 and iNK17). These cells can be distinguished by the receptors expressed on the cell surface (mainly NK1.1 and CD44) (Bennstein, 2017). For the interpretation of immunisation results in this thesis (Chapter 4), the main focus will be on type 1 iNKT cells, also known as mature iNKT (CD24⁻, CD69⁻, CD44⁺, NK1.1⁺).

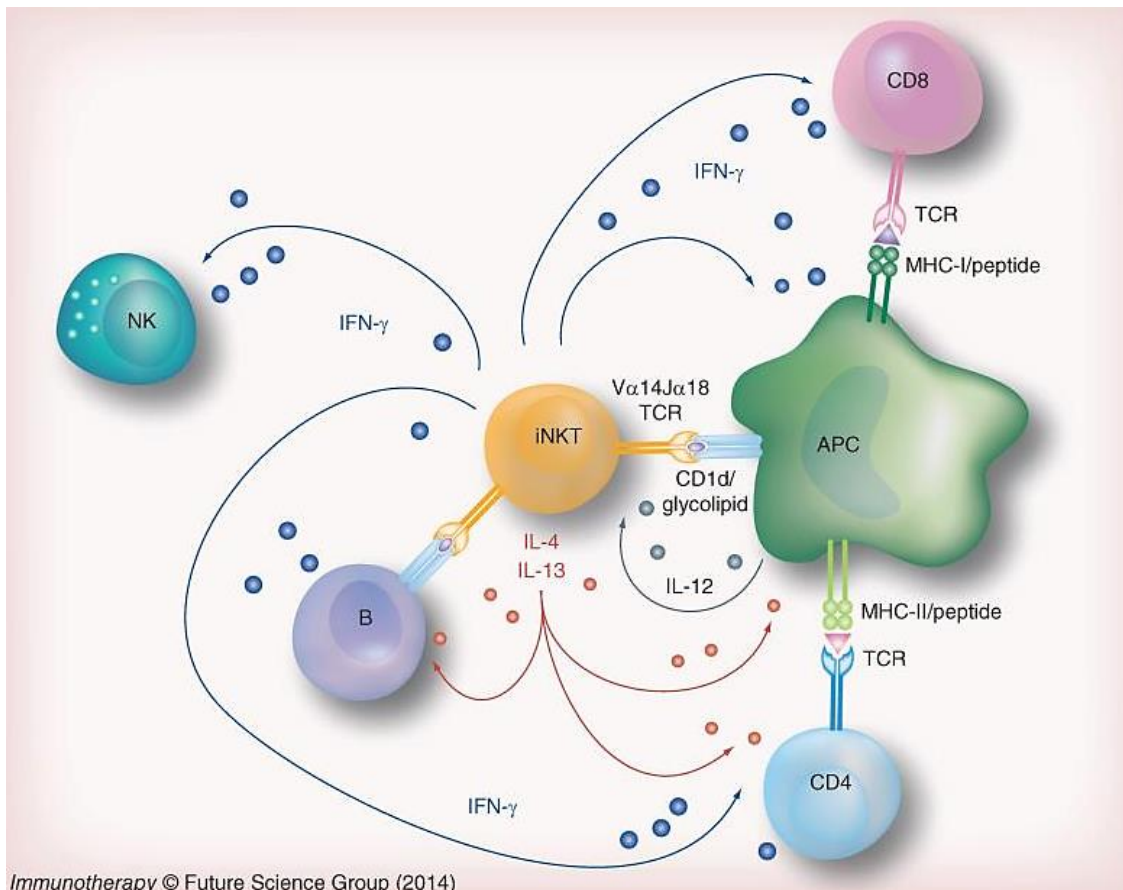


Figure 1.11. Invariant NKT cells and their role in immunity. iNKT cells express a specific antigen receptor that includes an invariant TCR α chain. These TCRs recognise specific glycolipid ligands bound to CD1d molecules, which are expressed mainly on APCs such as dendritic cells and B lymphocytes. After TCR ligation, iNKT cells rapidly secrete multiple Th1 and Th2 type cytokines, such as IFN- γ and IL-4. These cytokines, along with surface molecules expressed on activated iNKT cells, influence the activity of many other cells in the immune system, and contribute to transactivation of NK cells, maturation of DCs and enhancement of specific T-cell and B-cell responses and memory. Figure and legend are adopted from (Carreno et al., 2014).

Activated iNKT cells upregulate the expression of CD40L molecules on their surface, which stimulate DC production of interleukins (e.g., IL-12) (Caux et al., 1994). Additionally, as a result of DC-induced cellular activation, iNKT cells release IFN- γ and a range of other cytokines (Carnaud et al., 1999). The IL-12 produced through

interaction with DCs transactivates NK cells, leading to a further release of very high levels of IFN- γ (Figure 1.11)(Liu et al., 2005a).

The licensing or “help” by iNKT cells has been shown to be sufficient to provide the DCs with the capability to stimulate T cell responses to antigens they may have acquired (Fujii et al., 2007; Hermans et al., 2007; Hermans et al., 2003; Liu et al., 2005b). It is, therefore, possible to include an iNKT ligand in a vaccine as a form of immune adjuvant to promote CD8⁺ T cell responses antigens in the vaccine structure. Consequently, the iNKT cells themselves can be regarded as “cellular adjuvants” (Cerundolo and Kronenberg, 2010; Fujii et al., 2003). Furthermore, the licensing by iNKT may also replace the need for CD4⁺ T cells to act as helpers for the activation of CD8⁺ T cells (Gottschalk et al., 2015). In the multi-cellular grouping of DCs and T cells, the NKT cells provide the required CD40L co-stimulatory interactions to licence DCs (Fujii et al., 2003; Hermans et al., 2003; Nishimura et al., 2000), as well as interleukins and other soluble factors that induce activation of CD8⁺ (cytotoxic) T cells (Caux et al., 1994).

1.5 CANCER IMMUNOTHERAPY

Immunotherapy, in a broad sense, implies the use of either externally applied therapeutic antibodies, or boosting of intrinsic immune responses to fight disease (e.g., cancer), To date, several strategies have been developed to achieve this (Lee et al., 2018). For example, in cancer

immunotherapy, there are five ways to manipulate immune cells to fight cancer. One approach is targeting manufactured antibodies to cancer cell surface molecules to trigger apoptosis (Attarwala, 2010). Another way of using manufactured antibodies is to target cancer surface proteins and mark them for attack by antibody-dependent patient cytotoxic cells (Beurskens et al., 2012; Weiner et al., 2012). The third approach involves manufactured antibody-drug conjugates, or targeting chemotherapeutic drugs to the tumour; followed by immunostimulatory antibodies that act on immune cells (Dan et al., 2018). The fourth approach in immunotherapy is blocking the immunosuppressive effect in the tumour microenvironment, by using manufactured antibodies that enhance the immune response by blocking two key “checkpoints” that inhibit immune responses (Marhelava et al., 2019). In contrast, the fifth type of immunotherapy is immunisation using vaccines, therapeutic agents that are normally designed to induce adaptive immune responses against exogenous antigens, but are here induced to elicit TCL responses that target cells presenting cancer-specific neoantigens.

1.5.1 T cell vaccines targeting cancer cells

Vaccines that induce adaptive T cell responses can be used in immunotherapy for cancer treatments, usually in combination with chemotherapy and radiation (Vermaelen, 2019). Therapeutic vaccines are designed to target and eliminate already existing tumours. They are often considered as a supplementary therapy, and most of them are

still in various phases of pre-clinical and clinical development. So far, the only FDA-approved immunotherapy vaccine in the US has been Provenge (sipuleucel-T) for treatment of advanced prostate cancer (approved in 2010) (Brower, 2010; Dawson, 2010). In this technology, a recombinant antigen, that is specifically found in prostate cancer cells is used to stimulate T cells to fight cancer. Many other clinical trials for T cell therapies ultimately failed, mostly because the technology for the vaccine production needed further improvements.

It is important to note that in the case of cancer therapies, there is an additional challenge of having the primed T cells delivered to the tumour cells because the tumour microenvironment is immunosuppressive by its nature and as such represents a major obstacle for the efficiency of the vaccines (Vermaelen, 2019). In order to overcome the immunosuppression effects, vaccines are in some instances combined with immune checkpoint inhibitors (Couzín-Frankel, 2013; Pardoll, 2012).

The most sophisticated immunisation strategy involves extraction, *in vitro* stimulation, and adoptive transfer of autologous antigen-presenting cells (APC), in particular, dendritic cells (DCs) (Fan and Moon, 2015; Kandalaft et al., 2013). Clinical DC therapy trials have been reported for patients with bladder cancer (Zhang et al., 2012), melanoma (Carreno et al., 2015), pancreatic and lung cancer (Zhang et al., 2016a; Zhang et al., 2016b).

In the design of tumour-targeting vaccines, the antigen that is presented on tumour cells in the context of the MHC I complex, while absent from healthy tissues, has to be used, i.e. it is a "neoantigen". The most appealing neoantigens, when it comes to the T cell repertoire, are those against which there is no central tolerance, i.e. they are entirely "foreign" to the immune system. These are, for example, breakpoint peptides that arise from chromosomal rearrangement forming chimeric proteins, pro-viral antigens activated solely in the tumour, and mutated proteins resulting in novel antigens (Melief et al., 2015).

1.5.2 Carriers used in cancer vaccines

Most of the cancer neoantigens are intracellular; therefore the antigen-specific T cells kill the target cells that present these antigens in the context of MHC I. Physical link and specific stoichiometry of antigen to adjuvant molecules is required for maximising the antigen presentation while preventing overstimulation of iNKT cells. Consequently, it can lead to exhaustion of iNKT cells and prolonged inactivation (Parekh et al., 2005; Sullivan and Kronenberg, 2005). Such ratios can be achieved by using vaccine carriers.

Liposomes, immune-stimulating complexes and virus-like particles (VLPs) have been tested for display of antigens in multiple copies (Henry et al., 2015; McKee et al., 2012; Morein et al., 2004; Neumann et al., 2015; Prisco and De Berardinis, 2012; Sartorius et al., 2011; Yao et al., 2003).

One such type of biological particle can be derived from the Ff filamentous bacteriophages (Henry et al., 2015; Rakonjac et al., 2011). It has been reported that even wild-type Ff phages tend to show anti-tumorigenic effects (Dor-On and Solomon, 2015; Eriksson et al., 2009). In another study, by stimulating penetration of neutrophils into the tumour microenvironment, tumour-specific recombinant phages induced a strong anti-tumorigenic response (Eriksson et al., 2007). Furthermore, multiple antigens attached to a carrier proved to be much more efficient in inducing a T cell response than were the soluble antigens (De Berardinis et al., 2000; Demotz et al., 1990).

1.6 PHAGE-INDUCED IMMUNE RESPONSES

It has been demonstrated that phages can interact with the mammalian immune system and induce cellular responses *in vivo* and *in vitro* (Miernikiewicz et al., 2013; Van Belleghem et al., 2017; Weber-Dabrowska et al., 2000). Bacteriophages can enter mammalian cells by phagocytosis (Aronow et al., 1964; Wenger et al., 1978), either free or attached to the host bacteria. Spleen and liver have been identified as crucial organs for elimination of phages (Nungester and Watrous, 1934), as virions tend to accumulate in these sites where they are filtered out of circulation. Upon entry into the cells and lysosomal degradation of virions, phage DNA was shown to be sensed by endosomal PRRs (Hodyra-Stefaniak et al., 2015; Kazmierczak et al., 2014), or by cytoplasmic receptors (Carroll-Portillo and Lin, 2019). Filamentous

phages are natural carriers of CpG DNA motifs, and CpG-induced responses were detected when Ff phages were targeted to DCs (Sartorius et al., 2015).

Once phages reach the bloodstream and interact with the cells of the immune system (Wenger et al., 1978), they induce a cascade of cytokine production (Figure 1.13) (Van Belleghem et al., 2018). *In vitro* studies in human serum samples (Weber-Dabrowska et al., 2000), where blood samples from patients were tested for presence of IL-6 and TNF- α after phage-therapy for treatment of infections caused by drug-resistant bacteria, showed reduced levels of cytokine production after a long-term treatment (21 days). It was speculated that these results were most probably due to bacteriolytic effect of phages that resulted in release of LPS or other PAMPS from bacteria. On the other hand, some studies highlighted the anti-inflammatory effects of phages, that were not related to their antibacterial activity (Gorski et al., 2006; Zhang et al., 2018a, b).

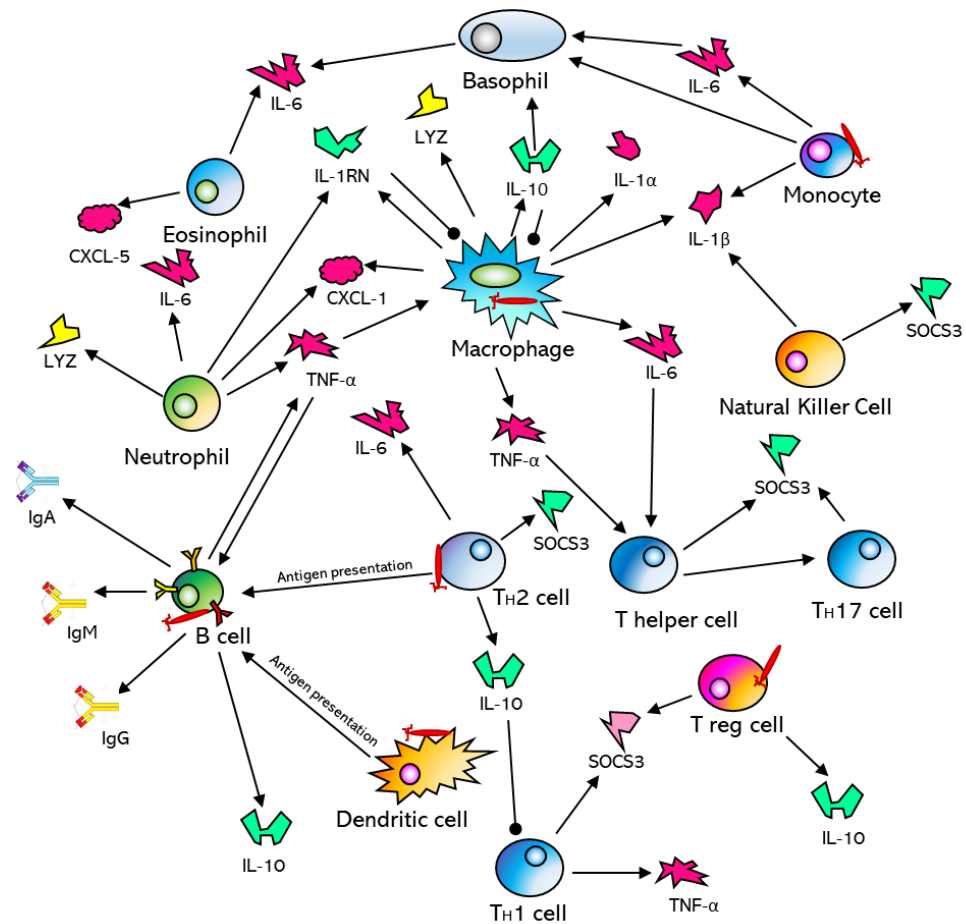


Figure 1.12. Interaction of bacteriophages with mammalian immune cells. Independent of the route of administration, phage (red rods) can enter the bloodstream and tissues and encounter immune cells in the blood. Phage could encounter these immune cells whilst they are bound to their bacterial host and taken up together by either macrophages or dendritic cells. Alternatively, these phages can directly interact with any of these immune cells by either interacting with cell surface molecules or receptors or taken up using a similar mechanism as observed with phage transcytosis. Once in contact with these immune cells, different pro- (pink) or anti-inflammatory (green) cytokines are induced, giving the phage the opportunity to influence the immune response. For example, the induction of IL1RN by the phage blocks the pro-inflammatory signals induced by IL1 α and IL1 β . Although it is known that phage can induce cytokine response, the precise cells responsible are currently not known. Furthermore, the uptake of phages by antigen presenting cells (APC; e.g., dendritic cells) leads to the activation of B cells and the production of specific antibodies against the phage. IL - interleukin; Ig - immunoglobulin; SOCS3 - suppressor of cytokine signalling; IL1RN - IL-1 receptor antagonist; CXCL1 - chemokine (C-X-C motif) ligand 1; TNF α - tumour necrosis factor α . Figure and legend adapted from (Van Bellegheem et al., 2018) with permission.

1.7 HYPOTHESIS AND AIMS OF THE RESEARCH

This thesis encompasses two major aims, featuring two medically relevant technological developments.

The first aim focuses on design of a vaccine based on filamentous phage as a carrier. This section is based on the hypothesis that *"Functionalised Ff phage displaying a model neoantigen in combination with fluorescently labelled α -GalCer can be used as an effective vaccine to elicit antigen-specific T cell responses"*. Objectives within the first aim were:

- a) Design and production of Ff-based vaccine displaying adjuvant molecule (α -GalCer-derived), and ovalbumin (OVA) as a model antigen (combined MHC I+II peptide).
- b) Assessment of the innate and adaptive immune responses *in vivo* in murine models.

The second aim is focused on development of Ff phage-derived nanoparticles and their use in diagnostic assays. This part of the thesis is based on the hypothesis that *"non-infectious filamentous phage-derived nanorods can be used in ultrasensitive diagnostic assays"*. Objectives within the second aim were:

- a) Design and establishment of protocols for production and purification of functionalised Ff-phage-derived short nanorods (named "BSFnano").
- b) Demonstration of a proof of concept ultra-sensitive lateral-flow-based assay using functionalised BSFnano particles.

Based on a large body of published work using orthogonally functionalised Ff, the full-length phage and BSFnano particles are promising candidates for development of immunoassays and immunotherapies. This thesis describes examples of the Ff and BSFnano functionalisation, production and applications in development of iNKT-recruiting vaccines and lateral flow diagnostic devices.

Chapter 2. MATERIAL AND METHODS

2.1 CHEMICALS, BUFFERS AND MEDIA

Agar

Bacteriological agar Acumedia® in powder form was purchased from Neogen (USA). Agar was added to nutrient media (1% final concentration) before autoclaving, then cooled to 50 °C and poured into Petri dishes under sterile conditions.

Agarose

Multipurpose agarose was purchased from Fisher Biotec, Australia. For agarose gels, 0.6 - 1.5% agarose was resuspended in 1× TAE buffer and heated in a microwave oven until dissolved, cooled to 50 °C and poured in appropriate gel chambers.

Alsever's Solution

D-glucose (20.5 g) (AnalaR, BDH), Na-citrate (7.9 g) (Sigma Aldrich), and NaCl (4.2 g) were dissolved in dH₂O and pH adjusted to 6.1 using 1 M citric acid (AnalaR, BDH). Water was added to the total volume of 1 L, and the buffer was stored at 4 °C until use. This saline solution prevents blood coagulation and stabilises the red blood cells (Rapoport, 1947).

Antibiotics

Antibiotics were purchased from GoldBio (USA) and Sigma-Aldrich (Australia). All antibiotics were dissolved in

sterile water and stored as 1000× stocks at -20 °C until use. Final concentrations of antibiotics in growth media were: 25 µg/mL for chloramphenicol (Cm), 50 µg/mL for kanamycin (Km), 60 µg/mL for ampicillin (Amp), and 25 µg/mL for tetracycline (Tet), unless otherwise stated.

Antibodies

Polyclonal antibodies specific to phage coat proteins pVIII (α -fd, F1, M13) and pIII, R164 (Rakonjac and Model, 1998) were donated from the Rockefeller University, New York, (USA). Monoclonal anti-pVIII antibody was purchased from Progen (Germany).

Monoclonal mouse antibodies for detection of displayed peptides, anti-FLAG (DYKDDDDK) was purchased from GeneScript (China); whereas antibody for detection of the combined MHCI/II OVA peptide (KISQAVHAAHAEINEAGRESIINEFKLTEWT) was custom made by ProteoGenix (France). Anti-fibronectin antibody was sourced from Sino Biological Inc. (China).

Secondary anti-mouse and anti-rabbit antibodies, conjugated to alkaline phosphatase (AP) or horseradish peroxidase (HRP), used for immunoblotting and ELISA assays were purchased from Sigma Aldrich, (USA).

Antibodies specific to murine cell-surface antigens, labelled with fluorescent dyes (Table 1) were either purified in-house at the Malaghan Institute for Medical Research, purchased from Biolegend, (USA), or Thermofisher, (USA).

Table 1. Antibodies used in murine models

Specificity	Fluorescent label	Supplier
CD44	BV711	Biolegend (cat# 103057, lot B264991)
CD8	BV421 FITC	Biolegend (cat# 100753, lot B235641) Biolegend (cat# 100706)
CD62L	Pe-Cy7	ThermoFisher (cat# 25-0621-81, lot E033434)
KLRG1	APC	Biolegend (cat# 561620, lot 7100981)
CD3	BV421 APC	Biolegend (cat# 562600, lot 6273589) Biolegend (cat#100312, lot B237984)
B220	BUV737 FITC	Biolegend (cat# 564449, lot B136876) Biolegend (cat# 103206, lot B247731)
CD4	PE	Biolegend (cat# 100408, lot B248731)
NK1.1	BV650	Biolegend (cat# 564143, lot 7048661)
CD69	Pe-Cy7	Biolegend (cat# 104512, lot B222011)
CD11c	APC	Biolegend (cat# 117510, lot B262130)

Azidohomoalanine

L-azidohomoalanine hydrochloride was purchased from Bachem (USA). The lyophilised powder was stored at -20 °C, and the stock solution was made fresh before use, by dissolving in water to a final concentration of 340 mM.

BCIP / NBT

SigmaFast™ BCIP®/NBT tablets were purchased from Sigma Aldrich (USA). One tablet dissolved in 10 mL water gives a buffered solution containing 10 mg of each 5-bromo-4-chloro-

3'-indolylphosphate and nitro-blue tetrazolium (BCIP/NBT), pH 9.5.

Blocking buffer for dipsticks

Odyssey® Blocking Buffer (1× PBS, 0.1% sodium azide) was purchased from Li-Cor Biosciences (USA), as a ready-to-use solution, and stored at 4 °C.

Blood lysis buffer (RBC lysis buffer)

Red blood cell (RBC) lysis buffer, was purchased from Qiagen (USA). This buffer leaves white blood cells intact while lysing the red blood cells.

CD1d-tetramer

CD1d-tetramer was sourced from NIH tetramer core facility, Emory University, Georgia, (USA).

Cell viability dyes

The cell viability was tested in dye exclusion assays (Thorntwaite and Leif, 1978) using Trypan blue, purchased from Gibco, Invitrogen (New Zealand). Trypan blue dye was stored at room temperature.

4,6-diamidino-2-phenylindole dihydrochloride (DAPI), which was purchased as a lyophilised powder from Invitrogen (New Zealand), and dissolved in MilliQ water. The solution was further diluted to a final stock concentration of 200 µg/mL in FACS buffer and stored in aliquots at 4 °C until use.

The Live/Dead® fixable blue (LDFB), cell staining kit, was purchased from Invitrogen, and stored at -20 °C. Working

solutions were prepared as per the manufacturer's instructions and stored at 4 °C for up to 6 weeks.

Complete Iscove's Modified Dulbecco's Medium (cIMDM)

Iscove's Modified Dulbecco's Medium (IMDM) was supplemented with 10% FCS, 2 mM Glutamax™, 10,000 U/mL penicillin and 100 µg/mL streptomycin, and stored at 4 °C.

DBCO-biotin

Biotin for click chemistry (dibenzyl-cyclooctyn-biotin, DBCO-biotin) was sourced from Click Chemistry Tools (USA) as a lyophilised powder. Upon reconstituting in DMSO to a final concentration of 5 M, the solution was dispensed into 6 - 7 µL aliquots in PCR tubes, and kept in the dark, in a zip-locked bag at -20 °C.

DIBAC-TAMRA dye

Fluorescent TAMRA dye, functionalized for click chemistry (dibenzyl-azacyclooctyn, DIBAC), was purchased as a lyophilised powder from Click Chemistry Tools, USA, and stored at -20 °C. Five-molar stock solution was prepared by dissolving the dye in DMSO. The solution was dispensed into 6 - 7 µL aliquots mini PCR tubes, and kept in the dark, in a zip-locked bag at -20 °C, to avoid degradation upon repeated thawing and light exposure.

Difco™ 2x YT (Yeast Extract Tryptone) Medium

Difco™ 2x YT from Becton, Dickinson and Co. Sparks (USA) was dissolved in water at 31 g/L and sterilised by autoclaving for 15 minutes at 121 °C before use.

Dimethyl sulfoxide (DMSO)

DMSO was purchased from Sigma Aldrich and stored at room temperature protected from light. To prevent the formation of ice crystals, 7 % DMSO was added to cells, phages and nanoparticles before storing the samples long term at -80 °C.

DNase I

DNase I was purchased from Roche (Germany) as a lyophilised powder, resuspended in water to a final concentration of 10 mg/mL, and stored in aliquots at -20 °C until use. Further dilutions were made in PBS.

Dulbecco's® Phosphate Saline Buffer (DPBS)

Sterile DPBS was purchased from Gibco, Thermo Fisher Scientific, and stored at room temperature and used under sterile conditions.

DyLight™ 550

Fluorescent dye for protein labelling, DyLight™ 550 NHS ester, was purchased in powder form from Thermo Fisher Scientific. After dissolving in dimethylformamide (DMF) to a final concentration of 1 mg/mL, 10 µL aliquots were stored at -20 °C.

Endotoxin detection kit

Limulus Amebocyte Lysate (LAL) kit was purchased from GeneScript and stored at 4 °C until use. The endotoxin standards were prepared as per the manufacturer's instructions and stored at -20 °C for no longer than 2 - 3

days. The LAL assay was used to detect lipopolysaccharides (LPS) in the vaccine samples (Harris and Feinstein, 1979).

Fluorescence-activated cell sorting (FACS) buffer

Cells for the fluorescence-activated cell sorting (Bonner et al., 1972) were resuspended in FACS buffer. The buffer was prepared from ethylene-diamine-tetra-acetic acid (EDTA), sodium-azide (NaN_3) purchased from Sigma Aldrich, and foetal bovine serum (FBS) sourced from Gibco, Invitrogen, by dissolving in 1× PBS to final concentrations of 1% EDTA, 0.01% NaN_3 and 2% FBS. The buffer was stored at 4 °C until use.

Glycerol

Glycerol (100%) was purchased from Sigma Aldrich, USA, and stored at room temperature. Stock solutions were made by dissolving in water to a final concentration of 60%. Stocks were sterilised by autoclaving and stored at 4 °C.

Gold nanoparticles

Streptavidin-conjugated gold nanoparticles (SAuNP) were purchased from Nanocs, Assay Matrix Pty Ltd., (Australia) and kept at -20 °C until used.

Iscove's Modified Dulbecco's Medium (IMDM)

Iscove's Modified Dulbecco's Medium (IMDM) was purchased in pre-sterilised bottles from Gibco, ThermoFisher Scientific, and stored at 4°C until use. This medium is suitable for high density cell cultures that are rapidly proliferating, and it represents a modification of Dulbeco's Modified Eagle

Medium (Eagle, 1971) by adding selenium, vitamins, amino acids and organic salts.

M9 minimal medium

Defined methionine-dropout minimal medium contained M9 salts (2.5 g/L NaCl, 15 g/L KH₂PO₄, 5 g/L NH₄Cl, and 33.9 g/L Na₂HPO₄) and was supplemented with glucose (1 g/L), thiamine (0.1%) and the following L- amino acids (µg/mL): phenylalanine (50), lysine (50), arginine (125), glycine (10), valine (35), alanine (42), tryptophan (20), threonine (35), serine (420), proline (230), asparagine (48), aspartic acid (52), glutamine (730), glutamic acid (935), tyrosine (18), isoleucine (40), leucine (40), histidine (50) and cysteine (50), as previously suggested in (Petrie, 2015).

Percoll solution

Percoll solution was freshly mixed prior to use: 15 mL Percoll from GE Healthcare Bio-Sciences AB (Sweden), 1 mL of Alserver's solution and 30 mL DPBS. Consisting of polyvinylpyrrolidone- (PVP) coated colloidal silica particles, this solution was used to ensure low viscosity and low density gradients when isolating cells (Liang et al., 1982).

Polyethylene glycol (PEG8000)

PEG8000 Fluka™, analytical grade powder, was purchased from Honeywell and stored at room temperature. Stock solutions were prepared in water, as 30% PEG800, 1 M NaCl, or 25% PEG800, 2.5 M NaCl, sterilised by autoclave, and stored at

room temperature until use for nanorod or phage precipitation (Sambrook and Russell, 2006).

Restriction enzymes

High-fidelity restriction enzymes, with reduced star activity, were used in cloning experiments (Sambrook and Russell, 2001). The restriction enzymes were purchased from New England Biolabs Inc. CutSmart® buffer (50 mM K-acetate, 20 mM Tris-acetate, 10 mM Mg-acetate, 100 µg/mL BSA, pH 7.9) was used for digests.

Ribonuclease A (RNase)

Lyophilised RNase type I-A from bovine pancreas was purchased from Sigma Aldrich, and stored at -20 °C.

Sodium chloride (NaCl)

NaCl was purchased from Sigma Aldrich (USA) and dissolved to 5 M solution in water. The stock solutions were autoclaved and stored at room temperature until used.

Sodium dodecyl sulphate (SDS)

SDS powder was purchased from Sigma Aldrich and stored at room temperature. The stock solution was prepared by dissolving in water to a final concentration of 10% (w/v).

Sodium Hydroxide (NaOH)

Sodium hydroxide pellets were purchased from Ajax FineChem (USA). Five-molar stock solution was made in water and stored at room temperature. NaOH was used to disassemble the phages (Sambrook and Russell, 2006).

Super Optimal broth with Catabolite repression (SOC)

Super Optimal broth (Sambrook and Russell, 2001) was prepared by dissolving MgSO₄ (4.8 g/L), yeast extract (5 g/L), tryptone (20 g/L), NaCl (0.5 g/L), KCl (0.2 g/L) and dextrose (3.6 g/L) in water. The solution was dispensed into 50 mL aliquots and sterilised by autoclaving. Stocks were kept at room temperature until used in sterile conditions.

TMB-ELISA reagent

TMB (3,3',5,5'-tetramethylbenzidine) soluble substrate for HRP detection (Olucha et al., 1985) was purchased from Thermo Fisher Scientific (USA) and stored at 4 °C.

Tris base

Tris base was purchased from GoldBio (USA). Stock solutions were prepared as 1 M, pH adjusted to 8.5, sterilised in autoclave and stored at room temperature until use.

Triton-X114

Triton X114, non-ionic detergent, was purchased from Sigma Aldrich and stored at room temperature until use for LPS removal from phage vaccine samples (Sartorius et al., 2018).

Tween® 20

Tween® 20 (polysorbate) was purchased from Prolab VWR (USA) and stored at room temperature until use in wash buffers for blots.

Urea

Urea was purchased from Pauling Industries (New Zealand). Six-molar urea was used in SDS-PAGE gels for pVIII protein for achieving effective separation of low molecular weights (Maniatis and Efstratiadis, 1980).

Water

Water used for this work was purified through two ion-exchange filters and two organic filters in a Barnstead NANOpure II system from Thermo Fisher Scientific.

2.2 *ESCHERICHIA COLI* STRAINS

All bacterial strains used in this work are derivatives of laboratory *Escherichia coli* strain K12 and are listed in Table 2. All *E. coli* strains were propagated at 37 °C in 2× YT liquid medium with continuous shaking at 200 rpm on an orbital shaker unless otherwise stated. The medium was supplemented with appropriate antibiotics (Section 2.1) as required. Long-term storage of all cultures was at -80 °C in 7% (v/v) DMSO, while cultures for short-term storage (1 - 2 weeks) were plated on 2× YT solid media supplemented with appropriate antibiotics when needed and stored at 4 °C.

Table 2. *E. coli* strains

Strain ID	Genotype	Reference
K561	<i>HfrC</i> λ^+ <i>relA1</i> <i>spoT1</i> T2 ^R (<i>ompF627</i> , <i>fadL701</i>), Δ <i>lacZ</i> , <i>lacI</i> ^q	The Rockefeller University Collection
K1030	<i>HfrC</i> , λ^- , S26 RIE, <i>fadL701</i> , <i>phoM510</i> , <i>mcrB</i> , <i>rrnB</i> <i>tonA22</i> , <i>garB10</i> , <i>ompF</i> , <i>relA1</i> , <i>pit10</i> , <i>spoT1</i> , T2R, <i>supD</i> <i>zed508::Tn10</i>	The Rockefeller University (Zinder-Model) collection
K2091	K561, <i>supD</i> , <i>zed508::Tn10</i>	(Sattar et al., 2015)
K2245	Δ (<i>araD-araB</i>)567, Δ <i>lacZ</i> 4787(<i>::rrnB-3</i>), λ^- , Δ <i>recO</i> 737, <i>rph-1</i> , Δ (<i>rhaD-rhaB</i>)568, <i>hsdR</i> 514; F'[: <i>Tn10 proAB</i> ⁺ <i>lacI</i> ^q Δ (<i>lacZ</i>)M15]	S. Kahnum, unpublished. Derivative of strain JW2549 (Baba et al., 2006).
JW3805-1	Δ (<i>araD-araB</i>)567, Δ <i>lacZ</i> 4787(<i>::rrnB-3</i>), λ^- , <i>rph-1</i> , Δ <i>metE</i> 774::Kan, Δ (<i>rhaD-rhaB</i>)568, <i>hsdR</i> 514	(Baba et al., 2006b)
K2449	K2091, Δ <i>metE</i> 774	This study

2.2.1 P1 Transduction

P1 transduction (Sternberg and Maurer, 1991) was used for generation of the *E. coli* methionine auxotroph strain. The donor strain was prepared from the Keio collection strain JW3805-1 (Table 2). The overnight culture (50 μ L) was diluted in 100 μ L of prewarmed 2 \times YT media supplemented with 10 mM CaCl₂ (2 \times YTC), and 50 μ L of the P1 phage master stock (10⁷ – 10⁸ pfu/mL) was added to a preheated (39 °C) flask

which was subsequently incubated for 5 - 10 min at 39 °C, without shaking to allow infection. Another 10 mL of pre-warmed YTC media was added, and cells were incubated for 4 - 6 h with continuous shaking at 200 rpm on an orbital shaker until lysis was observed. Several drops of chloroform were added and mixed using a vortex. The aqueous phase was centrifuged 10 min (6000 rpm SS34 / 4 °C) to remove the remaining cell debris, and the supernatant was filtered through a 0.45 µm filter and titrated on a 2× YT plate supplemented with 25 mg/L chloramphenicol and soft agar.

Recipient strain K2091 (Table 2) was prepared as an overnight culture in 2× YT at 37 °C. From this, 1 mL of cells were pelleted by centrifugation for 3 min at 10,000 rpm and washed twice in 1 mL of sterile 10 mM MgSO₄. The mixture containing 20 µL of the P1 lysate from the donor strain, and 100 µL of MgSO₄ (10 mM) was transferred into a 50 mL Falcon® tube and incubated at 39 °C for 10 min. Freshly prepared recipient cells (50 µL) were added, and the mixture was incubated for 10 min at 39 °C to permit the phage to adsorb to the cells, followed by the addition of 1 mL of pre-warmed 2× YT containing 10 mM Na-citrate. After incubating the mixture at 39 °C for 1 h, with aeration (200 rpm), the culture was centrifuged at 12,000 rpm for 2 min at room temperature. The pellet was washed twice in 10 mM MgSO₄ in equal volume as media and plated on the 2× YT plates containing 10 mM Na-citrate (YTC) and Km (50 µg/mL). Transductants were selected by overnight incubation at 39 °C, and lysogens were confirmed by plating dilutions on the YTC plates and incubating overnight at 30 °C. Transductants

were plated on 2× YT+ Km plates to obtain single colonies resistant to kanamycin.

To remove the Km^R marker from a selected colony, pCP20 transient transformation was used as described in (Baba et al., 2006b; Datsenko and Wanner, 2000). Briefly, in this method, plasmid pCP20 expresses Flp recombinase under a temperature-sensitive promoter pL and has a temperature-sensitive *ori* and an Amp^R marker. Once the plasmid is introduced into strains that carry the Keio collection Km cassettes, the specific open reading frame (ORF) is replaced and flanked by a sequence target of FRT recombinase, when incubated under pCP20 favourable conditions (30 °C).

2.3 MURINE MODELS

2.3.1 Maintenance and ethical approval

All experimental protocols for *in vivo* testing were approved by the Victoria University Animal Ethics Committee, (protocol reference: 23784 and 26384) and performed according to institutional guidelines. All mice were bred and housed in the Biomedical Research Unit of the Malaghan Institute of Medical Research, Wellington (New Zealand). The mouse diet contained meat-free rat and mouse rodent chow from Specialty Feeds (Western Australia) and acidified water, *ad libitum* while maintaining the 12-hour light/dark cycles. Gender and age-matched (6 - 10 weeks of age) mice were used for the immunisation experiments.

2.3.2 Murine strains

Original breeding pairs of the wild-type C57BL/6J mice were obtained from Jackson Laboratories, Bar Harbor (USA). These mice belong to the MHC haplotype subclass H-2b. The strains were maintained by mating between siblings.

OT-I transgene (derived from C57BL/6J) was provided by Frank Carbone from Melbourne University (Australia). This strain has the *Tcra-V2* and *Tcrb-V5* genes, which allow expression of a transgenic receptor for OVA₂₅₇₋₂₆₄ peptide. They produce CD8⁺ T cells that specifically recognise the OVA₂₅₇₋₂₆₄ peptide (OT-I cells) (Clarke et al., 2000; Hogquist et al., 1994).

2.4 GENERAL METHODS

2.4.1 Cloning

2.4.1.1 Plasmids and oligonucleotides

Oligonucleotides for PCR reactions and sequencing were purchased as a lyophilised powder from Integrated DNA Technologies Inc., IDT (USA). The stocks were made by dissolving in water to a final concentration of 10 mM, and stored at -20 °C. All the oligonucleotides and plasmids used in this study were designed *in silico* using Vector NTI® software, Thermo Fisher Scientific, and are listed in Table 3 and Table 4, respectively.

Table 3. Oligonucleotides

Name	Sequence ^a	Description
MR001	AAGGGAATTCATGAAGAAAAGCC TTGTTTTGAAG	pVIII from ATG + <i>EcoRI</i> Forward, T _m = 64 °C
MR002	AAAACCTGCAGCTATCAACTGGCT TTAGACGTAA	pVIII from GCT + <i>PstI</i> Reverse, T _m = 64 °C
rNano3:FnB F	TCCCGGCCCCAGCCGGCCGGAGGT CATGGACCGATTGTC	Amplification of p3:FnB from Rnano3:FnB; contains <i>SfiI</i> site; T _m =57.6 °C
rNano3:FnB R	TCCCGCGGCCCGCCTCGTTATCAA AGTGGAAGAAGCGT	Amplification of p3:FnB from Rnano3:FnB; contains <i>NotI</i> site; T _m =57.2 °C
JR436	CGTGAAAAAATTATTATTCGCAA TTC	Rnano3 forward sequencing primer (for sequencing of inserts, upstream of the MCS); T _m =66 °C
JR437	GAATTTTCTGTATGGGGTTTTC	Rnano3 reverse sequencing primer (for sequencing inserts, downstream of the MCS), T _m =66 °C, nt 1724-1702
metEfw	CAGTTCCGCAACGTTGTAG	Forward sequencing primer for $\Delta metE$ <i>E. coli</i> strain; (wt product ~2700 nt, $\Delta metE$ product ~500 nt).
metErev	ATTATCGTGTAACCGGACGC	Reverse sequencing primer for $\Delta metE$ <i>E. coli</i> strain; (wt product ~2700 nt, $\Delta metE$ product ~500 nt).
JR418	CGACATCATAACGGTTCTGGCAA	Forward sequencing <i>tac</i> promotor, for OVA and FLAG inserts in pGZ119EH
flas1	TCTTCTCTCATCCGCCAAAACAG C	Primer for sequencing downstream of gene IV

^a Underlined nucleotides refer to the restriction site stated in the third column.

Table 4. Plasmids

Name*	Description	Marker	Source
Helper plasmids			
pRnano3	Helper plasmid, derived from helper phage Rnano3 (R778; (Sattar et al., 2015), $\Delta(f1ori)$; ::pA15 <i>ori</i> , Km ^R), with multiple cloning site in gIII (<i>gIII::MCS</i>).	Km ^R	J. Zhou and J. Rakonjac, unpublished
pRnano3FnBP	Helper plasmid, derived from helper phage Rnano3 (R778; (Sattar et al., 2015), $\Delta(f1ori)$; ::pA15 <i>ori</i> , Km ^R), with multiple cloning site in gIII, displaying fibronectin-binding peptide (FnBP) fused to the N-terminus of mature pIII (<i>gIII::FnB</i>).	Km ^R	This study
p8Gly4	pRnano3 encoding Gly quartet fused to the N-terminus of the mature portion of pVIII (<i>gVIII 2^{am}::nGGGG</i> , S17L).	Km ^R	S. Bisset and J. Rakonjac, unpublished
p8Gly4FnBP	Helper plasmid p8Gly4 displaying fibronectin-binding peptide (FnBP) fused to the N-terminus of mature pIII (<i>gIII::FnB</i>).	Km ^R	This study
pHAS1	Helper plasmid pRnano3 containing mutations in <i>gVIII 2^{am}</i> , A9M, S17L, M28L, and deletion of N-domain in pIII (<i>gIIIC::MCS 3Cys</i>).	Km ^R	This study
pHAS8	Helper plasmid pRnano3 containing mutations in <i>gVIII -20^{am}</i> , A9M, S17L, M28L and deletion of N-domain in pIII (<i>gIIIC::MCS 3Cys</i>).	Km ^R	This study
pRnano38	Helper plasmid pRnano3 containing mutations in <i>gVIII -20^{am}</i> , A9M, S17L, M28L with multiple cloning site in gIII (<i>gIII::MCS</i>).	Km ^R	This study
Template plasmids			
pUC118	Phagemid vector, pUC <i>ori</i> , <i>f1ori</i> .	Amp ^R	(Vieira and Messing, 1987)
pBSF736	Plasmid resulting in replication and packaging of 736 nt ssDNA in the presence of Ff helper phage or helper plasmid.	Amp ^R	Rakonjac lab, unpublished
pBSF719	Plasmid resulting in replication and packaging of 719 nt ssDNA in the presence of Ff helper phage or helper plasmid.	Amp ^R	This study

pBSF529	Plasmid resulting in replication and packaging of 529 nt ssDNA in the presence of Ff helper phage or helper plasmid.	Amp ^R	This study
pVIII fusion plasmids			
pGZ119EH	An expression vector containing <i>tac</i> promoter and <i>colD ori</i> .	Cm ^R	(Lessl et al., 1992)
p8FLAG	Control plasmid for the mosaic display of FLAG-tag (DYKDDDDK) on wild-type pVIII expressed from the pGZ119EH vector.	Cm ^R	This study
pF1	Control plasmid pGZ119EH for the mosaic display of FLAG-tag (DYKDDDDK) on pVIII mutant containing an amber mutation in the signal sequence (-20 ^{am}) and suitable for azidohomoalanine incorporation without interference with assembly, (A9M, S17L, M28L).	Cm ^R	This study
p8OVA	Control plasmid for the mosaic display of OVA antigenic peptide KISQAVHAAHAEINEAGRESIINEFKLTEWT on wild-type pVIII expressed from the pGZ119EH vector.	Cm ^R	This study
pO1	Control plasmid pGZ119EH for the mosaic display of OVA peptide KISQAVHAAHAEINEAGRESIINEFKLTEWT on pVIII mutant containing an amber mutation in the signal sequence (-20 ^{am}) and suitable for azidohomoalanine incorporation without interference with assembly, (A9M, S17L, M28L).	Cm ^R	This study

2.4.1.2 Preparation of chemically competent cells

Competent cells were prepared as previously described (Sambrook and Russell, 2001). Briefly, an overnight culture was diluted 100x in 2x YT medium and incubated at 37 °C with shaking at 200 rpm until OD₆₀₀ reached 0.15 - 0.2. The culture was then cooled on ice for 30 min, and cells were harvested by centrifugation at 4 °C / 4000x g for 10 min. The resulting cell pellet was washed twice in a sterile solution of 100 mM CaCl₂ (pre-cooled to 4 °C), followed by resuspension in

a solution of 100 mM CaCl_2 and 10% glycerol. The final resuspension was dispensed into pre-cooled tubes (50 μL per tube). These cells were stored long-term at $-80\text{ }^\circ\text{C}$ until use for heat-shock transformation.

2.4.1.3 Preparation of electro-competent cells

An overnight culture was diluted 100x in 500 mL of 2x YT medium and incubated at $37\text{ }^\circ\text{C}$ with shaking at 200 rpm until OD_{600} reached 0.5 - 0.6. The culture was chilled for 30 min on ice in pre-cooled centrifuge bottles. Cells were pelleted by centrifugation at $4\text{ }^\circ\text{C}$ / 4000x g for 20 min. The supernatant was discarded, and the cells were resuspended in 500 mL of chilled sterile 10% glycerol. Centrifugation was repeated, and the cells were washed two more times in 500 mL of cold 10% glycerol. The final pellet was resuspended in an equal volume of glycerol and dispensed into 50 μL aliquots in pre-chilled tubes. Cells prepared in this way were stored long-term at $-80\text{ }^\circ\text{C}$ until use in transformation via electroporation.

2.4.1.4 Polymerase Chain Reactions (PCR)

Recombinant DNA techniques were used as described in (Sambrook and Russell, 2001). For PCR amplifications of DNA fragments used in cloning experiments, a proofreading PrimeSTAR High-fidelity DNA polymerase from Takara (Japan) was used. For all other PCR amplifications, Taq DNA polymerase was used. Each reaction mixture was set up on ice, in a total volume of 50 μL , containing 0.3 μM forward

and reverse primers (Table 3), 1 U polymerase, 1× amplification buffer, 25 ng template DNA, 0.3 mM dNTP mix, and PCR-grade water. Negative controls without the enzyme, or template, were both prepared for each amplification reaction. PCR products were purified from residual reagents using High Pure PCR Product Purification Kit, purchased from Roche.

2.4.1.5 Restriction endonuclease reactions

Plasmids and PCR products were incubated with appropriate enzymes and buffer according to the manufacturers' instructions. For cloning purposes, reactions were incubated overnight.

2.4.1.6 Ligation

A 3:1 molar ratio of insert to vector backbone was used per ligation. One U of T4 DNA ligase in T4 ligase ATP-buffer, purchased from Roche, was added in a total volume of 10 µL per reaction and incubated overnight at 16 °C (Sambrook and Russell, 2001).

2.4.1.7 Transformation by heat shock

The procedure for heat shock transformation used in this study is described in (Sambrook and Russell, 2001). Briefly, 25 ng DNA was added to 50 µL of chemically competent cells prepared as described in Section 2.4.1.2 and incubated on ice for 45 minutes. Cells were then exposed to 42 °C for 90

seconds and recovered on ice for 5 min. Nutrient-rich SOC medium was added up to 1 mL, and the transformed cells were left to recover for 1 h at 37 °C with continuous shaking at 200 rpm. Dilutions were plated on appropriate medium for selection of colonies and transformation efficiency (TE) was calculated as the number of transformed cells per µg DNA, using the formula:

$$TE = \frac{\text{Number of colonies} \cdot \text{dilution}}{\text{ng DNA used}} \cdot \frac{V_{total}}{V_{plated}}$$

2.4.1.8 Transformation by electroporation

Electro-competent cells prepared as described in Section 2.4.1.3 were transformed by electroporation of DNA into the cells when the high-efficiency transformation was required; chiefly in the nanorod production experiments. Briefly, 100 - 300 ng of the nanorod-production template plasmid pBSF529, or pBSF719 DNA was added to 50 µL of electrocompetent cells containing a helper plasmid. The cells were then transferred into pre-chilled 0.2 cm BioRad cuvettes using a Pasteur pipette, and pulsed at 2.5 kV (12.5 kV/cm) in a BioRad gene pulsar. SOC medium was added up to 1 mL, and cells were incubated at 37 °C for one hour with shaking at 200 rpm. Transformation efficiency was calculated in the same way as for the chemical transformation, as stated in Section 2.4.1.7.

2.4.1.9 Plasmid purification

Small scale purification of plasmids from 1.5 - 3 mL of the overnight culture was performed using High Pure Plasmid Isolation Miniprep Kit, purchased from Invitrogen, Thermo Fisher Scientific, according to the manufacturer's instructions. The midiprep kit from Invitrogen was used for large-scale DNA purifications from 100 - 200 mL of overnight cultures, according to the manufacturer's instructions.

2.4.1.10 DNA sequencing

The DNA sequences of all constructed recombinant plasmids and phages were confirmed by Sanger DNA sequencing at The Massey University Genome Service, Massey University, Palmerston North. The primers used for Sanger sequencing of are listed in Table 3.

2.4.2 Electrophoresis

2.4.2.1 Agarose gel DNA electrophoresis

Agarose gels (0.6% to 1.5% w/v), were prepared in 1× TAE buffer (40 mM Tris base, 20 mM acetic acid, 1 mM EDTA, pH 8.3), depending on the size of observed DNA fragments. One kb⁺ DNA ladder (100 ng) was loaded in one lane of each gel as a DNA size marker. Electrophoresis of DNA gels was carried out at 60 - 80 V for 1 - 2 h, followed by staining in ethidium bromide (EtBr) (10 µg/mL in 1× TAE, pH 8.3) for 20 min, and rinsing in water before imaging (Boffey, 1985).

All gels were visualised with the GelDoc XR gel documentation system and software, BioRad (USA).

2.4.2.2 SDS-PAGE and western blot

Proteins were analysed by SDS-PAGE (Laemmli, 1970; Ornstein, 1964; Tulchin et al., 1976). Samples were boiled for five minutes in 1× SDS-PAGE sample buffer (125 mM Tris-HCl, pH 6.8, 35% glycerol, 2.5% SDS, 0.025% BPB), before loading in the gel. To detect fusions with pIII coat protein, a 10% polyacrylamide gel was used, while for analysing the proteins displayed on pVIII a 16% polyacrylamide gel containing 6 M urea was used. The protein bands in polyacrylamide gels were visualised by staining overnight at room temperature in Coomassie blue. For more sensitive detection Pierce™ Silver Stain from Thermo Fisher was used, according to the manufacturer's instructions.

For immunoblotting of proteins, after separating them in SDS-PAGE, the proteins were transferred to nitrocellulose membrane (BioRad, 0.3 A, 45 min, on ice). The membrane was blocked with TBSTM buffer (30 mM Tris, 150 mM NaCl, pH 8.0, 0.05% Tween20, 5% skim milk), then incubated with the appropriate primary antibody, listed in Section 2.1, diluted 1:2,000 in TBSTM for 1 hour at 37 °C. The membranes were washed 5 times in 25 mL TBST and incubated with the appropriate secondary antibodies (1:10,000) overnight at 4 °C, or two hours at room temperature. When AP-conjugated antibodies were used, the membrane was washed 4 times in TBST and stained in alkaline phosphatase solution (NBT/BCIP

in Tris pH 9.5 buffer) (Section 2.1) before imaging on the GelDoc XR. The HRP-conjugated antibodies were visualised using enhanced chemiluminescence (ECL), Pierce™ ECL Western Blotting Substrate (Thermo Fisher Scientific) and imaged on the Azure c600, Custom Science (Australia).

2.4.2.1 Native phage agarose gels

Agarose gel electrophoresis was used for rapid detection and characterisation of native phages and phage-derived nanorods. Gels were prepared at 0.8 % agarose (w/v) in TAE buffer (pH 9.0). This pH was used instead of the standard 8.3 because the latter matches the isoelectric point of the Ff phages and nanorod variants containing serine instead of glutamic acid at position 2 in mature pVIII, used in this work. Samples of undiluted, 10-fold, and 100-fold diluted particles were mixed with 4× DNA loading dye (2% glycerol, 4× TAE, 10 mg/mL BPB), before loading the gel. Gel electrophoresis was carried out for 15 h at 20 V (1.5 V/cm) and stained in ethidium bromide (10 µg/mL EtBr, 1× TAE, pH 8.3) for 20 min to visualise free DNA and RNA in the sample. The native, intact particles should not be visible at this stage, since their DNA is inside the intact particle. To visualise the particles, the gel had to be soaked in 0.2 M NaOH for 45 min, to disassemble the protein structures and free the encapsulated DNA. After rinsing in water for 10 min, the gel was neutralised by soaking in 0.45 mM Tris (pH 7.1) and stained again in EtBr for another 20 min, followed by rinsing in water and imaging in GelDoc XR system.

2.4.2.2 Agarose gel electrophoresis of disassembled phages and phage-derived nanorods

Gels contained 0.8% to 1.2% (w/v) agarose (depending on the size of analysed ssDNA) in 1× TAE buffer, pH 8.3. Particles were disassembled by mixing with SDS buffer (1% SDS, 1× TAE, 5% glycerol, 0.25% BPB) and heating at 99 °C for 10-15 min. After equilibration to room temperature, the samples were loaded onto an agarose gel. Electrophoresis was carried out for 150 min at 3.7 V/cm; the gel was stained in EtBr for 20 min, followed by rinsing, and visualised with the GelDoc XR.

2.5 PHAGE AND NANOROD PURIFICATION AND QUANTIFICATION

Standard methods for phage production are described below. Improvements in method developments for Ff phages and nanoparticles are described in Section 3.2.2 and Section 5.2.2, respectively.

2.5.1 CsCl gradient ultracentrifugation

Caesium chloride gradient centrifugation was used to separate the phages from fine cellular debris that coprecipitated with PEG in the first step of phage precipitation from the supernatant of the producing culture (Rossomando and Zinder, 1968). About 1 mL of 1000-fold concentrated particles in 1× PBS buffer were mixed with 2 mL of 1× PBS buffer containing 1.5 g solid CsCl, mixed to homogenise and the volume was adjusted to 4 mL with 1× PBS,

to obtain a final CsCl concentration of 0.375 g/mL. Ultracentrifugation at 100,000× g at 18 °C for 16 h resulted in the formation of a density gradient. Depending on the amount of Ff phages or derived nanorods, they were either visible as a grey band or were not visually detectable. In both cases the particles were collected using a 25-gauge needle. When a visible band was observed, the tube was punctured just underneath the band. When a band was not visible, the centrifuge tubes were punctured at the bottom, and 100 µL (4 drops) fractions were collected in pre-labelled 1.7 mL Eppendorf tubes, as described (Sambrook and Russell, 2001).

The fractions were analysed by agarose gel electrophoresis of SDS-disassembled particles to detect the fractions that contained particles (Section 2.4.2.2). The fractions that contained the strongest Ff-derived DNA band, and no residual RNA and DNA, were combined and dialysed against 3,000 volumes of 1× PBS buffer at 4 °C for 24 hours (changing the buffer twice, after 2 and 6 hours), using 10 kDa cut-off Slide-a-Lyzer™ dialysis cassettes, purchased from Thermo Fisher Scientific.

2.5.2 LPS removal and LAL test

Limulus Amebocyte Lysate (LAL) assay was used for endotoxin detection in samples (Harris and Feinstein, 1979). The LAL kit was purchased from GenScript (USA). The reagents were prepared with LPS-free dH₂O, according to manufacturer's instructions, and stored at 4 °C for up to one week. The LPS

standard was prepared as 1 EU/mL stock in LPS-free dH₂O and stored at -20 °C for no longer than 5 days. Serial dilutions of the standard were prepared fresh for every assay.

Briefly, 100 µL of dilutions from purified vaccine samples were mixed with 100 µL of reconstituted LAL reagent and incubated at 37 °C for 40 min. A 100 µL aliquot of the chromogenic substrate was added and incubated for another 6 min at the same temperature, followed by adding 500 µL of the first colour stabiliser while swirling gently to avoid foaming. The same volumes of other colour stabilisers were added as directed by the manufacturer's instructions. The final solution was mixed well and transferred to a 96-well plate (100 µL per well, 2 wells for every sample dilution). The absorbance was measured at 545 nm wavelength and plotted as EU/mL = f(A₅₄₅) graph for the standard curves (Appendix 7.3.2).

2.5.3 Quantification of phages and phage-derived nanorods by densitometry

The phage vaccine particles were quantified by titration using an overlay plating method. A 100 µL aliquot of overnight *E. coli* K2091 (Table 2) culture of host bacteria was mixed with 3 mL of molten (50 °C) 2× YT soft agar (0.5%) and poured over the top of the 2× YT plate. Once the overlay had solidified, 5 µL of serial 100-fold dilutions of phage samples were spotted on the plate and left to dry. The plates were incubated at 37 °C overnight, and the following day zones of turbidity were counted as a single plaque-forming

units (pfu) (Kropinski et al., 2009). The titres were expressed as pfu per mL.

Ff-derived nanorods that do not carry any markers were quantified by densitometry of SDS-released ssDNA after separation by agarose gel electrophoresis (Rakonjac and Model, 1998). Each quantification gel was loaded with a series of known amounts of purified ssDNA to obtain a standard curve for densitometry. Images of EtBr-stained gels were analysed using ImageJ software (National Institutes of Health) and Microsoft Excel.

2.5.4 Fluorescent labelling

A fluorescent dye, DyLight™ 550 NHS ester (Section 2.1) was used for labelling the nanorods. Aliquots of BSF nano particles were diluted in 0.05 M Na-borate buffer (pH 8.5). The amount of dye for labelling was calculated using the formula (provided by the manufacturer):

$$\begin{aligned} \frac{mg_{protein}}{Mw_{protein}} \cdot F \cdot Mw_{dye} &= mg_{dye} & mg_{dye} \cdot \frac{V_{solvent}}{mg_{dye \text{ in } V}} \\ &= V_{dye \text{ solution}} \left(10 \frac{mg}{mL} \right) \end{aligned}$$

$Mw_{protein}$ - molecular weight in g/mol (for pVIII = $5.26 \cdot 10^3$ g/mol)

Mw_{dye} - molecular weight of dye (for DyLight 550 = 1,040 g/mol)

F - molar fold excess, if protein < 5 mg/mL, then F = 1-15; if protein \geq 5 mg/mL, then F = 8)

V_{solvent} - the volume of solvent that contains mg dye ($V=100$ μL)

$\text{mg}_{\text{dye in } V}$ - the amount of dye dissolved in V volume of solvent (1 mg)

The reaction was carried out for one hour at room temperature. The unbound dye was removed by dialysis using 10 kDa cut-off Slide-A-Lyzer™ dialysis cassettes in 3,000 volumes of 1× PBS buffer at 4 °C, changing the buffer twice as described before. The efficiency of labelling was examined by comparing the absorbance of samples at 280 nm and 557 nm. Labelled particles were analysed by native agarose gel electrophoresis and detected using the Azure c600 image analyser in red-green-blue (RGB) mode.

2.5.5 Microscopy of Ff phages and nanorods

2.5.5.1 Negative Staining Grid Preparation for TEM

All transmission electron microscopy images (micrographs) were collected by Jordan Taylor at the Manawatu Microscopy and Imaging Centre (MMIC), School of Fundamental Sciences, Massey University, Manawatū Campus. Purified phage or nanoparticle samples were diluted in RO water to a final concentration of 10^{10} pfu/mL. An 80 μL drop of the sample was placed in a glass Petri dish lined with Parafilm™ (Bemis Company Inc., USA). A formvar/carbon-coated 200 mesh copper grid (Agar Scientific, coated in the lab) with the film side facing down, onto the sample droplet and left for 4 minutes

to allow adsorption of phages onto the grid. The grid was carefully lifted and placed on the side of Whatman No1 filter paper to remove excess liquid.

The film with the adsorbed phages was placed on a drop of 2% uranyl acetate in MilliQ water and left for 4 min at room temperature to stain. Excess fluid was drained again, and the film was placed onto Whatman No1 paper to dry. Images were collected in TEM at 100 kV, FEI Tecnai G2 Spirit BioTWIN (Czech Republic).

2.5.5.2 On-grid gold labelling of Ff phage

Dilutions of biotinylated phages were made to 10^{10} pfu/mL in water. A carbon-coated grid was floated on the droplet of phage sample for 4 min, and excess liquid was drained on filter paper, as described above. The grid was washed by floating on the drop of water for 30 sec, then drained and blocked on a droplet of 0.02% BSA for 1 min. The washing step was repeated, and finally, phages were labelled with 0.01% streptavidin-gold nanoparticles, SA-AuNPs (5 nm) for 1 min, then drained again and stained with 2% uranyl acetate for 4 min.

2.6 IMMUNOLOGY METHODS AND VACCINE TRIALS

Phage-based vaccine samples were prepared in 1.1 – 1.2 mL aliquots and sent from Massey University, Palmerston North to the Malaghan Institute for Medical Research in Wellington (the MPI approval is listed in Appendix 7.1). All the *in*

vivo and *in vitro* experiments were performed with Kathryn Ferrand, at the Malaghan Institute of Medical Research. My contribution here was in designing and planning of the experiments and data analysis, while Kathryn Farrand handled the live animals and performed flow cytometry analyses.

2.6.1 Vaccination and tissue processing

2.6.1.1 Intravenous vaccination

Phage-based vaccines, conjugate-vaccine positive control, and negative DPBS buffer control were administered intravenously in 200 μ L volumes per mouse, using five mice per group. To inject the mice into the lateral tail vein, firstly they were warmed using a heat lamp, then placed into restrainers.

2.6.1.2 Blood

To assess activation of NKT cells in serum, six hours after the immunisation 6 - 8 blood drops were collected from the submandibular vein of live mice, using a 4 mm Goldenrod Animal Lancet. Microtubes (1.5 mL) containing 200 μ L of 10 mM EDTA/PBS were used for collecting the blood samples. The cells from the serum were pelleted at 420x g for 4 min, and the supernatant was removed. Pelleted cells were resuspended in 1 mL RBC lysis buffer (Material and Methods, Section 2.1) and incubated for 20 min at 37 °C with 5% CO₂. Lymphocytes were pelleted by centrifugation at 450x g, for 4 min,

supernatant was removed, and the pellet was resuspended in 200 μ L FACS buffer and aliquoted in a U-shaped 96-well plate for staining.

2.6.1.3 Spleen

Spleens from euthanised mice were collected into 24-well plates containing ice-cold IMDM, then mechanically dissociated through a 70 μ m cell strainer, while washing through with 15 mL IMDM in Falcon® tubes. Cells were pelleted at 400 \times g for 5 min at 4 °C and resuspended in 1 mL RBC lysis buffer (Section 2.1) and incubated for 5 min. The cells were then pelleted and resuspended in 1 mL FACS buffer for flow cytometry, or cIMDM (Section 2.1) for cell culture. Cells for counting were dispensed into a 96-well plate, kept on ice and processed as described in Section 2.6.1.5.

2.6.1.4 Liver

Intra-cardiac perfusion of the liver was performed on euthanised mice, with 5 - 10 mL PBS. The livers were cut out and placed into 24-well plate containing PBS, kept on ice. The livers were then mashed through a 70 μ m cell strainer, using the hard tip of the syringe plunger, while washing through with 50 mL of PBS, into Falcon® tubes, followed by centrifugation at 322 \times g for 10 min. The supernatant was removed by vacuum aspiration, and the pellet was resuspended in 46 mL of 33% Percoll solution, then centrifuged at 572 \times g for another 10 min at room temperature, without a centrifugal brake applied. The supernatant was removed, and

the cells were resuspended in 1 mL RBC lysis buffer, incubated at 37 °C for 5 min and centrifuged for 4 min at 894x g. The final pellet was resuspended in 2 mL of FACS buffer and prepared for flow cytometry analysis.

2.6.1.5 Viable cell count

Viable cells from single-cell suspensions (10 µL) of processed organs were stained with 1:20 dilution of trypan blue (190 µL) (Section 2.1). From this mixture, 10 µL was loaded onto a haemocytometer, where the live cells were identified as bright white cells, and the dark blue coloured cells were identified as dead cells (Thorntwaite and Leif, 1978). The total cell number was calculated using the formula:

$$N_{total} = N_{av1/9} \cdot 10^4 \cdot \text{dilution factor} \cdot V_{total}$$

N_{total} - total number of cells

$N_{av1/9}$ - the average number of cells counted in 1/9th of the field

V_{total} - the total volume of cell suspension

2.6.2 Flow cytometry data acquisition and analysis

Data for the individual particle analysis were acquired using a BD LSR-II flow cytometer, Beckton-Dickinson (USA). Parameters for identification of live cells were their forward scatter (FSC), and side scatter (SSC), which depends

on the cell size and shape (Thompson et al., 1985). The unlabelled cells were used to adjust the channel voltage. Single-labelled cells, with a single antibody or dye and CompBeads, were used for compensations in overlap signal from fluorophores (Szaloki and Goda, 2015). Gating strategies (Staats et al., 2019) will be presented in the Results (Section 4.2).

The cells were labelled for 10 min at room temperature with the same antibodies used in the experiment, at a 10-fold lower dilution than the concentrations used for labelling of the cells. If a combination of many different fluorophores was causing a rise in background signal, or if positive populations were hard to identify, fluorescence minus one (FMO) controls were used for gating. Cell samples were stained with all antibodies from the panel, except the one of interest.

2.6.2.1 CD8⁺ T cell responses ex vivo

Peripheral blood samples were collected from the submandibular vein of immunised mice, and leukocytes were stained with H-2Kb-OVA₂₅₇₋₂₆₄ pentamer-peptide complex. Pentamer 50 tests R-PE labelled Pro5 MHC, Cat#F2A-G, were sourced from Proimmune, Oxford (UK).

2.6.2.2 NKT markers surface staining

Single-cell suspensions were prepared as described in Section 2.6.1. The cells were washed and resuspended in FACS buffer prior to being dispensed into 96-well U-shaped bottom

plates. Thereafter cell pellets were collected by centrifugation at 2,500× g, for 2 min and the supernatant was discarded. FACS buffer (50 µL) containing 2.4G2 Fc-blocking reagent (prepared from the supernatant of 2.4G2 hybridoma cells) was applied for 10 min at 4 °C to prevent non-specific Fc-mediated binding to antibodies. The cells were washed twice with FACS buffer, and the supernatant removed the same way as described. The cells for fixing with live/dead fixable blue (1:1,000), needed to be washed for an additional 15 min at room temperature with PBS. After discarding the supernatant, cells were washed again with FACS buffer (150 µL), then resuspended in 50 µL of the mixture of surface antibodies (Table 1) in FACS buffer. The cells were resuspended in 4% paraformaldehyde (100 µL) and incubated at 4 °C for 30 min, followed by two washing steps in 200 µL of FACS buffer. Cells that are fixed in this way can be stored for 2 - 3 days at 4 °C, before analysing by flow cytometry.

2.6.3 Software used for data analysis

FlowJo software, version 10.5.3, Treestar Inc. (USA) was used for the analysis of flow cytometry standard (FCS) data. Microsoft Excel and GraphPad Prism™ for Mac OS X, GraphPad Software (USA) were used to create tables and graphs and for statistical analysis. FSC-A v FSC-W and SSC-A v SSC-W profiles were used for pre-gating the single live cells in example flow plots.

2.6.3.1 Statistical analysis

The statistical significance of data presented in figures and graphs is reported in tables as $p < 0.05$. The data were analysed using Prism™ 8.0 software. The graphs show the mean values and standard deviation (SD). For a single parameter in multiple groups, one-way ANOVA was used. To correct the errors from multiple groups comparisons, Tukey's post-test was used (Appendix 7.4).

2.7 DIAGNOSTIC ASSAYS USING FF-DERIVED PARTICLES

2.7.1 Dot blot

Membranes for dot-blot assay were prepared by placing a pair of 1 μ L dots, each containing 1 μ g of a capture reagent: collagen (test dot), anti-F1 phage monoclonal antibody (control dot). BSFnano particles bound to the membrane were detected using rabbit anti-Fd phage antibody, followed by the biotinylated anti-rabbit Ab and finally streptavidin-AP conjugate. The membranes were developed in alkaline phosphatase resolving buffer, as described earlier (Section 2.4.2.2).

Particles displaying FnBP (BSF.Gly₄.FnBP) or particles without displayed FnB (BSF.Gly₄) were mixed with a solution of analyte fibronectin (Fn) dissolved in PBS, or PBS only, as a negative control. Before soaking the membrane in the mixture, it was blocked for 2 h at room temperature with

PBSTM (1× PBS, 0.1% Tween, 5% skim milk) and dried for 1 h at 37 °C.

2.7.2 ELISA

In previous research (Sattar et al., 2015), the enzyme-linked immunosorbent assay (ELISA) (Harlow and Lane, 1999) was adapted for Ff-derived particles and used to confirm if the nanoparticles displayed the fusion proteins. In this study, ELISA was used for qualitative and quantitative analysis of functionalised BSFnano and Ff particles.

2.7.2.1 Qualitative ELISA for detection of fibronectin-binding peptide displayed on BSF nanorods

The FnBP-pIII fusion was confirmed by qualitative ELISA assay, as described earlier in Sattar et al. (2015). Nunc Immuno MaxiSorp™ 96-well microtiter plates (Sigma Aldrich, Denmark), were coated overnight at 4 °C with 100 µL of analyte, human plasma fibronectin (Sigma Aldrich) in Na-bicarbonate buffer, pH 9.5. The wells were washed twice with 200 µL 1× PBST buffer (PBS containing 0.05% Tween 20) and blocked for 1 h at room temperature with 300 µL of PBSTM (PBST + 5% skim milk), to minimise the unspecific binding of nanoparticles.

After rinsing the wells with PBST, a total of 10^8 nanoparticles were added to each well in a final volume of 100 µL, and incubated at room temperature for 1 h. Nanoparticles in the test group had the fibronectin-binding

peptide (FnBP) displayed on pIII, while nanorods from the control group had a full length pIII protein without the peptide fusion. After allowing the particles to attach to the analyte, the wells were washed 5 times with 300 μ L of PBST, to remove the unbound nanorods. To detect the bound functionalised nanorods, a pVIII-specific antibody (mouse anti-pVIII, or rabbit anti-fd, Section 2.1) was used in 1:500 dilution in PBSTM, incubated for 1 h at 37 °C. The wells were washed 5 times with 300 μ L PBST, followed by addition of the secondary antibody (HRP-conjugated anti-mouse, or anti-rabbit antibody, Section 2.1) in 1:10,000 dilution in PBSTM. After incubating the plate for another hour at 37 °C, the wells were washed 7 times with PBST before adding 100 μ L of 1-Step™ Turbo TMB-ELISA reagent (Section 2.1). After a 30 min of ELISA reagent incubation at room temperature, the reaction was stopped by adding an equal volume of 0.5 M H₂SO₄. The absorbance was detected at a wavelength of 450 nm.

2.7.2.2 ELISA assay for OVA-pVIII quantification

To detect and quantify OVA peptide displayed on Ff particles containing a mixture of "neat" pVIII and OVA-pVIII fusions, a somewhat unconventional ELISA assay was performed.

Briefly, Nunc Immuno MaxiSorp™ 96-well microtiter plates were coated by serial dilutions of synthetic OVA peptide (identical to the one displayed on the phage) that served as quantification standard. Each dilution was applied in

duplicate. Wells on the same plate were coated with the samples of Ff phage displaying the OVA peptide (Ff.OVA).

Coating was performed at room temperature for 1 h, followed by blocking with PBSTM at room temperature for 1 h. The OVA peptide in all wells was detected by adding a primary antibody, custom-raised against this specific OVA peptide (ProteoGenix, France) (Section 2.1) at 1:500 dilution in PBSTM. The plate was incubated for 1 h at 37 °C. After washing the unbound antibody five times with 1× PBST, the secondary HRP-conjugated antibody was added. The incubation of the secondary antibody, washing and detection using TMB-ELISA reagent, was performed using the same protocol as described in the previous section.

The standard curve was plotted based on quantification of the signal from OVA peptide dilutions $A_{450}=f(C_{OVA})$ and it served to quantify OVA peptide in the Ff.OVA-coated wells on the same plate (Appendix 7.3.5). It is important to note that even though the signal was very low for the OVA detection, it was consistent and reproducible.

Ideally, quantification by sandwich ELISA (Nakamura et al., 2007; Parker, 1998) would have been used in this study to monitor the amount of displayed. However, due to the availability of only one antibody that detects the OVA (MHC I+II) peptide used in this study, it was not possible to include a capture antibody in the assay. Further explanation for choosing this method can be found in Section 3.2.2.1.

2.7.3 Fibronectin dipstick assay

Previously prepared dipsticks (containing printed C and T lines), as described in (Sattar et al., 2015) were stored in the zip-lock bags, protected from light. Before use, dipsticks were blocked overnight at 4 °C in Odyssey® blocking buffer supplemented with 1:1,500 monoclonal anti-Fn antibody (Section 2.1) to minimise the unspecific binding of FnBP-displaying nanorods to potentially Fn-contaminated collagen on the T line, which would result in the false-positive signal. The 96-well microtiter plate that was used for the reaction mixtures was blocked with the same buffer without the antibody, under the same conditions. After blocking, the dipsticks were rinsed twice with PBST buffer and dried for 2 hours at 37 °C.

A total of 10^{11} particles per assay were mixed with serial dilutions of analyte in 1× PBS, in a total volume of 50 µL, in a 96-well plate and incubated at room temperature for 30 min.

Dried blocked dipsticks were dipped into the wells containing the reaction mixtures for 15 min at room temperature, then taken out of the wells and placed on the filter paper to dry at 37 °C for 1 h. Unlabelled BSFnano particles bound to the dipstick were visualised using anti-pVIII antibodies (Material and Methods, Section 2.1), followed by secondary AP-conjugated antibodies, using the same method as described in the western blotting (Section 2.4.2.2). Fluorescently labelled particles (DyLight® 550) were directly visualised using the Azure c600 fluoroimager.

The intensity of the signal from the T and C lines was quantified using ImageJ software.

Chapter 3. DESIGN OF FILAMENTOUS PHAGE-BASED VACCINE FOR IMMUNOTHERAPY

3.1 INTRODUCTION

This chapter describes design and production of vaccine particles, derived from a filamentous bacteriophages (Ff), for use as vaccines to stimulate T cell-mediated immune responses. In comparison to published work on nanoparticles used in immunotherapy (Kalkanidis et al., 2006), the novelty of this particular Ff-based vaccine design is that it allows independent control of the covalently attached antigenic peptides and glycolipid adjuvant molecules per particle.

The system for production of the vaccine is composed of a modified Ff phage, accessory plasmid, and a specific *E. coli* strain. Herein are the details of the Ff phage modifications and construction of the *E. coli* strain, as well as details of the plasmids. The plasmid used in this research was designed for expression of a translational fusion between the major coat protein pVIII and a peptide from a model protein antigen, ovalbumin (OVA), where a defined MHC I-binding sequence was adjoined to a defined MHC II-binding sequence. Specific modifications described in the following sections allowed to produce vaccine particles that were functionalised *in vivo*, with azide “handles” for attachment of α -GalCer as an adjuvant by “click” chemistry, while containing a high copy number of recombinantly expressed antigenic peptides. The levels of antigen and adjuvant

attached to the particles were quantified, and the amounts of each were subsequently optimised to achieve a high antigen to adjuvant ratio. A purification protocol for obtaining endotoxin-free particles was established.

3.1.1 Aim and objectives

The experiments described in this chapter were performed to optimise design, production and purification of novel phage vaccine for stimulating T cells, as well as to characterise the main features of the Ff-vaccine. The overall aim was to get the highest achievable ratio of antigen to adjuvant molecules on a single phage particle.

Antigenic OVA peptide (ISQAVHAAHAEINEAGRESIINEFKLTEWT), was combined with an analogue of the NKT cell-stimulating immune adjuvant α -GalCer that has been labelled with the fluorescent tag boron-dipyrromethene (BODIPY) and which also has a linker attached to facilitate "click" chemistry to the phage CI270A adjuvant [6-(BODIPY-COCH₂-S)-m α GC-PAB-CV-BCN] (for more details on the adjuvant molecule please refer to Appendix 7.2.1). In this thesis, this modified adjuvant molecule is referred to as BODIPY- α -GalCer.

Specific objectives were to:

- Design a production system for high-copy number display of OVA-pVIII fusions along the filamentous phage that at the same time display the azides for covalent attachment of the adjuvant.

- Optimise incorporation of the OVA-pVIII fusion into the particles.
- Optimise incorporation of an unnatural amino acid that contains an N_3 group (azidohomoalanine) into the particle, for chemical attachment of adjuvant molecules along the phage filament.
- Characterise and optimise the click-chemistry-mediated attachment, initially using the fluorescent dye (DIBAC-TAMRA) and streptavidin-gold nanoparticles (SA-AuNP), and then to use this information to attach fluorescently labelled glycolipid adjuvant, BODIPY- α -GalCer.
- Produce vaccine particles and purify from endotoxins for use in murine models for *in vivo* testing.

3.2 RESULTS

3.2.1 Design and construction of a new system for production of an improved Ff-based vaccine

The system for production was composed of a phage designed for the incorporation of an azide handle for adjuvant attachment, a plasmid required for expression of recombinant antigen-coat protein fusion, and a suitable host strain. All three components were constructed and tested prior to vaccine production, with the goal to make the vaccine particle as schematically presented in Figure 3.1.

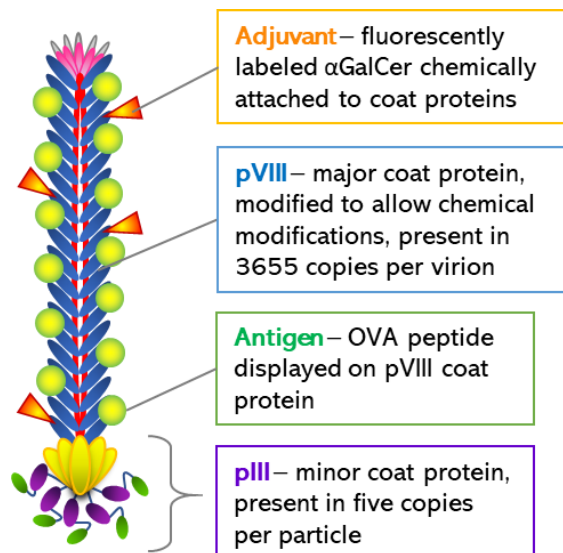


Figure 3.1. Schematic presentation of the vaccine particle design.

Symbols: gray ovals, protein pVII; pink ovals, protein pIX; blue ovals, major coat protein pVIII; yellow ovals, C domain of pIII; purple ovals, N2 domain of pIII; green ovals, N1 domain of pIII; orange triangles, adjuvant molecules BODIPY- α -GalCer; green circles, antigenic peptide model OVA.

3.2.1.1 Construction of an *Ff* phage mutant for azide display on the coat proteins

Firstly, azide groups had to be introduced into major coat protein pVIII to allow the attachment of BODIPY- α -GalCer to phage particles. *In vivo* incorporation of the unnatural amino acid azidohomoalanine, a methionine analogue that carries an $-N_3$ group, into *E. coli* proteins has been reported previously (Kiick et al., 2002). An *Ff* pVIII mutant that allows optimal azide display without disruption of the virion was described previously (Petrie, 2015). In this research, the method from Petrie and colleagues was adapted to fit the desired features of the vaccine particles, as described above.

The published work showed that incorporation of azidohomoalanine at the methionine residue of the wild-type pVIII (at position 28) (further explained in Section 3.2.1.3), not only fails to display the azide on the surface of the virion but also results in an unstable particle. This is because methionine in position 28 is within the hydrophobic helix portion of pVIII that forms the virion via hydrophobic interactions. Introducing a mutation that converts the methionine codon into leucine (M28L) prevents destabilisation once the azidohomoalanine is incorporated into the virion (Petrie, 2015). To allow the display of azides on the surface of the virion, a methionine has to be introduced, and this was accomplished by replacing alanine 9 of the mature protein with methionine (A9M) (Figure 3.2). The pVIII mutant generated for use in labelling is, therefore, pVIII A9M, M28L (Table 4).

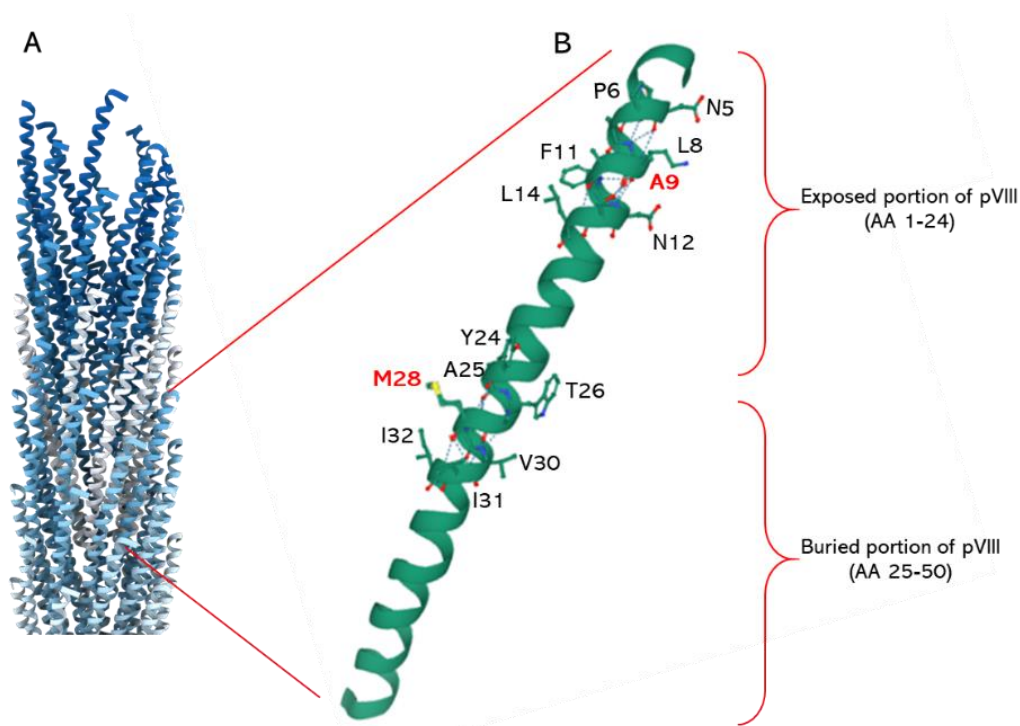


Figure 3.2. Molecular structure of major coat protein pVIII.

A. The structure of fd bacteriophage; **B.** The structure of a single pVIII subunit. Positions A9 and M28 indicating in red were replaced by M and L, respectively, in the phage R783, to allow incorporation of Aha at the position of ATG codons without compromising the virion assembly. Structures are based on PDB coordinates 1IFJ (A) and 2IFO (B); (Marvin et al., 2006)

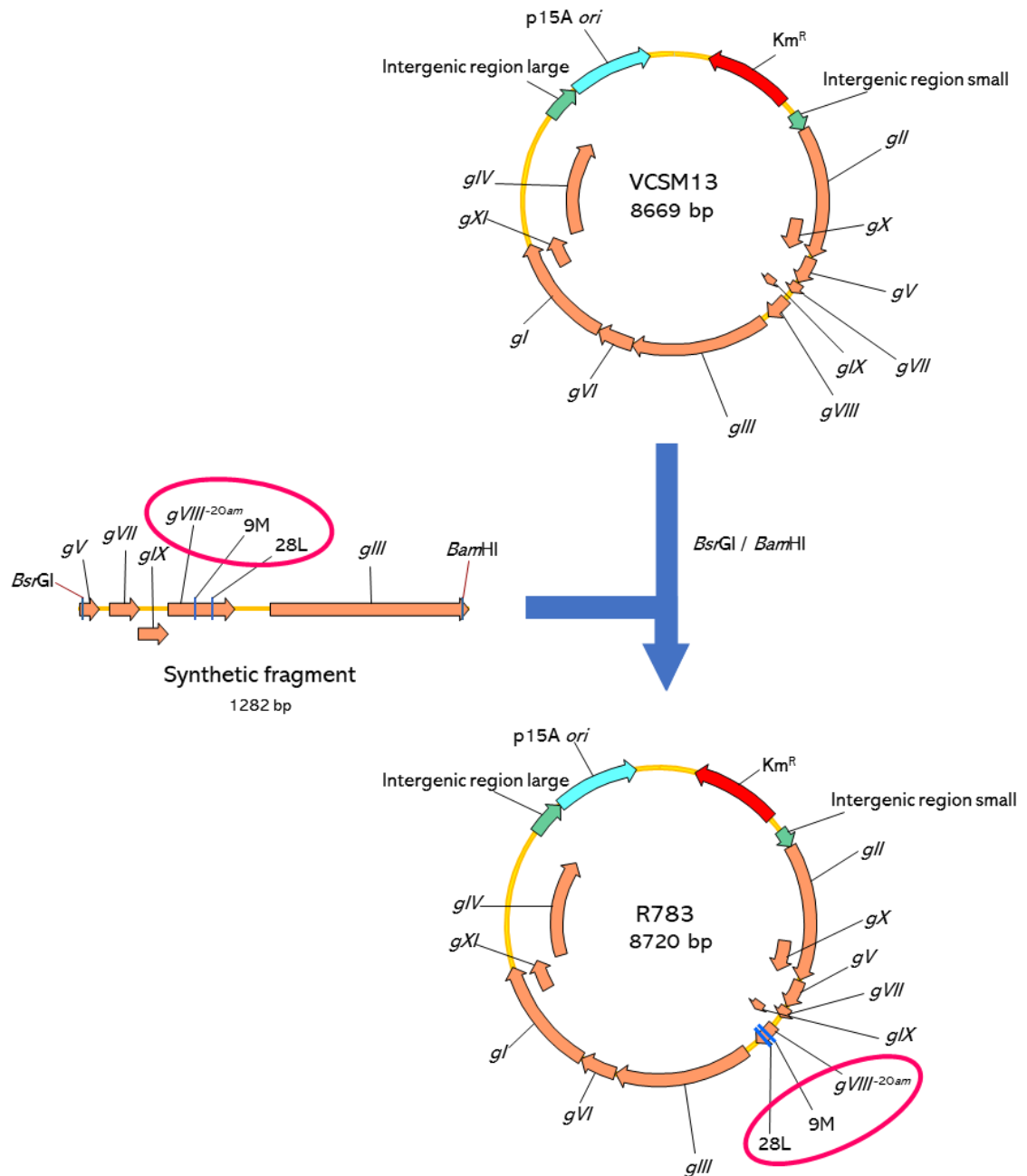


Figure 3.3. Construction of R783 phage strain.

The mutant phage R783 was constructed from a synthetic insert containing the mutations for azidohomoalanine incorporation (A9M, M28L), and an *amber* mutation in the signal sequence of the nascent pVIII (*gVIII-20am*) by cloning the insert into the phage VCSM13 at *BsrGI/BamHI* cut sites

(Figure 3.3). The role of *amber* mutation will be further explained in Section 5.2.1.

3.2.1.2 Plasmid design for expression of OVA-pVIII fusion

The Ff vaccine was designed to display an OVA peptide containing linked MHC class I and class II epitopes that bind the MHC molecules H2-K^b and I-A^d respectively, which are expressed in the C57BL/6J mouse strain to be used in the vaccine study (Material and Methods, Section 2.3.2). The OVA sequence used was 30 residues long: ISQAVHAAHAEINEAGRESIINEFKLTEWT (Table 5). Recombinant pVIII fusions displaying peptides longer than ten residues on every pVIII subunit prevents phage assembly (Iannolo et al., 1997). However, they can co-assemble into the virion in combination with the wild-type-length pVIII when both are expressed in the same cell (Figure 3.1). Therefore, to allow assembly of the 30-residue fusions of pVIII into an Ff virion, a plasmid expressing recombinant OVA-pVIII fusion protein was constructed and introduced into the host cells before infection with the phage, allowing assembly of “mosaic” particles.

The peptide fusion was driven by the *tac* promoter (Figure 3.4A), which is a hybrid of *trp* and *lac* promoters. This hybrid promoter is stronger than each *trp* and *lac* promoter, resulting, respectively, in a 3- and 11-fold increase in the transcript in comparison to the original promoters (de Boer et al., 1983). The peptide synthesis is induced by IPTG supplementation in growth media, as the *lac* repressor

controls the expression of the *tac*-promoter-driven genes. In addition to the inserts encoding the FLAG or OVA peptide fused to pVIII, the synthetic constructs also carried the *gVIII* mutations A9M, and M28L, necessary to match the phage-R783-encoded *gVIII* (Section 3.2.1.1, Figure 3.3). The *amber* mutation in *gVIII* was introduced to prevent toxicity during the cloning steps (Sattar et al., 2015). Table 5 shows the sequences of pVIII fusions.

Table 5. Amino acid sequences of phage pVIII fusions.

Strain	pVIII seq ^a	M _w (kDa)	#AA
wt Ff	MKK*LVLKASVAVATLVPMLSFAAEGDDPAKMAFDLQALATEYIGYAWAMVVVIVGATIGIKLFKKFTSKAS*	5.26	50
R783	MKK*LVLKASVAVATLVPMLSFAAEGDDPAKMAFDLQALATEYIGYAWAMVVVIVGATIGIKLFKKFTSKAS*	5.31	50
R783.OVA	MKK*LVLKASVAVATLVPMLSFAAISQAVHAAHAEINEAGRESIINFELTEWTGGAFRMAFDLQALATEYIGYAWAMVVVIVGATIGIKLFKKFTSKAS**	8.43	78
R783.FLAG	MKK*LVLKASVAVATLVPMLSFAADYKDDDDKGGGAKMAFDLQALATEYIGYAWAMVVVIVGATIGIKLFKKFTSKAS**	6.02	57

^aResidues in grey belong to the signal sequence of pVIII protein; mature protein is in black letters; green sequences are peptides fused to N-terminus of mature pVIII; red letters represent the flexible linkers between displayed peptide and pVIII protein; blue letters represent cut sites for cleaving the peptide from pVIII protein. Highlighted in yellow are mutations for chemical modifications of phage, as described in Section 3.2.1.1. Molecular weights and numbers of amino acids in mature pVIII proteins are listed in the third and fourth column, respectively.

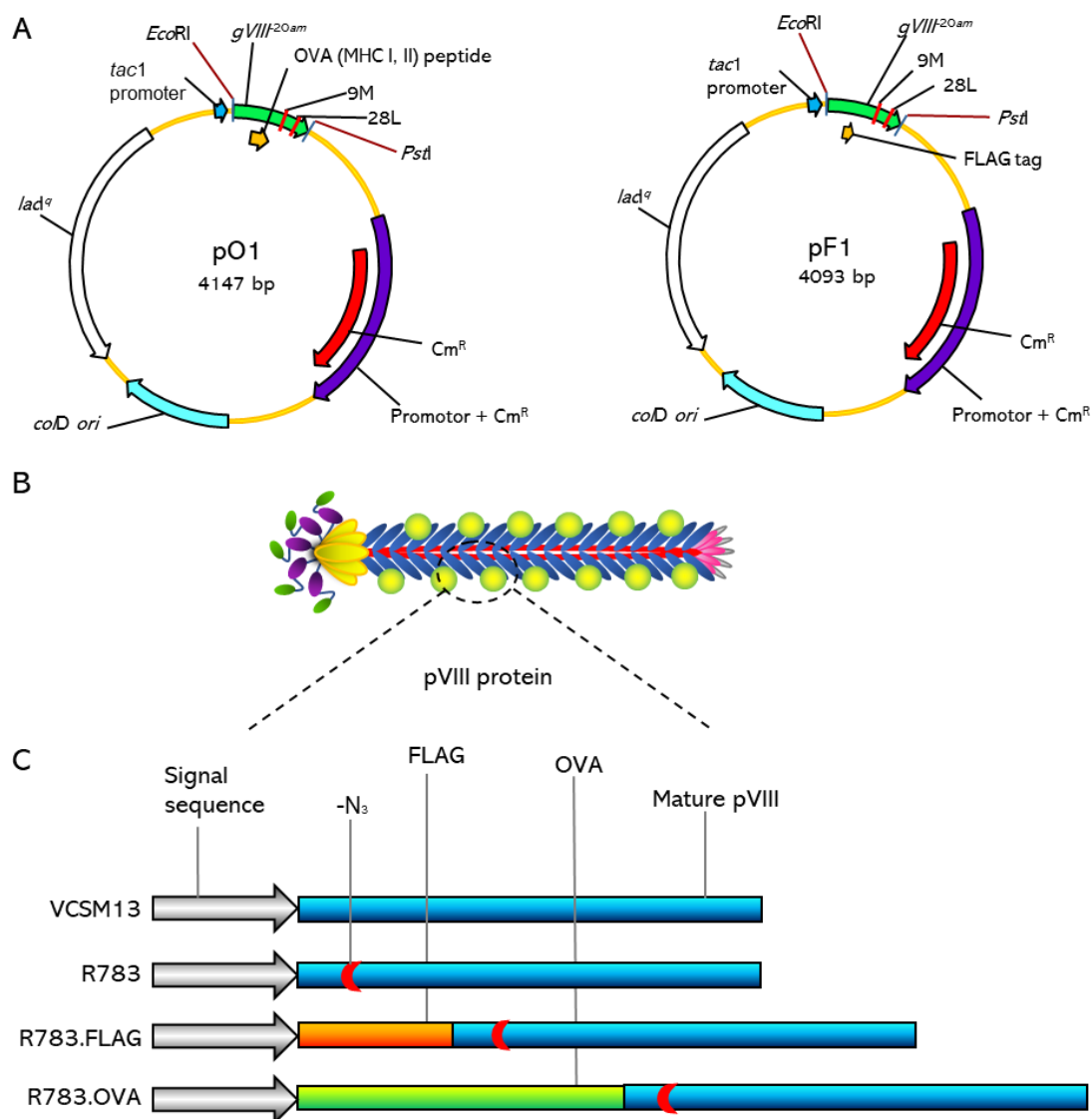


Figure 3.4. Schematic presentation of OVA peptide and FLAG-tag fusions. **A**, pO1 and pF1 plasmids expressing, respectively, OVA-peptide-pVIII and FLAG-tag-pVIII fusions. **B**, Schematic representation of the filamentous phage particles displaying peptide-pVIII protein fusions (R783.FLAG or R783.OVA). **C**, Comparison of the pVIII proteins of wild type Ff phage protein pVIII (VCSM13), mutant phage pVIII modified for click chemistry (R783), FLAG-tag-pVIII fusion and OVA-peptide-pVIII fusion. **Symbols**: grey arrows, signal sequences of pVIII; blue rectangles, mature pVIII protein; orange rectangle, FLAG-tag peptide; green rectangle, OVA antigen peptide; red husks, azide groups in mature pVIII protein as handles for modifications via click chemistry.

DNA sequences encoding OVA-pVIII fusion, and a control FLAG tag-pVIII (Table 4), were custom-synthesised. These

synthetic inserts were cloned into *EcoRI* and *PstI* sites of expression vector pGZ119EH and named pO1 and pF1, respectively (Figure 3.4A). The recombinants were identified by double digestion using *EcoRI* and *PstI* restriction endonucleases (Figure 3.5B).

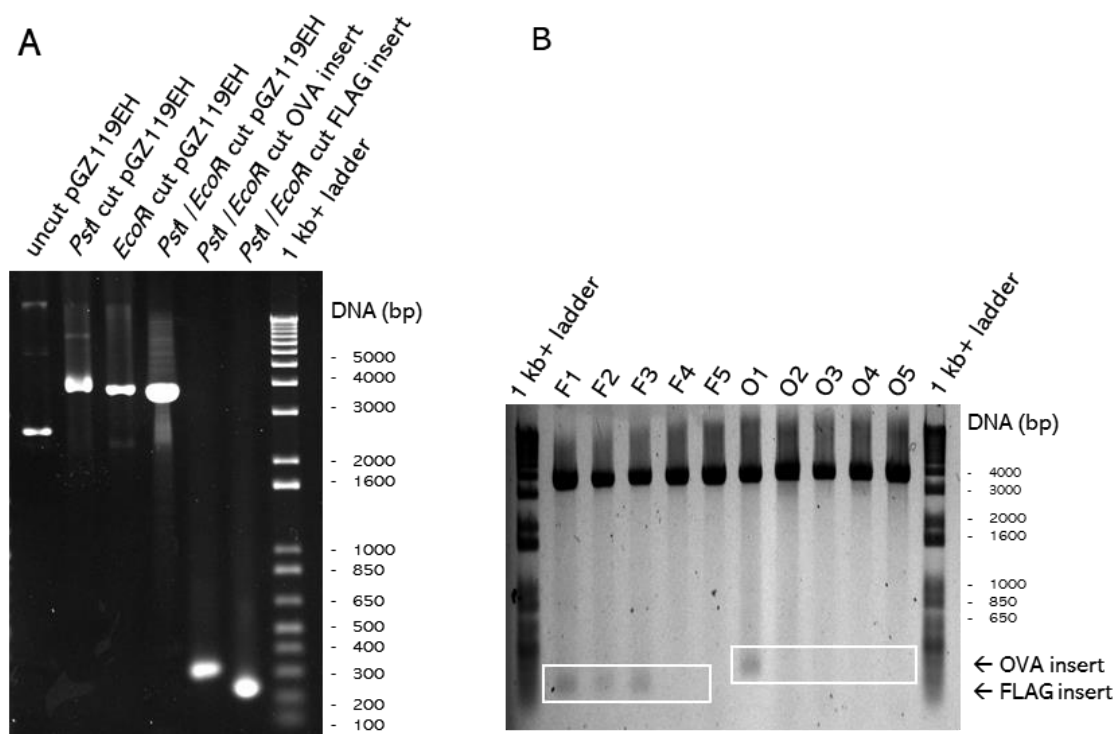


Figure 3.5. Agarose gel analysis of the cloning steps of the pVIII fusion constructs.

A, Vector pGZ119EH (Table 4) and synthetic inserts containing OVA-pVIII and FLAG-pVIII fusion were cut using *PstI* and *EcoRI* restriction enzymes; **B**, *PstI*/*EcoRI* restriction enzyme digests identification of recombinant plasmids that contain the OVA-pVIII and FLAG-pVIII inserts. Lanes: F1-F5, FLAG-pVIII candidate clones; O1-O5, OVA-pVIII candidate clones. The linear dsDNA ladder 1kb+ (Life Technologies) was used as a standard.

3.2.1.3 *E. coli* host strain for production of Ff-based vaccine

To produce azide-functionalised Ff particles using R783 phage, it was essential to construct an *E. coli* strain in which the cellular concentration of methionine can be

manipulated. The Ff-producing strain had to be transformed into a methionine auxotroph, a strain that cannot synthesise methionine on its own, hence the concentration of this amino acid is controlled by the availability of methionine in the growth medium. Varying the concentration of methionine, and its ratio to the unnatural amino acid azidohomoalanine (Figure 3.6) in the minimal medium, it is possible to gauge the intracellular concentrations of these two amino acids. Consequently, this allows the incorporation of azidohomoalanine into the phages during its assembly, to achieve the desired frequency of the azides displayed on phage coat proteins.

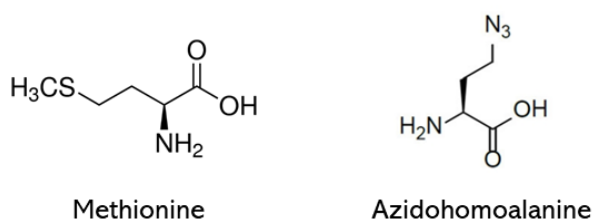


Figure 3.6. Structural formulas of methionine and azidohomoalanine.

Methionine is synthesised in *E. coli* from homoserine (Figure 3.7), which in turn is synthesised from aspartate by two successive reductions of the side chain carboxyl group (Blanco et al., 2003). Methionine auxotrophy, without affecting other amino acid synthesis pathways, can be achieved by introducing a null mutation in the gene encoding the enzyme that catalyses the final step in this biosynthesis pathway. However, there is redundancy in this step in that *E. coli* has two genes, *metE*, and *metH*, which

encode two enzymes that catalyse S-methylation of homocysteine to methionine (Caspi et al., 2014).

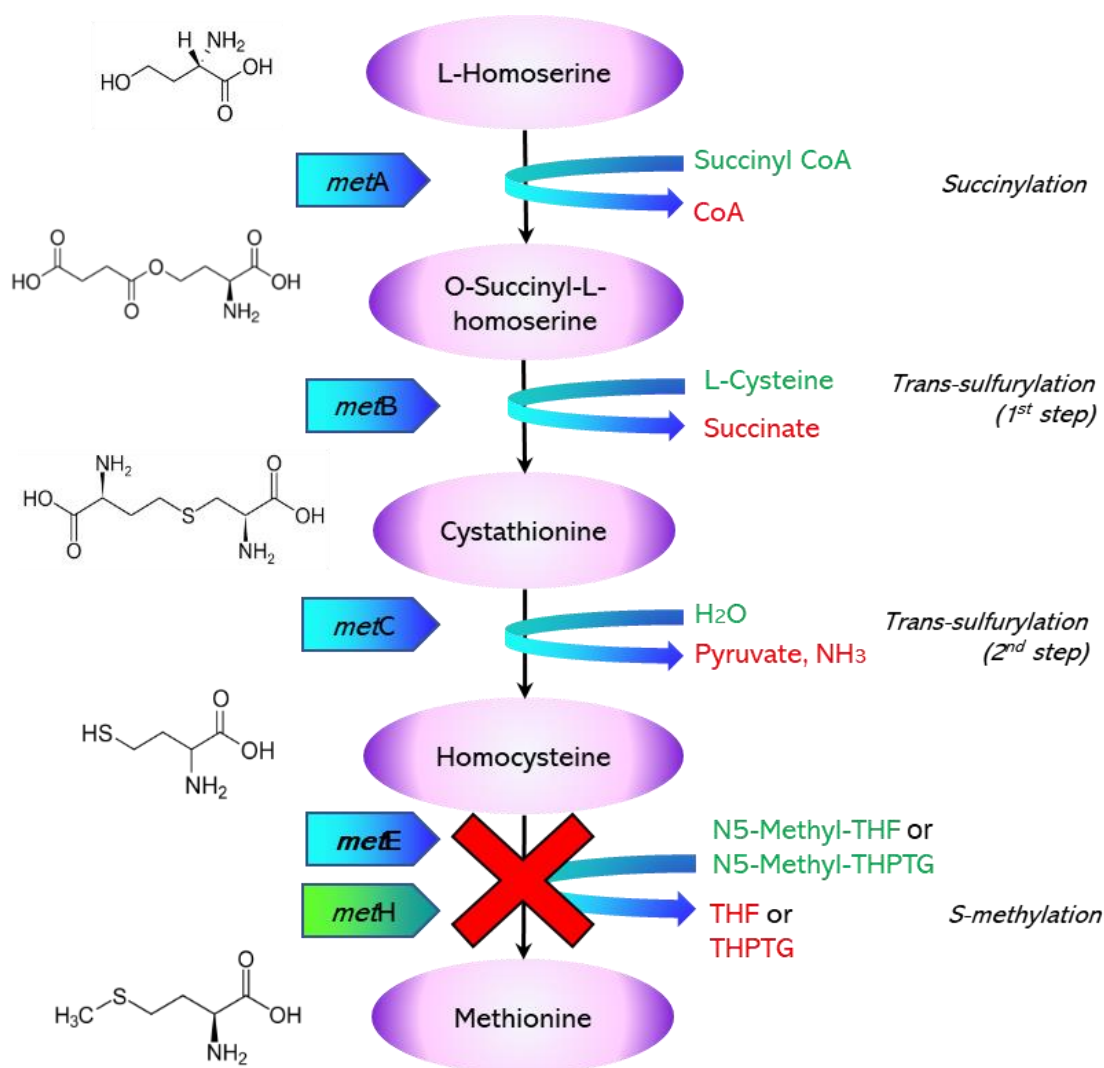


Figure 3.7. Methionine biosynthesis pathway in *E. coli*.

Blue shapes with writing represent essential genes; green shape with writing represents a non-essential gene. The red cross marks the point of introduced knock-out mutation from strain JW3805-1 into K2091. Purple ovals present the main reaction products, with molecular formulas shown on the left side. Writings in green represent molecules going into biochemical reaction; writings in red represent by-products of a chemical reaction. For simplicity, black arrows represent the flow of the methionine biosynthesis pathway; blue arrows represent individual reactions noted in italic on the right side of the scheme. Figure adapted from (Matthews and Hondorp, 2013).

This redundancy would typically mean that both genes would have to be mutated to gain methionine auxotrophic strain. *MetH*, however, requires B₁₂ (cobalamin) supplementation for function (Weissbach and Brot, 1991), in minimal medium, hence a strain with deletion of the *metE* gene is a conditional methionine auxotroph in this medium (in the absence of vitamin B₁₂). Intracellular methionine concentration in a $\Delta metE$ mutant can, therefore, be controlled by varying its concentration in the media.

To construct the methionine auxotrophic strain, a $\Delta metE774::Kan$ knock-out mutation was introduced into strain K2091 by P1 (generalised) transduction from a donor strain, JW3805-1 of the *E. coli* knock-out collection [Table 2; (Baba et al., 2006b)]. The strain of choice for the phage production was K2091 (Table 2) which contains a *lacI^q* mutation, permitting tight control of the *lac* promoter used to drive the expression of various constructs, as described in Section 3.2.1. Another relevant allele is *supD*, which suppresses the *amber* stop codon in pVIII (Hoffman and Wilhelm, 1970). Phage with *amber* mutation in their genome can only replicate in hosts that carry a suppressor gene for that particular mutation (e.g., *supD* for *amber*). The *supD* mutation in the host strain is required to suppress an *amber* stop codon by inserting a serine residue.

After isolating and clonally purifying the transductants, the Km^R marker (flanked by two *FRT* sites) was removed using the cognate FLP recombinase expressed from a temperature-sensitive promoter pL in pCP20 plasmid (Cherepanov and

Wackernagel, 1995), as described in Section 2.2.1, and the new strain was named K2449. The deletion of *metE* gene in the new strain was confirmed by sequencing, using primers metEfw and metErev (Table 3).

3.2.1.4 Optimising the conditions for azidohomoalanine incorporation into the phage

To efficiently incorporate the azidohomoalanine into phage, it is essential to use a methionine concentration that will allow bacterial growth and phage production, but not to provide an excess of methionine, so that azidohomoalanine is utilised for the synthesis of phage proteins. To determine the dependence of *E. coli* K2449 growth in different methionine concentrations, a dose-response growth experiment was carried out in a methionine “dropout” medium (M9MM, Section 2.1), at a series of increasing methionine concentrations (Figure 3.8).

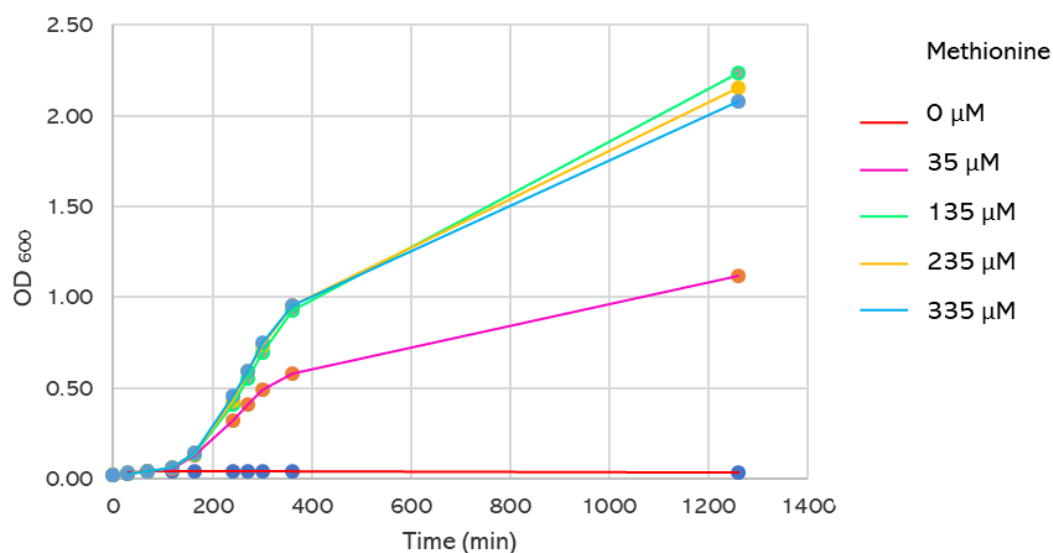


Figure 3.8. Methionine-dependent growth of *E. coli* strain K2449.

An M9-based defined medium (containing glucose and 17 amino acids) described in Material and Methods (Section 2.1), was supplemented with several different concentrations of methionine. Bacterial growth was monitored by measuring optical density at set time intervals during the day (0-380 min), and after the overnight incubation (>1200 min).

There was no significant difference in bacterial growth in M9 minimal medium containing 135 μM , 235 μM , or 335 μM methionine, while the lowest concentration of methionine, 35 μM , was suboptimal (Figure 3.8). In previous work (Petrie, 2015), the reported concentration of methionine in the M9 met-dropout medium for phage growth in ΔmetE strain was 235 μM . The same author also reported that supplementation with 10 mM azidohomoalanine in this medium should allow incorporation of 60 - 70 azide groups per virion into the phage mutant containing pVIII, A9M, M28L (genome length 7666 bp, 1028 nm, 3213 pVIII). This number of adjuvant copies per virion is too high for the vaccine design applied in this thesis. Given that the adjuvant to be attached to the virion for vaccine design is very potent in mice (I. Hermans 2018, personal communication, 21 June), it was

expected that it would be required at a low copy number per particle; therefore, lower azidohomoalanine concentrations (1 mM, 5 mM and 10 mM) were tested, followed by quantification of incorporated azides per particle (Section 3.2.3.1).

3.2.2 Production of azide- and antigen-displaying phage particles

As indicated in Section 3.1, there are well-established protocols for phage production and purification, both from nutrient-rich and dropout media. For this research, however, the protocols had to be optimised (Figure 3.9) so that the vaccine carriers have modified pVIII protein suitable for attachment of the fluorescently tagged glycolipid molecule BODIPY- α -GalCer by click chemistry. At the same time, the vaccine particles were designed to display the 30-residue long antigenic OVA peptide (Table 5) in a “mosaic” manner along the filament (OVA-pVIII fusion). Detailed general protocols for phage growth and purification are described in Material and Methods, Section 2.5.

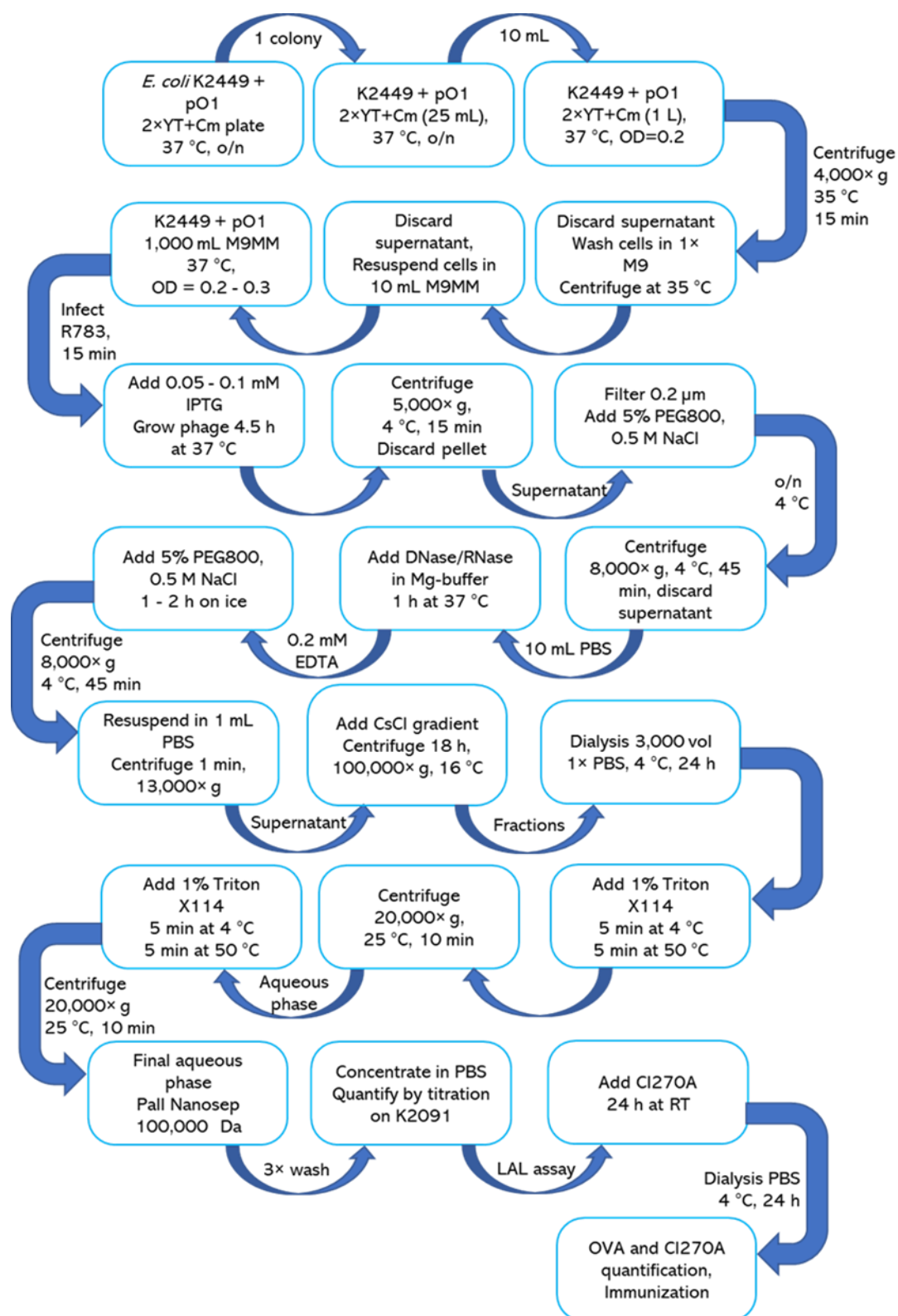


Figure 3.9. Flow-diagram of the optimised production and purification of Ff-vaccine carrying long peptide antigens and the click-chemistry-attached glycolipid adjuvants.

For the vaccine particles, strain K2449 was transformed with pO1 or pF1 plasmid and plated on 2× YT+Cm plates. After overnight incubation, a single colony was picked and cultivated overnight at 37 °C in 25 mL of liquid media. The following day, the overnight culture was diluted 1:100 in fresh media and incubated until the OD₆₀₀ reached 0.2. The cells were pelleted by centrifugation (15 min, 4000× g) at 35 °C, and the supernatant was removed. Cells were washed in the warm M9 salts to remove any nutrients from the previously used culture media, then pelleted again. The supernatant was removed, and the cells were resuspended in M9 medium supplemented with methionine, with and without azidohomoalanine (as stated for specific experiments) and incubated at 37 °C until an OD₆₀₀ was between 0.2 and 0.3. The culture was then inoculated with R783 phage (m.o.i. 50) from a purified stock (described in Section 3.2.1.1) in PBS and incubated for 15 min at 37 °C without shaking, to allow adsorption of phages to the F-pili and infection of the host cells. In the next step, the production of pVIII fusions from the accessory plasmid was induced by IPTG (0.05 - 0.1 mM), followed by phage growth at 37 °C for 4.5 hours with aeration (200 rpm). After the incubation was completed, bacteria were pelleted by centrifugation (5000× g, 4 °C, 15 min), and the culture supernatant containing the phages was filtered through a 0.2 µm filter (to eliminate bacteria) into pre-chilled sterile centrifuge bottles.

Phages were concentrated by PEG precipitation and subsequently purified by CsCl gradient centrifugation, as described in Material and Methods, Section 2.5. The CsCl-

purified phages (Figure 3.10), however, still contain lipopolysaccharides (LPS) from bacterial cells, along with other residual debris, making them unsuitable for *in vivo* administration. To remove these impurities, subsequent two-step washing with Triton X114 was carried out as described in Section 2.5.2, and the residual detergent was removed by centrifugal ultrafiltration (Pall® ultra; MWCO 100 kDa). The purified vaccine particles were resuspended in sterile LPS-free Dulbecco's phosphate-buffered saline (DPBS) and tested for endotoxin presence with a *Limulus* Amebocyte Lysate (LAL) assay kit. Phage enumeration was determined by plaque assay (Adams, 1959), and the titres were recorded as pfu/mL.

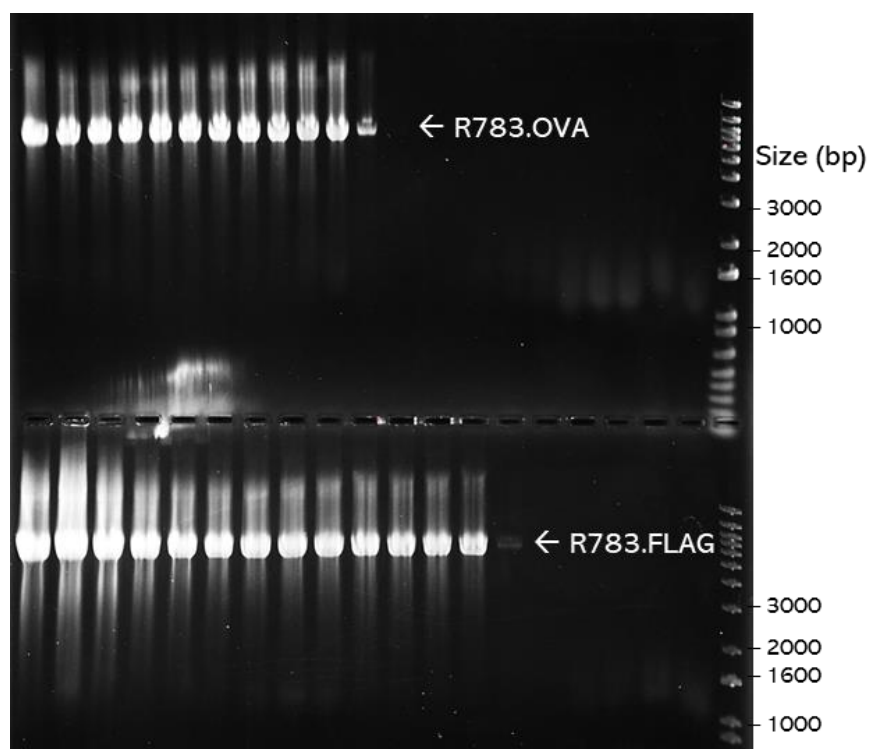


Figure 3.10. Agarose gel electrophoresis of phage fractions

The US Pharmacopeia (USP) recommendations for endotoxin levels in vaccine production range between 10 EU/mL and 200,000 EU/mL, depending on the type of vaccine (Brito and

Singh, 2011). For recombinant proteins and polysaccharides, the most relevant description of the vaccine used in this research, the upper limit is set at 20 EU/mL. Therefore, the desired purification level of Ff vaccine was achieved after two washes with Triton X114. An example of such purification experiment is shown in Figure 3.11.

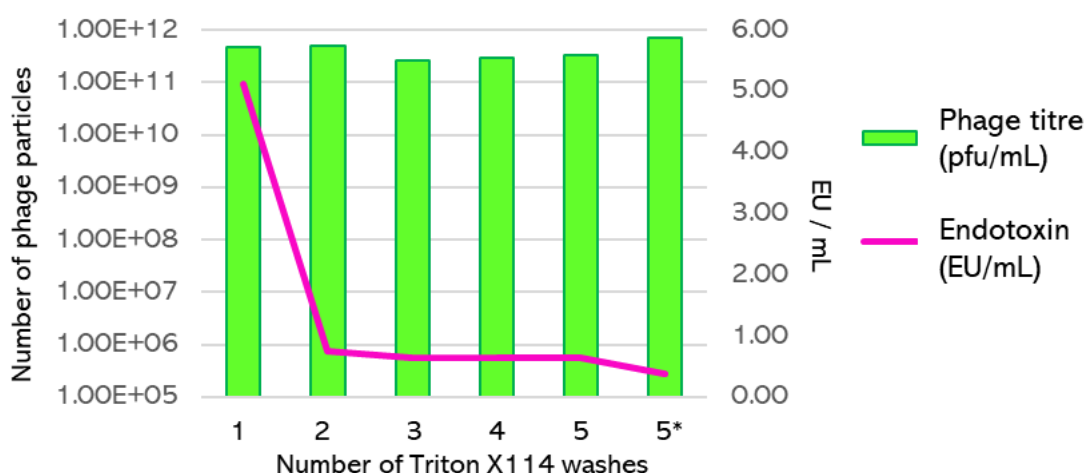


Figure 3.11. Efficacy of Triton X-114 treatments for removal of residual LPS from R783.OVA vaccine samples.

After CsCl and dialysis, phage vaccine samples were treated with Triton X-114 in five consecutive washing steps, as described in Section 2.5.2. The sample after the final wash (5*) was concentrated 3-fold by ultrafiltration. Numbers of phages are presented as plaque-forming units (pfu/mL), estimated by titration after each washing step. Endotoxin levels are shown as endotoxin units (EU/mL) estimated by LAL assay, as described in Section 2.5.2

After the Triton X114 treatment, R783.OVA and R783.FLAG final vaccine samples for immunisation gave values of 1.92 EU/mL and 3.58 EU/mL, respectively.

3.2.2.1 Long antigen peptide is displayed as protein fusion on phage coat protein

Quantification of the displayed OVA peptide on Ff particles was essential to establish whether a high antigen load had been achieved in the particle vaccine. Phages displaying OVA antigen at the pVIII coat protein were produced and purified as described in Section 2.5. SDS-PAGE and western blots were used for detection of the OVA-pVIII fusion. For detailed methods, refer to Section 2.4.2.2. A phage ELISA assay was used for quantification of OVA peptide per phage particle (Figure 3.12), as described in Section 2.7.2.2.

Initially, a custom-made antibody for C-terminus of pVIII was designed, with intention to compare and quantify the signal on western blots from N-terminally attached ovalbumin peptide (OVA-pVIII fusion) and pVIII without the peptide. However, the difference in protein sizes was 3 kDa and it was not possible to separate them clearly enough to perform such analysis (data not shown).

As an alternative approach for this study, an ELISA assay (Section 2.7.2.2) was used for quantification of the OVA peptide, and it is important to note that this is not a conventional way of performing peptide quantification. Nevertheless, this was the only possible solution at the time, since only one, custom made antibody was available for the detection of MHC I+II OVA peptide. It was noted that the ELISA signal was indeed very low, even with the highest peptide concentration applied (Appendix 7.3.56) and these values were reproducible and consistent through the study.

This might have been due to the insufficient binding of the peptide to the wells, or low quality of the designed antibody.

Immobilised phage particles (R783.OVA) were efficiently detected with OVA-specific antibodies in the samples where the peptide fusion was induced with 0.05 mM IPTG. No signal over background levels was detected in control samples where OVA-pVIII fusion expression was not induced with IPTG (R783.OVA, no IPTG), or when phages were produced without the pO1 display plasmid (R783) (Figure 3.12). For details of quantification of peptide copies per phage particle, refer to Appendix 7.3.56.

A higher concentration of IPTG was also tested (1 mM), resulting in Ff.OVA displayed up to 1900 peptide copies per R783 phage particle. The amount of virion produced, in that case, however, was lower by a factor of 100 in comparison to the cultures containing 0.05 mM or 0.1 mM IPTG (data not shown). Hence, for further production, 0.05 mM and 0.1 mM IPTG were chosen for optimal phage yields and peptide display.

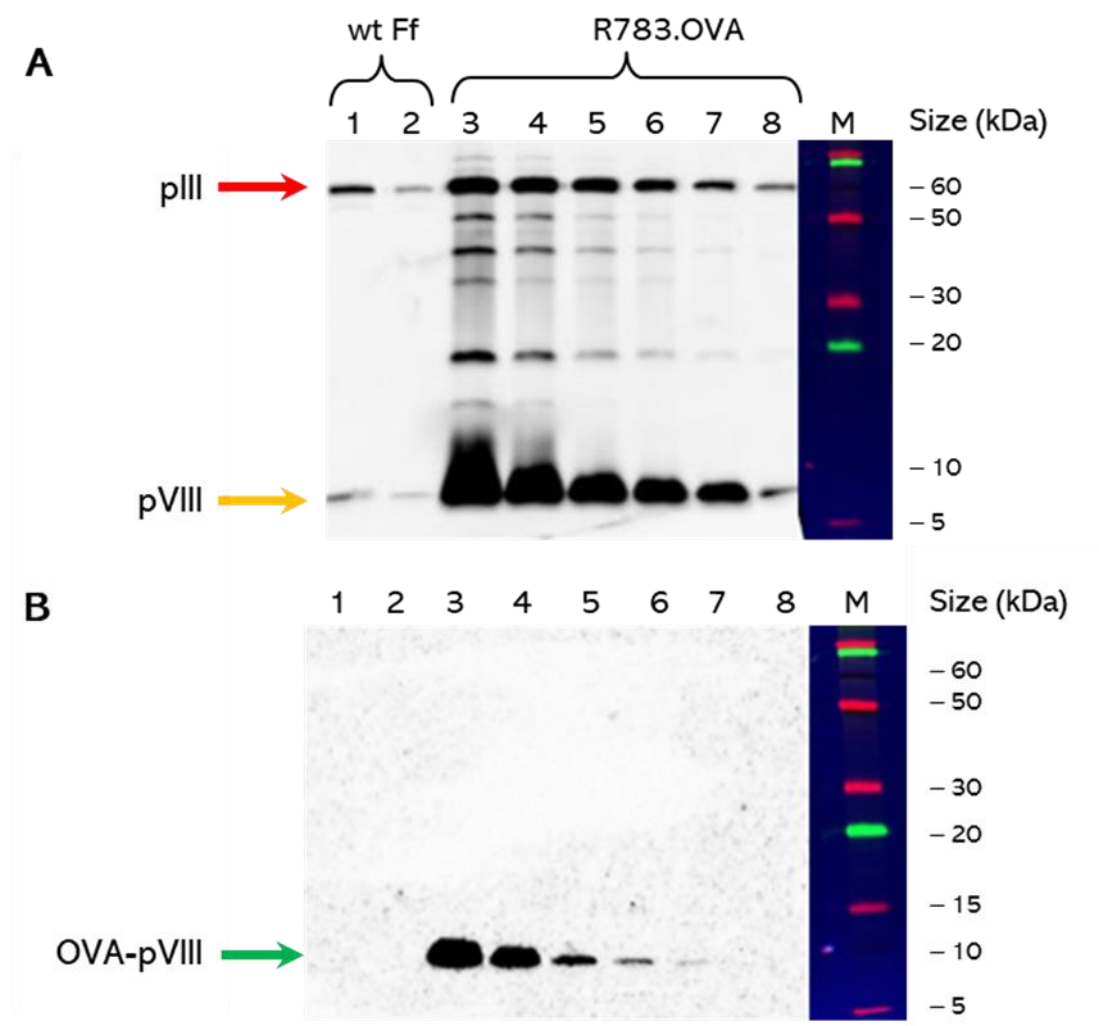


Figure 3.12. Immuno-detection and quantification of OVA peptide displayed along the phage filaments.

A, Detection of the virion proteins by western blotting using rabbit anti-f1 and HRP-conjugated anti-rabbit Ig. Bands between pVIII and pIII in lanes 3 - 7 could be either multimers of pVIII coat protein, visible at high concentrations of Ff phages, or residual proteins from *E. coli* that are specifically detected by anti-f1 rabbit polyclonal antibody. **B**, Detection of the OVA-pVIII fusion by western blot analysis of the same samples as in A, using affinity-purified rabbit anti-OVA. **Lanes (A and B)**: 1, 2, wild-type Ff (VCSM13); 3 - 8, serial dilutions of R783.OVA mutant phage displaying OVA peptide on pVIII; M, protein size marker, pre-stained Novex Sharp® (kDa). **Symbols**: red arrow, pIII coat protein; yellow arrow, pVIII protein; green arrow, OVA-pVIII fusion; red bars, control R783 phages; yellow bars, R783.OVA particles without IPTG induction; green bars, R783.OVA phage induced with 0.05 mM IPTG.

3.2.3 Cycloaddition allows controlled modifications of phage coat proteins

Azide-alkyne cycloaddition is one of the “click chemistry” tools, first introduced in 2001 (Kolb et al., 2001). The reaction occurs in aqueous solution and is irreversible, forming covalent bonds in biomolecules, suitable for biological systems (Takayama et al., 2019). Here, copper-free click chemistry was used to attach the glycolipid adjuvant molecule, BODIPY- α -GalCer (Figure 3.14), which has a fluorescent tag. Firstly, the efficiency of the phage modification was monitored and optimised using two “reporter” molecules functionalised for click chemistry, a fluorescent dye (DIBAC-TAMRA), and DBCO-biotin (Section 2.1). Fluorescent dyes allow easy detection and quantification of the average numbers of fluorescent molecules per phage particle by fluorescence spectroscopy. On the other hand, biotin-functionalised particles can be decorated by streptavidin-conjugated gold particles (5 nm), allowing direct visualisation of covalently attached biotin by TEM and counting the numbers of attached gold particles per individual phage (Section 3.2.3.2).

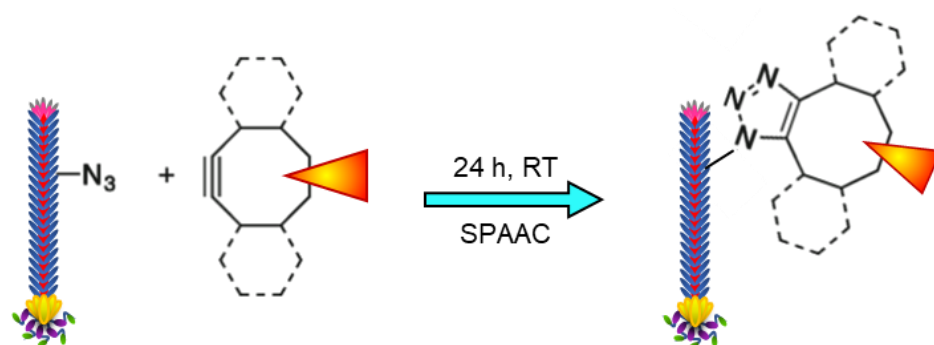


Figure 3.13. Schematic presentation of alkyne cycloaddition to azide-displaying phage.

The phage coat protein was genetically modified to allow incorporation of unnatural amino acid azidohomoalanine in the position that allows exposure of the azide (N_3) to the solvent. The molecule of interest (orange triangle) was functionalized for click chemistry with a cyclooctyne group, and the reaction was carried out at room temperature for 24 h. SPAAC, strain promoted azide-alkyne cycloaddition.

The chemical reaction for the labelling of azide-displaying phages is schematically presented in Figure 3.13. Briefly, phage samples in 1× PBS were mixed with a concentrated solution of the desired molecule, and the mixture was incubated at room temperature for 24 h. The non-reacted excess reagent was removed by dialysis (MWCO 10 kDa) over 24 h at 4 °C in 3,000 volumes of 1× PBS in three steps. In the first 1000 volumes when the sample contained most of the unreacted dye, dialysis was performed for 2 - 3 hours, then the buffer was changed with fresh 1000 volumes and dialysed another 4 - 6 hours, followed by the last 1000 vol dialysis overnight. Labelled phages were PEG-precipitated and resuspended in fresh PBS before measuring the absorbance.

3.2.3.1 Modified phages are covalently labelled with the fluorescent dye

DIBAC-TAMRA

The absorption spectra of DIBAC-TAMRA attached to phages (Figure 3.14B) was measured over the wavelength range of 240 to 650 nm (Figure 3.15). The number of dye molecules (N) was calculated as $N=n \cdot N_A$, where N_A [1/mol] = $6.02 \cdot 10^{23}$ is Avogadro's number; n [mol] = m [g] / M_w [g/mol], is number of mols, for each dilution, at 558 nm, the DIBAC-TAMRA maximum absorption wavelength. These values were then used for calculating the labelling efficiency of pVIII protein (the number of TAMRA molecules per virion). For quantification of the TAMRA molecules, a standard curve $A_{MAX}=f(c_{dye})$ was generated by measuring the absorbance of DIBAC-TAMRA free molecules in serial dilutions of known concentrations at $A_{MAX}=558$ nm. Labelled phage particles were measured in the range of 240 - 600 nm (Figure 3.15). For detailed quantification refer to Appendix 7.3.3.

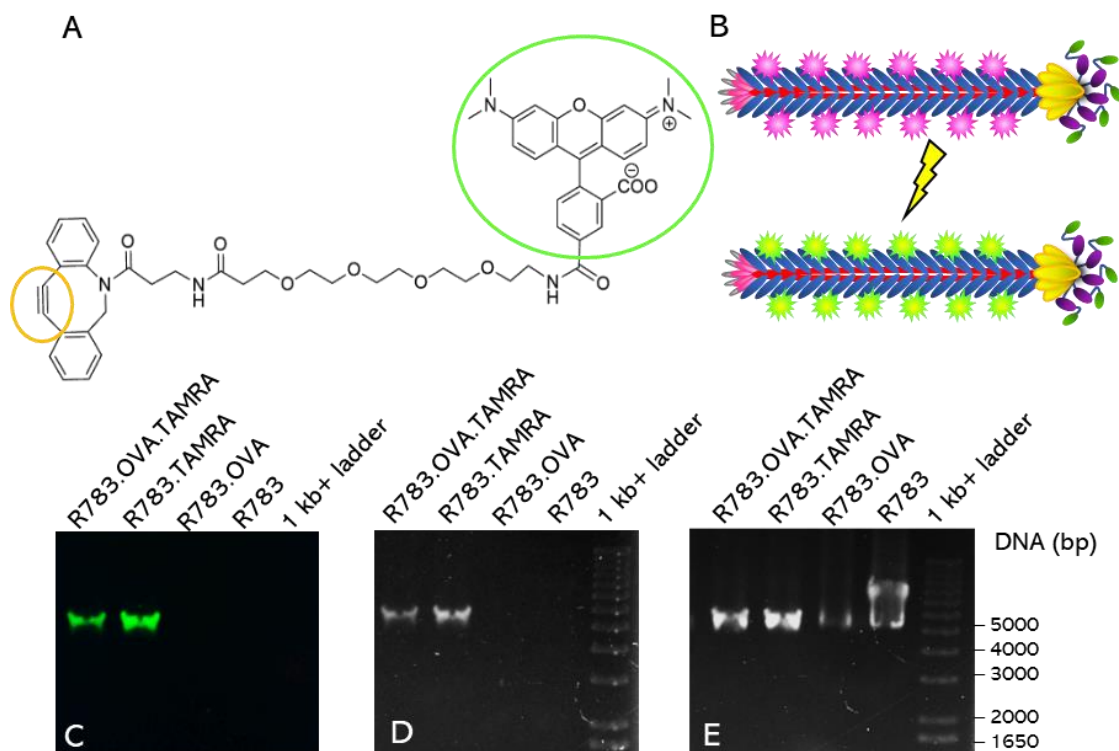
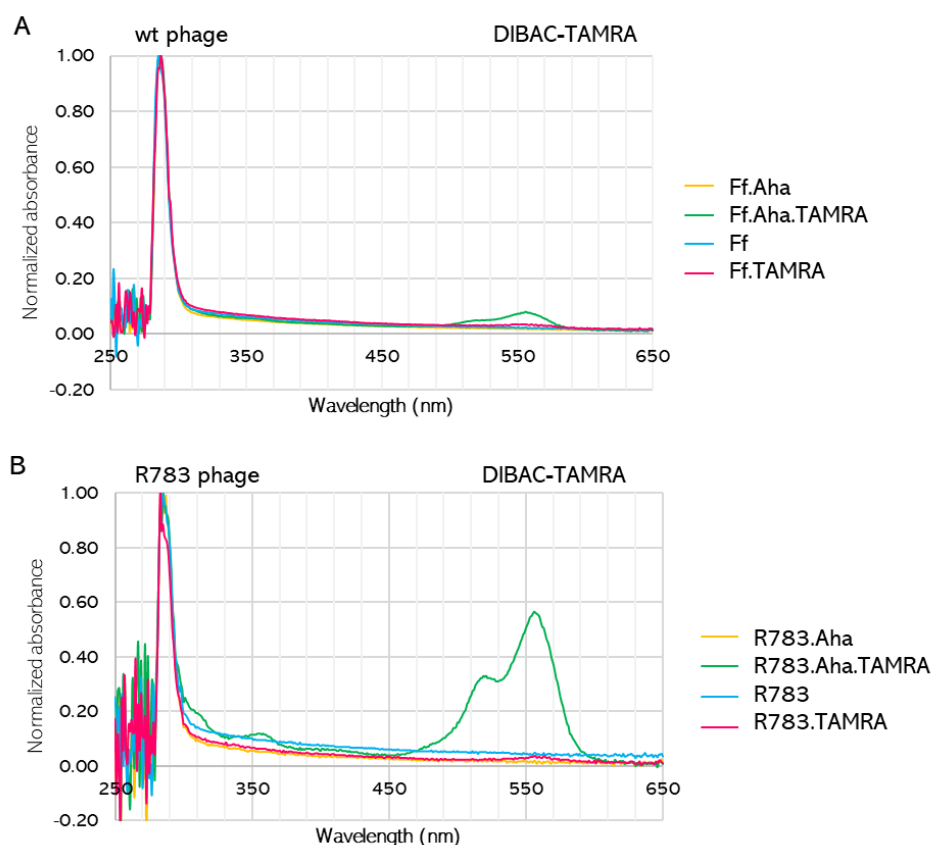


Figure 3.14. Fluorescent labelling of Ff phages via pVIII-displayed azide handles.

A, Structure of DIBAC-TAMRA molecule, composed of a fluorescent dye TAMRA (circled in green) connected with a short PEG linker to the azide-reactive group DIBAC-amine (dibenzo-azacyclooctyne-amine) for click chemistry (alkyne group circled in yellow). **B**, Schematic representation of TAMRA-labelled Ff phages, detected as pink in the visible spectral region (top) or fluorescing green (bottom) as seen in (C). **C - E**, TAMRA labelling analysed by agarose gel electrophoresis of native Ff particles (as described in Section 2.4.2.1). **C**, Fluorescent bands of the native TAMRA-conjugated phages in an unstained gel detected by Azure c600 fluoroimager; **D**, UV image of EtBr-stained gel (detecting TAMRA), **E**, UV image of EtBr-stained phage DNA after processing the gel in NaOH to disassemble the Ff particles, as described in Section 2.4.2.1. The double-stranded linear DNA ladder 1 kb+ (Life Technologies) was used to monitor the migration of gel bands during the electrophoresis, but not for size comparison of ssDNA from the phage particles.



Sample	1	2	3	4	5	6	7	8
Phage	(A) VCSM13				(B) R783			
1 mM Aha	+	+	-	-	+	+	-	-
DIBAC-TAMRA	-	+	-	+	-	+	-	+
$A_{558\text{ nm}}$	0.015	0.070	0.013	0.030	0.001	0.139	0.012	0.008
TAMRA per phage (molecules)	0	34	0	17	0	351	0	11
Labeled pVIII (%)	0	0.93	0	0.46	0	9.64	0	0.31

Figure 3.15. Quantification of fluorescent dye on phages labelled via click chemistry.

Wild-type phage VCSM13 that has no exposed methionine residues in pVIII, used as a control was prepared under the same conditions as mutant phage R783 containing exposed A9M, functionalized for click chemistry. Phages were produced in M9 met-dropout medium, supplemented either with methionine alone (135 μM) or with azidohomoalanine (10 mM); therefore, the particles were either displaying azide or methionine on pVIII, respectively. Azide-alkyne cycloaddition reaction with purified phages was performed as described in Section 3.2.3. A_{MAX} for phage particles and DIBAC-TAMRA are 269 nm and 558 nm, respectively. **A**, Phage control group VCSM13 (1-4); **B**, mutant phage R783 (5-8).

TAMRA-labelling efficiency of R783 phage was 9.6% of the total number of pVIII per virion when particles were produced in media containing 10 mM azidohomoalanine (Figure 3.15) and limited methionine (135 μ M). This was equivalent to 351 dye molecules per phage particle that has 3,655 copies of pVIII. The maximal concentration of azidohomoalanine in media that allows phage assembly is 10 mM (Petrie, 2015). Wild-type phage VCSM13 had 0.93% labelling efficiency, or 34 molecules per virion when incubated under the same conditions. This low level of TAMRA can be attributed to labelling of the minor coat proteins via the methionine residues that are exposed to solvent, and labelling of the co-precipitated *E. coli* proteins. The background signal at 558 nm wavelength in phage samples that were not labelled (samples 1, 3, 5, and 7 in Figure 3.15) would correspond to about 10 molecules of fluorescent dye per particle, which was similar to previously reported findings (Petrie, 2015).

3.2.3.2 Gold nanoparticles are attached to modified phages via click chemistry

Click chemistry was also used to attach DBCO-biotin to azides displayed on purified R783 and VCSM13 phages. On-grid attachment of streptavidin-conjugated gold particles (SA-AuNPs) and transmission electron microscopy (TEM) allowed direct counting of the gold nanoparticles per virion. On average, there were 41 gold nanoparticles per R783 phage (Figure 3.16A), and only one per control VCSM13 phage (Figure 3.16B), prepared under the same conditions.

A relatively smaller number of nanogold particles per virion was observed, in comparison to the number of the TAMRA molecules per virion detected in Section 3.2.3.1. This finding can be explained by steric interferences, where a 5 nm sphere is expected to block 6 ± 2 pVIII subunits (Marvin et al., 1994; Petrie, 2015). It should also be noted that the biotinylated phages prepared for TEM imaging were immobilised on carbon grids, as described in Section 2.5.5.2, before binding of SA-AuNPs. This means that, theoretically, only one side of phages was exposed to solvent in the reaction. Finally, four molecules of biotin interact with one streptavidin. Hence, the number of gold particles per virion is expected to be at least four-fold lower in comparison to the number of TAMRA molecules.

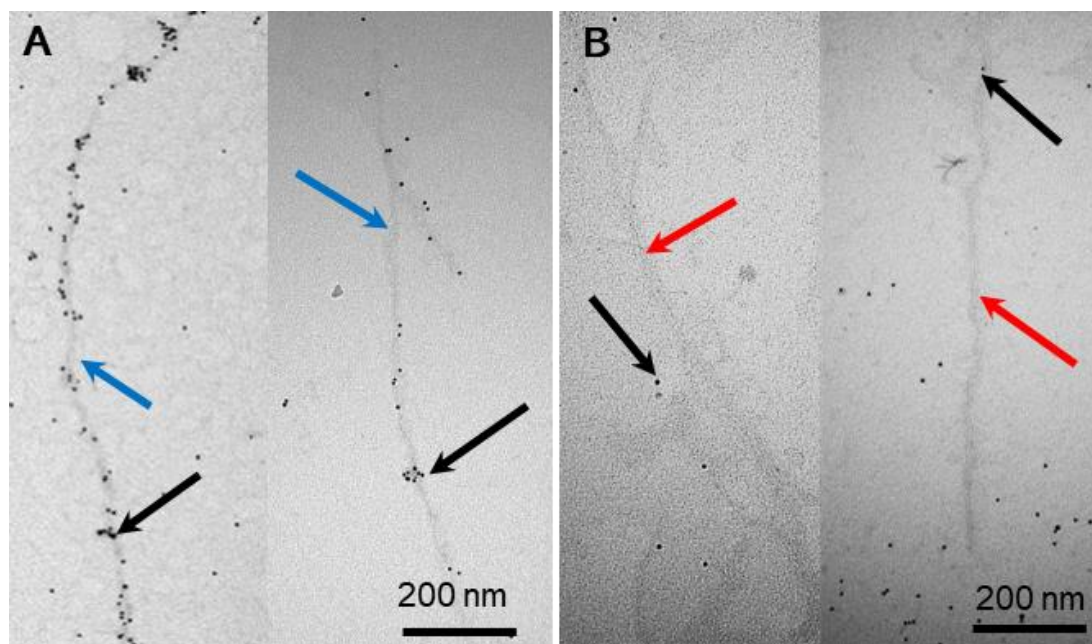


Figure 3.16. Electron micrograph of gold-coated phages. Phage particles grown in M9 met-dropout media supplemented either with methionine alone (135 μ M) or with azidohomoalanine (10 mM azidohomoalanine). Biotin-labelled purified phages were on-grid exposed to Streptavidin-conjugated gold nanoparticles (5 nm), stained and imaged by TEM. **A**, mutant phage R783; **B**, control wild-type phage VCSM13. **Symbols**: blue arrows, phage R783; black arrows, streptavidin-conjugated gold nanoparticles (SA-AuNP); red arrows, control phage VCSM13. The scale bars are 200 nm.

3.2.4 Fluorescently labelled glycolipid adjuvant BODIPY- α -GalCer chemically attached to phage particles

When labelling phages with the BODIPY- α -GalCer fluorescently tagged adjuvant molecule, it was expected that the number of α -GalCer per phage would be similar to that of the TAMRA, given the molecule sizes and potential steric effects. When phages were grown in media supplemented with 10 mM azidohomoalanine, this number appeared to be too high for the vaccine design, given the low yields of phage production

in methionine-dropout media. Considering that the ratio of antigen to α -GalCer should be high, lowering the azidohomoalanine concentration in phage production media was a desirable option.

BODIPY- α -GalCer synthesised at the Ferrier Research Institute (Cheng, 2014) was further modified for click chemistry to obtain the CI270A molecule (Appendix 7.2.1) (Compton, Painter, unpublished) and was provided by Prof Gavin Painter and Dr Benji Compton. Given that this adjuvant molecule was highly hydrophobic and was expected to form a precipitate in PBS solution, different conditions for labelling the phage particles were tested (data not shown). Mixtures of phages and adjuvant in different ratios of PBS and DMSO (a standard non-polar solvent) were incubated for 24 h at room temperature. Even though phage particles were stable when stored long-term at 7% DMSO, concentrations of $\geq 50\%$ DMSO seemed to have caused degradation of virions, as no phage particles were detected by agarose gel electrophoresis after incubation in 50% DMSO. Interestingly, when BODIPY- α -GalCer was incubated with phages in the reaction containing only PBS, it did not form a visible precipitate at the concentrations used for labelling (15 nM BODIPY- α -GalCer for $5 \cdot 10^8$ pfu in 0.5 mL). In contrast, when BODIPY- α -GalCer was resuspended in PBS in the absence of phages, at the same concentrations used for labelling, the pellet was formed. When the phage samples were examined after reaction with BODIPY- α -GalCer on an agarose gel, the R783 phage band showed the fluorescence attributable to

BODIPY- α -GalCer. Some smearing was observed, most likely reflecting different levels of modification and thereby non-uniform hydrophobicity and charge within the virion population, similarly to smearing observed within the TAMRA-labelled virion population (Figure 3.17 C, D).

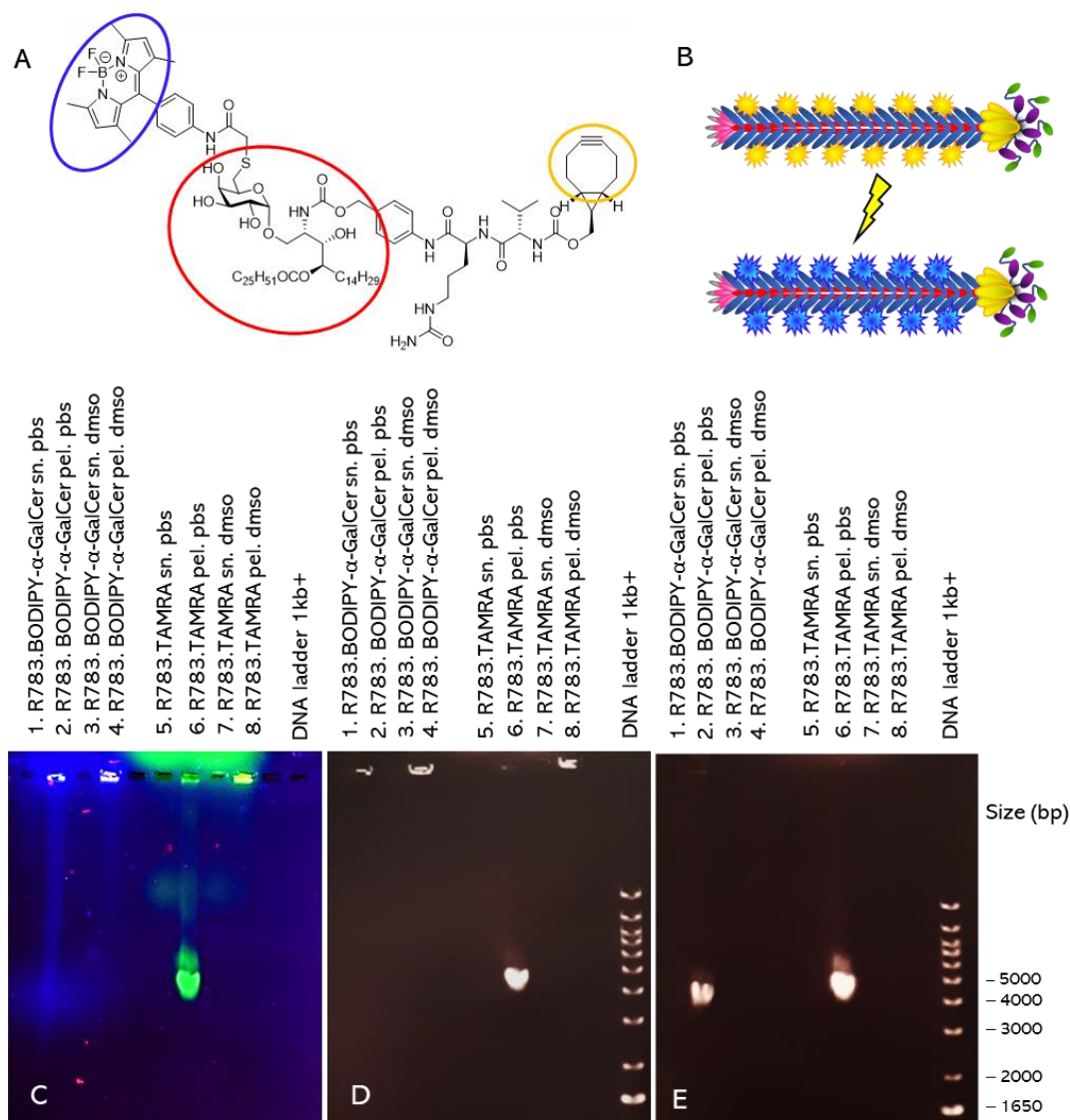


Figure 3.17. Fluorescent labelling of R783 phages with the BODIPY-α-GalCer adjuvant via pVIII-displayed azide handles.

A, Structure of BODIPY-α-GalCer molecule, composed of a glycolipid adjuvant, α-GalCer (circled in red), functionalized with cyclooctyne for click chemistry (circled in orange) and labelled with BODIPY fluorescent dye (circled in blue). The linkers between these groups are short amino acid sequences susceptible to cathepsin cleavage. **B**, Schematic representation of BODIPY-α-GalCer -labelled Ff phages, detected as orange in the visible spectral region (top) or fluorescing blue (bottom) as seen in (C). **C - E**, BODIPY-α-GalCer and TAMRA phage-labelling reactions analysed by agarose gel electrophoresis of native Ff particles (as described in Section 2.4.2.1). **C**, Fluorescent bands of the native TAMRA-conjugated and BODIPY-α-GalCer-conjugated phages in an unstained gel detected by Azure c600 fluoroimager; **D**, UV image of EtBr-

stained gel (detecting TAMRA); **E**, UV image of EtBr-stained phage DNA after processing the gel in NaOH to disassemble the Ff particles, as described in Section 2.4.2.2. **Lanes**: supernatant (**1**) and pellet (**2**) from PEG precipitated R783.BODIPY- α -GalCer after the reaction in PBS; supernatant (**3**) and pellet (**4**) from PEG precipitated R783.BODIPY- α -GalCer after the reaction in DMSO; supernatant (**5**) and pellet (**6**) from PEG precipitated R783.TAMRA labelled in PBS; supernatant (**7**) and pellet (**8**) from PEG precipitated R783.TAMRA labelled in DMSO. DNA size marker is 1 kb+ double-stranded linear DNA ladder, and as such is not used for a direct comparison of DNA sizes of ssDNA from particles. This marker has been used only for tracking the progress of electrophoresis.

Following the optimisation of azide-alkyne cycloaddition for labelling phage particles with displayed peptides along the filament, R783.OVA phage vaccine samples were labelled with BODIPY- α -GalCer (Figure 3.17). The adjuvant was quantified using fluorescence spectroscopy analysis of tagged and untagged probes.

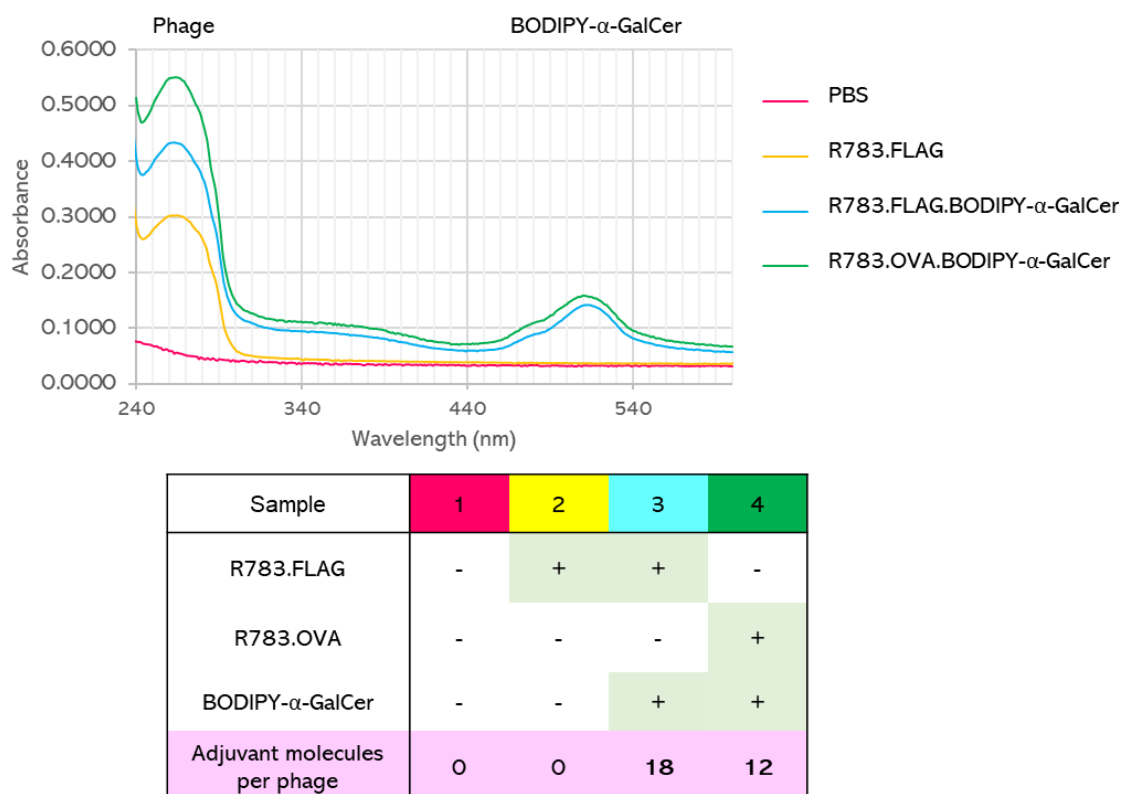


Figure 3.18. Quantification of chemically attached adjuvant molecules on phage particles displaying antigenic peptides.

Phage R783, prepared as described in Section 3.2.2, displaying either control peptide FLAG-tag (blue), or antigen model OVA (green), were chemically modified to carry fluorescently labelled adjuvant molecule BODIPY-α-GalCer. Azide-cycloaddition on purified phages was performed as described in Figure 3.13. The particles were PEG-precipitated and resuspended in PBS before measuring the absorbance. Phage control is R783 without displayed peptides on pVIII. Buffer control was 1× PBS. A_{MAX} for phages is 269 nm, and for BODIPY A_{MAX} is 513 nm when attached to phage particles. For detailed analysis, please see the Appendix 7.3.4.

Samples: 1, buffer control PBS; 2, negative control, unlabelled R783.FLAG phage; 3, control phage R783.FLAG with attached BODIPY-α-GalCer molecules; 4, R783.OVA phage with attached BODIPY-α-GalCer molecules.

3.3 DISCUSSION

One of the possible applications of Ff phages is in vaccines as drug delivery vehicles (Bakhshinejad et al., 2015; Sioud, 2019). As the pVIII protein is present in thousands of copies per phage particle, it can be used for display of multiple antigenic and adjuvant molecules along the filament (Kneissel et al., 1999; van Houten et al., 2006). In the current study, for the first time, filamentous phage VCSM13 was modified to carry pVIII proteins that allow chemical modifications post-production, while at the same time displaying long peptide fusions to pVIII in the mosaic display mode (combined with “neat” pVIII copies without displayed peptides). A synthetic fragment, with -20_{am}, A9M, M28L mutations were cloned into *BsrGI/BamHI* site of VCSM13 phage, resulting in a mutant strain named R783. The new strain carried 3655 copies of pVIII protein (8720 nt).

Initially, plasmids for peptide expression were designed to have OVA- and FLAG- fusions between the signal sequence and N-terminus of the mature portion of the wild-type pVIII (plasmids p8OVA and p8FLAG, Table 4). However, these constructs had to be adjusted to incorporate the modified pVIII with mutations required for click chemistry, as the assembly of two different pVIII subunits in the same particle was not favourable (data not shown). A study from 2003 (Li et al., 2003) showed that mutations at the N-terminus of the phage coat protein pVIII can affect the infectivity and assembly of phage. Additionally, mutations in central domain (AA 12-19) of pVIII can influence the

binding affinity of N-terminally displayed peptides (Kuzmicheva et al., 2009).

Thus, plasmids expressing pVIII fusions (pO1 and pF1, Table 4) were created. These plasmids carried matching mutations in the pVIII sequence as phage R783 (-20_{am}, A9M, M28L).

When designing the production system and having in mind the length of desired antigenic peptide, there were alternative options for displaying peptides. Enzymatic attachment (Hess et al., 2012) was considered as one possible approach for this research, using SrtA enzyme from *S. pyogenes*; however, there were several advantages of recombinant peptide-pVIII fusions (di Marzo Veronese et al., 1994; Minenkova et al., 1993; van Houten et al., 2006) over the enzymatic attachment. The main advantages are production reproducibility and lower cost, as no enzyme or synthetic peptide was required, since in the plasmid system the peptide is expressed and displayed on the particles while they are assembled during growth of the culture.

As the phage particles were modified to additionally display azidohomoalanine instead of methionine on protein pVIII, a methionine auxotroph host was designed, as suggested by (Petrie, 2015). A *metE* knock-out gene from Keio collection (Table 2) (Baba et al., 2006a) was transduced into K2091 laboratory strain and the conditions were adjusted to display the desired numbers of azide residues. Once the host strain and the plasmids were created, the next step was to optimise the growth conditions in minimal media. Previously reported concentrations of azidohomoalanine were

substantially higher (10 mM), aiming to maximise the number of this unnatural aminoacid into the virions (Petrie, 2015). On the other hand, phage-based vaccine design in this thesis aimed to gauge the number of incorporated azidohomoalanine residues to achieve a low ratio of azide-attached adjuvant molecules to displayed peptide antigens. Therefore, a ten-fold lower concentration of azidohomoalanine in growth media (1 mM) was used in this study.

In a report published during the course of this thesis work, α -GalCer was added to the Ff phage as admix. Hydrophobic interactions appeared to have been sufficient to associate some small amount of α -GalCer with the phage filament (Sartorius et al., 2018). The published method has drawbacks in that it incurs a huge loss of starting material and precludes control of the amount of displayed adjuvant. In this thesis fine-tuning the conditions of the phage growth and gauging the amounts of displayed azide ($-N_3$) groups permitted production of the Ff vaccines with controllable numbers of attached adjuvant molecules. Also, to allow easy detection, α -GalCer pre-labelled with a fluorescent dye (BODIPY) was conjugated to the phage filament. In the current study, for the first time, an adjuvant molecule was attached to phages via azide-alkyne cycloaddition and monitored *in vivo* for the immune response in murine models. More detailed comparison of the effectivity of the phage-based vaccine from current study, and from Sartorius et al. (2018) will be provided in the Discussion section of the Chapter 4.

In comparison to previous phage purification methods, here an additional 0.2 μm filtration step was introduced after collecting the culture supernatant, to remove residual bacteria. Moreover, PEG precipitation was shortened from overnight incubation at 4 °C to 1 - 2 hours on ice. Having the two PEG-precipitation steps completed in one day instead of three (Sattar, 2013), significantly shortened the time phage were exposed to proteolytic enzymes (Maurizi, 1992) from the bacterial supernatant. This could have potentially improved the stability of displayed antigenic peptides on the pVIII coat protein.

Ff phage preparations contain LPS (a pyrogen) contaminants unless subjected to specific removal procedures (Dor-On and Solomon, 2015). Given that the use of pyrogen *in vivo* is not ethical and LPS is an adjuvating molecule that interferes with analysis of α -GalCer activity (Ando et al., 2013), the phage vaccine preparations had to be subjected to LPS removal procedures. In this research, two methods were analysed for the LPS removal: (i) using the endotoxin removal magnetic beads that contained covalently bound polycationic ligands for LPS-binding (Miltenyi Biotec, USA) or (ii) detergent Triton X114. The Triton X114 method removed the LPS from phage samples by several washes in this detergent (Teodorowicz et al., 2017), combined with modified temperature treatments. The method for removing the LPS from phage vaccines is described in Section 3.2.2. with the main difference from previous research being that instead of incubating the solution at 4 °C for 30 min followed by

incubation at 37 °C for 10 min, in this research each incubation step was only 5 minutes.

Although endotoxin removal using magnetic beads offered a simple and easy-to-use protocol and was generally recommended for recombinant protein purifications (Razdan et al., 2019), in case of filamentous phage particles, they did not show favourable recovery (data not shown). The reason was most probably because phages tend to adhere to solid surfaces themselves; therefore, an alternative option was sought. Accordingly, it has been reported that purification of LPS from biopharmaceuticals can indeed result in product loss (Razdan et al., 2019). Washing samples with non-ionic detergent (Triton X114) in a series of heat / cold cycles proved to be sufficient for the removal of endotoxins while keeping the sample recovery at satisfactory levels (Figure 3.11). An additional advantage of using detergent, in comparison to magnetic beads, was the option to purify larger volumes of phages, simply by mixing the samples with more detergent. On the other hand, the magnetic beads have a specific limited capacity of endotoxin that can be purified ($4.2 \cdot 10^6$ EU/mL according to the manufacturer's instructions) which was not sufficient for large-scale phage preparations.

To optimise the OVA peptide (ISQAVHAAHAEINEAGRESIINEFKLTEWT) display on pVIII, gauging of the recombinant fusion expression by increasing IPTG concentration in the medium was performed. Given that pVIII fusions can be toxic to *E. coli* cells if overexpressed leading to low production of the Ff phage, the effect of

IPTG concentration on Ff phage production was monitored in the first instance. It was observed that the phage production in K2449 *E. coli* strain (Table 2) did not show much variation when the fusion was induced with 0.05 mM, 0.1 mM and 1 mM IPTG in nutrient-rich media (2× YT). In contrast, growing recombinant phages in methionine-dropout medium supplemented with azidohomoalanine was more sensitive to overexpression of the pVIII fusions, with the yields dropping 100-fold when 1 mM IPTG was used (data not shown). In this study, the optimal balance between the amount of displayed antigen and concentrations of produced phage particles was found to be at 0.05 mM IPTG (used in vaccines in Section 4.2.2) and 0.1 mM IPTG (used for the vaccines tested in Sections 4.2.3 and 4.2.4). These conditions did not decrease the Ff titres relative to the no-IPTG control. Under the optimum production conditions (0.1 mM IPTG in the M9 minimal medium), the 30-residues-long OVA peptide fusion constituted about 25% of the major coat protein subunits in the virion. Initially, western-blot was used for detecting the presence of pVIII and the phage-encoded pVIII fusion, using a custom-made anti-pVIII antibody that recognises epitope at the C terminus of pVIII. However, due to the similar mobility of pVIII and OVA-pVIII fusion in SDS-PAGE, it was not possible to detect them both at the same time. This problem was overcome by using an ELISA assay and custom-made OVA-peptide-specific antibody for quantification of OVA peptide. This approach, described in Section 2.7.2.2, used direct binding of OVA peptide or OVA-displaying phage to the wells of the microtitre plate. Although sandwich ELISA assay

is commonly accepted approach, it was not feasible, given that only one OVA-specific antibody was available. Later on, authors who worked on similar vaccine design (Sartorius et al., 2018) used N-terminal sequencing for quantification of peptide fusion. However, in their report, the pVIII displayed only SIINFEEKL portion of the ovalbumin peptide, and they reported 15 - 20% of pVIII subunits in the virion carrying this short sequence. A 30-mer-pVIII fusion should theoretically have a decreased efficiency of incorporation into the virion relative to 8-mer (SIINFEEKL)-pVIII fusion (Petrenko, 2018). The higher incorporation of a pVIII fusion displaying 30 residues achieved in this thesis is therefore unexpected. The higher incorporation of a longer peptide fusion observed here might be due to differences in: media, phage strains and their pVIII sequences, purifications techniques, and detection methods.

Having successfully isolated Ff particles with and without displayed peptides (OVA and FLAG), the next step was to optimise the click chemistry for attachment of glycolipid adjuvant BODIPY- α -GalCer. Firstly, fluorescent dye (TAMRA) functionalised for azide-alkyne cycloaddition was tested in order to establish the relationship between the azide concentration and the copy number of covalently attached reporter molecules (Petrie, 2015).

A signal equivalent to 10 - 11 DIBAC-TAMRA fluorescent dye molecules per phage particle was identified as a background signal in the samples produced in the absence of Aha (Figure 3.15). This means that for more sensitive detection (e.g., one molecule per particle), a different detection method

would have to be considered and optimised. When mutant and wild-type phages, with and without dye labelling, were tested, the only highly positive signal was detected R783 A9M, M28L mutant produced in the azidohomoalanine-enriched medium (Figure 3.2). Quantification showed that about 9.6% of pVIII (351 pVIII proteins per particle) in this sample contained the fluorescent dye attached via click chemistry; in agreement with findings by (Petrie, 2015).

Additionally, phage VCSM13 that contains the wild type pVIII showed some labelling under the same conditions, which can be explained by the position of the sole methionine residue in pVIII subunit (at position 28) in the phage structure. Even though this methionine is embedded deep inside the pVIII structure of Ff (Figure 3.2), there is a probability that, the azide in small number of pVIII subunits could still be accessible and therefore labelled with azides. This, however, was not significant, giving a positive signal in only 0.93%, or 34 pVIII subunits (out of 3655) per virion.

Phage and Ff-derived particles decorated with fluorescent dye via click chemistry could be used in diagnostic applications for rapid detection and visualisation. One possibility is to visualise fluorescently labelled Ff particles accumulated in tissues, for example when targeting tumour cells or DCs (Bar et al., 2008; Ju and Sun, 2017; Sartorius et al., 2015), which could be assessed by confocal microscopy. In a similar manner, *in vivo* distribution of fluorescent phages has been quantified throughout the tumour tissue by using fluorescent tomographic imaging (Kelly et al., 2006).

As an additional strategy to test the attachment by click chemistry, a possibility of attaching streptavidin-labelled gold nanoparticles (SAuNP, 5 nm) to click chemistry-attached ligand biotin was also explored here. Interestingly, the numbers of attached gold nanoparticles were lower than those of TAMRA. There are several reasons for this. Firstly, in the process of labelling with SAuNP only one side of the phage is physically exposed to the solvent, while the other side is occluded due to the interaction with to carbon-coated microscope grid. Secondly, with the spheres being almost the same diameter as the width of the filamentous phages, it was expected that some of the pVIII subunits carrying biotin will be covered and unreachable for a reaction. Thirdly, the stoichiometry of streptavidin to biotin reaction is 1:4 (Jain and Cheng, 2017); and finally each SAuNP is functionalised with multiple streptavidin groups, therefore single bead attaches to multiple biotins on the phage. The numbers of beads observed here corresponded to previously reported ones (Petrie, 2015).

Overall, strain promoted azide-alkyne cycloaddition (Tummatorn et al., 2012) proved to be a desirable tool for controlled modifications of proteins that display azide groups on the surface of phage particles. These solvent-exposed azide groups served as "handles" to attach non-peptide molecules along the filaments. This was a particularly useful tool when designing the Ff-based vaccine, where adjuvant and antigen concentrations ideally needed to be controlled independently of each other. After establishing the protocols for post-purification

modifications (Section 3.2.1.4), and quantification of attached molecules (Section 3.2.3), the next step was to produce OVA-displaying phage particles and attach fluorescently labelled adjuvant BODIPY- α -GalCer via azide cycloaddition.

As mentioned in Section 3.2.4, for this research the adjuvant molecule α -GalCer had been modified at the Ferrier Research Institute to include a BODIPY tag and linker for click chemistry, which was named CI270A (Appendix 7.2.1; for simplicity in this thesis it is referred to as BODIPY- α -GalCer). This is the first time that such a molecule has been made for testing *in vivo*; therefore, in planned *in vivo* studies (described in the next chapter), it was necessary to compare the activity of BODIPY- α -GalCer to unmodified α -GalCer. The first challenge with BODIPY- α -GalCer was the solubility. This compound is highly hydrophobic, and when dissolved in DMSO added to PBS or water, it instantly precipitated, even in low concentrations. For this reason, trials of labelling in various DMSO : water ratios were conducted (data not shown). Even though Ff phages are highly stable and usually stored at 7% DMSO long term at -80 °C, higher DMSO concentrations (e.g., $\geq 50\%$) severely impaired Ff structure (as measured by infectivity) after 24 hours. Since BODIPY- α -GalCer (33 μ M) did not form a precipitate when mixed with concentrated Ff particles ($\sim 10^{12}$ pfu/mL) in PBS, it was possible for the reaction to occur in this buffer.

When supernatants and pellets of PEG-precipitated labelled Ff samples, both from DMSO and PBS, were examined by gel electrophoresis (Figure 3.17), it was observed that some of the dye precipitated in the control reactions that did not include phage. However, in lanes containing reactions that included phage particles, BODIPY- α -GalCer migrated as a smear, separately from phages (Figure 3.17 E).

In conclusion, the recombinant phage constructs were produced, purified and chemically modified with antigenic peptide and adjuvant molecules. The first vaccine samples contained higher ratio of adjuvant to antigen molecules, while the second batch had the high antigen to adjuvant ratio, as initially planned at the beginning of this research.

Chapter 4. ASSESSING THE PHAGE-BASED VACCINE-INDUCED IMMUNE RESPONSES IN MURINE MODELS

4.1 INTRODUCTION

This chapter describes an evaluation of innate responses (NKT cells) and adaptive cellular immune responses (peptide-specific CD8⁺ T cells) to the phage-based vaccine described in the previous section. For simplicity, from here onwards the filamentous phage will be referred to as Ff. It is essential to note that this refers to the R783 mutant strain, described in Chapter 3, which was used for production of all vaccine samples. All *in vivo* experiments were conducted in C57BL/6J mice; animal immunisations, tissue processing and flow cytometry analyses were conducted at the Malaghan Institute of Medical Research, with Kathryn Farrand. To test the structural requirements for favourable activity of the vaccine Ff.OVA, specifically the dose requirement for adjuvant and antigen, several different designs of Ff vaccines were prepared, where the antigen and adjuvant doses were altered, or the antigen was absent entirely to test for non-specific immune activity (listed in Table 6). In the experiments conducted, the Ff vaccines were compared to a previously validated vaccine that was composed of the same antigenic peptide OVA (MHC I+II) covalently conjugated to a single α -GalCer molecule, which served as a positive control

(Appendix 7.2.2) (Anderson et al., 2015; Compton et al., 2015).

During this research another study was published describing Ff-based vaccines carrying antigenic OVA peptide and non-covalently associated α -GalCer adjuvant (Sartorius et al., 2018). The novelty presented in this thesis was the ability to separately control the amounts of adjuvant molecules attached to phages. This was achieved by introducing the site-directed covalent attachment of α -GalCer adjuvant via click chemistry on displayed azide groups displayed on the major coat protein. In contrast, uncontrolled spontaneously phage-bound α -GalCer was used in the Sartorius et al. (2018) report. Furthermore, in this thesis, a combined MHC I and MHC II presented antigen-derived peptide sequences were displayed on the phage, in contrast to solely MHC I antigen-derived peptide in the (Sartorius et al., 2018) paper. The intention had been to evaluate CD4⁺ T cell responses to the MHC class II epitope in addition to the CD8⁺ T cells responses reported in this chapter. However, this was not achieved due to time constraints.

Additionally, as an essential step in evaluation of the vaccine, the adjuvant activity of molecule BODIPY- α -GalCer (described in Chapter 3) has been tested *in vivo* for the first time. The sections to follow will describe immunisation with vaccines containing different ratios of antigen and adjuvant molecules displayed along the Ff filament, and an evaluation of the ability of these vaccines to elicit immune responses. The important objective was to

establish how well these vaccines functioned compared to the validated conjugate that had a simple 1:1 ratio of antigen to adjuvant (Anderson et al., 2015; Compton et al., 2015).

4.1.1 Aim and objectives

The overall aim of the experiments described herein was to analyse the potential of Ff-based vaccines to stimulate T cell-mediated immune responses *in vivo*. The specific objectives were to:

- Analyse the potential of Ff.BODIPY- α -GalCer vaccine to present α -GalCer molecule to CD1d on iNKT cells *in vivo*.
- Analyse the OVA-specific CD8⁺ T cell adaptive immune responses in murine models immunised with Ff.OVA.BODIPY- α -GalCer vaccine and compare this response to the 1:1 molecular ratio of antigen : adjuvant conjugate vaccine.

4.2 RESULTS

For the *in vivo* testing of the Ff-based vaccine efficiency and potential use in immunotherapy, several different groups of vaccine samples were prepared. Detailed strategy for vaccine production was described in Chapter 3, and the final Ff-vaccine samples are listed in Table 6.

Table 6. Characterisations of vaccine samples for experiments in murine models.

Section	Samples*	OVA	α -GalCer**	OVA:BODIPY- α -GalCer
4.2.1	<ul style="list-style-type: none"> • Ff.FLAG • Ff.FLAG.BODIPY-α-GalCer 	n/a	4.4 μ g	n/a
4.2.2	<ul style="list-style-type: none"> • Ff.FLAG • Ff.OVA • Ff.OVA.BODIPY-α-GalCer • Ff.FLAG.BODIPY-α-GalCer 	127 ng	800 ng	1 : 25
4.2.3 4.2.4	<ul style="list-style-type: none"> • Ff.FLAG • Ff.OVA • Ff.OVA.BODIPY-α-GalCer • Ff.FLAG.BODIPY-α-GalCer • Ff.OVA+Ff.FLAG.BODIPY-α-GalCer admix • Ff.OVA+BODIPY-α-GalCer admix 	8.75 μ g	80 ng	28 : 1

*Phage vaccine samples prepared using the recombinant R783 phage strain. The table does not include control groups for immunisation trials; these will be listed in appropriate sections.

**The vaccine particles carried molecule BODIPY- α -GalCer (Section 3.2.4), the amounts calculated here are α -GalCer equivalents since each molecule consisted of α -GalCer, a fluorescent dye, a linker and a functional group for click chemistry.

4.2.1 Early iNKT (3 days) cell activation by a phage-displayed BODIPY- α -GalCer conjugate

The initial experiment was designed to assess whether the BODIPY- α -GalCer molecule can induce iNKT cell activation and proliferation when covalently attached to pVIII coat proteins of Ff particles. BODIPY- α -GalCer is a modified variant of α -GalCer with a significant fluorescent moiety (BODIPY) on the galactose (Appendix 7.2.1). This experiment was relevant because the BODIPY moiety may have impeded recognition via the iNKT cell TCR. Additionally, the glycolipid needs to be cleaved away enzymatically (by cathepsins), from the Ff particle once acquired by antigen-

presenting cells. Therefore, there was a risk that this cleavage was prevented once attached to the phage. Five animals per group (Figure 4.1) were immunised with 200 μ L of Ff-based vaccine (Ff.FLAG.BODIPY- α -GalCer) in PBS. The negative controls were PBS alone and phage without the BODIPY- α -GalCer molecule (Ff.FLAG). The positive control was free BODIPY- α -GalCer molecule. The doses were equivalent to 4.4 μ g of α -GalCer. It is important to note that this is a relatively high amount of adjuvant molecule to be administrated via *i.v.* route. In this assay, the iNKT cell activation after three days was compared in livers and spleens of immunised mice (Figure 4.1).

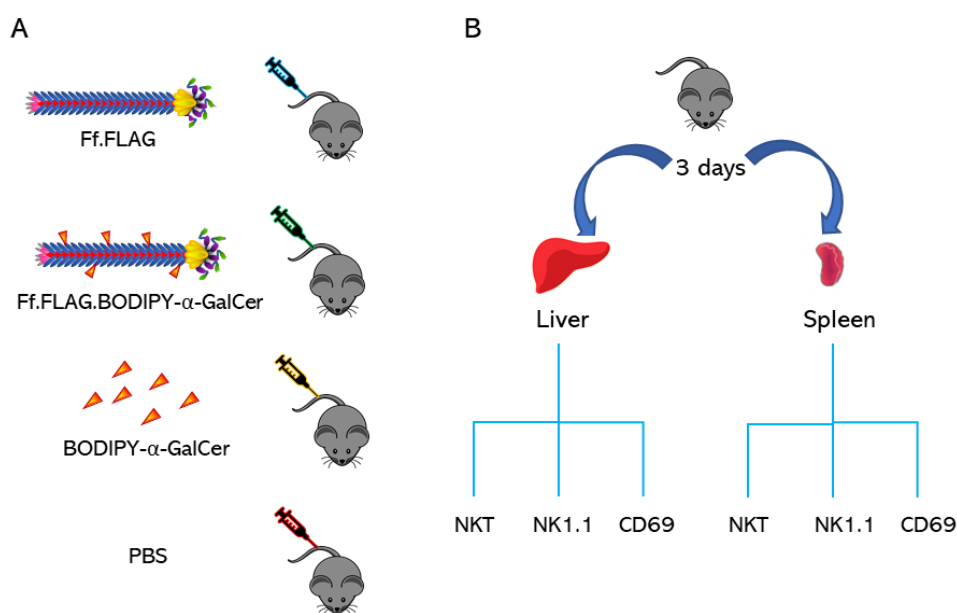


Figure 4.1. Schematic presentation of vaccine trials.

A, Immunisation of mice groups using phage particles with and without attached adjuvant molecule (Ff.FLAG.BODIPY- α -GalCer and Ff.FLAG, respectively). Free BODIPY- α -GalCer was used as a positive control, and PBS was used as a buffer control. **B**, Five mice per group were immunised on day 0. Spleens and livers were harvested on the third day for analysis of NKT numbers and characterisation of iNKT cells (positive for NK1.1 or CD69 markers).

The anti-CD3 antibody was used as a marker to identify the TCR-CD3⁺ cells within the lymphocyte populations, thereby labelling all T cells. A fluorescently labelled α -GalCer-loaded CD1d tetramer, in conjunction with α -GalCer, was applied to label the iNKT cells specifically, given that only iNKT cells contain TCR that recognises CD1d- α -GalCer complex. The gating strategy for cell analysis is presented in Figure 4.2. This consisted of gating out any cellular aggregates, followed by exclusion of dead cells identified with a live/dead fixable dye. The cells of interest within a broad lymphocyte gate were identified by back-gating on staining for CD3. A channel was also used to exclude highly auto-fluorescent cells. An antibody to B220, an isoform of CD45, was used to identify and exclude B cells, as they can attract non-specific binding by the α -GalCer-loaded CD1d tetramer. Finally, antibodies to the activation marker CD69, and NK1.1, were used in conjunction with the tetramer and anti-CD3 to identify the iNKT cells and define activation status. It is important to note that iNKT cells express intermediate levels of CD3.

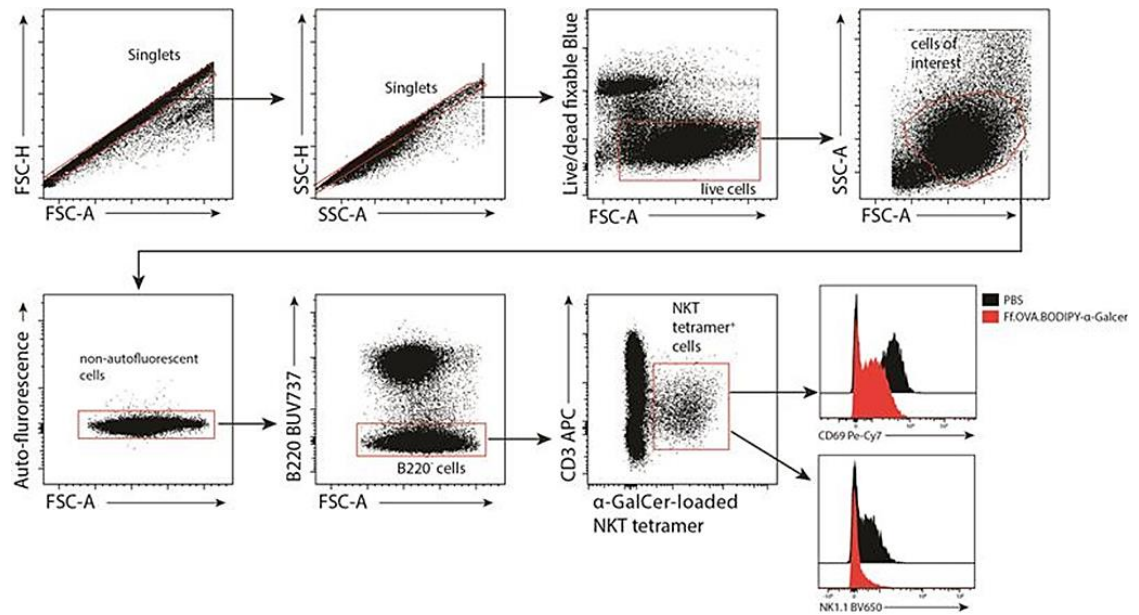


Figure 4.2. Gating strategy for iNKT cell analyses by flow cytometry.

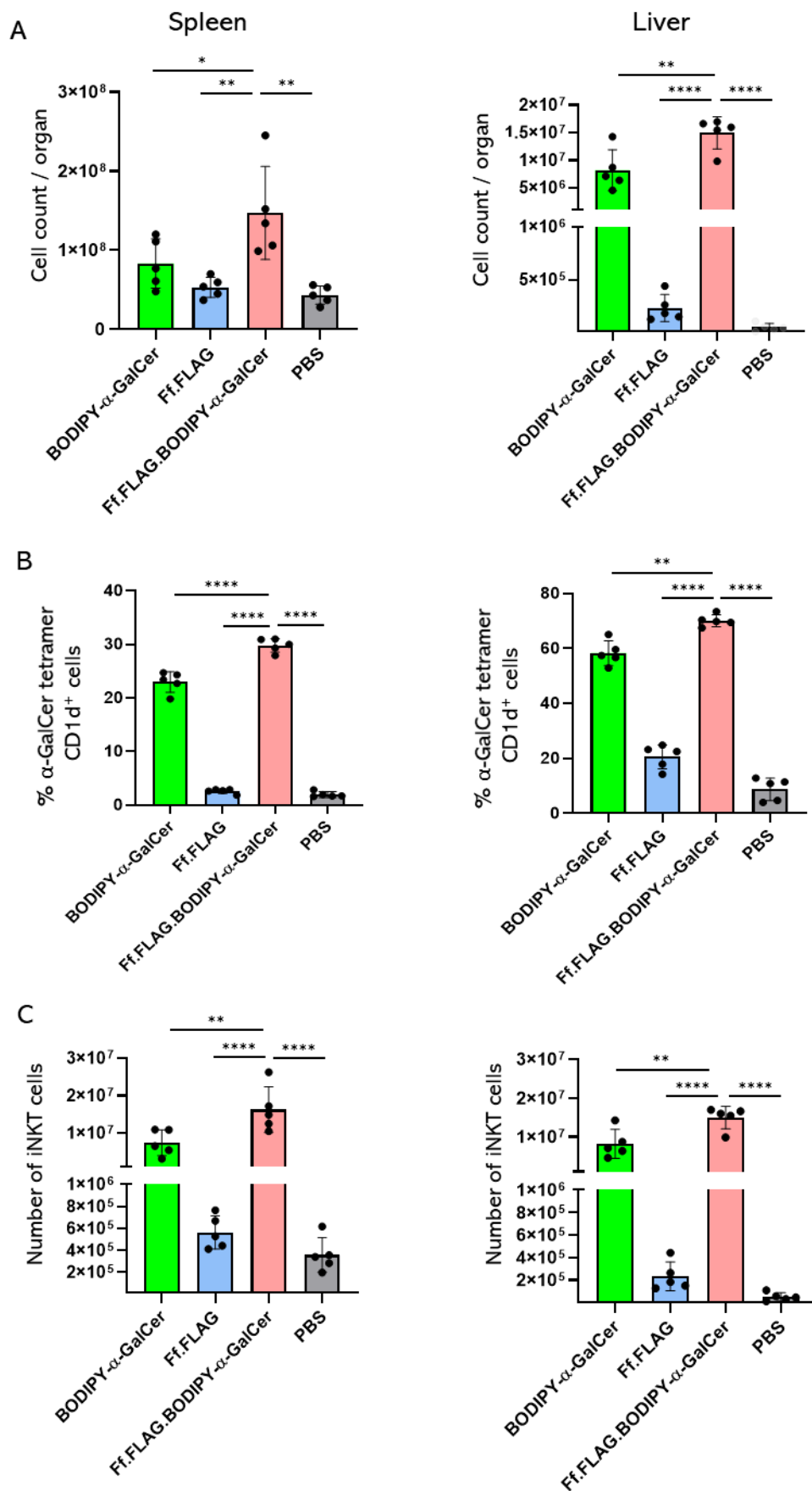


Figure 4.3. Total cell count comparison and iNKT composition in the liver and spleen three days after BODIPY- α -GalCer stimulation.

A, Total cell count per organ of the spleen (left) and liver (right) of immunised animals. Cell count is proportional to the organ sizes. **B**, Mean percentages of CD3^{int} α -GalCer tetramer CD1d⁺ cells for each experimental group. **C**, Numbers of iNKT cells per organ from each experimental group. Error bars represent SD; dots represent values from the individual animals. One-way ANOVA analysis and Tukey's multiple comparisons test were used to calculate the statistical significance, (**** $p \leq 0.0001$, *** $p \leq 0.001$; ** $p \leq 0.01$; * $p \leq 0.05$) presented in Appendix 7.4.1.

The results of the 3-day post-vaccination analysis are presented in Figure 4.3. The first obvious difference was enlarged spleen and liver size (documented as a total cell count) in experimental groups that were injected with samples containing adjuvant BODIPY- α -GalCer, either in free form or attached to the phages. An increase in iNKT cell proportion based on upregulation of all live cells in these same animals CD69 and NK1.1 markers (Figure 4.3B), suggesting iNKT cells accounted for at least some of the increased cell number in each organ. In fact, animals treated with the adjuvant compounds had significantly increased numbers of iNKT cells when compared to PBS and Ff.FLAG treated groups (Figure 4.3C). The total number of iNKT cells in the spleen and liver was increased 10 to 100-fold (Figure 4.3). The animals injected with the phage-displayed BODIPY- α -GalCer resulted in a significantly higher titre of the iNKT cells in comparison to the free BODIPY- α -GalCer-injected group in both the liver and spleen ($p < 0.01$), highlighting an advantage to phage-mediated delivery. Of interest, there was a small but significant increase in percentage of iNKT cell in the livers of animals

that received Ff.FLAG, when compared to PBS control (Appendix 7.4.1). Perhaps this could be suggesting some low levels of iNKT cell stimulation induced by the phages alone.

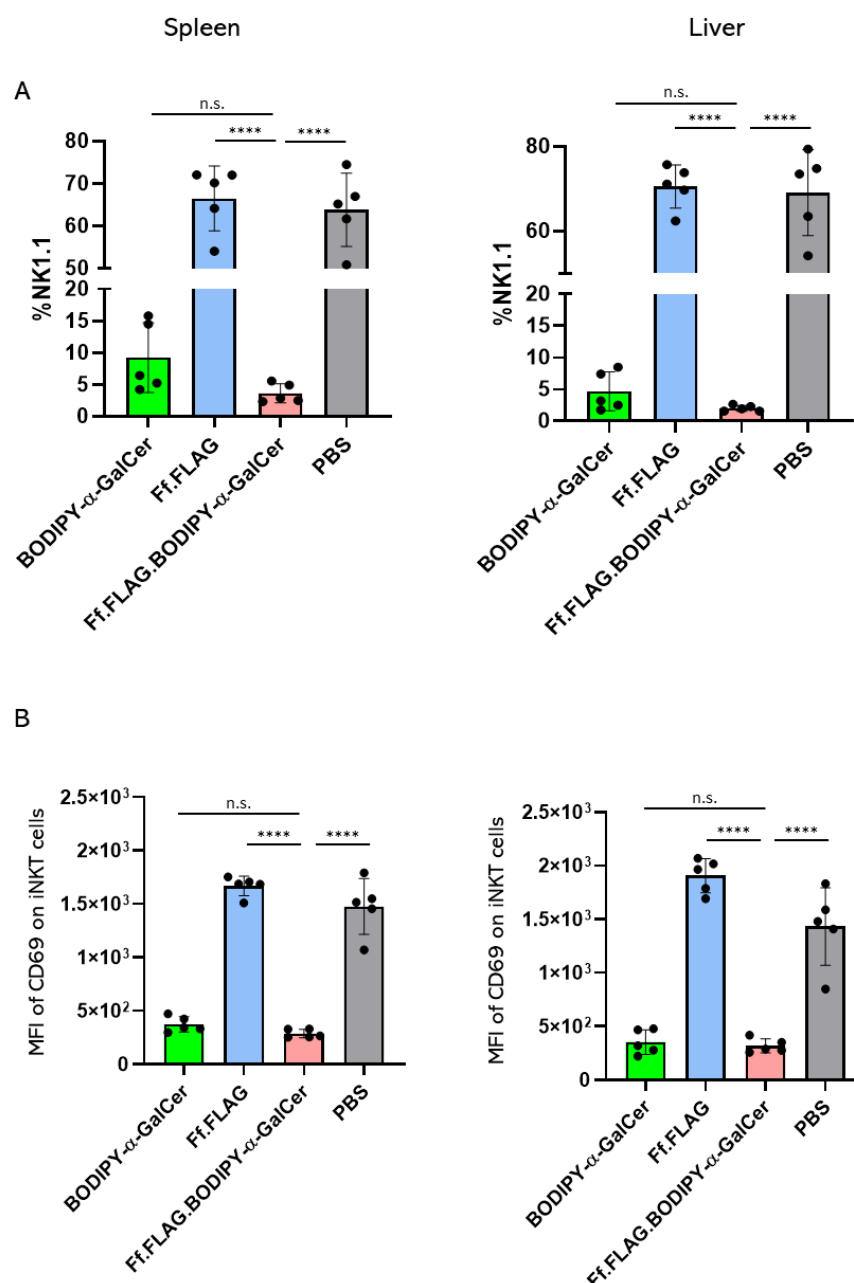


Figure 4.4. iNKT cells analysed for the presence of the NK1.1 and CD69 markers.

Both NK1.1 and CD69 markers were expected to be downregulated three days post-immunisation in vaccine groups injected with the adjuvant molecule BODIPY- α -GalCer. **A**, Mean percentage of NK1.1⁺ iNKT cells of all gated iNKT cells in each experiment group. **B**, Mean fluorescence intensity (MFI) of CD69 on iNKT cells for each experiment group. Error bars represent SD; dots represent values from the individual animals. One-way ANOVA analysis and Tukey's multiple comparisons test were used to

calculate the statistical significance (**** $p \leq 0.0001$, *** $p \leq 0.001$; ** $p \leq 0.01$; * $p \leq 0.05$) presented in Appendix 7.4.1.

Three days after immunisation with BODIPY- α -GalCer-containing vaccine, it was expected that activated iNKT cells would have downregulated the marker NK1.1 on the cell surface in addition to the rapid increase of the total cell numbers. The frequencies (in percentages) of NK1.1⁺ cells within the iNKT population from five animals were plotted (**Figure 4.4A**). There was a significantly reduced frequency observed in the groups that received BODIPY- α -GalCer (free or phage-conjugated) vs. corresponding controls (PBS or phage; $p < 0.0001$), indicative of BODIPY- α -GalCer-triggered iNKT activation (Appendix 7.4.1), which aligned with the trends observed in Figure 4.3.

The iNKT cells from this experiment were analysed for another early marker of activation, CD69 (Bennstein, 2017), as presented in Figure 4.4B. Although this marker is typically initially upregulated (in the hours immediately after activation), its kinetics of expression can vary depending on strength of stimulus. With a strong ligand like α -GalCer, CD69 declines to sub-baseline levels by day three. This type of response was observed in the groups injected with BODIPY- α -GalCer, with a significantly lower number of CD69⁺ cells in comparison to the controls. The increase in iNKT cell proportion in liver ($p = 0.01$) seen when Ff.FLAG was compared to PBS control, perhaps further supports the idea

that there was some limited iNKT cell activity induced with phage alone, as mentioned earlier.

Upon establishing that the vaccine-induced changes in iNKT cell population size and phenotype were equally detectable in livers and spleens of immunised mice, in the following experiments, only spleens were harvested.

4.2.2 Ff-derived OVA vaccine testing at a low antigen to BODIPY- α -GalCer ratio

Having established that iNKT cells are activated by BODIPY- α -GalCer, it was assumed that their “cellular adjuvant” activities would be stimulated by recombinant Ff vaccines. The capacity of a Ff.OVA.BODIPY- α -GalCer vaccine to stimulate T cell responses was therefore evaluated in mice. This vaccine is an Ff phage construct (R783), displaying OVA (MHC I + MHC II) antigenic peptide as a major coat protein pVIII fusion, and BODIPY- α -GalCer via covalent attachment to pVIII-displayed azides using the click chemistry (Section 3.2.4). A group immunised with PBS alone was used to monitor background T cell levels, whereas a group immunised with a 1:1 direct α -GalCer : OVA peptide conjugate vaccine was used as a positive control as it is known to induce the proliferation of OVA-specific T cells (Anderson et al., 2015). It is important to note that OVA- α -GalCer is a chemical conjugate of the same OVA peptide (MHC I + MHC II) attached to the α -GalCer molecule (Appendix

7.2.2), via the same enzymatically cleavable linker as the one in the OVA peptide used for the Ff-based vaccine.

To determine whether BODIPY- α -GalCer caused a stronger adaptive response when attached to phage particles vs. administered as a free adjuvant, a control group injected with Ff.OVA mixed with free BODIPY- α -GalCer was included. For this control, the Ff.OVA phage displayed the OVA peptide in the same manner and numbers per phage as the test vaccine, evaluated by ELISA (Appendix 7.3.6). Another control group was immunised with phages that were OVA antigen-negative, expressing a short peptide, FLAG-tag (Ff.FLAG). A further group was immunised with a version of Ff.FLAG that was decorated with the BODIPY- α -GalCer covalently attached to pVIII-displayed azides using the click chemistry, in the same manner as in the vaccine (Ff.FLAG.BODIPY- α -GalCer). This is the same BODIPY- α -GalCer-displaying vaccine as used in the previous section for testing the iNKT activation, but with lowered BODIPY- α -GalCer concentration (Table 6). The reason for lowering the adjuvant concentration from 4.4 μ g/dose to 800 ng/dose was to bring it closer to standardly used 200 ng/dose for *in vivo* studies in α -GalCer controls (I. Hermans 2019, personal communication, 18 February). The level of iNKT cell activation seen in the previous experiment suggested that modifications to α -GalCer had not compromised iNKT cell activation. Moreover, the levels of activation with BODIPY- α -GalCer were comparable to those observed with previously used unmodified α -GalCer molecule

(I. Hermans 2019, personal communication, 18 February). Therefore, for the assessment of adaptive immune responses, a lower dose was expected to be sufficient for the positive control vaccine (OVA- α -GalCer 1 : 1 conjugate) to induce strong T cell responses. Vaccine groups displaying the OVA peptide carried 127 ng/dose of antigenic peptide, and BODIPY-labeled adjuvant equivalent to 800 ng/dose of α -GalCer. This composition gave a total 1:25 ratio of OVA: α -GalCer in the phage-based vaccines.

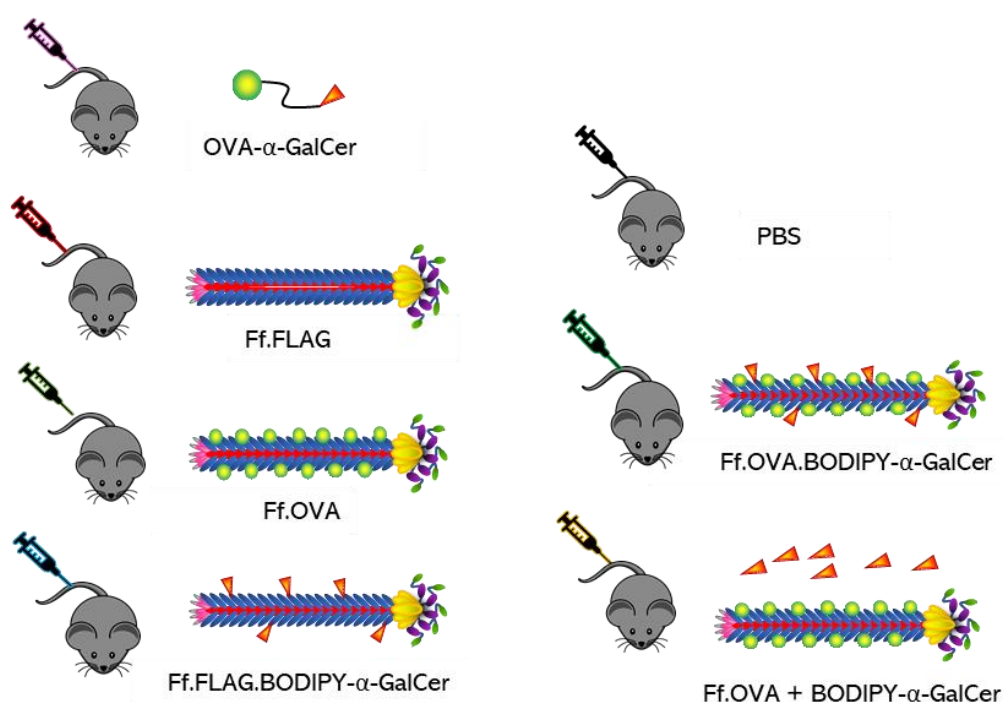


Figure 4.5. Mice groups for immunisation with phage vaccines. The positive control was OVA- α -GalCer conjugate molecule (Appendix 7.2.2), buffer background control group was PBS alone. Phage group carrying FLAG-tag was used as a phage control group, with and without displayed adjuvant (Ff.FLAG, and Ff.FLAG.BODIPY- α -GalCer). Test group (Ff.OVA.BODIPY- α -GalCer) was compared to vaccine particles without adjuvant (Ff.OVA), and with separately administered adjuvant molecules (Ff.OVA + BODIPY- α -GalCer). Blood samples were collected, and spleens harvested from five mice per group, seven and nine days, respectively, after immunisation.

Five animals in each group were immunised with 200 μ L of each of the seven vaccine preparations i.v. as described in Section 2.6.1. Cartoons of the structures are given in Figure 4.5.

4.2.2.1 OVA-specific CD8⁺ T cell responses

The mice groups from Figure 4.5 were monitored for the presence of an expanded pool of OVA-specific CD8⁺ T cells in blood seven days after vaccination *in vivo* with the Ff-based vaccines. Gating for the OVA-specific T cells by flow-cytometry is presented in Figure 4.6, and the results are presented in Figure 4.7. Briefly, aggregates and dead cells were excluded, and a general lymphocyte “gate of interest” was determined by back-gating based on staining with anti-CD8 antibody. The B cells were then excluded, and assessment of CD44 fluorescent OVA-pentamers were used in conjunction with anti-CD8 to detect the OVA-specific CD8⁺ T cells. Here “OVA-pentamer” refers to OVA-loaded complex of five covalently conjugated soluble MHC I H-2K^b molecules (corresponding to the MHC I haplotype in C57BL/6J murine line used in the vaccination trial). The pentamer had been loaded with an epitope from OVA protein (SIINFEKL), hence it binds specifically to the OVA-specific TCR on the OVA⁺ CD8⁺ T cells. Therefore, OVA-pentamer can be used to detect the OVA-specific T cells that have undergone clonal expansion as a result of vaccine-elicited activation. Assessment of upregulation of CD44, an activation marker,

was used to further distinguish memory and effector CD8⁺ T cells from their naïve counterparts.

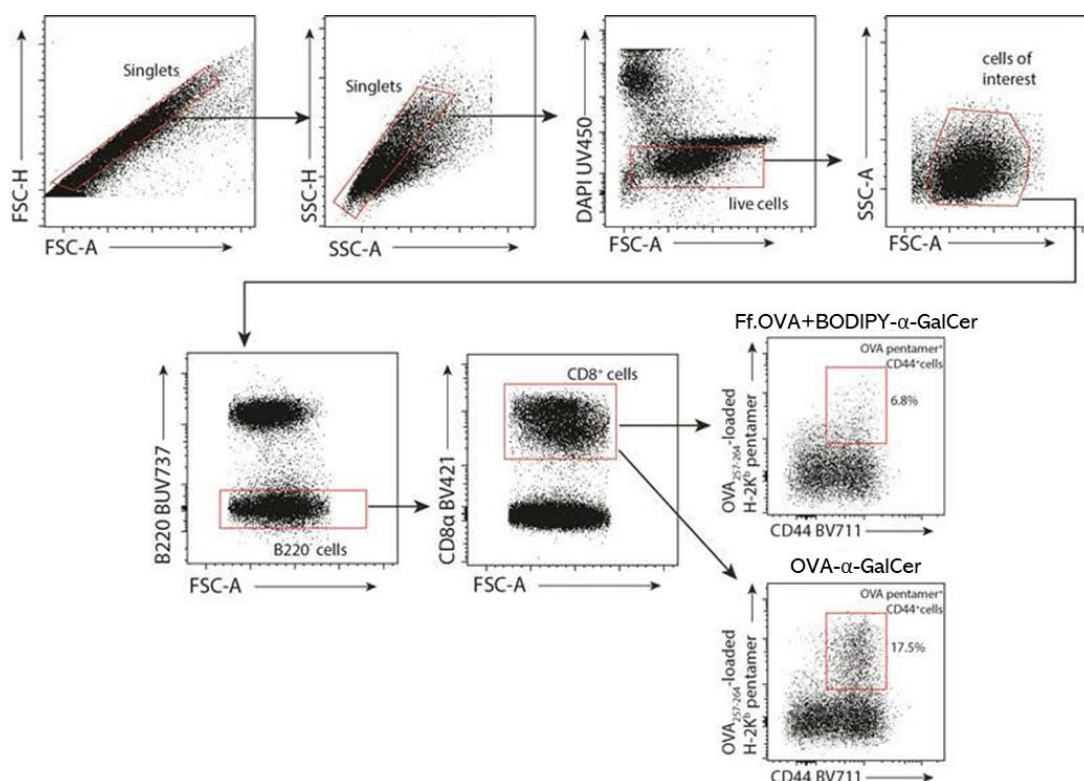
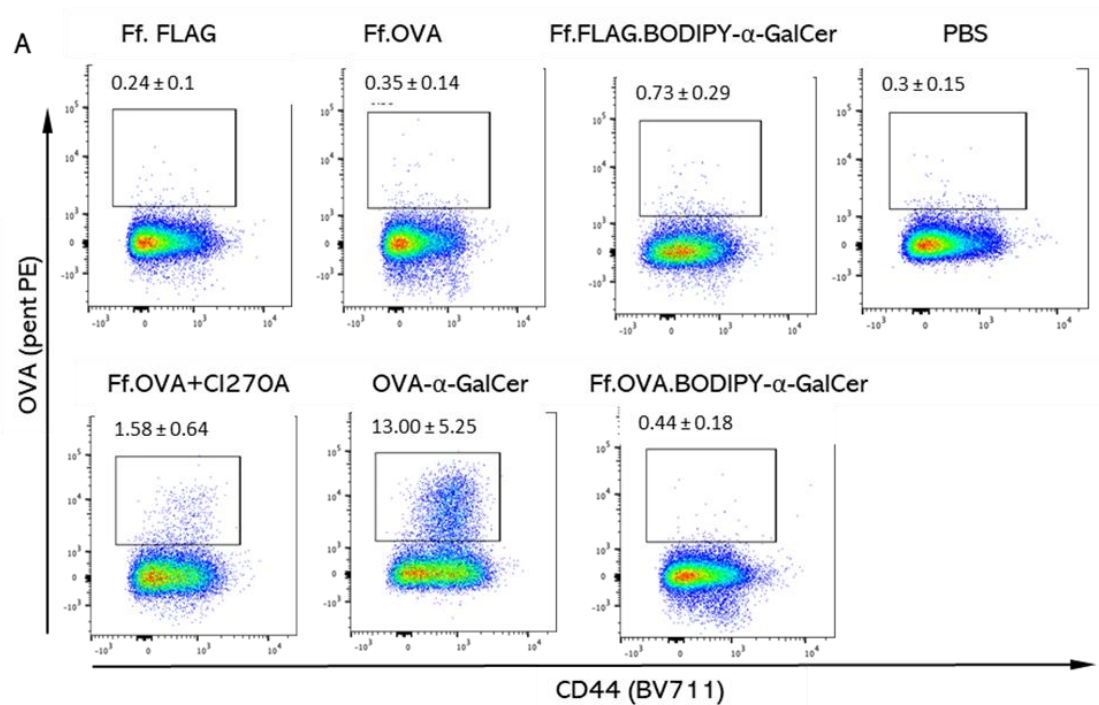


Figure 4.6. Representative plots for gating strategy from OVA-α-GalCer vaccinated group for analysis of vaccine-induced CD8⁺ T cell by fluorescence-activated cell sorting.

Cells were first gated for singlets, to exclude clumps and then for viability. After excluding the B cells (B220⁺), "cells of interest" - a broad lymphocyte gate - was determined by backgating based on staining with anti-CD8. Then OVA-specific CD8⁺ T cells were identified with anti-CD8 and OVA pentamer, with the expected upregulation of CD44 used to help define the population.



B

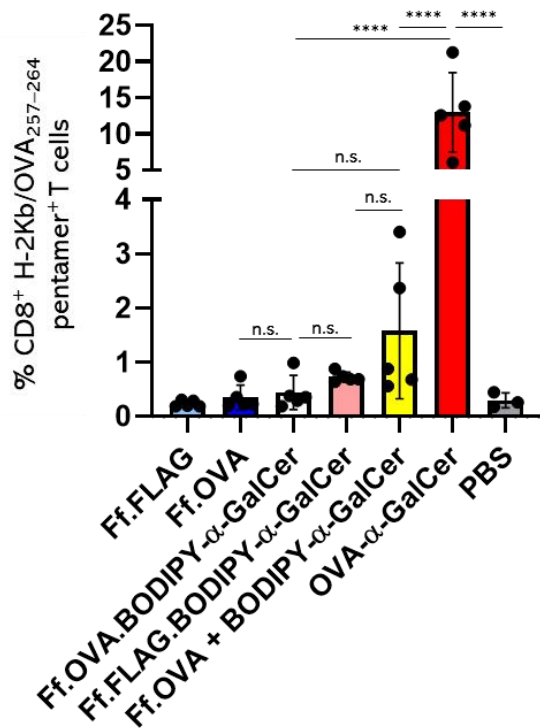


Figure 4.7. Detection of OVA-specific CD44^{hi} CD8⁺T cells in blood seven days post-immunisation.

A, Representative flow cytometry plots from each of the seven experimental groups, showing analysis of gated CD8⁺ cells. Mice groups were immunised as shown in Figure 4.5, and the blood samples were analysed seven days after the immunisation. Buffer control was PBS, and positive control was OVA- α -GalCer conjugate vaccine. OVA-specific T cells were gated as indicated by the squares in each plot, defined as CD44^{hi} OVA pentamer⁺ cells. The numbers indicate mean percentage of OVA-specific cells within the CD8⁺ population, and standard deviation, for each experimental group of 5 animals. **B**, Graph of mean percentage of OVA-specific cells within the CD8⁺ population per treatment group, with standard deviation and individual scores shown. Summary plot of OVA-specific CD8⁺ T cells in all animals. One-way ANOVA analysis and Tukey's multiple comparisons test were used to calculate the statistical significance (**** $p \leq 0.0001$, *** $p \leq 0.001$; ** $p \leq 0.01$; * $p \leq 0.05$) presented in Appendix 7.4.2.

It was hypothesised that the 25-fold higher OVA antigen dose on the Ff particles would provoke a stronger OVA-specific CD8⁺ T cell response compared to the OVA- α -GalCer conjugate used as a control. However, as presented in Figure 4.7D, there were only limited T cell responses to the Ff vaccines, whereas the conjugate vaccine induced a statistically significant response. Furthermore, it had been anticipated that there would be an advantage to including the antigen and adjuvant in the one phage; however, again this was not the case. In fact, the highest OVA-specific T cell responses induced with the phage in any animal were observed in the group where Ff.OVA was admixed with the adjuvant (yellow bar, Ff.OVA + BODIPY- α -GalCer). Although, the variations in that group were high with a positive outcome in only 2 out of 5 mice, (top two dots in the yellow bar), and the overall response for this group was not statistically different over those seen in animals injected with the other phage or buffer

controls (Appendix 7.4.4). Overall, the flow cytometry analysis showed $1.58 \pm 0.64\%$ OVA-specific CD8⁺ T cells in Ff.OVA + BODIPY- α -GalCer group.

Interestingly, when the conjugate vaccine control OVA- α -GalCer (red bar) is omitted from the statistical analysis, in order to assess if the phage-based vaccine induced any T cell activity (Appendix 7.4.4), the admix group of Ff-vaccine with the adjuvant molecule (Figure 4.7, yellow bar) showed the significant increase in percent of OVA-specific CD8⁺ T cells ($p = 0.0497$) relative to the buffer control (Appendix 7.4.4).

4.2.2.2 iNKT cell activation after nine days

The low OVA-specific CD8⁺ T-cell activation by the Ff-based vaccines in previous experiment (Figure 4.7) was unexpected given the robust proliferation of iNKT cells that the BODIPY- α -GalCer-conjugated phage vaccines have induced in the trial experiment, on par and with the positive control vaccine (Figure 4.3) and raised the possibility that the lower dose of adjuvant BODIPY- α -GalCer used (800 ng) compared to the first experiment (4.4 μ g) was an issue. As the adaptive immune response induction was proposed to be via iNKT cell-mediated DC activation, it was necessary to establish that the iNKT cells had indeed been activated at the lower dose. To this end, iNKT cells from spleen were analysed at the end of the experiment (at day 9; Figure 4.8). Proliferation of stimulated iNKT cells peaks three days after the stimulation with α -GalCer (Van Kaer et al.,

2015), after which their numbers slowly drop. However, iNKT cell levels remain above baseline for many days, with NK1.1 and CD69 still downregulated. At the outset of this study, it was known that analysis on day 7 can be used as a readout successful iNKT cell stimulation with the 1:1 conjugate vaccine (Holz et al., 2020). Although conducted here at day 9, it was anticipated that successful iNKT cell stimulation would still be reflected by increased iNKT cells numbers and/or downregulation of NK1.1 and CD69.

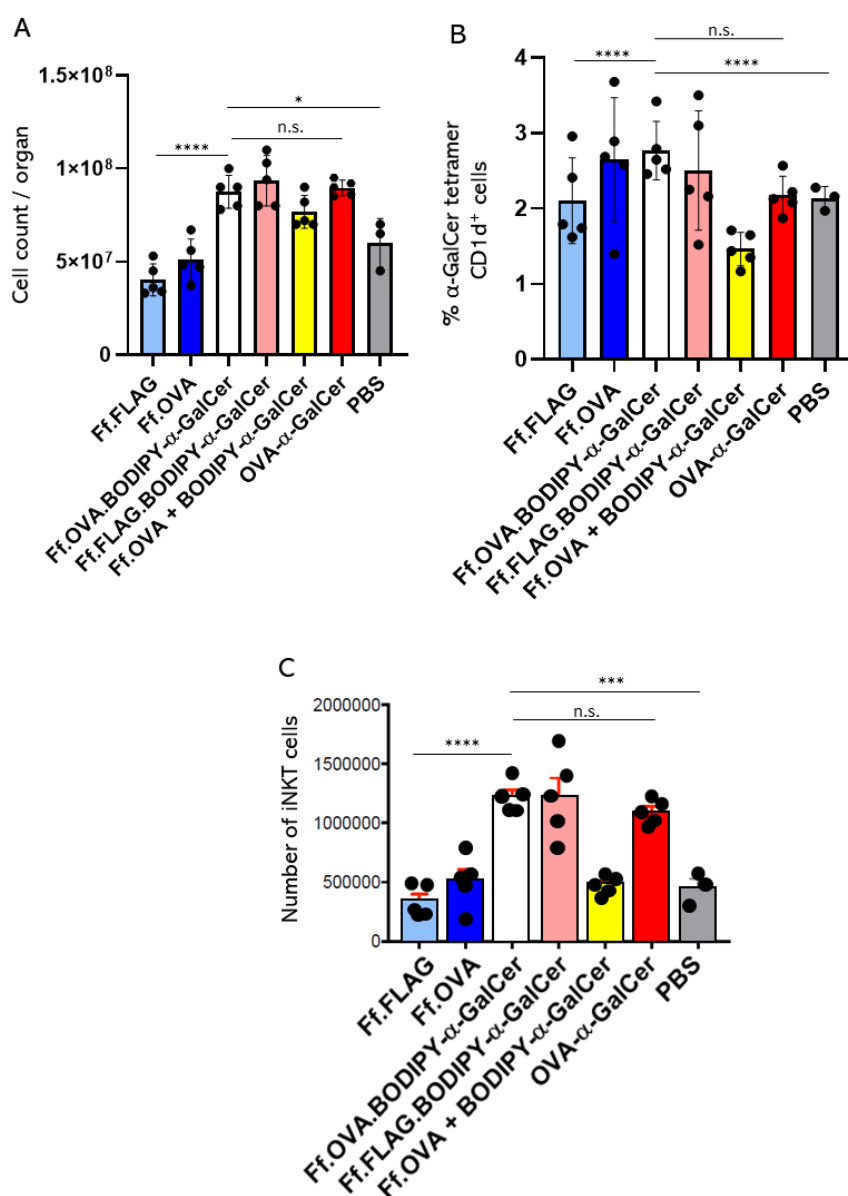


Figure 4.8. Analysis of iNKT cells in spleen nine days after vaccination. **A**, Total cell count per organ of immunised animals. Cell count is proportional to the organ sizes. **B**, Mean percentages of CD3^{int} α -GalCer tetramer CD1d⁺ cells for each experimental group. **C**, Numbers of iNKT cells per organ from each experimental group. Error bars represent SD; dots represent values from the individual animals. One-way ANOVA analysis and Tukey's multiple comparisons test were used to calculate the statistical significance (**** $p \leq 0.0001$, *** $p \leq 0.001$; ** $p \leq 0.01$; * $p \leq 0.05$) presented in Appendix 7.4.3.

Analysis of iNKT cell numbers did show increases were significantly higher than in animals injected PBS control (Figure 4.8C). Similar trends were observed in the conjugate OVA- α -GalCer positive control, and in groups where BODIPY- α -GalCer molecule was chemically attached to Ff. Perhaps surprisingly, in the group where Ff.OVA was mixed with BODIPY- α -GalCer (yellow bar), which had induced a limited OVA-specific T cell response, no obvious expansion of the iNKT cell population was observed.

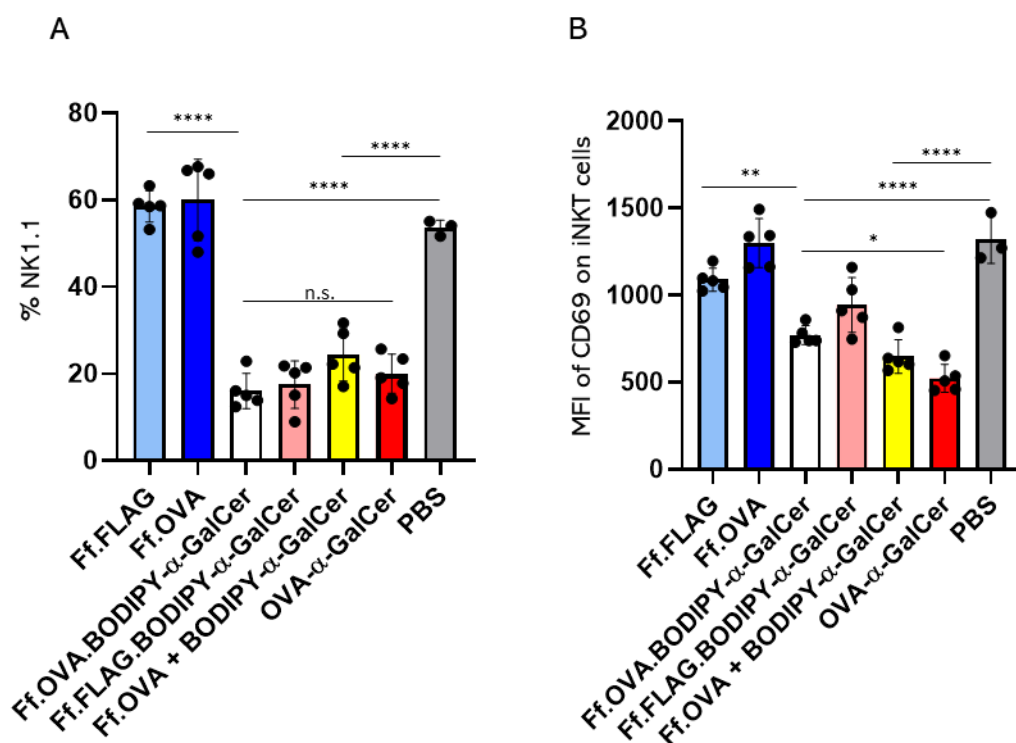


Figure 4.9. iNKT cells from spleen analysed for the presence of the NK1.1 and CD69 markers.

Both NK1.1 and CD69 markers were expected to be downregulated nine days post-immunisation in vaccine groups injected with the adjuvant molecule BODIPY- α -GalCer. **A**, Mean percentage of NK1.1⁺ iNKT cells of all gated iNKT cells in each experiment group. **B**, Mean fluorescence intensity (MFI) of CD69 on iNKT cells for each experiment group. Error bars represent SD; dots represent values from the individual animals. One-way ANOVA analysis and Tukey's multiple comparisons test were used to calculate the statistical significance (**** $p \leq 0.0001$, *** $p \leq 0.001$; ** $p \leq 0.01$; * $p \leq 0.05$) presented in Appendix 7.4.3.

The iNKT populations gated using the strategy outlined in Figure 4.2 were analysed for the expression levels of NK1.1, and CD69 markers in the same manner as in Section 4.2.2. All groups immunised with vaccines containing BODIPY- α -GalCer showed similar downregulation of NK1.1⁺ as the control OVA- α -GalCer group (Figure 4.9A), while there was accompanying a trend towards reduced expression of CD69 marker (Figure 4.9B). The marginal increase in the OVA-specific CD8⁺ T-

cells in the group vaccinated Ff.OVA admixed with BODIPY- α -GalCer, therefore, did not correlate with the proliferation of iNKT cells.

Based on the statistically significant increase in the iNKT cells in this experiment (day 9; Figure 4.8C), it can be concluded that activation of iNKT cells has occurred in groups exposed to chemically phage-attached BODIPY- α -GalCer. Therefore, the lack of OVA-specific T cell response to Ff-based vaccines could not be attributed to a general loss of iNKT cell functions. However, it remains puzzling that the group with admixed Ff.OVA + BODIPY- α -GalCer did not show significant difference in iNKT cell numbers.

4.2.3 Ff-derived OVA vaccine testing at a high antigen to BODIPY- α -GalCer ratio

4.2.3.1 OVA-specific CD8⁺ T cell responses on day 7

A reason for low immunogenicity of the Ff-based vaccines could have been the low dose of the antigen injected (127 ng per dose). To achieve a higher dose, a third set of vaccine samples with an increased antigen : adjuvant ratio was prepared to substantially increase the Ff particles therefore carried covalently attached BODIPY- α -GalCer molecules equivalent to 80 ng of α -GalCer, and 1.4 μ g of OVA peptide per vaccine dose, having the OVA : BODIPY- α -GalCer molecules. This was therefore a >ten-fold increase in OVA

peptide per injected dose compared to the previously prepared vaccines, giving a molar ratio of 45:1 (Table 6).

In analysing the new vaccines, all adjuvant and antigen doses in Ff-based vaccines were equivalent across the different treatment groups. In addition to the seven experimental groups used in the previous section (Figure 4.5), one more control group was added. To compare the iNKT stimulation from BODIPY- α -GalCer adjuvant molecules when they are attached to a separate phage particle (rather than being applied as a free molecule), additional group was included. This group received a mix of antigen-carrying phage and adjuvant-carrying phage (Ff.FLAG.BODIPY- α -GalCer + Ff.OVA). Seven days after mice had been injected, blood samples were analysed for levels of OVA-specific CD8⁺ T cells by flow cytometry to assess the antigen-specific immune responses induced by the different Ff-vaccines. Figure 4.10 shows the results of this analysis, where levels of CD44^{hi} OVA⁺ CD8⁺ T cells were evaluated. The gating strategy was the same as in the earlier experiment (Figure 4.6).

There were two ways to assess this experiment with respect to OVA-specific CD8⁺ T-cell induction: (i) comparison of Ff vaccines to the conjugate OVA- α -GalCer (Figure 4.10B); (ii) comparison of Ff-based vaccines to the PBS buffer control without the positive OVA- α -GalCer control (Appendix 7.4.4), same as in the previous experiment (Section 4.2.2.1).

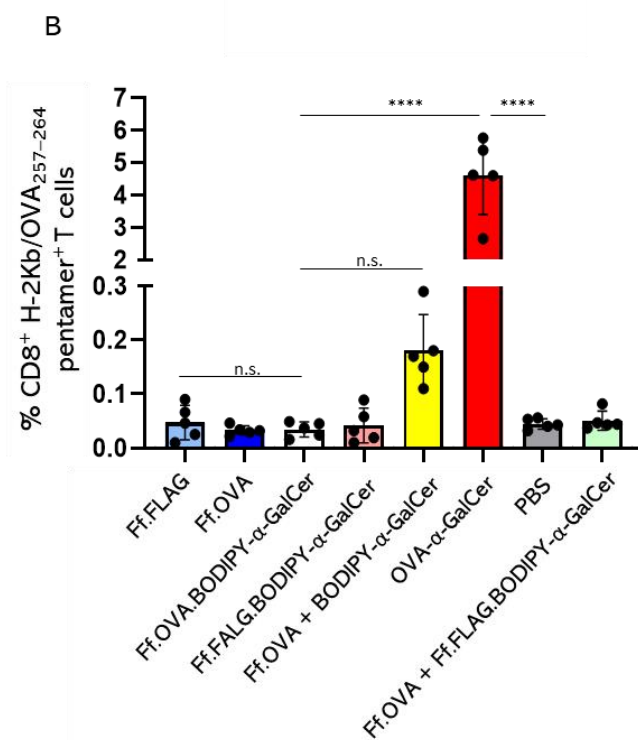
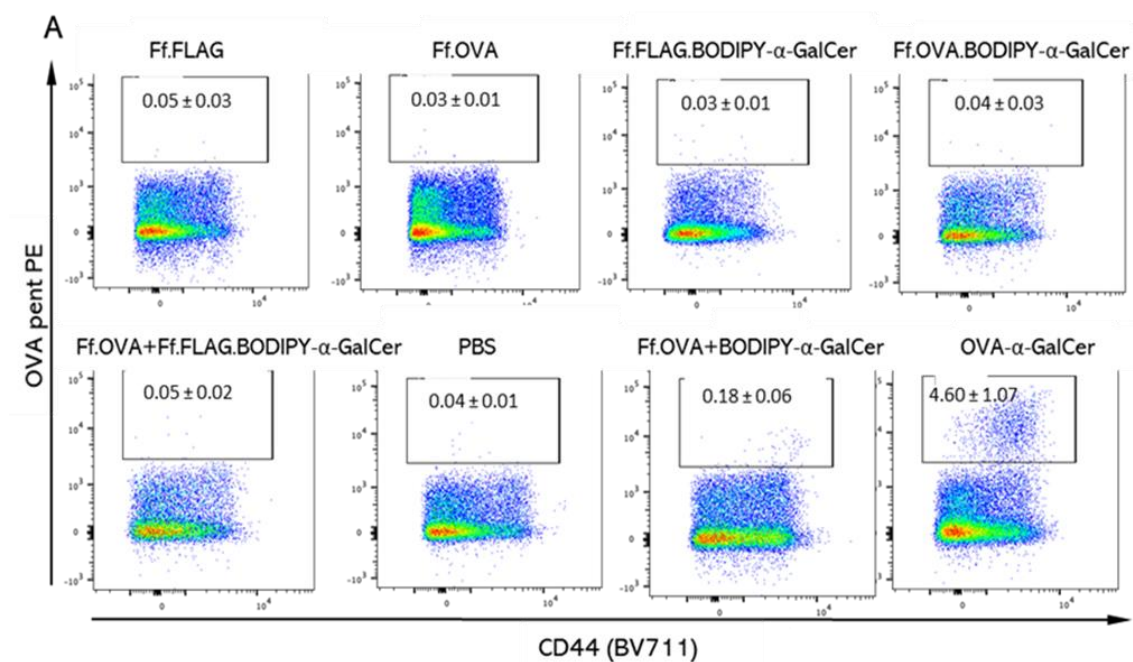


Figure 4.10. Detection of OVA-specific CD44^{hi} CD8⁺ T cells in blood seven days post-immunisation.

A, Representative flow cytometry plots from each of the seven experimental groups, showing analysis of gated CD8⁺ cells. Mice groups were immunised, as shown in Figure 4.5 with additional control group added (bottom left plot). The blood samples were analysed seven days after the immunisation. Buffer control was PBS, and positive control was OVA- α -GalCer conjugate vaccine. OVA-specific T cells were gated as indicated by the squares in each plot, defined as CD44^{hi} OVA pentamer⁺ cells. The numbers indicate mean percentage of OVA-specific cells within the CD8⁺ population, and standard deviation, for each experimental group of 5 animals. **B**, Graph of mean percentage of OVA-specific cells within the CD8⁺ population per treatment group, with standard deviation and individual scores shown. Summary plot of OVA-specific CD8⁺ T cells in all animals. One-way ANOVA analysis and Tukey's multiple comparisons test were used to calculate the statistical significance (**** $p \leq 0.0001$, *** $p \leq 0.001$; ** $p \leq 0.01$; * $p \leq 0.05$) presented in Appendix 7.4.4).

The only treatment that induced a significant rise in CD44^{hi} OVA-specific CD8⁺ T cells compared to PBS-injected controls was again the positive control, 1:1 conjugate vaccine OVA- α -GalCer (Figure 4.10). Thus, in answer to the first question, the Ff vaccines performed poorly compared to the synthetic conjugate. To ask the second question - whether the Ff vaccines induced a response at all - the results from the group injected with the positive control (direct antigen- α -GalCer conjugate vaccine) was omitted from the statistical analysis. This analysis showed some responsiveness in the group where Ff.OVA was admixed with the adjuvant (yellow bar; Ff.OVA + BODIPY- α -GalCer), which was significant ($p < 0.0001$) when compared to the PBS control (Appendix 7.4.4). These findings were consistent with the previous experiment (Section 4.2.2) and suggested that increasing dose of OVA peptide (in this case by more than

10-fold), could not increase the immunogenicity of the Ff-based vaccines.

4.2.3.2 iNKT cell activation after eight days

Because the BODIPY- α -GalCer dose had been further reduced in the vaccines used in this experiment, it was necessary to confirm that iNKT cells had been activated. This second reduction in adjuvant numbers was for technical reasons, as the phage growth conditions were re-optimised to increase the expression of pVIII-antigen fusion in order to allow highest possible numbers of antigenic peptides displayed per phage (Section 3.2.2.1). The impact of vaccination on iNKT cells in spleens was analysed at the end of the experiment, at day 8 (Figure 4.11).

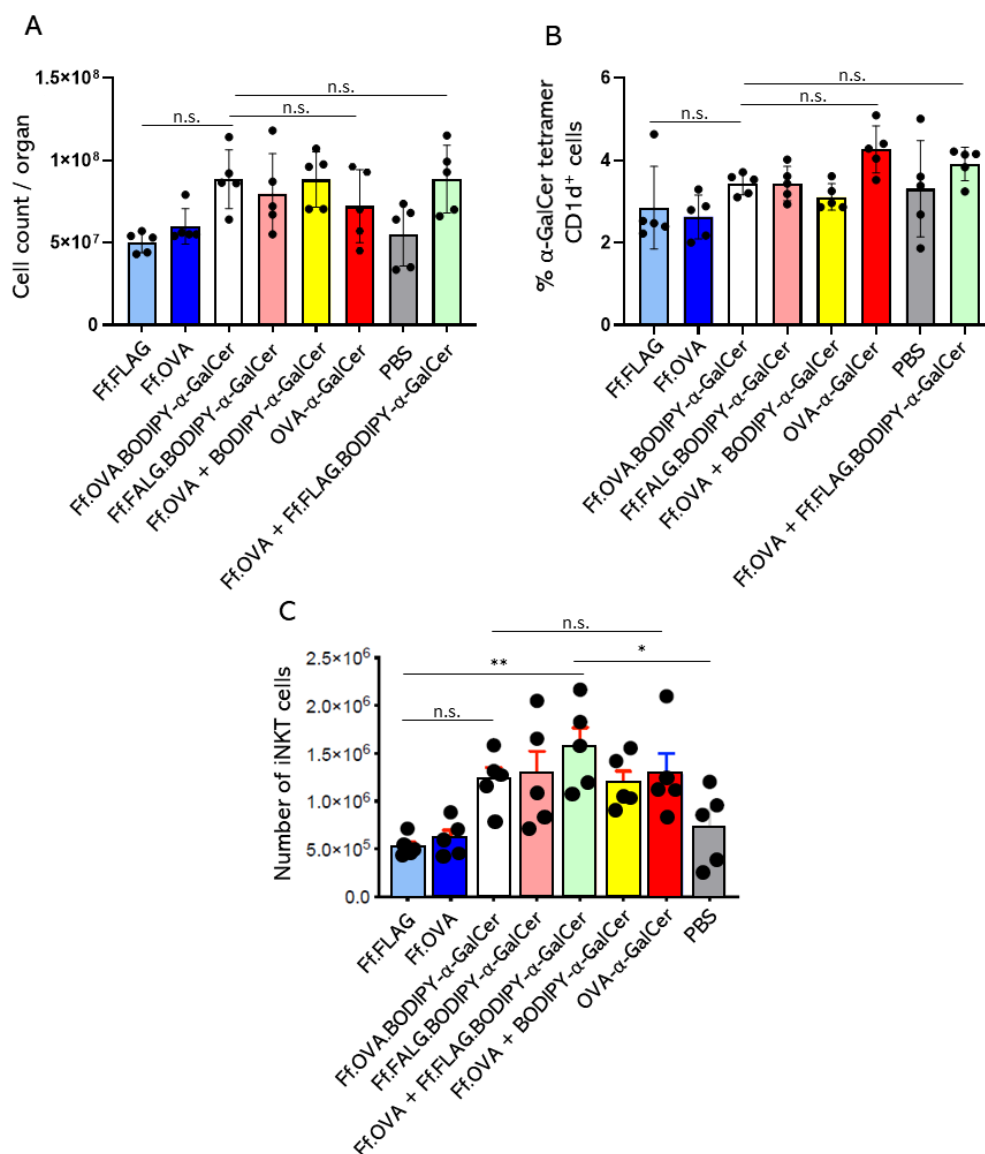


Figure 4.11. Total cell count comparison and iNKT composition in the spleen eight days after the phage-based vaccine stimulation.

A, Total cell count per organ of immunised animals. Cell count is proportional to the organ sizes. **B**, Mean percentages of CD3^{int} α-GalCer tetramer CD1d⁺ cells for each experimental group. **C**, Numbers of iNKT cells per organ from each experimental group. Error bars represent SD; dots represent values from the individual animals. One-way ANOVA analysis and Tukey's multiple comparisons test were used to calculate the statistical significance (**** $p \leq 0.0001$, *** $p \leq 0.001$; ** $p \leq 0.01$; * $p \leq 0.05$) presented in Appendix 7.4.5.

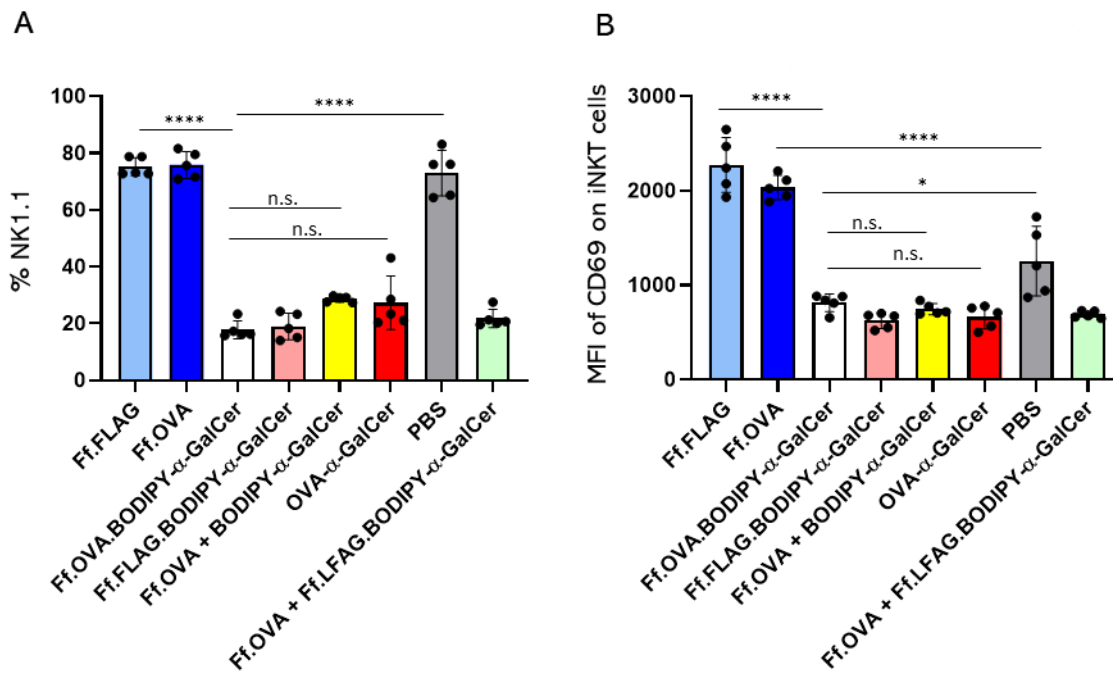


Figure 4.12. iNKT cells from spleen analysed for the presence of the NK1.1 and CD69 markers.

Both NK1.1 and CD69 markers were expected to be downregulated eight days post-immunisation in vaccine groups injected with the adjuvant molecule BODIPY- α -GalCer. **A**, Mean percentage of NK1.1⁺ iNKT cells of all gated iNKT cells in each experiment group. **B**, Mean fluorescence intensity (MFI) of CD69 on iNKT cells for each experiment group. Error bars represent SD; dots represent values from the individual animals. One-way ANOVA analysis and Tukey's multiple comparisons test were used to calculate the statistical significance (**** $p \leq 0.0001$, *** $p \leq 0.001$; ** $p \leq 0.01$; * $p \leq 0.05$) presented in Appendix 7.4.5.

There was a repeated trend towards increased iNKT expansion in all BODIPY- α -GalCer treated groups relative to the buffer control (Figure 4.11C), but there was no significant difference when compared to groups that were injected with phage in the absence of adjuvant molecules (Appendix 7.4.5). Only Ff.OVA + Ff.FLAG.BODIPY- α -GalCer showed a significant increase in iNKT numbers when compared to the buffer control

group ($p \leq 0.05$) and Ff-vaccines without BODIPY- α -GalCer molecule ($p \leq 0.01$).

Additionally, the iNKT cells were analysed for the NK1.1 (Figure 4.12A) and CD69 markers (Figure 4.12C). The results observed here confirmed the previous findings that BODIPY- α -GalCer molecule from the Ff-vaccines could induce activation of iNKT cells by stimulating them with the α -GalCer glycolipid. As seen in the earlier analysis (Figure 4.9) Ff-vaccine groups without adjuvant molecules (Ff.OVA and Ff.FLAG) again showed a significant upregulation of CD69 marker on iNKT cells ($p \leq 0.0001$), when compared to the buffer control group (Figure 4.12C). This was the opposite effect from the ones seen in adjuvant-carrying vaccine groups, indicative of some, as yet unknown, impact of the Ff phage on iNKT cells. Overall, it can be concluded that the iNKT cells had been activated with the lower dose of BODIPY- α -GalCer attached to Ff phages.

4.2.4 *In vitro* T cell proliferation

With the Ff based vaccines inducing a marginal OVA-specific CD8⁺ T cell response *in vivo*, even when the dose of antigen attached was substantially increased (8.75 vs. 0.127 μ g/dose; Table 6), and despite the evidence of iNKT cell activation, it was speculated that the antigen was unable to be cleaved from the vaccine to be effectively presented by DCs to T cells. Therefore, an *in vitro* T cell proliferation assay was used to determine whether the

peptide SIINFEKL derived from the phage vaccine was presented to OVA-specific CD8⁺ T cells by DCs. The readout of this assay is based on the fact that antigen-specific CD8⁺ T cells will divide after exposure to peptides presented by DCs. The spleens and lymph nodes from OT-I mice (Section 2.3.2) were used as a source of naïve T cells for this experiment. The OT-I mouse is a transgenic model engineered to express MHC I-restricted OVA-specific TCR. All T cells in this mouse are therefore CD8⁺ T cells, displaying TCR that is specific for SIINFEKL presented on H-2K^b MHC class I molecules (Carbone et al., 1992; Hogquist et al., 1994). Due to a very low frequency of naïve antigen-specific T cells in wild-type murine models, this strain has been particularly useful in studying T-cell development and generation of primary adaptive T cell responses (Clarke et al., 2000). Due to the lack of CD4⁺ T-cells, the OT-I mouse is devoid of iNKT cells (which are CD4⁺ in murine models). In this experiment, the OT-I mouse was used to by-pass the requirement for clonal selection and expansion and test activation of already developed OVA-specific CD8⁺ T cells.

Briefly, T cells from the lymph nodes of naïve OT-I mice were cultured with syngeneic DCs for 72 hours with the titrating doses of the vaccines used in the previous experiment (Section 4.2.3). Assessment of T cell proliferation was tested by the addition of a radio-labelled nucleotide to the culture media (³H-thymidine, or 3dT). Once the cells were stimulated to divide, all newly formed cells incorporated the radio-labelled nucleotide into their DNA, resulting in radioactivity increase with every subsequent

generation. The level of radioactive label was measured after washing the free ^3H -thymidine from the media in wells to assess the level of radioactivity acquired by the cells. The total radioactivity incorporated was used as a measure of proliferative activity, which was compared between samples where the cells were exposed to different vaccines (Figure 4.13). Counts per minute (CPM) was plotted against SIINFEKL peptide molar concentrations in each case.

Importantly, given that iNKT cells are not present in OT-I mice, they cannot contribute to the proliferative responses assayed. Free soluble SIINFEKL peptide was used as a positive control in this assay. This short OVA peptide does not need to be processed to be presented to OT-I CD8^+ T cells, which is why the cell proliferation (measured as increase in radioactive signal) was expected at very low peptide concentrations. Another control was OVA protein alone, which has to be processed by DCs for its epitope to be presented on MHCI to OVA-specific CD8^+ T-cells.

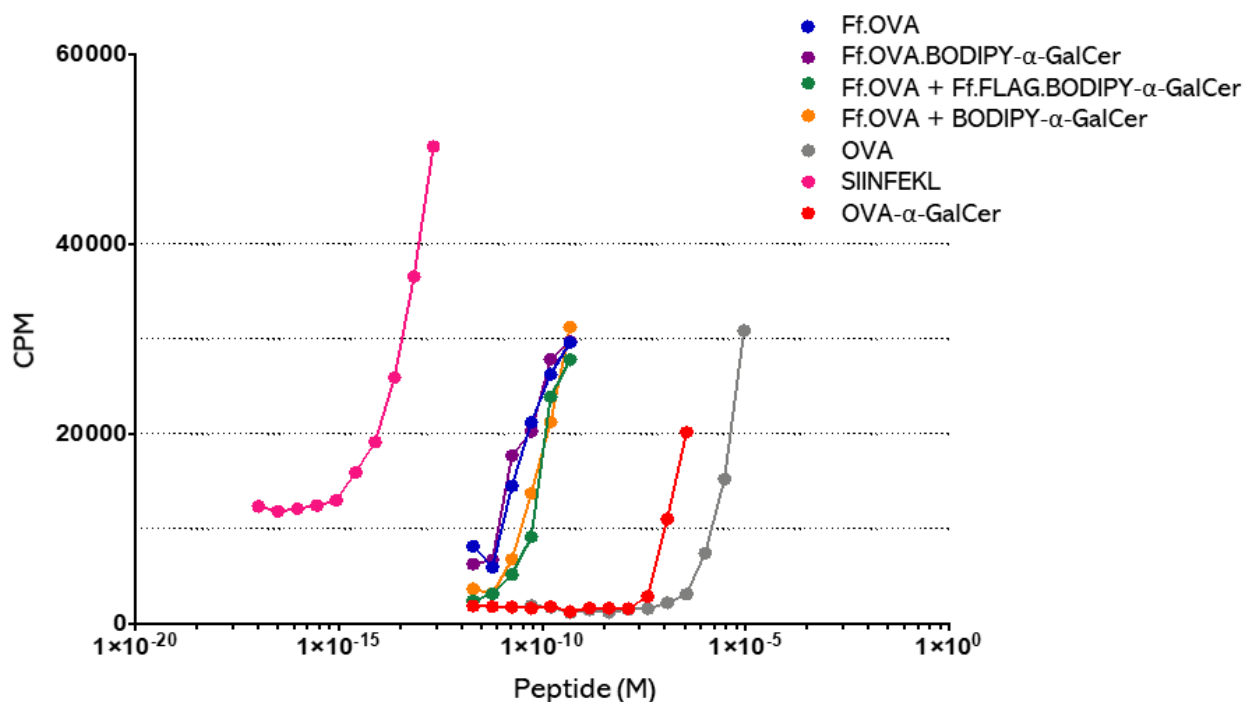


Figure 4.13. *In vitro* proliferation assay.

LN and DC enriched splenocytes from OT-I mice were pulsed with different concentrations of OVA peptide, as described in Chapter 3. CPM, counts per minute. Data presented are from three OT-I TCR transgenic mice per group.

The DCs used in the experiment were generated from the bone marrow precursors and were of 71.7% purity, based on the expression of the DC marker CD11c. The T cells from OT-I mice, taken from the lymphoid tissues to be used as responders, were at 77% purity, based on expression of CD3 (data not presented). As expected, the free peptide induced T cell proliferation at the lowest doses among all samples (Figure 4.13; EC₅₀ $\sim 10^{-14}$ M). All phage vaccines clustered on the plot at concentrations between 10^{-12} and 10^{-10} M, much lower than the OVA- α -GalCer 1 : 1 conjugate, whose EC₅₀ was about 10^6 -fold higher than that of the phage-presented OVA peptide. Incorporation of the peptide into Ff phage, therefore, does not inhibit its presentation by DCs, and

this is unlikely to be the reason why the vaccines failed to induce high clonal proliferation and expansion of the OVA-specific CD8⁺ T cells *in vivo*. This is interesting, because the 1 : 1 conjugate vaccine gave a strong response *in vivo* in the wild-type mice, whereas only one of the OVA peptide-displaying vaccines induced marginal increase of the OVA-specific CD8⁺ T-cells (Figure 4.7 and Figure 4.10). Further work is therefore needed to establish why the Ff-based vaccines were not strongly immunogenic *in vivo*, despite effectively presenting both the adjuvant *in vivo* and antigen *in vitro*.

4.3 DISCUSSION

The vaccine designed in this project, described in Chapter 3, was expected to effectively induce CD8⁺ T-cell response that is applicable to cancer immunotherapy. One of the anticipated advantages of Ff-based vaccine when compared to a synthetic 1:1 conjugate design (Compton et al., 2015) was utilising the ability of Ff phages to carry high numbers of physically connected antigenic peptides and adjuvant molecules, with the additional possibility to gauge their ratios.

Initially, analysis was conducted three days after vaccination, to determine the iNKT cell induction by the novel phage vaccine. This experiment provided insights into efficiency of adjuvant presentation to CD1d molecule when attached to the filamentous phage vs administered as a free compound. Importantly, the adjuvant molecule

(BODIPY- α -GalCer; Appendix 7.2.1) used in this research had the glycolipid component α -GalCer, a fluorescent dye (BODIPY) and AAC-reactive group (DBCO), and was compared when used as a free (admixed) adjuvant or covalently attached to the phage. As expected, groups that carried adjuvant molecules, either free or Ff-attached, showed significant stimulation of iNKT proliferation, monitored by CD1d-binding TCRs. Additionally, the activation dynamics was monitored by downregulation of CD69 and NK1.1 markers (Figure 4.4).

In this initial experiment, a relatively high dose of α -GalCer was used (4.4 μ g), compared to 200 ng used in the *in vivo* experiments in earlier work on synthetic 1:1 conjugates (Anderson et al., 2014). It was important to take into consideration that the BODIPY- α -GalCer molecule (Appendix 7.2.1) was structurally different than the α -GalCer alone. Therefore, the first *in vivo* experiment was performed to assess if the BODIPY- α -GalCer molecule could be presented to iNKT cells when attached to phages.

When the glycolipid from α -GalCer binds to the CD1d groove, the fatty acid chain always goes to the A' pocket, while the sphingosine chain always goes to the F' pocket of the binding groove within the α -chain (Figure 1.10). This leaves the polar carbohydrate head free to interact with the TCRs of iNKT cells (Borg et al., 2007). In order to access the α -GalCer, phage displaying this adjuvant have to be taken up and processed by APCs, and the linkers connecting α -GalCer

to the phage and BODIPY fluorescent marker have to be cleaved by cathepsins. Only the α -GalCer as an active molecule, once released, can be presented on CD1d in order for iNKT cells to be stimulated.

Short time-course (3 days) experiments testing iNKT cell activation showed that the phage vaccine carrier was as efficient in activating iNKT cells when loaded with BODIPY- α -GalCer adjuvant molecules as was the free BODIPY- α -GalCer (Figure 4.3), indicating that attachment to the phage does not impair α -GalCer presentation.

The next step was to lower the dose of adjuvant molecules from 4.4 μ g, which is considered relatively high for i.v. route, down to 800 ng (Table 6), and test the OVA-carrying vaccine in mice. Previous studies showed that the immune response was better when focused to the antigens conjugated to filamentous phages, relative to the same antigens conjugated to the standard carriers (Sartorius et al., 2011; van Houten et al., 2010; van Houten et al., 2006). This was observed even without adjuvant molecules attached to the particles, and with only one round of immunisation, without booster doses. Here the aim was to induce antigen-specific immune responses in murine models, using a vaccine displaying combined MHC I- and MHC II-specific OVA epitopes, in order to stimulate both the CD8⁺ and CD4⁺ T cells. According to earlier research using this long OVA peptide (Compton et al., 2015), optimal T cell responses are reached when α -GalCer adjuvant is delivered to the same APCs as the peptide antigen, therefore boosting the CD1d-restrictive

iNKT cells that additionally induce antigen-specific CD8⁺ T cell responses.

When looking at the OVA-specific T cell populations from this research, filamentous phages loaded with adjuvant and antigen molecules resulted, however, in very poor responses. When carrying 127 ng of antigenic peptide per dose, Ff-based vaccine was inferior to covalently conjugated OVA- α -GalCer molecule at a 1:1 ratio. The doses of all vaccine samples within a single trial were made to contain equal amounts of α -GalCer (Table 6). It is essential to note that there is a close temporal relationship that is needed between the presentation of OVA and α -GalCer (Hermans et al., 2003). The administration of antigen and adjuvant has to be simultaneous, or within an hour of each other, to elicit the strongest responses. Therefore, the low number of OVA-specific CD8⁺ T cells in Ff-vaccinated groups after seven days might have been due to poor priming, if the antigen and adjuvant molecules were released from the phage at different rates. In this context, the different structure of BODIPY- α -GalCer molecule, when compared to a free α -GalCer molecule, may have altered the kinetics with which the adjuvant was acquired, processed and presented to iNKT cells.

Furthermore, when analysing iNKT cells stimulated by glycolipid adjuvants, the timeframe plays a critical role in results obtained. Their peak numbers are achieved after three days post-immunisation, keeping their phenotypic characteristics more or less the same until the day 7 (Bennstein, 2017; Chiba et al., 2008; Van Kaer et al., 2015).

Therefore, by obtaining the results after nine days of initial vaccine dose, without a boost vaccine at day seven, it was not certain what to expect in terms of CD69 and NK1.1 phenotype markers. Nevertheless, when doses of BODIPY- α -GalCer were lowered to the equivalent of α -GalCer 800 ng, iNKT cells downregulated expression of NK1.1 markers in all expected groups of immunised mice, with adjuvant either being attached to the phage particles or administered as a free compound (Figure 4.9). On the other hand, when looking at the total number of iNKT cells in these groups (Figure 4.8), free Ff.OVA + BODIPY- α -GalCer showed no difference when compared to the PBS control, while covalently attached adjuvant to phage particles, with or without antigenic peptide (Ff.OVA.BODIPY- α -GalCer, and Ff.FLAG.BODIPY- α -GalCer) showed similar results as the positive control (OVA- α -GalCer conjugate). These data indicate that there might be a differential effect on iNKT cell activation according to whether the adjuvant molecule is free or attached to the phage carrier, with attached delivery being superior.

Finally, the immune response to a vaccine with a substantially increased ratio of antigen to adjuvant was tested as described in Section 4.2.3. However, similar to the results observed in the previous experiment, Ff-based vaccine did not induce antigen OVA-specific CD8⁺ T cell responses when compared to the 1 : 1 conjugate vaccine (OVA- α -GalCer). Perhaps surprisingly, some reactivity was consistently observed in the group of admixed Ff.OVA +

BODIPY- α -GalCer (Figure 4.7 and Figure 4.10), but much lower than the response to the OVA- α -GalCer 1 : 1 conjugate. The activity seen in this group was similar to the previously reported Ff-based vaccine, where adjuvant α -GalCer was admixed (Sartorius et al., 2018). Interestingly, this work lacked a positive control (a 1 : 1 conjugate of antigen and α -GalCer), hence their experiments were not gauged against a "gold standard". Because of the similarities between the research topic of this thesis and the mentioned publication, a more detailed discussion is provided in the following paragraphs.

In Sartorius et al. (2018) study four mice were vaccinated i.v. on day 0, followed by booster doses on day 14, and analysis of T cells from spleens on day 21. To compare with the current study, here 5 mice were immunised on day 0, without a booster dose, and T cells were collected from the blood on day 7. Booster doses and longer periods between vaccination and analyses of the adaptive CD8⁺ T-cell responses might have contributed to different results observed between the published work and this thesis. More detailed comparison of technical differences between these two studies is presented in Table 7.

Table 7. Comparison of the i.v. vaccine results with the published similar experiment.

Key	Sartorius et al. (2018)	This study
Phage	fdOVA	R783.OVA (a f1-M13 chimera) (Section 3.2.1.1)
OVA antigen fusion	MHCI-pVIII	A-MHCII-MHCI-cathepsin cut site-M-pVIII
Adjuvant molecule	α -GalCer	BODIPY-linker- α -GalCer-cyclooctyne
Adjuvant attachment	Hydrophobic interactions	Covalent bonds
Positive control OVA- α -GalCer	No	Yes
LPS	Not stated	< 4 EU/mL
Mice	C57BL/6; 4 / group	C57BL/6J; 5 / group
Vaccination	i.v.	i.v.
Booster dose	Yes, day 14	No
Adaptive immune response	Assessed on day 21	Assessed on day 7
Analysis	CD8 ⁺ H-2Kb/OVA ₂₅₇₋₂₆₄ dextramer ⁺ T cells from spleen (Figure 3)	CD8 ⁺ H-2Kb/OVA ₂₅₇₋₂₆₄ pentamer ⁺ T cells from blood (Figure 4.10)
% OVA-specific CD8 ⁺ T cells	0.4% PBS 0.5% Fd.OVA 1.4% Fd.OVA.GalCer	0.04% PBS 0.03% Ff.OVA 0.04% Ff.OVA.BODIPY- α -GalCer 0.18% Ff.OVA + BODIPY- α -GalCer 4.6% OVA- α -GalCer
Cytokines assayed	IL-2, IFN- γ (Figure 3)	IL-12 p70 (data not presented)

Overall, even though these two studies have used filamentous phages, OVA peptide and α -GalCer adjuvant for the immunotherapy vaccine, the methods in vaccine design, vaccination protocol, and analysis of the immune responses are significantly different. Nevertheless, both showed that admix of Ff phage displaying OVA peptide and α -GalCer resulted in the increase in OVA-specific CD8⁺ T cells in the intravenous infection over Ff-OVA phage of about 3-fold (Figure 4.10 in this study vs Figure 3D in Sartorius et al. 2018). Importantly, in Sartorius et al. (2018) vaccination

protocol included a boost at day 14 and the OVA-specific CD8⁺ T-cells were analysed at 21st day, hence the response should have been much higher in comparison to this thesis work where no boost was included and the OVA-specific CD8⁺ T-cells were analysed much earlier, on day 7 after immunisation. Nevertheless, results of this study, and the similarly limited response reported by Sartorius et al. (2018) suggest that the phage-based vaccines induce a weak OVA-specific CD8⁺ T cell response.

Driven by these results, an additional assay was performed *in vitro* (Section 4.2.4) on T cells derived from OT-I mice, with the same vaccine samples as in Section 4.2.3. Based on the structure of the conjugate OVA- α -GalCer vaccine (Appendix 7.2.2), it is expected that this molecule would have to be acquired and processed by APCs to present SIINFEKL peptide on the MHC I complexes on the cell surface. That means that a long OVA (MHC I+II) peptide would have been required at higher concentrations than SIINFEKL in order to induce the same proliferation response (Figure 4.13), as SIINFEKL is freely available to directly bind to MHC I on the cell surface without a need for uptake by DCs and processing.

Interestingly, the data from this experiment show that phage particles carrying OVA peptide were more efficiently acquired and processed when compared to OVA- α -GalCer 1 : 1 conjugate containing long OVA peptide (MHC I+II), or the complete native OVA protein. The 6-log lower concentration of Ff-phage-displayed long OVA peptide required for OVA-

specific CD8⁺ T cells in proliferation assay in comparison to the OVA- α -GalCer 1 : 1 conjugate suggests much more efficient presentation of the antigen by DCs. It is possible that the reason for this superior presentation could be an additional adjuvant effect of the Ff phages in this *in vitro* assay. It had been reported that the phages can act as adjuvants due to the unmethylated CpG motifs from ssDNA within Ff, which are known PAMPs. Phages were found to stimulate TLR-9 receptors on APCs *in vitro* (Sartorius et al., 2015) causing enhanced immune responses relative to OVA protein or peptide alone. In support of this, Ff phages are known to be highly immunogenic, even when applied at low doses and in the absence of adjuvant (Sartorius et al., 2015). This could be beneficial for the vaccine designs, as if true, there would be no need for additional adjuvant molecules. Considering that Ff phages are extremely stable, it remains puzzling how they release the ssDNA and expose the CpG motifs from the encapsulated particle to act as TLR agonists. They require harsh conditions to be degraded and to release the DNA ($\text{pH} \geq 10$; $\text{pH} \leq 2$; SDS detergent; $+70\text{ }^{\circ}\text{C}$) (Sattar et al., 2015). Nevertheless, it is important to note that, for example, TLR2 agonists (e.g., Pam3Cys, lipopeptide derived from Gram-negative bacterial membrane) could shut down antigen processing if administered before the antigen delivery. Consequently, CpG motifs derived from the Ff phage ssDNA backbone may result in downregulation of processing needed for maturation of DCs.

When it comes to monitoring the immune responses, there are quite profound cytokine responses from iNKT cells, that

could have been assayed (Figure 1.12), especially in the early days after vaccination. For example, iNKT cells make IL-4 and IFN- γ (Chang et al., 2015), and a whole host of other cytokines that cross-activate DCs, which then produce IL-12 p70 (Albarran et al., 2005; Coquet et al., 2008; Coquet et al., 2007). Interleukin 12, in turn, cross-activates NK cells, and the NK cells produce more IFN- γ (Figure 1.11). All these responses can be measured and interpreted in relation to α -GalCer-induced activation. However, IL-12 p70 is only particularly useful as IL-12 is APC-related cytokine, therefore changes in its concentration should indicate whether the APCs were activated. Nevertheless, for this study, a serum IL-12 p70 assay at a single time-point was performed and was negative for all groups apart from those injected with α -GalCer (data not shown). This assay was hard to interpret in terms of DC activation dynamics, as it only contained a single data point. A more comprehensive approach is needed to measure the kinetics of cytokine induction in response to new adjuvants (BODIPY- α -GalCer or Ff phage) that were unknown prior to this work.

Apart from IL-12 p70 that provides a profile of transactivation events induced by α -GalCer, another cytokine of interest would be IL-4, which is produced by iNKT cells. IL-4 profile could be used to tease apart the levels of iNKT activation, specifically the marginal OVA-specific CD8⁺ T cell increase in Ff.OVA admixed with BODIPY- α -GalCer, and no detectable increase in Ff-OVA-BODIPY- α -GalCer vaccinated

groups. In the future work intracellular cytokines can be analysed to characterise NKT or T cells functionally. Analysis of T cell response by this technique would have been very challenging in the context of experiments presented in this thesis, as not much of a T cell response was observed by flow cytometry with OVA pentamers (Figure 4.7, Figure 4.10).

Activated CD8⁺ T cells produce cytokines such as IFN- γ , TNF- α and TNF- β (Slifka and Whitton, 2000). Therefore, another option that could have been considered is to examine T cell functionality by looking for IFN- γ production by T cells using the ELISpot assay (Schmitt et al., 2001). This technique would provide information on T cell activation which cannot be determined simply by identifying OVA-specific CD8⁺ T cells using MHC I. Additionally, IFN- γ has other beneficial effects in tumour immunotherapies, as it can damage the tumour blood vessels that supply nutrients, resulting in cell necrosis and death (Qin et al., 2003) and inhibits the tumour cell proliferation (Bromberg et al., 1996; Chin et al., 1996). Therefore, if there would have been IFN- γ detected, this could have indicated better anti-tumour vaccine outcomes.

To better understand the positive responses of individual animals that were outliers, demonstrating high number of OVA-specific CD8⁺ T cells in the admix control group (yellow bar in Figure 4.7 and Figure 4.10), a further examination of these mice in more detail would be needed, including increasing the sample size. Larger experimental groups would

need to be used to assess if phages were able to present antigen to T cells *in vivo*.

One alternative might have been to investigate the T cells in other organs, in case OVA specific CD8⁺ T cells had homed to these organs (e.g., spleen) and were not represented in the blood. It could be possible that a weak response is measured from blood samples of immunised animals, yet a larger cohort of T cells might have been observed in some other organs, particularly the lymphoid organs such as spleen and lymph nodes. In the future experiments, to not miss out on any potential OVA-positive T cells, pentamer staining could be performed on T cells isolated from lymphoid tissues as well. However, it should be noted that in previous studies of α -GalCer-adjuvanted vaccines, responses in blood have been highly predictive of responses that accumulate in lymphoid tissue, or indeed other organs such as the lung and liver (I. Hermans 2020, personal communication, 26 May).

If the Ff-vaccines had induced significant immune response, the next step would have been a tumour challenge, using B16.OVA melanoma model. In such experiments, the vaccine would have been tested for its ability to provide T cell-mediated protection. Unfortunately, since there was no robust evidence that a challenge-experiment would provide any different information than what was observed, it was not used in this study.

It is known that specific sub-populations of DCs differ in their ability to cross-present antigens. For example, cDC1s

have a heightened capacity for cross-presentation *in vivo* and are therefore likely to be involved in vaccine-induced CD8⁺ T cell responses to the peptide in the phage constructs. If the low induction of the CD8⁺ T cell responses by phage vaccines was due to a failure to be targeted to the right APCs (e.g., cDC1s) *in vivo*, vaccines could be further modified in such way that the phage particles display recombinant variable domains of antibodies (e.g., scFv) that recognise cell surface molecules involved in antigen uptake by the correct DC type (Caminschi et al., 2012). One of the cell surface molecules that these DCs express is Clec9A (Lahoud et al., 2011). Therefore, it would be sensible to display the variable domains of anti-Clec9A mAb on pIII protein of Ff particles to target the phage directly to the appropriate APCs.

Overall, design and production of the Ff-based vaccine were successfully achieved, and the glycolipid adjuvant incorporated into the phage was efficiently presented to iNKT cells. Additionally, the peptide antigen from the vaccine was effectively acquired and presented to antigen-specific CD8⁺ T cells by APCs *in vitro*. However, at this point, it remains unknown why the vaccine displaying BODIPY- α -GalCer did not induce significant OVA-specific CD8⁺ T cell responses *in vivo*, while the admixed vaccine elicited only marginal response. This should be investigated further as outlined above.

Chapter 5. NOVEL FUNCTIONALISED BIOLOGICAL NANORODS FOR DIAGNOSTIC APPLICATIONS

5.1 INTRODUCTION

While in the previous two chapters, filamentous phages were modified and tested as vaccine carriers, here the intention was to develop phage-derived biological non-infectious nanoparticles and examine their potential applications in diagnostic assays. The reasoning behind it is that, even though Ff show an extraordinarily wide range of possible modifications, applications of Ff phage as nanoparticles in diagnostics and tissue targeting are at the proof of concept stage. Their use outside of the laboratory faces regulatory restrictions and consumer concerns because these Ff are genetically modified replicating bacteriophages that carry antibiotic resistance genes. Hence, Ff could replicate in *E. coli* within the gut, and spread antibiotic resistance genes to gut microbiota by horizontal gene transfer.

Non-biological nanoparticles, on the other hand, are widely used in medical and nanotechnology applications. Problems linked to these structures include the toxicity of the particles themselves and sustainability issues due to the use of toxic chemicals in production. When considering the range of modifications of the nanoparticles for their use, Ff phages have an advantage over many biological and non-biological counterparts. Phages can be orthogonally functionalised with peptide- or non-peptide molecules due

to the distinct protein composition along the shaft, and at two opposite ends, however, their diffusion properties and high length to diameter ratio can cause difficulties in some applications.

To eliminate these drawbacks of filamentous phages, a new type of short Ff-derived bio-nano particles were developed in the Rakonjac research group at Massey University (Bisset, Zhou, Khanum, Rakonjac, Leon, unpublished). These nanorods, named BSFnano (Biological Scalable Ff-derived Nanorods) that are non-infectious and do not carry any antibiotic resistance genes, have the potential to be used outside of the laboratory. In this thesis, BSFnano was used for the development of diagnostic tests, as proof of principle for the applications in point of care diagnostics or food and environment contamination assays.

This chapter describes production optimisation and functionalisation of the BSFnano, as well as modifications that were introduced as "handles" for site-specific post-production chemical alterations, such as click chemistry (described earlier in Section 3.2.3) or "tag and modify" chemistry. The nanorods were then used for the development of dipstick assays, demonstrating their applicability using a test analyte, fibronectin. Fluorescent labelling of functionalised BSFnano particles was performed in conjunction with direct visualisation of the dipstick assay result (Section 5.2.4.4). The unlabelled particles were used in conjunction with immunodetection to achieve ultrasensitive detection (100,000 molecules/ μ L; Section 5.2.5).

5.1.1 Aim and objectives

The purpose of the experiments described in this chapter was to develop functionalised BSFnano particles using a novel two-plasmid system, thereby eliminating the helper phage which was used in earlier production method (Sattar et al., 2015). This chapter also presents the development of dipstick assays using functionalised BSFnano particles.

Specific objectives were to:

- Construct and test the production efficiency of several different helper plasmids containing handles for functionalisation of BSFnano rods.
- Establish and characterise the BSFnano fluorescent labelling to be used for particle visualisation in diagnostic applications.
- Perform proof-of-concept lateral flow (dipstick) diagnostic assays for detection of fibronectin.

5.2 RESULTS

5.2.1 Helper plasmids for site-directed functionalising BSFnano via specific chemical handles.

The production system has been developed earlier in Rakonjac research lab at Massey University, using a nanorod replicon template plasmid (Figure 1.6) which serves as the source of the BSFnano ssDNA backbone (Table 4). Here the research focus was on developing helper plasmids that encode all the

proteins required for the production of functionalised nanorods (Figure 1.5). By engineering specific modifications in the helper plasmids, one can produce a range of different functionalities displayed on the nanorods (Table 8).

5.2.1.1 Helper plasmids for site-specific chemical conjugations

Helper plasmids for site-specific chemical conjugations, named pHAS1 and pHAS8, were designed to allow two possible chemical modifications on particles, after their production. One of them is known as "tag and modify", and the other one is "click" chemistry.

The tag and modify method is a chemical modification that requires unpaired and accessible cysteine residues. Full-length pIII contains six cysteine residues forming four intra-domain bridges, Cys7–Cys36, Cys46–Cys53, Cys188–Cys201, and Cys354–Cys371, two in N1, and one each in the N2 and C domains (Kremser and Rasched, 1994). No other exposed cysteine residues are present in the particle. pIII was modified by deleting the N1 domain and part of the N2 domain (Figure 5.2), removing five out of eight cysteine residues and leaving a short segment of the N2 domain containing an unpaired cysteine residue. The C domain with the remaining two cysteine residues that form a disulphide bridge is sufficient for assembly of the nanoparticle. Given that there are five copies of pIII per particle, five unpaired cysteine residues per nanorod were available to serve as tags for covalent modification.

Another benefit of removing the pIII N-terminus is that it eliminates the immunodominant component of the nanorod, a vital property if particles were to be used as vaccine carriers. This idea will be further discussed in Section 5.2.1.1.

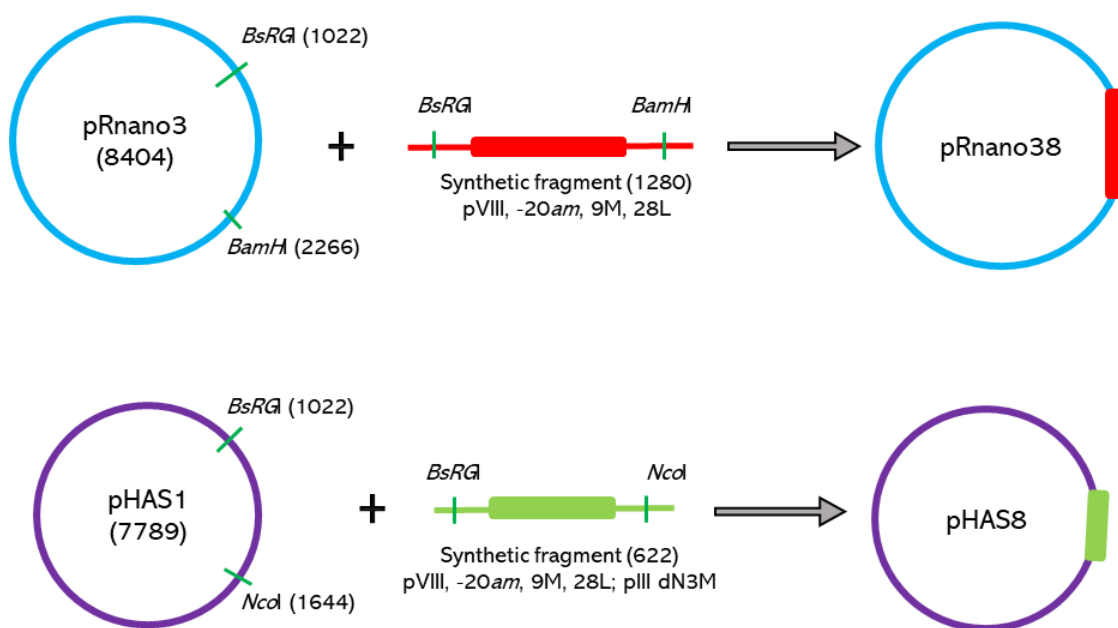


Figure 5.1. Construction of helper plasmids pHAS8 and pRnano38.

A synthetic insert containing an amber mutation in position -20 of gVIII, and point mutations A9M, M28L was cloned into helper plasmid pRnano3 at BsrGI / BamHI cut sites to introduce mutations required for inserting azide-containing non-natural amino acid azidohomoalanine solely in the solvent-exposed position in the major coat protein pVIII. A synthetic insert containing the same mutations on pVIII, and additional deletion of N1 and a portion of N2 domain of pIII (pIIIdN3M) was cloned into helper plasmid pHAS1 at BsrGI / NcoI cut sites to introduce mutations required for inserting azide-containing azidohomoalanine in the major coat protein pVIII and exposing 5 unpaired cysteine groups on phage minor coat protein pIII.

Helper plasmid pRnano38 (Table 4) was the same as pHAS8 (Figure 5.1), except that pIII was present in full-length (it contained the N1 and N2 domain). Both plasmids contained modifications that allowed the incorporation of azides in

the exposed portion of the major coat protein (pVIII A9M, M28L). As described in Section 3.2.3, where this method was used to attach adjuvant molecules onto the vaccine phage particles, azidohomoalanine incorporation *in vivo* during the nanorod assembly creates additional functionalisation site on the nanorods. Displayed -N₃ group of azidohomoalanine on particle surface serves as a handle to chemically attach desired molecules (Petrie, 2015).

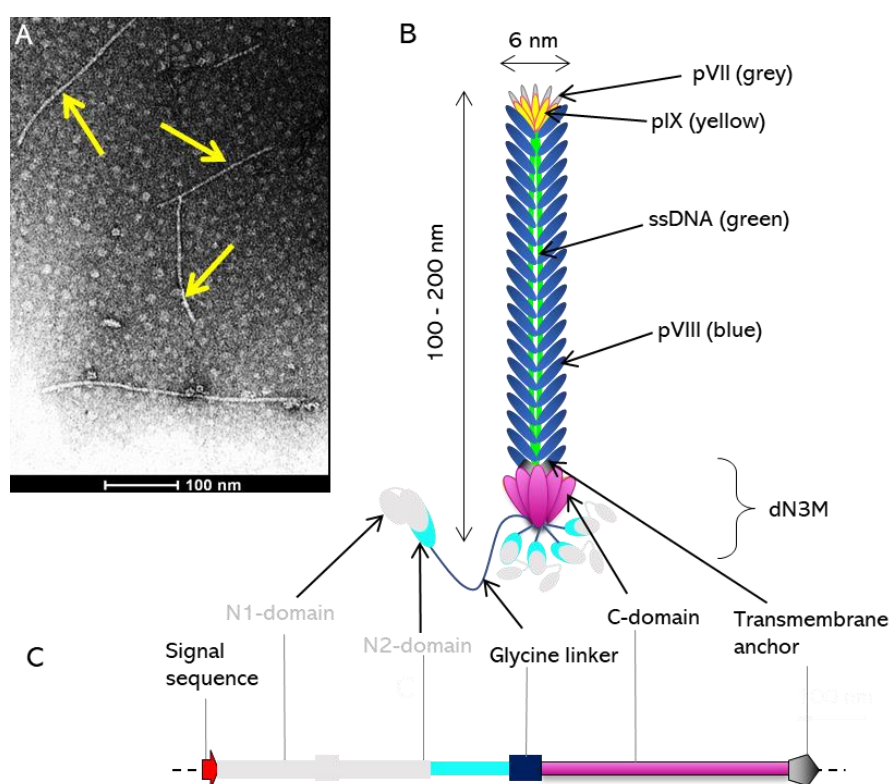


Figure 5.2. BSFnano functionalised for chemical modifications.

A, Micrograph of BSFnano particles produced from pHAS1 helper plasmid and pBSF529 template plasmid in *E. coli* K2449 strain. Yellow arrows, pointing at BSFnano particles; the scale bar is 100 nm. **B**, Schematic representation of BSFnano with five unpaired cysteine residues and 15 methionine residues per particle exposed at the endcap (pIII); **C**, domain organisation of pIII with indicated deletion of N1 and part of N2 domain. **Symbols**: yellow ovals, protein pIX; grey ovals, protein pVII; green line, ssDNA from pBSFnano template; blue ovals, coat protein pVIII; pink ovals, C-domain of minor coat protein pIII (dN3M).

Maximal concentration of azidohomoalanine in the growth medium, above which particle assembly becomes severely compromised, results in incorporation of this unnatural amino acid into phage proteins at about 10% of ATG codons, meaning that one azide can be incorporated per 10 ATG codons (Chapter 3). If azide is to be displayed at the pIII end of the nanorod, at least 10 methionine codons have to be present for the display of one azide per particle.

In the pHAS8 helper plasmid expressing N-terminal deletion of pIII, the truncated wild-type pIII (dNpIII) described above would have one solvent-exposed methionine. With five copies of pIII present per virion, a total of five exposed methionine residues were present per particle. To increase the odds of azide incorporation into most nanorods in the population, two additional *met* codons were introduced into the solvent-exposed portion of dNpIII, giving a total of 15 methionine residues per particle. The resulting modified pIII was named dN3M (Figure 5.2).

To avoid pVIII toxicity to *E. coli* in the course of plasmid construction and purification, and to stimulate the production of short nanorods by decreasing the amount of pVIII in the cells, a suppressible *amber* stop codon was introduced into *gVIII* of the helper plasmids. A stop codon at position 25 (or position 2 of mature pVIII; glutamic acid) was used in pHAS1, whereas in pHAS8 it was used at position 4 (serine; within the signal sequence, -20). Suppressor D (*SupD*) in the *E. coli* strain used in this work was superior by a factor of 100 in terms of phage production when pVIII contained the *amber* stop codon (at position 2 of

mature pVIII) to the commonly used Suppressor E (*SupE*) (J. Rakonjac, unpublished). The former suppressor introduces serine instead of glutamic acid in the mature pVIII in the mutant containing *amber* codon at position 25, increasing the pI of the nanorod from pH 6.8 to 8.3. In contrast, *amber* codon in position 4 does not result in a change of the pVIII amino acid sequence (or pI) in *SupD* strain.

5.2.2 Optimised production and purification generate high yields of nanorods

The BSFnano particles were functionalised for detection of soluble analyte (fibronectin). To produce nanoparticles in high yields, while ensuring the integrity of the displayed peptides (such as FnBP on pIII), the production and purification had to be optimised (Figure 5.3).

Briefly, the host strains (Table 2) for the production of BSFnano were first transformed with a helper plasmid that carries a Km^R marker (Table 4). Overnight culture of a single transformed cell was then used to make electrocompetent cells, as described in Section 2.4.1.3. To produce particles by these cells, template plasmid pBSFnano, carrying an Amp^R marker, was introduced (Table 4). After overnight incubation, nanorods were PEG precipitated and purified away from DNA and RNA that are typically released by the host cells during culturing, and co-precipitated with nanorods. Nanorods were separated from cellular impurities by CsCl gradient ultracentrifugation.

BSFnano particles were produced in high yields, using the method described in Figure 5.3, giving 10^{14} - 10^{15} particles/mL in the final 1000-fold concentrated sample or 10^{14} - 10^{15} particles per litre of the original *E. coli* culture. Given that these particles are non-infectious, they could not be titrated as phage plaques. Therefore, the quantities of nanorods were estimated based on the amounts of the single-stranded nanorod-encapsidated DNA, using densitometry, as described in Material and Methods, Section 2.5.3.

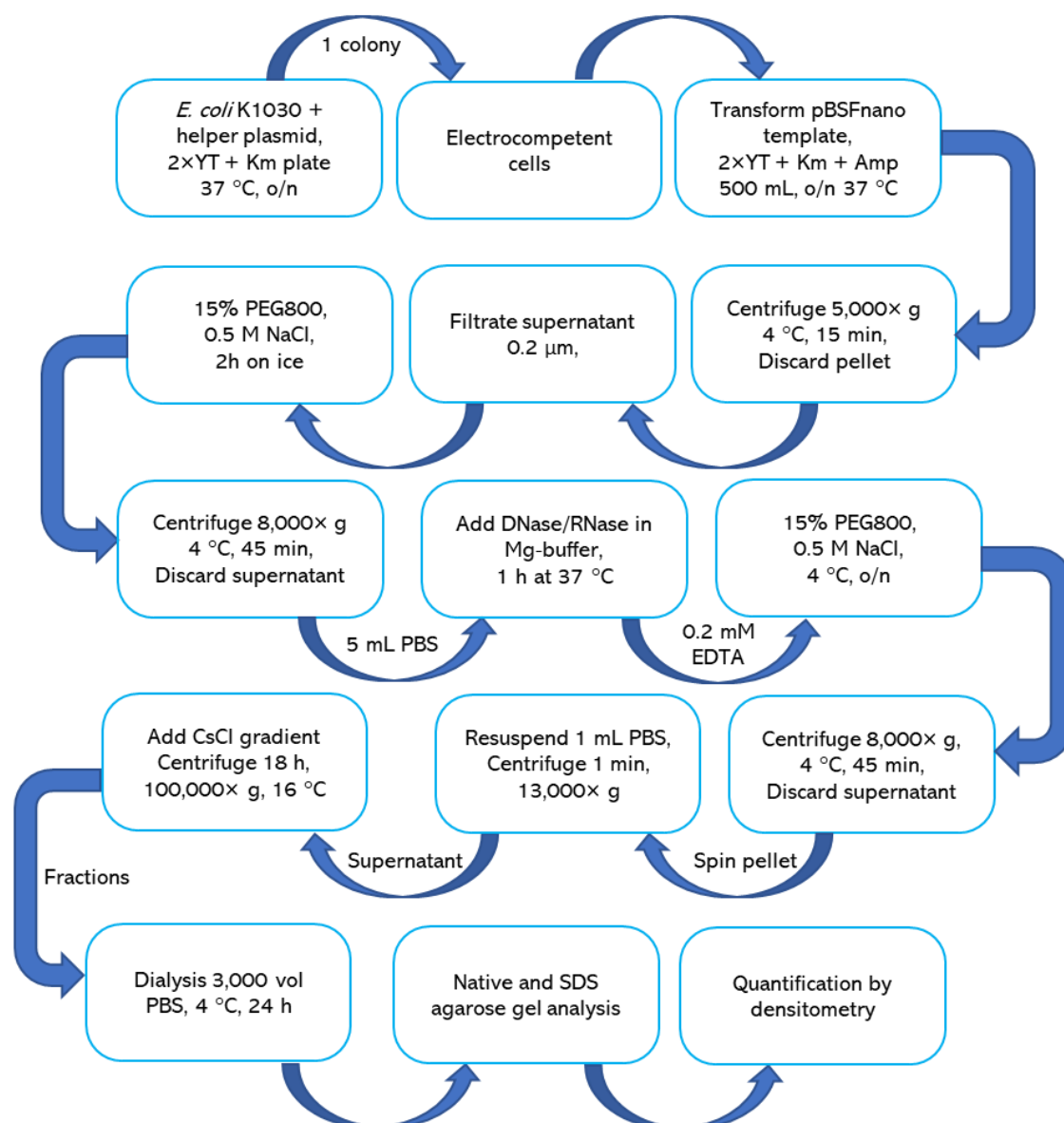


Figure 5.3. Flow diagram of optimised production and purification of BSFnano particles.

When produced from the pBSF529 replication cassette, and a helper phage with the full-length pIII and unmutated pVIII, the ssDNA was packaged into nanorods that were 75 nm in length (Khanum, S., unpublished). Interestingly, when BSF529.HAS1 nanorods were imaged using TEM (Section 2.5.5) (Figure 5.2A), only one unit-length nanorod (75 nm) was detected in five particles, while most particles were >150

nm long. Analysis of pHAS8 and pHAS38 by native agarose gel electrophoresis (Figure 5.4A) showed a ladder of bands. This is in contrast with the BSF529 nanorods obtained using pRnano3 helper that contained no mutations in pVIII (Khanum, S., unpublished) where most nanorods are unit-length (75 nm). BSF529.HAS8 nanorods separated into two major bands (Fig. 5.3A), whereas BSF529.HAS38 separated in a ladder of >6 bands, with the strongest signal coming from the top band (Figure 5.4B).

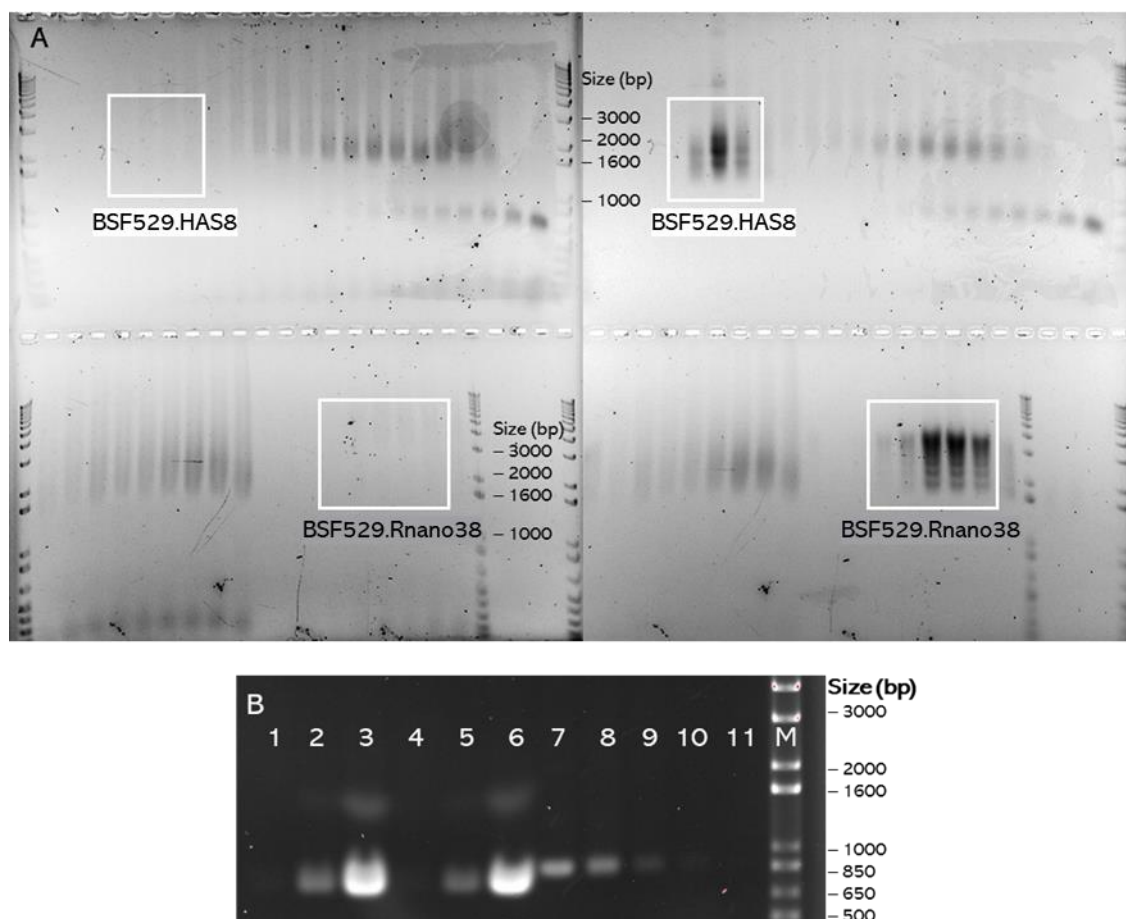


Figure 5.4. BSF529 nanorod purification monitored by agarose gel electrophoresis.

A, Detection of native particles in fractions collected after CsCl ultracentrifugation, as described in Section 2.5.1. **Left**: UV image of EtBr stained gel, (detecting free DNA only); **Right**: UV image of EtBr-stained nanorod DNA after processing the gel in NaOH to disassemble the nanorods. White squares indicate where native nanorods were detected. **B** Agarose electrophoresis of the SDS-disassembled BSF529 particles. This gel was used for quantification, as described in Section 2.5.3. **Lanes**: 1-3, ten-fold dilutions of BSF529.HAS8; 4-6, ten-fold dilutions of BSF529.Rnano38; 7-11, quantification standard (serial dilutions of ssDNA standard of known amounts, prepared from BSF719 nanorods); M, DNA size marker 1 kb⁺ double-stranded linear DNA ladder, as such was not used for a direct comparison of DNA sizes of ssDNA from particles. This marker has been used only for tracking the progress of electrophoresis, due to the lack of appropriate size markers for ssDNA or native virions.

The ladder observed in native nanorods samples could be due to the presence of particles of different lengths, or different charges. For example, if different bands correspond to the nanorods of different lengths, the fastest-migrating bands would be the nanorods of unit length (containing a single 529-nt circular ssDNA backbone or "genome"). In contrast, the slower-migrating bands in the ladder would correspond to the double-length and multiple-length nanorods, containing two or more sequentially packaged ssDNA genomes. Alternatively, virions containing different discrete charges would also be expected to run as separate bands. A statistical analysis of a large number of particles from multiple TEMs will be required to determine whether the nanorod populations obtained from pBSF529 using pHAS8 and pHAS38 helper plasmids are due to the charge or length differences.

While protein pIII in full-length Ff phage makes up only 2% of the total mass, in BSFnano it counts for 22% of total nanorod mass. Therefore, due to the significant contribution of pIII to the nanorods, it can be expected that the truncated vs. full-length pIII in the two variants will influence the properties of the two types of nanorods. However, despite the different physical properties, production of BSF529.HAS8 and BSF529.Rnano38 was similar, with the amounts of the pure nanorods after the CsCl gradient purification step (Figure 5.4B) estimated at $8.34 \cdot 10^{14}$ particles/mL and $1.00 \cdot 10^{15}$ particles/mL, respectively. Furthermore, the termination step of assembly, and in turn, the nanorod length, depends on direct interaction between

pIII and pVIII (Rakonjac et al., 1999). This interaction may have been compromised by A9M and M28L mutations in pVIII of BSF529.HAS8 and BSF529.Rnano38 nanorods.

To label the particles with an unnatural amino acid *in vivo*, *E. coli* host culture must be grown in the M9 minimal medium, as was described in Section 3.2.1.3 for the phage vaccine production. However, because the nanorods are much smaller than Ff, they require higher concentrations of PEG800 (15% for nanorods vs 5% for Ff phages) for precipitation from the culture supernatant. This higher PEG concentration resulted in crystallisation of salts during precipitation (data not shown). Therefore, the concentration of nanorods produced in minimal media would have to be carried out by a method that is different from PEG precipitation. Rich *E. coli* growth media (e.g., 2x YT) did not compromise the BSFnano purification by 15% PEG precipitation. Several other combinations of helper and template plasmids were used to test the production and purification of nanorods, resulting in various BSFnano constructs, listed in Table 8.

Table 8. Nanorods constructs

Nanorods	Helper plasmid	Template plasmid	Comments
BSF529.HAS1	pHAS1	pBSF529	Modified pVIII for click chemistry; 529 nt; deletion of N-domain in pIII
BSF529.HAS8	pHAS8	pBSF529	Modified pVIII for click chemistry; 529 nt; deletion of N-domain in pIII, displaying cysteine residues for "tag and modify" chemistry.
BSF529.Rnano38	pRnano38	pBSF529	Modified pVIII for click chemistry; 529 nt; with multiple cloning site in pIII (<i>gIII</i> :MCS)
BSF719	pRnano3	pBSF719	Wild type pVIII control; 719 nt; ssDNA standard for quantification.
BSF529	pRnano3	pBSF529	Wild type pVIII control; 529 nt
BSF719.FnBP	pRnano3::FnBP	pBSF719	Fn detection; 719 nt; wt pVIII, FnBP-pIII Fn detection, 719 nt
BSF529.FnBP	pRnano3::FnBP	pBSF529	Fn detection; 529 nt; wt pVIII, FnBP-pIII
BSF529.Gly ₄	p8Gly ₄	pBSF529	Control for BSF.Gly ₄ .FnBP; 529 nt GGGG-pVIII
BSF719.Gly ₄	p8Gly ₄	pBSF719	Control for BSF.Gly ₄ .FnBP; 719 nt GGGG-pVIII
BSF719.Gly ₄ .FnBP	p8Gly ₄ ::FnBP	pBSF719	Fn detection; 719 nt; GGGG-pVIII, FnBP-pIII
BSF529.Gly ₄ .FnBP	p8Gly ₄ ::FnBP	pBSF529	Fn detection; 529 nt; GGGG-pVIII, FnBP-pIII

5.2.4 BSF-nanorods for fibronectin detection

5.2.4.1 Construction of FnBP-pIII-fusion-expressing helper plasmid

Filamentous phages and Ff-nano particles designed for detection of fibronectin were previously produced using a helper-phage-driven nanorod assembly system (Sattar et al., 2015). In this system, helper phage Rnano3::FnBP served as a vector for the display of a detector molecule, fibronectin-binding peptide (FnBP), on pIII coat protein. In work described in this thesis, a new plasmid-based nanorod production system was used to produce fibronectin-detection nanorods, such that the FnBP-pIII fusion was expressed from a helper plasmid instead of a helper phage. The coding sequence of FnBP was amplified using Rnano3::FnBP phage DNA (Sattar et al., 2015) as a template and inserted into the multiple cloning site (MCS) within *gene III* (*gIII*) of the helper plasmid p8Gly₄, to allow fusion with the mature portion of pIII.

Given that the FnBP-pIII fusion is the only source of pIII in the nanorod-producing cells, all five copies of pIII in the nanorods are encoded by the fusion gene. FnBP is a fibronectin-binding domain of *Streptococcus pyogenes* Serum Opacity Factor (SOF) (Rakonjac et al., 1995). The FnBP domain of SOF belongs to a conserved family of the high-affinity fibronectin-binding domains of Streptococci and Staphylococci (Pilka et al., 2006). The nanorods produced using the helper plasmid used in this experiment, p8Gly₄, also have an N-terminally displayed peptide GGGG (Gly₄) on

every copy of the major coat protein pVIII (Bisset and Rakonjac, unpublished). The presence of the tetra-glycine peptide in the nanorods produced using p8Gly₄ was confirmed by mass spectroscopy (S. Bisset and J. Rakonjac, unpublished). GGGG is a motif that is used for enzymatic attachment of molecules that contain a C-terminal LPETG peptide, using enzyme Sortase A from *Staphylococcus aureus* (SrtA_{au}). Any molecule, including fluorescent dyes, or paramagnetic beads conjugated to the LPETG peptide (Zong et al., 2004), could potentially be enzymatically attached to these functionalized nanorods via the GGGG motif.

The template plasmid used for production of the nanorods gives rise to a 719-nt circular ssDNA genome in the presence of a helper plasmid. Nanorods produced by the cells transformed with the pBSF719 template plasmid and p8Gly₄FnBP or p8Gly₄ helper plasmids were named BSF719.Gly₄.FnBP and BSF719.Gly₄, respectively (Table 8). The former are nanorods for detection of fibronectin, and the latter is the control group. These nanorods were purified using the protocol developed in this thesis (Section 5.2.2) and analysed to determine the length, presence of FnBP-pIII fusion and finally to develop a lateral flow assay.

5.2.4.2 Characterisation of the BSF719.Gly₄.FnBP and BSF719.Gly₄ nanorods

Agarose gel electrophoresis of the BSF719.Gly₄ nanorods produced using helper plasmid p8Gly₄ shows a ladder of bands on the native gel. This indicates the production of nanorods that are not only unit length (containing a single 719-nt

circular ssDNA genome), but also double- and multiple-length, containing two or more sequentially packaged ssDNA (Figure 5.5C). The ladder contained seven strong bands, each representing a particle population that contains a discrete number of sequentially packaged ssDNA "genomes". Interestingly, BSF719.Gly₄.FnBP nanorods generated using p8Gly₄::FnBP helper plasmid (containing the FnBP insert) demonstrated a dominant unit-length band in native agarose gel electrophoresis, and a faint ladder, hence these nanorods are predominantly single unit-length (Figure 5.5C). Purified nanorods were also analysed by transmission electron microscopy (TEM), as described in Section 2.5.5.1. Due to a tendency of the Ff-derived nanorods to aggregate under the conditions of TEM, distribution of the nanorod lengths is skewed towards adjoined, intertwined or aggregated particles (Figure 5.5A). Nevertheless, a much higher proportion of single unit-length particles was observed in the BSF719.Gly₄.FnBP nanorod sample in comparison to the control nanorods lacking FnBP, in agreement with the native agarose gel electrophoresis analyses (Figure 5.5C). Given that the nanorod production system for BSF719.Gly₄.FnBP and BSF719.Gly₄ is identical, apart from the FnBP-encoding insert, it is unclear why only the latter resulted in an increased proportion of multi-length nanorods.

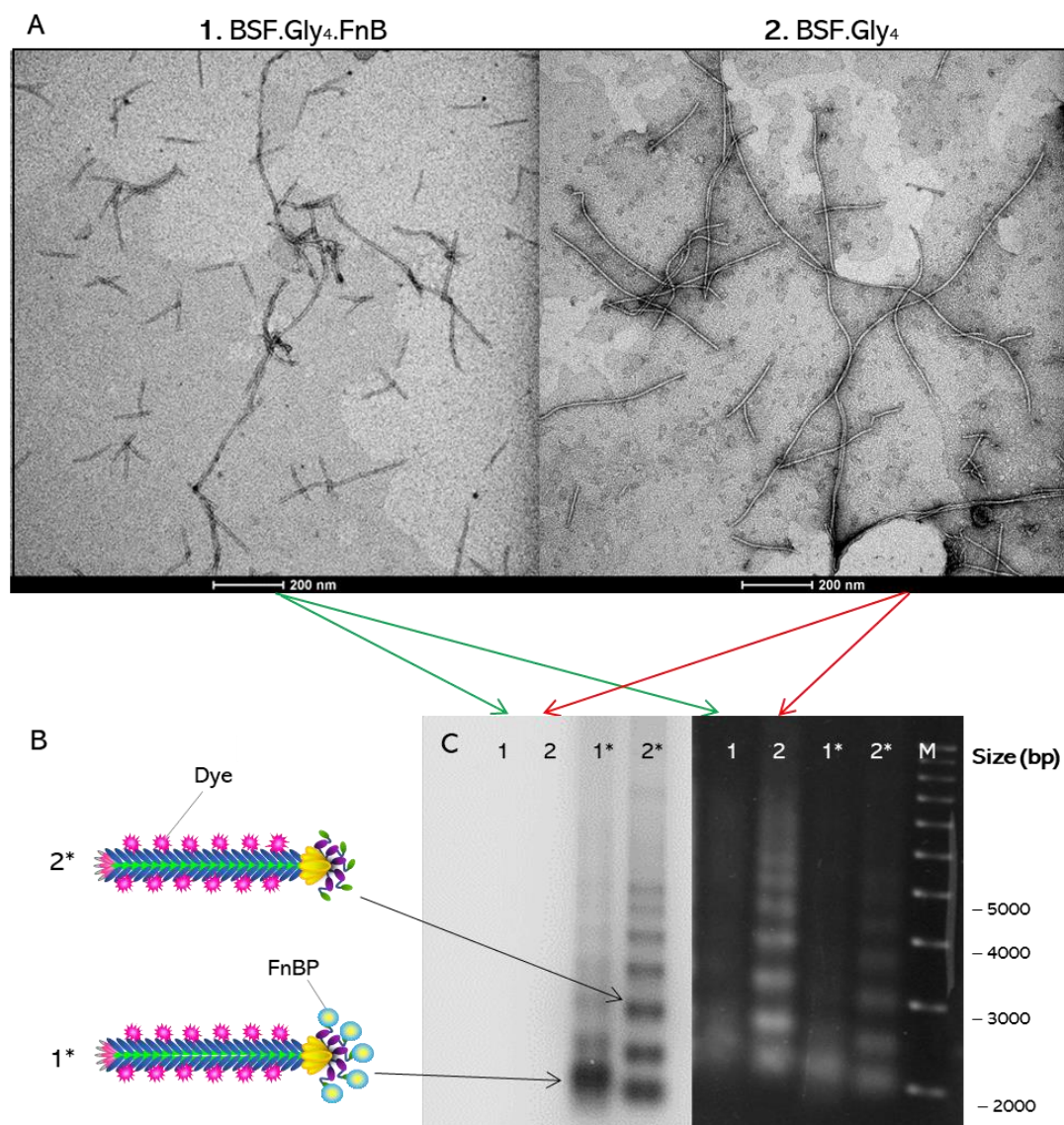


Figure 5.5. Characterisation of BSF719.Gly₄.FnB and BSF.Gly₄ nanorods. **A**, Micrograph of BSF719.Gly₄.FnB (1) and BSF719.Gly₄ (2) produced from pBSF719 template using BSF719.Gly₄.FnB and BSF.Gly₄ helper plasmids, as described in Section 5.2.2. The scale bar represents 200 nm. **B**, Schematic representation of DyLight 550-labelled BSFnano particles functionalized for fibronectin detection, seen as pink (pink stars) in the visible spectral region; **C**, Native fluorescently labelled (1*, 2*), and unlabelled (1, 2) particles, separated by agarose gel electrophoresis as described in Section 2.4.2.1. **Left**: UV image of unstained gel (detecting DyLight 550-labelled nanorods only); **Right**: UV image of EtBr-stained nanorod DNA after processing the gel in NaOH to disassemble the nanorods in situ. The DNA size marker is 1 kb⁺ double-stranded linear DNA ladder, and as such is not used for a direct comparison of DNA sizes of ssDNA from particles. This marker has been used only for tracking the progress of electrophoresis, due to lack of appropriate size markers for ssDNA.

5.2.4.3 Confirmation of FnBP-pIII fusion in the nanorods

Peptides displayed on the Ff phages and derived nanorods are susceptible to degradation by proteases during assembly and purification. To confirm that the intact fusion was indeed present in the nanorods, SDS-PAGE and western-blot analysis of the nanorod proteins using pIII-specific antibodies were performed (Figure 5.6).

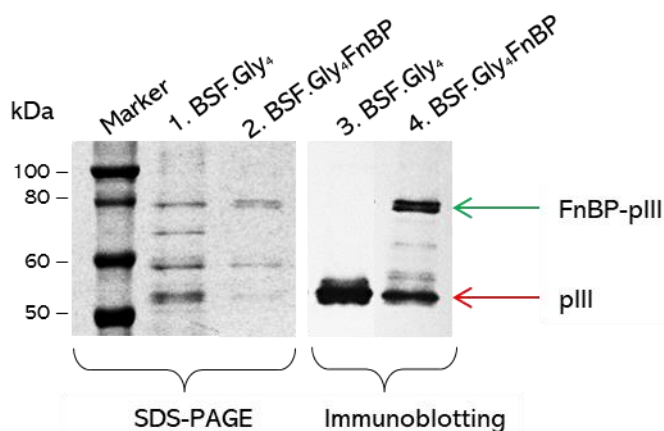


Figure 5.6. Detection of FnBP-pIII fusion in BSFnano particles functionalized for fibronectin detection.

Purified BSFnano particles were analysed by SDS-PAGE analysis. **Left:** All proteins in the gel were detected by Coomassie blue staining; **Right:** FnBP-pIII fusion was detected by western blotting using a pIII-specific antibody (Rakonjac and Model, 1998) as described in Section 2.4.2.2. **Lanes:** M, molecular weight standard (kDa); BSF.Gly₄, control particles without the fusion protein; BSF.Gly₄.FnBP, particles displaying FnBP-pIII fusion.

Nanorods containing FnBP-pIII fusion showed a band detected by pIII-specific antibody at 80 kDa, corresponding to the expected mobility of the fusion. However, an additional band of similar strength, corresponding to the unmodified pIII found in the control nanorods, was also detected, demonstrating proteolytic removal of the FnBP from about half of the pIII copies in the nanorods. Assuming that the

full-length fusion represents about 40% of pIII in the nanorods, it is expected that, on average, the BSF719.Gly₄.FnBP nanorods each have two FnBP-pIII fusions per particle. This is a much-improved display frequency relative to the nanorods produced using the helper phage, where only 10% of pIII in the nanorods were FnBP fusions, displaying on average 0.5 FnBP-pIII fusion per particle, or one peptide fusion per two particles (Sattar, 2013). Increased preservation of the fusion, when the helper plasmid was used for the nanorod production instead of helper phage, was most likely achieved by the significantly shortened purification time, due to the elimination of the part of the protocol necessary for the removal of the full-length helper phage.

Display of functional FnBP on the nanorods was demonstrated by a nanorod ELISA assay detecting immobilised fibronectin (Figure 5.7) performed as described in Section 2.7.2.1. Briefly, a 96-well plate was coated with fibronectin and binding of the BSF719.Gly₄.FnBP nanorods were quantified using phage-specific antibodies that recognise the coat protein pVIII.

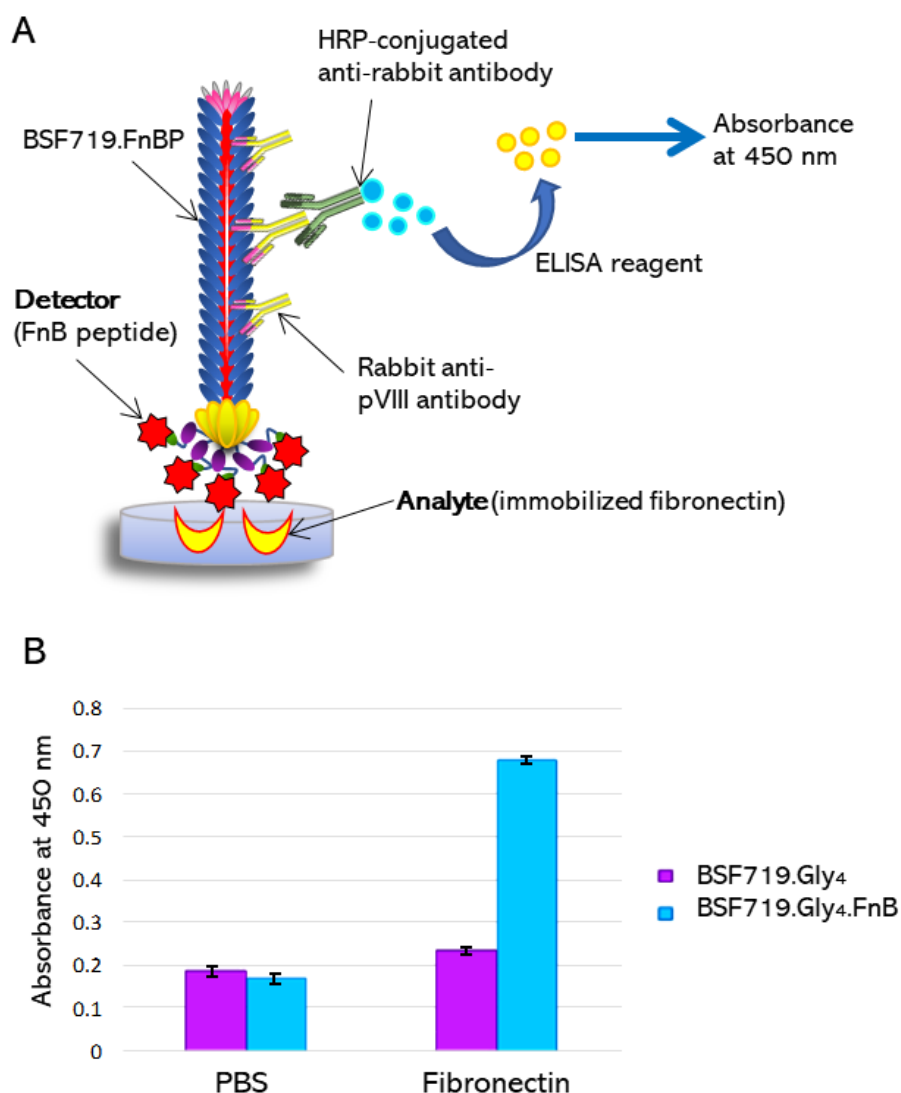


Figure 5.7. ELISA assay monitoring binding of the FnB-displaying nanorods to immobilised Fn.

A, Schematic representation of using BSF-nano particles in ELISA tests. Analyte fibronectin (yellow husk shapes) is immobilised onto an ELISA plate. The detector molecule displayed at one end of the nanorod (red star) binds to the analyte. Unbound particles are washed away, and attached particles are detected using an antibody against major coat protein of nanorods, as described in Section 2.7.1. **B**, Graph showing plotting the ELISA signal for analysed sample and controls. BSF719.Gly₄ control particles; BSF719.Gly₄.FnBP detector particles. Columns labelled as PBS denote the control wells coated with the phosphate buffer saline (PBS). A total of $2 \cdot 10^8$ nanorods was used in each assay. Data are presented as an average of duplicates; error bars represent SD.

No signal was detected above the background when control particles (BSF719.Gly₄) without the detector probe were used. The significant binding was observed with detector particles displaying the fibronectin-binding peptide (BSF719.Gly₄.FnBP) in the wells that contained the analyte (Fn), and no signal over the background value in the control wells from which the analyte was omitted.

5.2.4.4 Fluorescent labelling of nanorods via NHS-ester chemistry

BSF719.Gly₄.FnBP and BSF719.Gly₄ nanorods were fluorescently labelled for direct visualisation with DyLight™ 550 amine-reactive fluorescent dye (Alexa Fluor™ 555, TRITC, and Cy3™). DyLight™ 550 is an N-hydroxysuccinimide (NHS)-ester derivative that gives pink-to-red fluorescence (Figure 5.5). Ester moiety forms stable amide bonds with N-terminal α -amino groups, and ϵ -amino groups of the lysine residues (Koniev and Wagner, 2015). Therefore, allowing labelling of all proteins that make up the nanorod, and have a lysine side-chain amine exposed to the solvent. Each major coat protein pVIII has two exposed primary amines.

Given that each nanorod contains at least 294 copies of pVIII, it was expected that the fluorescent signal would come dominantly from the labelling of this protein. Fluoroimager scan (Azure c600) of the agarose gel containing DyLight™ 550-labelled native nanorods showed that their bands in the gel were intrinsically fluorescent, demonstrating that they were successfully labelled with the dye. Mobility of the labelled nanorods in agarose gel

electrophoresis appeared similar to those of unlabelled native nanorods (Figure 5.5C).

5.2.5 BSFnano-based lateral flow assay for the detection of fibronectin

Fibronectin detection using lateral flow dipstick assay was previously developed for phage, and Ff-nano particles (Sattar et al., 2015) produced using a helper phage. The sensitivity of that assay was 0.08 ng/ μ L of fibronectin, equivalent to 0.35 fmol/ μ L or $2 \cdot 10^8$ molecules/ μ L. Figure 5.8. shows a schematic representation of the fibronectin dipstick assay; experimental procedures are described in Material and Methods, Section 2.7.3. The control line was a monoclonal anti-pVIII antibody, and the test line was collagen. Collagen binds strongly to the analyte (fibronectin), via an epitope that is different from the one that interacts with FnBP (detector) (Pilka et al., 2006).

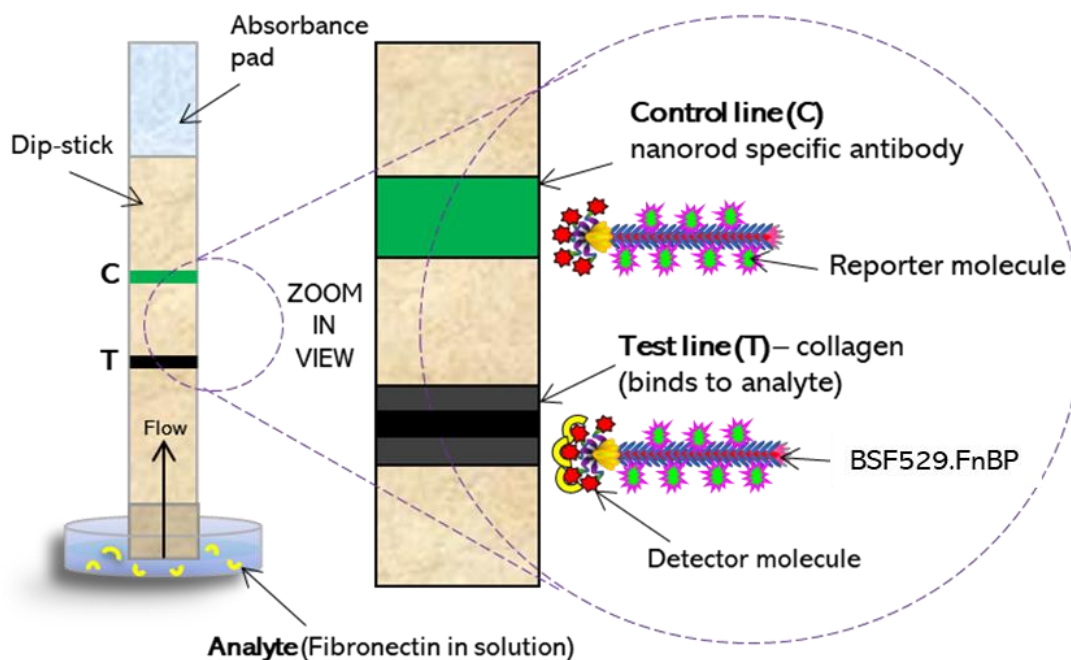


Figure 5.8. Lateral flow dipstick assay. Schematic representation of diagnostic assay for fibronectin detection using functionalised BSFnano particles. Analyte from the solution, fibronectin (yellow husk shapes) binds to the detector molecule displayed at the tip of the nanorod (red star). Test line (T), the collagen that captures fibronectin which travels with detector nanorods. Control line (C), a monoclonal antibody against the major coat protein of the nanorods. All the particles can bind to the C line.

Figure 5.9A shows detection of soluble fibronectin using fluorescently labelled BSF529.Gly₄.FnBP nanorods, prepared as described in Section 2.5.4 and conjugated to DyLight™ 550 as described in Section 2.5.4. For this assay, 1 µg of fibronectin was used in 100 µL of the mixture with 10¹¹ BSF529.Gly₄.FnBP particles. Using fluorescent dye as a reporter molecule shortened the time for analyte detection from about 3.5 hours to 30 min, as this test was based on direct fluorescence, and not on immunodetection of nanorods. The background signal along the dipstick was, however,

relatively strong (Figure 5.9A), resulting in limited sensitivity.

To achieve maximal sensitivity, the dipstick assay combined with immunodetection of nanorods was performed (Figure 5.9B). In this experiment, BSF529.FnBP nanorods were produced using the pBSF529 template plasmid (Table 8), that give rise to shorter nanorods in comparison to the BSF719 nanorods (75 nm vs 100 nm). Furthermore, BSF529.FnBP nanorods do not contain the GGGG peptide on pVIII. These changes were made to shorten the nanorod length and remove the glycine layer on the surface of the nanorod formed by GGGG display on every pVIII. This was believed to improve the diffusion of nanorods within the dipstick matrix and decrease non-specific binding to the dipstick surface.

A total of 10^{11} particles were mixed with serial dilutions of fibronectin dissolved in PBS. After the assay was performed, nanorods were visualised by immunodetection using rabbit polyclonal anti-pVIII primary, and rabbit-IgG-specific secondary AP-conjugated antibody that does not interact with the mouse antibodies in the printed control line. Particles that carried analyte (fibronectin), bound to the FnBP (BSF529.FnBP), were expected to bind to the test line, and the signal was expected to correlate to the amount of fibronectin in the assay. All particles should bind to the control line (Figure 5.8). Interestingly, the lowest Fn concentration that gave the signal and hence, the sensitivity limit of this assay was 0.04 pg/ μ L, equivalent to 0.167 attomoles/ μ L or 100,000 molecules/ μ L. A weak signal

was detected in the absence of Fn. Nanorods without detector molecule (BSF529) were used as a negative control; they gave no signal.

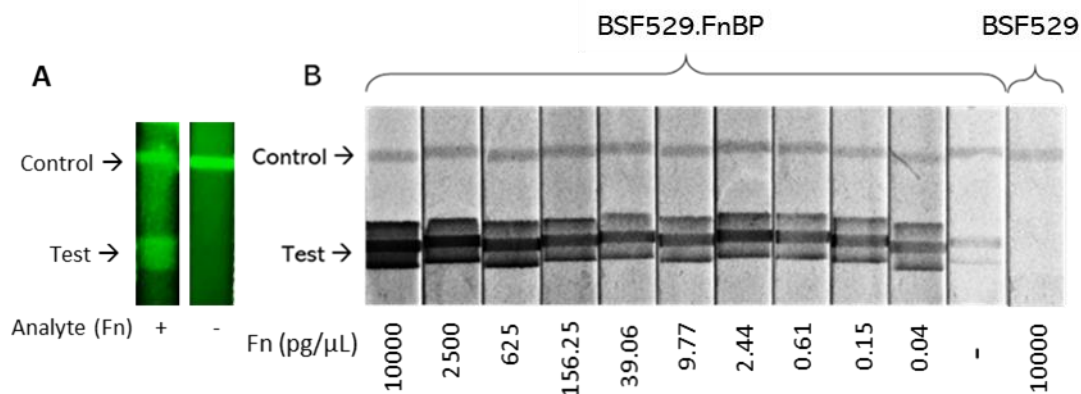


Figure 5.9. Fibronectin detection using FnBP-displaying nanorods in the lateral-flow dipstick assay.

A, Fibronectin dipstick assay using fluorescently labelled BSF719.Gly₄.FnBP nanorods. Signal was detected using fluoroimager (Azure c600). A total of 10^{11} nanorods were mixed with 1 μ g of fibronectin diluted in PBS (100 μ L final volume), or PBS alone, and incubated for 30 min at room temperature. Test strips were dipped into the mixture, allowing lateral flow for 15 min. Particles that carry Fn bound to Test line were visualised on the bottom line, as described in Figure 5.6. Control line captured all the BSFnano particles (BSF529.FnB and BSF529). **B,** Series of fibronectin dilutions analysed using BSFnano-based dipstick assay. Each assay contained 10^{11} nanorods in the total volume of 100 μ L; Fn concentrations are indicated below each stick.

It is important to note is that the fibronectin detection dipstick assay yielded unspecific binding and a strong false-positive signal when the membrane was blocked with milk-containing blocking buffers because milk contains fibronectin. The false-positive signal was minimised by using a commercial blocking buffer that was non-mammalian-based (Odyssey®) and adding anti-fibronectin

antibody at 1:1,500 dilution to the blocking buffer to block most of fibronectin that was present in the solution.

5.3 DISCUSSION

In the previous study (Sattar et al., 2015), short Ff-derived nanorods (named Ff-nano; equivalent to BSF221) were successfully produced and functionalised; however, the yields of nanoparticles were extremely low. Additionally, even though these nanorods could not replicate and do not contain any antibiotic resistance genes, a full-length helper phage had to be used as a source of proteins required for replication and particle assembly. A long helper phage posed a challenge of full-length Ff particles production alongside Ff-nano, and then in much higher numbers relative to nanoparticles. Despite multi-step purification protocol used to eliminate full-length phage, it was not possible to obtain phage-free nanorods (Sattar et al., 2015).

Consequently, it was hypothesised that a two-plasmid assembly system (described in Section 1.2.1) could be optimised to provide high yields of pure functionalised nanoparticles for diagnostic applications in the absence of full-length phage. During this research, purified BSFnano particles, with and without the tetra-glycine handles (described in Section 5.2.1), were used in a lateral-flow dipstick assay to detect fibronectin. A fibronectin-detection assay was chosen as a proof of concept, given that it has been reported to provide a strong, measurable, qualitative and quantitative signal when FnBP-displaying

nanorods Ffnano.FnBP (BSF221.FnBP) of identical virion protein composition were used (Sattar et al., 2015).

Lateral flow immunoassays are ranked on their performance based on specificity and sensitivity (Tan et al., 1999). Interestingly, the dipstick assay in this research showed a detectable signal at the T line for Fn concentration of 0.04 pg/ μ L (Figure 5.9). In contrast, Sattar et al. (2015) reported that the lowest Fn concentration where there was a signal at the T line on test strips was 80 pg/ μ L. The dipstick assay based on these nanorods produced using the new helper-plasmid system was therefore 2,000-fold as sensitive as was the identical assay reported for the phage-system-produced 50 nm nanorods (Sattar et al., 2015).

To compare these results with the LFIA kits for fibronectin detection currently available on the market (Creative Diagnostics, USA), the sensitivity limit is reported to be 10 pg/ μ L. This dipstick assay uses gold nanoparticles, coated with fibronectin-specific antibodies.

Depending on the desired properties of a diagnostic assay, displayed functionalisation handles on pVIII protein along the nanorod could be utilised to modify the strength of the signal, or to decrease the time for the signal readout (Li et al., 2010b). For rapid identification of analytes in the field, for example in food production (Ching et al., 2015), quality control (van Dam et al., 2013), and environmental testing (Mei et al., 2013), dye-labelled nanoparticles could be used for generating a visual signal with dipstick assays. Furthermore, for a higher resolution and quantification, the

detection of labelled nanorods could be enhanced with hyperspectral imaging (Daeschlein et al., 2017; Vresak et al., 2016).

However, the central part of this research was the development and improvement of BSFnano production and nanotechnology. Therefore, further discussion will focus on what are the advantages and possible reasons for the observed increase in the sensitivity of diagnostic.

There could be three possible reasons that have contributed either separately, or in synergy, to high sensitivity of fibronectin detection when using functionalised BSFnano particles. Firstly, the two-plasmid system produces only nanorods and therefore does not require extra purification steps to separate nanorods from the full-length helper phages. This, in turn, decreases the time needed to concentrate the nanorods from the crude culture supernatants that contain *E. coli* proteases. Therefore, by decreasing the opportunity for the displayed detector molecule to be proteolyzed, an increased proportion of the FnBP detector display was achieved. Overall, two detector peptides (FnBP) were displayed per BSFnano particle, in contrast to one peptide per two particles in Ff-nano display system of Sattar et al. (2015). An increased avidity of the particles was observed, and most probably resulted from the display of more than one detector molecule in proximity to each other, at the pIII tip of the nanorod.

The second improvement was the pBSFnano plasmid, which contained the replication-assembly cassette that has both

positive and negative f1 *ori*. In contrast, pSS3 only possess positive *ori*. Consequently, this meant that a smaller culture volume (1 L vs 8 L) was required to produce the same number of particles, resulting in faster processing and concentration of the particles.

Finally, the third improvement was the increase of pVIII : FnBP (reporter : detector) ratio due to the higher number of pVIII per nanorod. Initially, it was thought that the increased length of the nanorod (75 nm vs 50 nm) might be a concern for its diffusion in the lateral flow assay. However, the experimental data demonstrated that the longer nanorods did not impair its diffusion during the assay. This finding may be because the increase in the length of the nanorod is still comparably much smaller than the difference between either the size of the nanorods and the full-length phage. The BSF529 monomer, even though 50% longer than Ff-nano, it is still 1/10th the size of the full-length Ff phage.

When designing the helper plasmids that would provide displayed functional groups on the coat proteins, the copy number and position of displayed functionalities depends on the virion protein that is used as the platform. For example, use of pVIII as a display platform allowed high copy numbers of displayed peptide along the nanorod. The exact number of displayed peptides depends on the number of pVIII subunits per nanorod, which in turn is in direct correlation to the length of the ssDNA genome. As described earlier, (Figure 1.7B) the length of the genome can be adjusted by inserting

or deleting the DNA sequences between initiator and terminator of the BSFpn replication cassette.

On the other hand, the use of the minor coat proteins (most often pIII) as platforms, allows the display of up to five copies per particle, at one of the particles' ends (Figure 5.2). Using minor proteins at opposite ends (e.g., pVII/pIX, pIII/pVI) as display platforms for two different functionalities would create functionally asymmetrical particles with two separately controlled reactive groups at two different ends.

Helper plasmid designs incorporated an *amber* mutation within *gVIII* sequence to prevent toxicity of this protein during its expression in a non-suppressor *E. coli* host strain. The nanorods that were produced from the helper plasmids containing *gVIII*^{2_{am}} showed a smear on the native agarose gels. In contrast, BSFnano produced from helper plasmids with *gVIII*-20_{am} produced relatively sharp bands when the electrophoresis was performed at pH 8.3 (typical conditions for gel electrophoresis). This was due to the change of the isoelectric point (pI) of protein pVIII (and presumably that of the whole nanorod) from 6.8 to 8.3 in the helper plasmids containing *gVIII*^{2_{am}} due to incorporation of serine instead of glutamic acid by the host suppressor strain.

Filamentous phages, and therefore Ff-derived nanoparticles, are very stable over a wide pH range. In order to obtain the sharp bands in native gels from particles that carry an *amber* mutation in position 2 of mature pVIII protein (or codon 25 in *gVIII*), the pH of TAE buffer was increased from

8.3 to 9.0, which was above the pI of the particles. This change resulted in avoiding the particles of multiple different charges and therefore sharpening the bands. Importantly, this pH was not high enough to disassemble the nanorods during gel electrophoresis.

Additionally, when observing similar production of two nanorods, BSF529.HAS8 and BSF529.Rnano38, the former containing truncated pIII lacking N1N2 domain, and the latter with full-length pIII protein (Section 5.2.1), it could be concluded that the deletion of N-domain from pIII did not prevent particle assembly. This finding was in accordance with the previous research on the deletion of pIII from Ff phage particles, where it was observed that only C-domain was essential for particle assembly (Rakonjac et al., 1999). Hence, the BSFnano rods behave the same way as Ff phages, in terms of particle assembly and release of the particles from the *E. coli* membrane, as presented in the last stage of the phage life cycle (Figure 1.4).

Besides the LFIA-based tests (introduced in Section 1.3.1), BSFnano rods could be used in immuno-PCR for ultrasensitive diagnostics in forensics or the detection of explosives (Liu et al., 2016b). In such assays, instead of detecting the whole nanorods bound to the analyte, like in dipsticks, the bound particles could be lysed by heat (95 °C for 10 min) or with low pH solutions. These conditions would cause the release of the encapsulated ssDNA, which is then amplified and quantified by qPCR analysis. However, in comparison to the lateral flow immunoassay, iPCR requires highly trained staff and sophisticated laboratory equipment (real-time PCR

machine). When looking at the lab-based tests, ELISA is still routinely used as a gold standard for immuno-based assays (Cazacu et al., 2003).

.

Chapter 6. CONCLUSIONS AND FUTURE DIRECTIONS

6.1 CONCLUSIONS

This thesis is composed of two separate streams of technological developments. The first line of research was towards Ff-based vaccines that stimulate cytotoxic T cell responses. A recombinant phage-based construct that carried a high ratio of antigenic peptide to adjuvant molecules was successfully manufactured as a vaccine to be tested in murine models. The vaccine was efficiently acquired by APCs *in vitro* and was successfully presented to iNKT cells *in vivo*. Further optimisation is required to achieve efficient adaptive T-cell immune responses *in vivo*.

The second line of research was towards technological improvements of a previously developed diagnostic assay using novel functionalised biological nanorods, named BSFnano. The dipstick diagnostic assay developed during this research was 2,000 times more sensitive than a previously reported assay. (Sattar, 2015). The new nanorods developed in the current study show promising potential for use in the rapid and sensitive detection of biomolecules.

6.2 FUTURE DIRECTIONS

In the future, a proposed outline of work is required to optimise the phage-based vaccine for immunotherapy, and to further develop BSFnano technology:

6.2.1 Future developments of the Ff-based vaccine

For the applications of phage display technology in drug delivery, it is common to express specific peptides, antibodies or receptor-sensitive proteins on the surface of modified virions (Willats, 2002). In one study, a synthetic peptide was used to improve the transdermal delivery of human growth hormone and insulin (Chen et al., 2006). Similarly, (Hofmeister et al., 2015) engineered phage-based nanocarriers guided by "PREY" peptide to bind to the atherosclerotic vasculature. To improve the T cell responses *in vivo*, a phage-based vaccine can be optimised by displaying scFvs derived from monoclonal antibodies that will target the vaccine to the appropriate subset of dendritic cells specialised for inducing CD8⁺ T-cell responses (e.g., anti-Clec9A mAb for targeting to CLEC9A⁺XCR1⁺ cDCs) (Park et al., 2017).

It is important to note that, based on the findings in this thesis, it is expected that recombinant fusion of additional peptides to the Ff proteins (e.g., pIII) is likely to result in a further decrease of phage yields under the conditions required for incorporation of azide groups in recombinant antigen-pVIII fusion. With the production already diminished

by an order of magnitude due to antigen-pVIII fusion, this will likely make it impossible to obtain a sufficient number of phages for vaccination.

One alternative to the recombinant display of cell-targeting peptides is chemical attachment to purified particles. Click chemistry can be utilised for this, in the same way as the adjuvant display, provided that the molecule of interest (e.g., anti-Clec-9A mAb) has an alkyne functional group required for this reaction (e.g., DBCO, or DIBAC) (Hein et al., 2008). If click chemistry is used for attachment of additional molecules on Ff-based vaccine particles, optimisation of reaction conditions would have to be considered. Due to utilising the azide groups displayed on pVIII protein, this would result in competing with the adjuvant attachments. If a lesser amount of adjuvant is attached to the particle, this may result in a decrease of the iNKT cell activation *in vivo*. On the other hand, if the phage production conditions were to be shifted towards higher azide display, there is an increased cost of production and a high potential of decreasing the copy numbers of antigenic peptides.

Another option to attach cell-targeting functionalities on the phage particles, after they are purified from culture media, is to use an enzymatic attachment. Important to note that this would be a more targeted approach and would not compete with the adjuvant attachments via azide groups. For example, short peptides (AAGGGG or GGGG) can be displayed on pIII or pIX, that would allow enzymatic attachment of LPETA- or LPXTG- containing molecules (e.g., anti-Clec-9A

mAb) by using the enzyme Sortase A derived from *S. pyogenes* (SrtA_{py}), or *S. aureus* (SrtA_{au}), respectively (Hess et al., 2012).

Furthermore, the vaccine could be redesigned so that the adjuvant BODIPY- α -GalCer is chemically attached to the N-terminus of a displayed peptide with cathepsin cutting sites, instead of directly to the pVIII phage protein. In the current vaccine design, phages carry a mixture of OVA-pVIII, OVA(BODIPY- α -GalCer)pVIII, BODIPY- α -GalCer.pVIII and free pVIII. If adjuvant molecule α -GalCer be chemically or enzymatically attached to the N terminus of Ff-displayed OVA peptide, the OVA-pVIII fusions will be mosaic, with some of them displaying α -GalCer in addition to OVA (α -GalCer-OVA-pVIII). These fusions displaying α -GalCer covalently conjugated to OVA would ensure that the adjuvant is presented to the APC at the same time as OVA antigen. This design could solve the problem of iNKT and CD8⁺ T-cell localisation to the same APCs. In this way, the key prerequisite for induction of adaptive CD8⁺ T-cell response, coordinating the appropriate rate of release of antigen vs. α -GalCer *in vivo* would be fulfilled, so that peptide and adjuvant are optimally presented by the same APCs (Prendergast et al., 2018). Additionally, recombinant expression of peptide antigen, followed by enzymatic or chemical attachment of the adjuvant molecules, would still allow modifications of the OVA: α -GalCer ratio by controlling the concentrations of added adjuvant, while keeping the two molecules directly attached to each other.

6.2.2 Adaptation of BSFnano purification and concentration protocols for vaccine applications

BSFnano particles could be used as vaccine particles instead of filamentous phage. Unlike Ff phages, which are genetically modified viruses, BSFnano do not carry any protein-encoding genes; therefore, obtaining the regulatory approvals for their use outside of the laboratory should be possible. Ideally, BSFnano would be functionalised to target dendritic cells (as stated above), while loaded with antigens and adjuvants in a manner that would induce CD8⁺ T cell responses. To achieve this, alterations in particle purification protocol have to be considered. The optimisation is particularly needed in the case of azidohomoalanine incorporation into pVIII coat protein that occurs in the presence of minimal medium. Salts in this medium precipitate in 15% PEG800, preventing purification of short nanorods using PEG precipitation. To avoid the PEG precipitation step, protocols for a concentration of particles from the large volume of culture media will need to be optimised for a particular application. Some suggestions include membrane filtration, chromatography and crossflow filtration.

6.2.3 Future developments of the BSFnano-based technology

BSFnano can be used for diagnostic purposes in the rapid, sensitive detection of trace molecules (e.g., toxins, explosives, viruses, biomarkers for diseases). To increase

the speed of the readout signal, additional techniques of particle detection have to be explored. This can be achieved by attaching visible dye molecules for spectrophotometric detection or hyperspectral analysis and quantification (Vresak et al., 2016). Alternatively, peptides that nucleate paramagnetic nanocrystal assembly along the nanorod (Neltner et al., 2010) could also be attached to pVIII. In a recent paper (Ross et al., 2019) carbon-labelled nanoparticles were used in a multiplex LFIA, combined with the smartphone detection for allergens. Potentially, similar assays could be developed with BSFnano technology. "Quantum phages" have been recently designed at MIT, USA (Park et al., 2016), with a potential application in distribution of energy from solar panels; therefore, BSFnano could potentially be used in photoelectronic detectors.

At the time of writing this thesis, there was a global pandemic outbreak of SARS-CoV-2 virus. The need for rapid diagnostic tests for the antigen particles, as well as vaccines, spread across the world as a number one priority. Even though this was not the topic of the research done for this thesis, it is important to acknowledge the possibility of the BSFnano applications for this purpose.


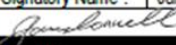
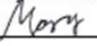
The nanorods-based LFIA from this study (Section 5.2.5) could be modified to detect the virus particles, and therefore ensure the rapid responses in case isolation or hospitalisation is needed. One of the critical bottlenecks in controlling the pandemic is the number of tested individuals (Binnicker, 2020; Vashist, 2020). Currently, the gold standard for diagnose is PCR amplification of the viral

genetic material (Mardani et al., 2020; van Kasteren et al., 2020). However, gene-based tests are relatively expensive, time-consuming and restricted to trained personnel and laboratory equipment. These test are also dependent on “cold-chain” dependent chemicals. In contrast, a point of care dipstick tests are quick and easy to use. Direct antigen testing is currently being rolled out in the USA to to enable population surveillance that will help control the pandemic (Service, 2020).

Besides diagnostic applications of the BSFnano technology, targeted drug delivery in nanomedicine is a growing field. For example, modified nanorods could be utilised as drug delivery vehicles, similar to Ff-based vaccine described in Chapter 3. Recently, researchers (Finbloom et al., 2018) tested the delivery of doxorubicin via three different virus-like particles (VLPs) to glioblastoma. Drugs that target the brain diseases have an additional obstacle to cross, the blood-brain barrier (BBB). One way of delivering the drug molecules through the BBB is to chemically attach them to the genetically modified BSFnano that display BBB-targeting peptides (Diaz-Perlas et al., 2017). Furthermore, research from (Frenkel and Solomon, 2002) showed that Ff phages can easily cross the blood-brain barrier (BBB) in murine models, even without carrying any BBB-transporting peptides. Therefore, the potential of BSFnano to penetrate BBB remains to be explored in the future.

Chapter 7. APPENDICES

7.1 MPI APPROVAL FOR TRANSFER OF PHAGES

FOR Microorganisms/Cell Cultures/GMO's Invertebrates Vertebrate Lab Animals Plants Zoo Animals	Ministry for Primary Industries Manatū Ahu Matua 		
AUTHORITY TO MOVE UNCLEARED BIOSECURITY RISK GOODS <small>Authorised under section 25 of the Biosecurity Act 1993 for the movement of uncleared risk goods held in facilities approved to the following MPI/EPA facility standards:</small>			
<div style="display: flex; justify-content: space-between;"> <ul style="list-style-type: none"> ▪ Standard for Facilities for Microorganisms and Cell Cultures: 2007a (154.03.02) ▪ Standard for Transitional & Containment Facilities for Invertebrates (154.02.08) ▪ Standard for Containment Facilities for Vertebrate Laboratory Animals (154.03.03) <ul style="list-style-type: none"> ▪ Standard for Containment Facilities for Plants: 2007 (155.04.09) ▪ Standard for Containment Facilities for Zoo Animals (154.03.04) </div> <p style="text-align: center;">**The goods being moved are subject to all conditions specified in the original Permit to Import. Ensure you are aware of these**</p>			
Uncleared Biosecurity Risk Goods			
Description & Quantity of Goods ² :	Filamentous phage (Ff) strains (R783) Ff.FLAG and Ff.OVA resuspended in small volumes of PBS. Details about the quantity will be included with the parcel and transfer paperwork.		
Applicable BACC Number(s):	N/A		
Applicable MPI Permit to Import Number(s):	N/A		
Applicable HSNO Approval Number(s):	Massey (GMO04/MU016 S67A); Malaghan APP201737		
Single or Multiple Movement ⁴ :	Multiple		
Movement Details			
Proposed Date of Movement:	21/01/2019 To be completed by 21/01/2020		
Proposed Method of Transport & Management of Biosecurity Risks:	Transport by tracked NZ courier service. Each sample will be individually labelled and packaged in 3 layers.		
Sending Facility			
Applicant Name:	Marina Rajic	Department (if applicable):	IFS
Email or Fax:	m.rajic@massey.ac.nz	Phone Number:	+64 6 350 5237
Facility Name:	Massey University	MPI Reg ⁿ . Number:	3088
Facility Operator:	Massey University	Relevant Facility Standard:	154.03.02
Facility to be Charged:	Massey University	Purchase Order # (if available):	IFS to pay
Authorised Signatory Name ³ :	James Connell	Date:	14/12/2018
Signature:			
Receiving Facility			
Receiving Persons Name:	Prof Ian Hermans	Department (if applicable):	
Email or Fax:	ihermans@malaghan.org.nz	Phone Number:	+64 4 499 6914 ext 823
Facility Name:	Malaghan Institute, Victoria University of Wellington	MPI Regn. Number:	612
Facility Operator:	Malaghan Institute Graham Le Gros	Facility standard approved to	154.03.02
Declaration: I agree to receive the uncleared risk goods named in this authorisation and comply with the regulatory requirements in accordance with this authorisation and the relevant facility standard. (Not required for export)			
Receiving facility Authorised Signatory Name ³ : Mark Yang		Date: 15/01/2019	
Signature: 			

Conditions	
A.	A copy of this form & the applicable HSNO approval controls must accompany the goods during movement.
B.	The goods being moved are subject to all conditions specified in the original Permit to Import and relevant HSNO approval ⁵ .
C.	The method of transport must ensure the containment of the risk good(s) in accordance with Section 8 of AS/NZS 2243:3:2002, & the IATA Dangerous Goods Regulations/Live Animal Regulations, where applicable).
D.	Packages/consignments must be labelled with senders and receivers contact details and the nature of the contents.
E.	Packages/consignments of goods that have been moved under this authorisation must only be opened within the receiving facility.

MPI USE ONLY	Your Application is <u>APPROVED</u> / NOT APPROVED	Movement Authority #: NS053
	Inspector Name: Nicki Sherratt	Specialist Adviser Name:
	Signature: <i>N Sherratt</i> Date: 17/01/18	Signature: Date:

Email this completed & signed form to containmenttransfers@mpi.govt.nz or your primary MPI Inspector

Important Information

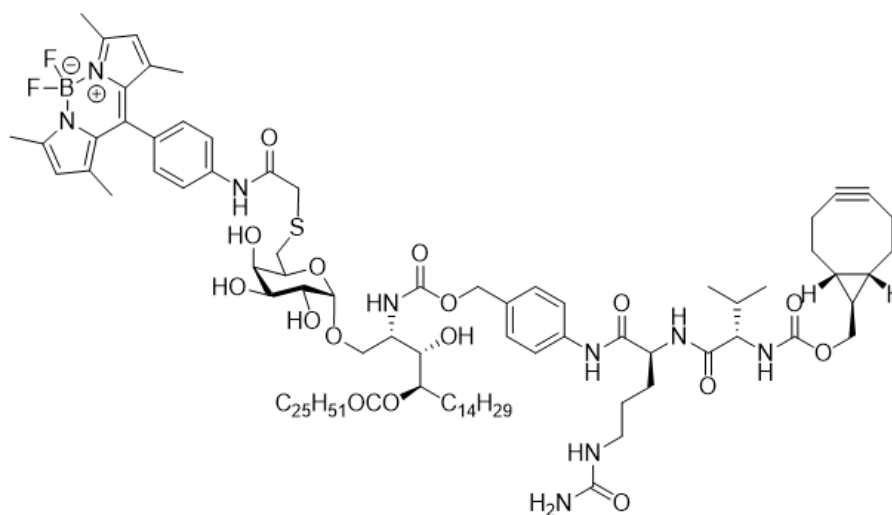
1. All applicable parts of the form must be completed.
2. Sufficient information must be provided to describe the nature and quantity of the organisms being moved, including scientific name and, where applicable, individual identifier, gender, number of vials/containers etc.
3. 'Authorised Signatories' are persons that have been authorised by the facility operator to sign movement request authorities, and have been approved as such by MPI. Authorisation must be in writing, have been accepted as such by MPI, and recorded in the facility documentation prior to receipt of movement authority requests.
4. This form may be used for one-off (single) movements or multiple movements of the named uncleared risk goods. It is not necessary to name the number of multiple movements that may occur.
5. In order to inform the receiving facility of the conditions specified in the original Permit to Import, a copy of the conditions should accompany the consignment or sent to the receiving facility separately. It is the responsibility of the Operator of the receiving facility to ensure that the risk goods being received are held subject to the conditions specified in the original Permit to Import.
6. No movement of risk goods must be initiated prior to receiving MPI approval.
7. All conditions of the authorisation must be complied with. Compliance will be subject to verification by MPI.
8. Failure to comply with this authorisation, or any part(s) of it, is an offence under section 154(N)(6) of the Biosecurity Act 1993 and may be subject to penalties under that Act.

Additional Conditions

7.2 CHEMICAL STRUCTURES

7.2.1 BODIPY- α -GalCer adjuvant molecule (CI270A)

CI270A: 6-(BODIPY-COCH₂-S)-m α GC-PAB-CV-BCN



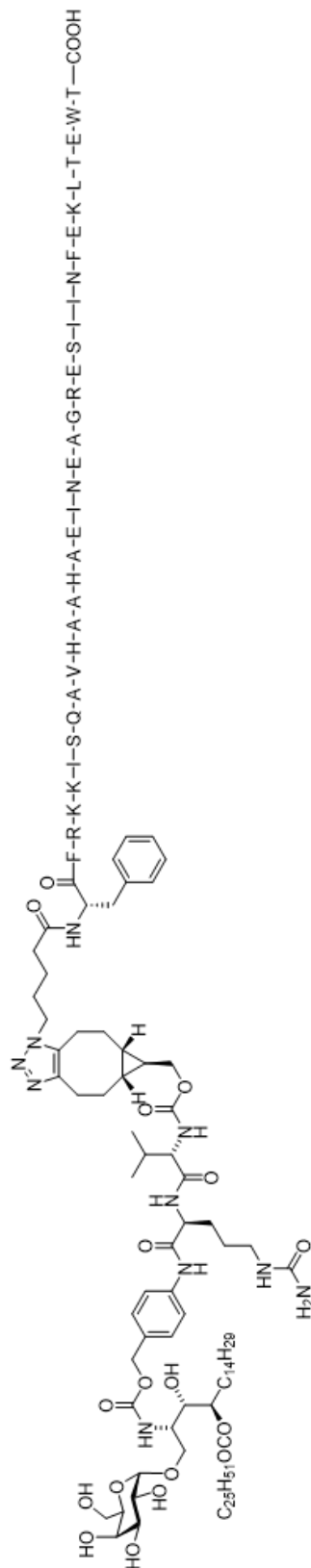
Chemical Formula: C₁₀₁H₁₅₈BF₂N₉O₁₆S

Exact Mass: 1834.1608

Molecular Weight: 1835.2888

7.2.2 Conjugate vaccine molecule (CI038)

CI038: M α GC-PAB-CV-BCN-FFRK-K-ISQAVHAAHAEINEAGR-E-SIINF-EKL-TEWT



Chemical Formula: C₂₆₉H₄₂₉N₆₁O₇₀

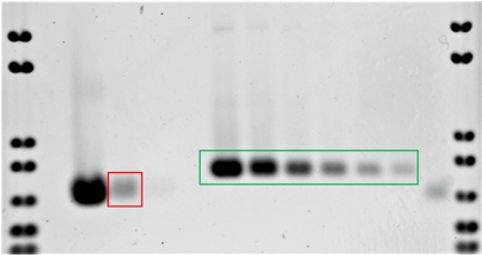
Exact Mass: 5634.1885

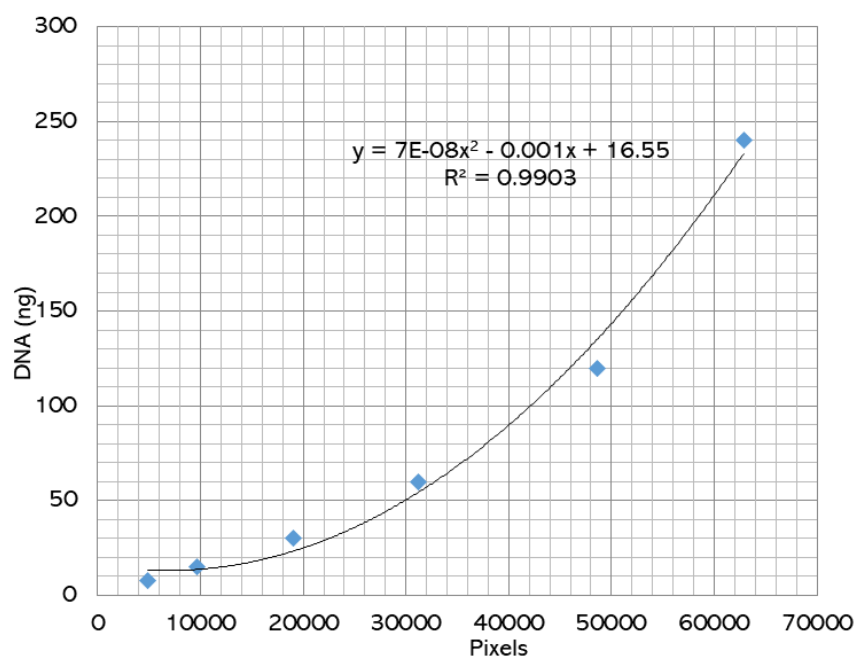
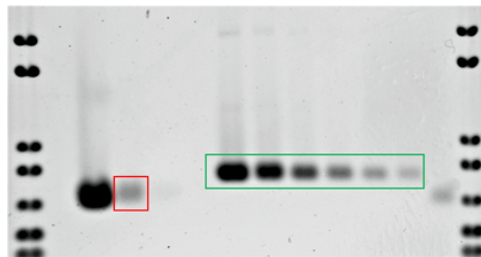
Molecular Weight: 5637.7480

7.3 QUANTIFICATION AND MOLECULE ANALYSIS

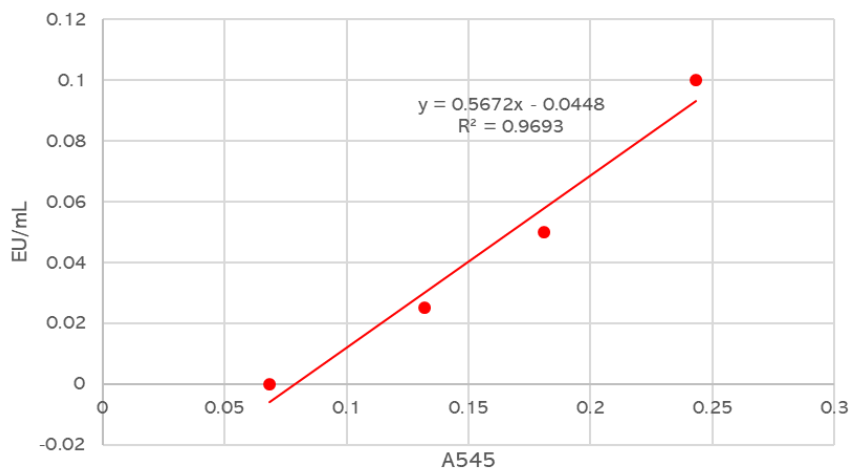
7.3.1 BSFnano particle quantification

Base	Mw	#BSF719	total BSF719			
A	313.2	150	46,980.00			
T	304.2	196	59,623.20			
G	329.2	167	54,976.40			
C	289.2	206	59,575.20			
Total (g/mol)		719	221,154.80			
Molecules (Avogadro)		6.02E+23				
particles/g DNA			2.7221E+18			
particles/ng DNA			2.7221E+09			
Standard for calibration						
NanoZap	Pixels	ng (ssDNA)	ssDNA std. (ng/uL)	loaded ssDNA (uL)		
1	62852.969	240.00	40.00	6.00		
2	48570.546	120.00	20.00	6.00		
3	31217.233	60.00	10.00	6.00		
4	19074.714	30.00	5.00	6.00		
5	9705.903	15.00	2.50	6.00		
6	4898.305	7.50	1.25	6.00		
Sample	Pixels	DNA (ng)/lane	sample (uL)/lane	DNA (ng)/sample (uL)	DNA (ng)/ sample (mL)	particles/mL
pHAS1+Zap537 in 2091	93691.983	5.373E+02	0.53	1.023E+03	1.023E+06	2.786E+15



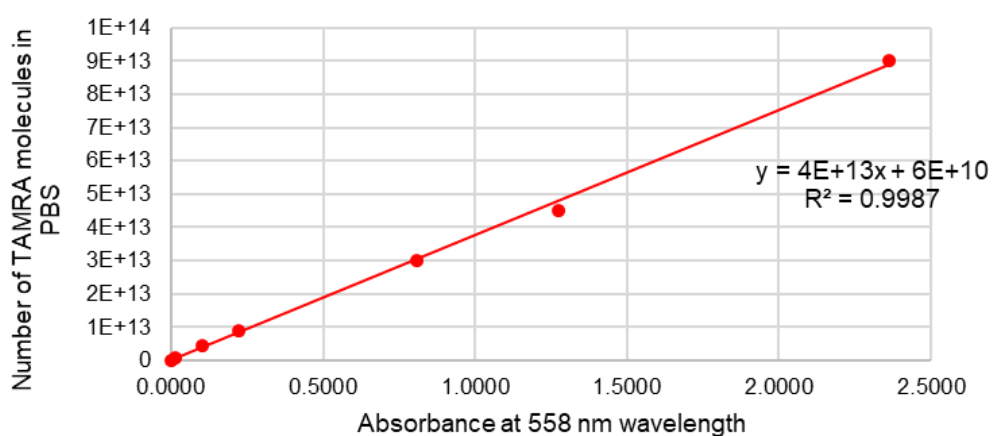
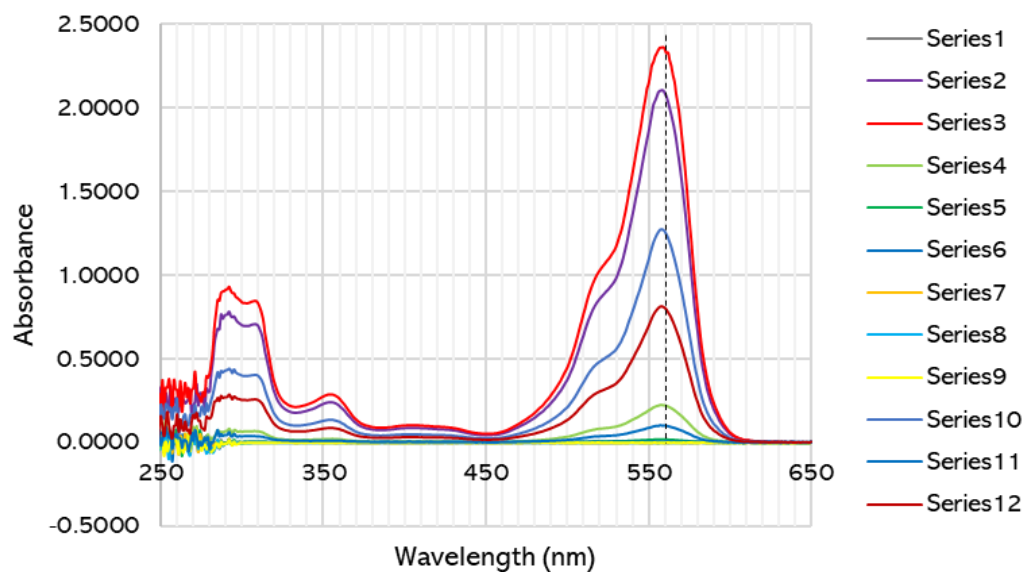


7.3.2 Endotoxin quantification via LAL assay

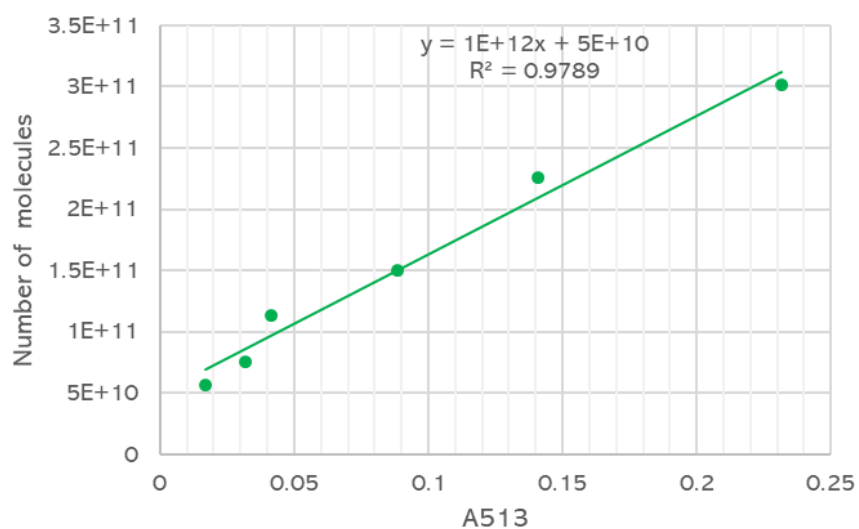
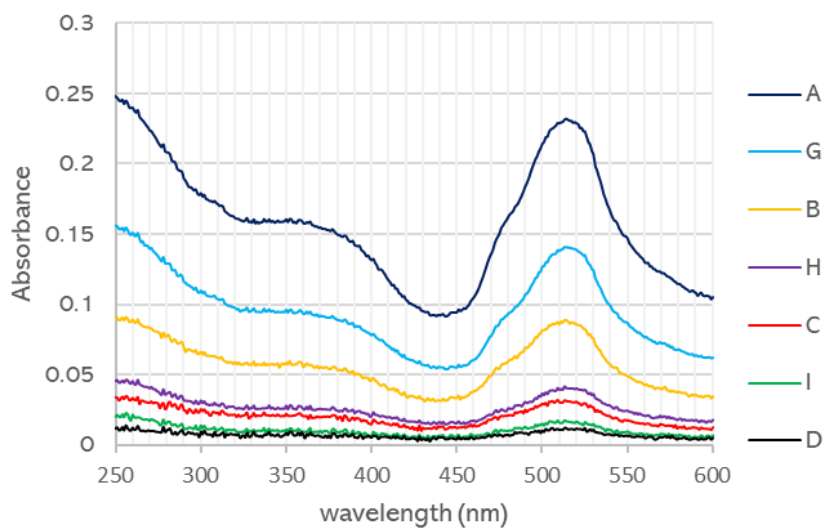


Std curve		EU/mL				
Sample	Blank	0	0.01	0.025	0.05	0.1
A545	0.0433	0.1118	0.1944	0.1752	0.2242	0.2866
Std-blank	0	0.0685	0.1511	0.1319	0.1809	0.2433

7.3.3 TAMRA fluorescence quantification

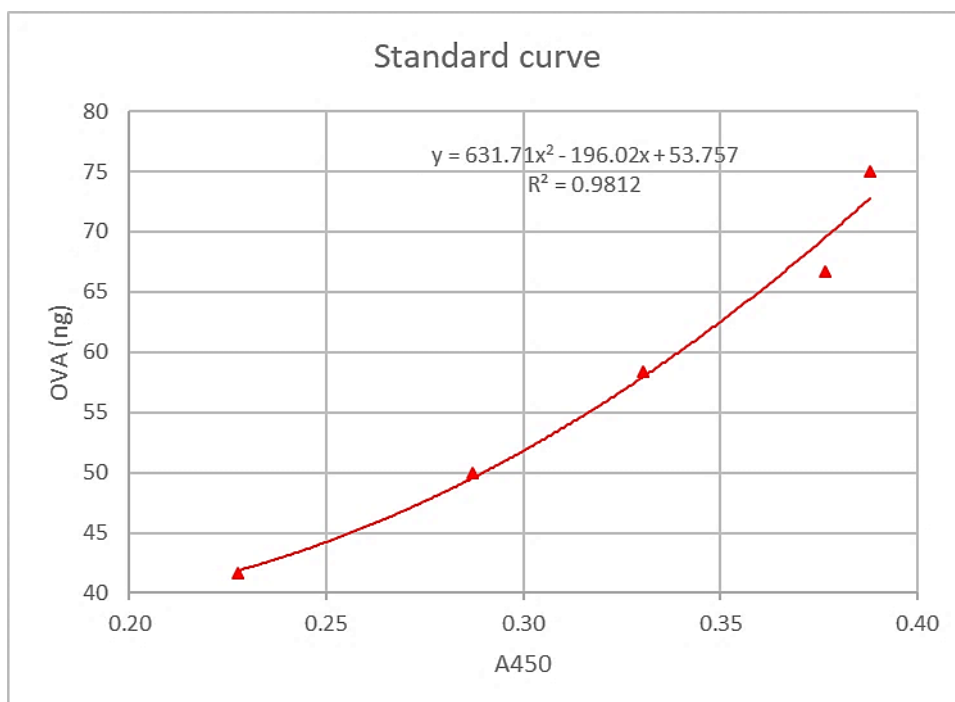


Series	1	2	3	4	5	6
M (mol/L)	-	3.00E-05	3.00E-07	3.00E-08	3.00E-09	3.00E-10
n (mol)	-	1.50E-08	1.50E-10	1.50E-11	1.50E-12	1.50E-13
N	-	9.03E+15	9.03E+13	9.03E+12	9.03E+11	9.03E+10
Series	7	8	9	10	11	12
M (mol/L)	3.00E-11	3.00E-12	3.00E-13	1.50E-07	1.50E-08	1.00E-07
n (mol)	1.50E-14	1.50E-15	1.50E-16	7.50E-11	7.50E-12	5.00E-11
N	9.03E+09	9.03E+08	9.03E+07	4.52E+13	4.52E+12	3.01E+13

7.3.4 BODIPY- α -GalCer quantification via fluorescence

Sample	A	G	B	H	
A513	0.2318	0.141	0.0886	0.0412	
N	3.01E+11	2.26E+11	1.51E+11	1.13E+11	
Sample	C	I	D	E	F
A513	0.0317	0.0171	0.0118	0.0065	0.0021
N	7.53E+10	5.65E+10	3.76E+10	1.88E+10	9.41E+09

7.3.6 Example of OVA-pVIII fusion quantification



	A₄₅₀	
BSA	0.0486	
PBS	0.0461	
Na-carb	0.0508	
R783.OVA	0.2759	0.2918
Calculation		
pfu/mL	8.53E+09	8.53E+09
pfu total	1.07E+09	1.07E+09
true signal	0.2274	0.2433
ng OVA/mL	41.84826	43.45934
g OVA/mL	4.18E-08	4.35E-08
Mw OVA (g/mol)	3365	3365
N Av	6.02E+23	6.02E+23
N (OVA)/mL	7.49E+12	7.77E+12
N (OVA) total	9.73E+11	1.01E+12
pVIII / phage	3655	3655
pVIII total	3.9E+12	3.9E+12
OVA/phage	910	945
% fusion	25%	26%

7.4 STATISTICAL ANALYSES

7.4.1 iNKT cell activation in spleen and liver (Section 4.2.1)

Cell count per organ (spleen) - Figure 4.3A

Number of families	1								
Number of comparisons per family	6								
Alpha	0.05								
Tukey's multiple comparisons test	Mean Diff.	95.00% CI of diff.	Significant?	Summary	Adjusted P Value				
BODIPY- α -GalCer vs. Ff.FLAG	30280000	-31848757 to 92408757	No	ns	0.5204	A-B			
BODIPY- α -GalCer vs. Ff.FLAG.BODIPY- α -GalCer	-63800000	-125928757 to -1671243	Yes	*	0.0431	A-C			
BODIPY- α -GalCer vs. PBS	40000000	-22128757 to 102128757	No	ns	0.2908	A-D			
Ff.FLAG vs. Ff.FLAG.BODIPY- α -GalCer	-94080000	-156208757 to -31951243	Yes	**	0.0026	B-C			
Ff.FLAG vs. PBS	9720000	-52408757 to 71848757	No	ns	0.9691	B-D			
Ff.FLAG.BODIPY- α -GalCer vs. PBS	103800000	41671243 to 165928757	Yes	**	0.0011	C-D			
Test details	Mean 1	Mean 2	Mean Diff.	SE of diff.	n1	n2	q	DF	
BODIPY- α -GalCer vs. Ff.FLAG	83400000	53120000	30280000	21715598	5	5	1.972	16	
BODIPY- α -GalCer vs. Ff.FLAG.BODIPY- α -GalCer	83400000	147200000	-63800000	21715598	5	5	4.155	16	
BODIPY- α -GalCer vs. PBS	83400000	43400000	40000000	21715598	5	5	2.605	16	
Ff.FLAG vs. Ff.FLAG.BODIPY- α -GalCer	53120000	147200000	-94080000	21715598	5	5	6.127	16	
Ff.FLAG vs. PBS	53120000	43400000	9720000	21715598	5	5	0.633	16	
Ff.FLAG.BODIPY- α -GalCer vs. PBS	147200000	43400000	103800000	21715598	5	5	6.76	16	

Cell count per organ (liver) - Figure 4.3A

Number of families	1							
Number of comparisons per family	6							
Alpha	0.05							
Tukey's multiple comparisons test	Mean Diff.	95.00% CI of diff.	Significant?	Summary	Adjusted P Value			
BODIPY- α -GalCer vs. Ff.FLAG	7959420	3682619 to 12236221	Yes	***	0.0004	A-B		
BODIPY- α -GalCer vs. Ff.FLAG.BODIPY- α -GalCer	-6778800	-11055601 to -2501999	Yes	**	0.0017	A-C		
BODIPY- α -GalCer vs. PBS	8141777	3864976 to 12418578	Yes	***	0.0003	A-D		
Ff.FLAG vs. Ff.FLAG.BODIPY- α -GalCer	-14738220	-19015021 to -10461419	Yes	****	<0.0001	B-C		
Ff.FLAG vs. PBS	182357	-4094444 to 4459158	No	ns	0.9993	B-D		
Ff.FLAG.BODIPY- α -GalCer vs. PBS	14920577	10643776 to 19197378	Yes	****	<0.0001	C-D		
Test details	Mean 1	Mean 2	Mean Diff.	SE of diff.	n1	n2	q	DF
BODIPY- α -GalCer vs. Ff.FLAG	8191950	232530	7959420	1494852	5	5	7.53	16
BODIPY- α -GalCer vs. Ff.FLAG.BODIPY- α -GalCer	8191950	14970750	-6778800	1494852	5	5	6.413	16
BODIPY- α -GalCer vs. PBS	8191950	50173	8141777	1494852	5	5	7.703	16
Ff.FLAG vs. Ff.FLAG.BODIPY- α -GalCer	232530	14970750	-14738220	1494852	5	5	13.94	16
Ff.FLAG vs. PBS	232530	50173	182357	1494852	5	5	0.1725	16
Ff.FLAG.BODIPY- α -GalCer vs. PBS	14970750	50173	14920577	1494852	5	5	14.12	16

% α -GalCer tetramer⁺ CD1d⁺ cells in spleen - Figure 4.3B

Number of families	1							
Number of comparisons per family	6							
Alpha	0.05							
Tukey's multiple comparisons test	Mean Diff.	95.00% CI of diff.	Significant?	Summary	Adjusted P Value			
BODIPY- α -GalCer vs. Ff.FLAG	20.4	18.21 to 22.59	Yes	****	<0.0001	A-B		
BODIPY- α -GalCer vs. Ff.FLAG.BODIPY- α -GalCer	-6.84	-9.030 to -4.650	Yes	****	<0.0001	A-C		
BODIPY- α -GalCer vs. PBS	21.03	18.84 to 23.22	Yes	****	<0.0001	A-D		
Ff.FLAG vs. Ff.FLAG.BODIPY- α -GalCer	-27.24	-29.43 to -25.05	Yes	****	<0.0001	B-C		
Ff.FLAG vs. PBS	0.63	-1.560 to 2.820	No	ns	0.8428	B-D		
Ff.FLAG.BODIPY- α -GalCer vs. PBS	27.87	25.68 to 30.06	Yes	****	<0.0001	C-D		
Test details	Mean 1	Mean 2	Mean Diff.	SE of diff.	n1	n2	q	DF
BODIPY- α -GalCer vs. Ff.FLAG	22.98	2.578	20.4	0.7655	5	5	37.69	16
BODIPY- α -GalCer vs. Ff.FLAG.BODIPY- α -GalCer	22.98	29.82	-6.84	0.7655	5	5	12.64	16
BODIPY- α -GalCer vs. PBS	22.98	1.948	21.03	0.7655	5	5	38.85	16
Ff.FLAG vs. Ff.FLAG.BODIPY- α -GalCer	2.578	29.82	-27.24	0.7655	5	5	50.33	16
Ff.FLAG vs. PBS	2.578	1.948	0.63	0.7655	5	5	1.164	16
Ff.FLAG.BODIPY- α -GalCer vs. PBS	29.82	1.948	27.87	0.7655	5	5	51.49	16

% α -GalCer tetramer CD1d⁺ cells in liver - Figure 4.3B

Number of families	1							
Number of comparisons per family	6							
Alpha	0.05							
Tukey's multiple comparisons test	Mean Diff.	95.00% CI of diff.	Significant?	Summary	Adjusted P Value			
BODIPY- α -GalCer vs. Ff.FLAG	37.82	30.79 to 44.85	Yes	****	<0.0001	A-B		
BODIPY- α -GalCer vs. Ff.FLAG.BODIPY- α -GalCer	-11.78	-18.81 to -4.748	Yes	**	0.001	A-C		
BODIPY- α -GalCer vs. PBS	49.6	42.57 to 56.64	Yes	****	<0.0001	A-D		
Ff.FLAG vs. Ff.FLAG.BODIPY- α -GalCer	-49.6	-56.63 to -42.57	Yes	****	<0.0001	B-C		
Ff.FLAG vs. PBS	11.78	4.752 to 18.82	Yes	**	0.001	B-D		
Ff.FLAG.BODIPY- α -GalCer vs. PBS	61.38	54.35 to 68.42	Yes	****	<0.0001	C-D		
Test details	Mean 1	Mean 2	Mean Diff.	SE of diff.	n1	n2	q	DF
BODIPY- α -GalCer vs. Ff.FLAG	58.34	20.52	37.82	2.458	5	5	21.76	16
BODIPY- α -GalCer vs. Ff.FLAG.BODIPY- α -GalCer	58.34	70.12	-11.78	2.458	5	5	6.778	16
BODIPY- α -GalCer vs. PBS	58.34	8.736	49.6	2.458	5	5	28.54	16
Ff.FLAG vs. Ff.FLAG.BODIPY- α -GalCer	20.52	70.12	-49.6	2.458	5	5	28.54	16
Ff.FLAG vs. PBS	20.52	8.736	11.78	2.458	5	5	6.78	16
Ff.FLAG.BODIPY- α -GalCer vs. PBS	70.12	8.736	61.38	2.458	5	5	35.32	16

Spleen #NKT - Figure 4.3C

Number of families	1								
Number of comparisons per family	6								
Alpha	0.05								
Tukey's multiple comparisons test	Mean Diff.	95.00% CI of diff.	Significant?	Summary	Adjusted P Value				
BODIPY- α -GalCer vs. Ff.FLAG	6795996	454675 to 13137317	Yes	*	0.0336	A-B			
BODIPY- α -GalCer vs. Ff.FLAG.BODIPY- α -GalCer	-8889060	-15230381 to -2547739	Yes	**	0.005	A-C			
BODIPY- α -GalCer vs. PBS	6999940	658619 to 13341261	Yes	*	0.028	A-D			
Ff.FLAG vs. Ff.FLAG.BODIPY- α -GalCer	-15685056	-22026377 to -9343735	Yes	****	<0.0001	B-C			
Ff.FLAG vs. PBS	203944	-6137377 to 6545265	No	ns	0.9997	B-D			
Ff.FLAG.BODIPY- α -GalCer vs. PBS	15889000	9547679 to 22230321	Yes	****	<0.0001	C-D			
Test details	Mean 1	Mean 2	Mean Diff.	SE of diff.	n1	n2	q	DF	
BODIPY- α -GalCer vs. Ff.FLAG	7357540	561544	6795996	2216455	5	5	4.336	16	
BODIPY- α -GalCer vs. Ff.FLAG.BODIPY- α -GalCer	7357540	16246600	-8889060	2216455	5	5	5.672	16	
BODIPY- α -GalCer vs. PBS	7357540	357600	6999940	2216455	5	5	4.466	16	
Ff.FLAG vs. Ff.FLAG.BODIPY- α -GalCer	561544	16246600	-15685056	2216455	5	5	10.01	16	
Ff.FLAG vs. PBS	561544	357600	203944	2216455	5	5	0.1301	16	
Ff.FLAG.BODIPY- α -GalCer vs. PBS	16246600	357600	15889000	2216455	5	5	10.14	16	

Liver #NKT - Figure 4.3C

Number of families	1								
Number of comparisons per family	6								
Alpha	0.05								
Tukey's multiple comparisons test	Mean Diff.	95.00% CI of diff.	Significant?	Summary	Adjusted P Value				
BODIPY- α -GalCer vs. Ff.FLAG	7959420	3682619 to 12236221	Yes	***	0.0004	A-B			
BODIPY- α -GalCer vs. Ff.FLAG.BODIPY- α -GalCer	-6778800	-11055601 to -2501999	Yes	**	0.0017	A-C			
BODIPY- α -GalCer vs. PBS	8141777	3864976 to 12418578	Yes	***	0.0003	A-D			
Ff.FLAG vs. Ff.FLAG.BODIPY- α -GalCer	-14738220	-19015021 to -10461419	Yes	****	<0.0001	B-C			
Ff.FLAG vs. PBS	182357	-4094444 to 4459158	No	ns	0.9993	B-D			
Ff.FLAG.BODIPY- α -GalCer vs. PBS	14920577	10643776 to 19197378	Yes	****	<0.0001	C-D			
Test details	Mean 1	Mean 2	Mean Diff.	SE of diff.	n1	n2	q	DF	
BODIPY- α -GalCer vs. Ff.FLAG	8191950	232530	7959420	1494852	5	5	7.53	16	
BODIPY- α -GalCer vs. Ff.FLAG.BODIPY- α -GalCer	8191950	14970750	-6778800	1494852	5	5	6.413	16	
BODIPY- α -GalCer vs. PBS	8191950	50173	8141777	1494852	5	5	7.703	16	
Ff.FLAG vs. Ff.FLAG.BODIPY- α -GalCer	232530	14970750	-14738220	1494852	5	5	13.94	16	
Ff.FLAG vs. PBS	232530	50173	182357	1494852	5	5	0.1725	16	
Ff.FLAG.BODIPY- α -GalCer vs. PBS	14970750	50173	14920577	1494852	5	5	14.12	16	

Spleen %NK1.1 - Figure 4.4A

Number of families	1							
Number of comparisons per family	6							
Alpha	0.05							
Tukey's multiple comparisons test	Mean Diff.	95.00% CI of diff.	Significant?	Summary	Adjusted P Value			
BODIPY- α -GalCer vs. Ff.FLAG	-57.27	-68.90 to -45.65	Yes	****	<0.0001	A-B		
BODIPY- α -GalCer vs. Ff.FLAG.BODIPY- α -GalCer	5.61	-6.015 to 17.23	No	ns	0.5284	A-C		
BODIPY- α -GalCer vs. PBS	-54.61	-66.24 to -42.99	Yes	****	<0.0001	A-D		
Ff.FLAG vs. Ff.FLAG.BODIPY- α -GalCer	62.88	51.26 to 74.51	Yes	****	<0.0001	B-C		
Ff.FLAG vs. PBS	2.66	-8.965 to 14.28	No	ns	0.9124	B-D		
Ff.FLAG.BODIPY- α -GalCer vs. PBS	-60.22	-71.85 to -48.60	Yes	****	<0.0001	C-D		
Test details	Mean 1	Mean 2	Mean Diff.	SE of diff.	n1	n2	q	DF
BODIPY- α -GalCer vs. Ff.FLAG	9.246	66.52	-57.27	4.063	5	5	19.93	16
BODIPY- α -GalCer vs. Ff.FLAG.BODIPY- α -GalCer	9.246	3.636	5.61	4.063	5	5	1.953	16
BODIPY- α -GalCer vs. PBS	9.246	63.86	-54.61	4.063	5	5	19.01	16
Ff.FLAG vs. Ff.FLAG.BODIPY- α -GalCer	66.52	3.636	62.88	4.063	5	5	21.89	16
Ff.FLAG vs. PBS	66.52	63.86	2.66	4.063	5	5	0.9258	16
Ff.FLAG.BODIPY- α -GalCer vs. PBS	3.636	63.86	-60.22	4.063	5	5	20.96	16

Liver %NK1.1 - Figure 4.4A

Number of families	1							
Number of comparisons per family	6							
Alpha	0.05							
Tukey's multiple comparisons test	Mean Diff.	95.00% CI of diff.	Significant?	Summary	Adjusted P Value			
BODIPY- α -GalCer vs. Ff.FLAG	-65.88	-76.53 to -55.23	Yes	****	<0.0001		A-B	
BODIPY- α -GalCer vs. Ff.FLAG.BODIPY- α -GalCer	2.66	-7.988 to 13.31	No	ns	0.8898		A-C	
BODIPY- α -GalCer vs. PBS	-64.42	-75.07 to -53.77	Yes	****	<0.0001		A-D	
Ff.FLAG vs. Ff.FLAG.BODIPY- α -GalCer	68.54	57.89 to 79.19	Yes	****	<0.0001		B-C	
Ff.FLAG vs. PBS	1.46	-9.188 to 12.11	No	ns	0.9788		B-D	
Ff.FLAG.BODIPY- α -GalCer vs. PBS	-67.08	-77.73 to -56.43	Yes	****	<0.0001		C-D	
Test details	Mean 1	Mean 2	Mean Diff.	SE of diff.	n1	n2	q	DF
BODIPY- α -GalCer vs. Ff.FLAG	4.66	70.54	-65.88	3.722	5	5	25.03	16
BODIPY- α -GalCer vs. Ff.FLAG.BODIPY- α -GalCer	4.66	2	2.66	3.722	5	5	1.011	16
BODIPY- α -GalCer vs. PBS	4.66	69.08	-64.42	3.722	5	5	24.48	16
Ff.FLAG vs. Ff.FLAG.BODIPY- α -GalCer	70.54	2	68.54	3.722	5	5	26.05	16
Ff.FLAG vs. PBS	70.54	69.08	1.46	3.722	5	5	0.5548	16
Ff.FLAG.BODIPY- α -GalCer vs. PBS	2	69.08	-67.08	3.722	5	5	25.49	16

Spleen CD69 MFI - Figure 4.4B

Number of families	1							
Number of comparisons per family	6							
Alpha	0.05							
Tukey's multiple comparisons test	Mean Diff.	95.00% CI of diff.	Significant?	Summary	Adjusted P Value			
BODIPY- α -GalCer vs. Ff.FLAG	-1294	-1555 to -1034	Yes	****	<0.0001	A-B		
BODIPY- α -GalCer vs. Ff.FLAG.BODIPY- α -GalCer	86.8	-174.0 to 347.6	No	ns	0.7777	A-C		
BODIPY- α -GalCer vs. PBS	-1102	-1363 to -841.6	Yes	****	<0.0001	A-D		
Ff.FLAG vs. Ff.FLAG.BODIPY- α -GalCer	1381	1120 to 1642	Yes	****	<0.0001	B-C		
Ff.FLAG vs. PBS	192	-68.82 to 452.8	No	ns	0.1932	B-D		
Ff.FLAG.BODIPY- α -GalCer vs. PBS	-1189	-1450 to -928.4	Yes	****	<0.0001	C-D		
Test details	Mean 1	Mean 2	Mean Diff.	SE of diff.	n1	n2	q	DF
BODIPY- α -GalCer vs. Ff.FLAG	375.6	1670	-1294	91.16	5	5	20.08	16
BODIPY- α -GalCer vs. Ff.FLAG.BODIPY- α -GalCer	375.6	288.8	86.8	91.16	5	5	1.347	16
BODIPY- α -GalCer vs. PBS	375.6	1478	-1102	91.16	5	5	17.1	16
Ff.FLAG vs. Ff.FLAG.BODIPY- α -GalCer	1670	288.8	1381	91.16	5	5	21.43	16
Ff.FLAG vs. PBS	1670	1478	192	91.16	5	5	2.978	16
Ff.FLAG.BODIPY- α -GalCer vs. PBS	288.8	1478	-1189	91.16	5	5	18.45	16

Liver CD69 MFI - Figure 4.4B

Number of families	1								
Number of comparisons per family	6								
Alpha	0.05								
Tukey's multiple comparisons test	Mean Diff.	95.00% CI of diff.	Significant?	Summary	Adjusted P Value				
BODIPY- α -GalCer vs. Ff.FLAG	-1553	-1932 to -1175	Yes	****	<0.0001	A-B			
BODIPY- α -GalCer vs. Ff.FLAG.BODIPY- α -GalCer	35	-343.6 to 413.6	No	ns	0.9933	A-C			
BODIPY- α -GalCer vs. PBS	-1079	-1458 to -700.6	Yes	****	<0.0001	A-D			
Ff.FLAG vs. Ff.FLAG.BODIPY- α -GalCer	1588	1210 to 1967	Yes	****	<0.0001	B-C			
Ff.FLAG vs. PBS	474.2	95.56 to 852.8	Yes	*	0.012	B-D			
Ff.FLAG.BODIPY- α -GalCer vs. PBS	-1114	-1493 to -735.6	Yes	****	<0.0001	C-D			
Test details	Mean 1	Mean 2	Mean Diff.	SE of diff.	n1	n2	q	DF	
BODIPY- α -GalCer vs. Ff.FLAG	353	1906	-1553	132.3	5	5	16.6	16	
BODIPY- α -GalCer vs. Ff.FLAG.BODIPY- α -GalCer	353	318	35	132.3	5	5	0.374	16	
BODIPY- α -GalCer vs. PBS	353	1432	-1079	132.3	5	5	11.53	16	
Ff.FLAG vs. Ff.FLAG.BODIPY- α -GalCer	1906	318	1588	132.3	5	5	16.97	16	
Ff.FLAG vs. PBS	1906	1432	474.2	132.3	5	5	5.067	16	
Ff.FLAG.BODIPY- α -GalCer vs. PBS	318	1432	-1114	132.3	5	5	11.91	16	

7.4.2 OVA-specific T cell responses (Section 4.2.2)

OVA⁺ CD8⁺ T cells - Figure 4.7

Number of families	1					
Number of comparisons per family	21					
Alpha	0.05					
Tukey's multiple comparisons test	Mean Diff.	95.00% CI of diff.	Significant?	Summary	Adjusted P Value	
Ff.FLAG vs. Ff.OVA	-0.114	-4.587 to 4.359	No	ns	>0.9999	A-B
Ff.FLAG vs. Ff.OVA.BODIPY- α -GalCer	-0.206	-4.679 to 4.267	No	ns	>0.9999	A-C
Ff.FLAG vs. Ff.FLAG.BODIPY- α -GalCer	-0.492	-4.965 to 3.981	No	ns	0.9998	A-D
Ff.FLAG vs. Ff.OVA + BODIPY- α -GalCer	-1.342	-5.815 to 3.131	No	ns	0.9588	A-E
Ff.FLAG vs. OVA- α -GalCer	-12.76	-17.23 to -8.287	Yes	****	<0.0001	A-F
Ff.FLAG vs. PBS	0.06067	-5.225 to 5.104	No	ns	>0.9999	A-G
Ff.OVA vs. Ff.OVA.BODIPY- α -GalCer	-0.092	-4.565 to 4.381	No	ns	>0.9999	B-C
Ff.OVA vs. Ff.FLAG.BODIPY- α -GalCer	-0.378	-4.851 to 4.095	No	ns	>0.9999	B-D
Ff.OVA vs. Ff.OVA + BODIPY- α -GalCer	-1.228	-5.701 to 3.245	No	ns	0.9731	B-E
Ff.OVA vs. OVA- α -GalCer	-12.65	-17.12 to -8.173	Yes	****	<0.0001	B-F
Ff.OVA vs. PBS	0.05333	-5.111 to 5.218	No	ns	>0.9999	B-G
Ff.OVA.BODIPY- α -GalCer vs. Ff.FLAG.BODIPY- α -GalCer	-0.286	-4.759 to 4.187	No	ns	>0.9999	C-D
Ff.OVA.BODIPY- α -GalCer vs. Ff.OVA + BODIPY- α -GalCer	-1.136	-5.609 to 3.337	No	ns	0.9818	C-E
Ff.OVA.BODIPY- α -GalCer vs. OVA- α -GalCer	-12.55	-17.03 to -8.081	Yes	****	<0.0001	C-F
Ff.OVA.BODIPY- α -GalCer vs. PBS	0.1453	-5.019 to 5.310	No	ns	>0.9999	C-G
Ff.FLAG.BODIPY- α -GalCer vs. Ff.OVA + BODIPY- α -GalCer	-0.85	-5.323 to 3.623	No	ns	0.996	D-E
Ff.FLAG.BODIPY- α -GalCer vs. OVA- α -GalCer	-12.27	-16.74 to -7.795	Yes	****	<0.0001	D-F
Ff.FLAG.BODIPY- α -GalCer vs. PBS	0.4313	-4.733 to 5.596	No	ns	>0.9999	D-G
Ff.OVA + BODIPY- α -GalCer vs. OVA- α -GalCer	-11.42	-15.89 to -6.945	Yes	****	<0.0001	E-F
Ff.OVA + BODIPY- α -GalCer vs. PBS	1.281	-3.883 to 6.446	No	ns	0.9838	E-G
OVA- α -GalCer vs. PBS	12.7	7.535 to 17.86	Yes	****	<0.0001	F-G

Test details	Mean 1	Mean 2	Mean Diff.	SE of diff.	n1	n2	q	DF
Ff.FLAG vs. Ff.OVA	0.236	0.35	-0.114	1.402	5	5	0.115	26
Ff.FLAG vs. Ff.OVA.BODIPY- α -GalCer	0.236	0.442	-0.206	1.402	5	5	0.2078	26
Ff.FLAG vs. Ff.FLAG.BODIPY- α -GalCer	0.236	0.728	-0.492	1.402	5	5	0.4962	26
Ff.FLAG vs. Ff.OVA + BODIPY- α -GalCer	0.236	1.578	-1.342	1.402	5	5	1.354	26
Ff.FLAG vs. OVA- α -GalCer	0.236	13	-12.76	1.402	5	5	12.87	26
Ff.FLAG vs. PBS	0.236	0.2967	-0.06067	1.619	5	3	0.05299	26
Ff.OVA vs. Ff.OVA.BODIPY- α -GalCer	0.35	0.442	-0.092	1.402	5	5	0.09279	26
Ff.OVA vs. Ff.FLAG.BODIPY- α -GalCer	0.35	0.728	-0.378	1.402	5	5	0.3813	26
Ff.OVA vs. Ff.OVA + BODIPY- α -GalCer	0.35	1.578	-1.228	1.402	5	5	1.239	26
Ff.OVA vs. OVA- α -GalCer	0.35	13	-12.65	1.402	5	5	12.76	26
Ff.OVA vs. PBS	0.35	0.2967	0.05333	1.619	5	3	0.04659	26
Ff.OVA.BODIPY- α -GalCer vs. Ff.FLAG.BODIPY- α -GalCer	0.442	0.728	-0.286	1.402	5	5	0.2885	26
Ff.OVA.BODIPY- α -GalCer vs. Ff.OVA + BODIPY- α -GalCer	0.442	1.578	-1.136	1.402	5	5	1.146	26
Ff.OVA.BODIPY- α -GalCer vs. OVA- α -GalCer	0.442	13	-12.55	1.402	5	5	12.66	26
Ff.OVA.BODIPY- α -GalCer vs. PBS	0.442	0.2967	0.1453	1.619	5	3	0.1269	26
Ff.FLAG.BODIPY- α -GalCer vs. Ff.OVA + BODIPY- α -GalCer	0.728	1.578	-0.85	1.402	5	5	0.8573	26
Ff.FLAG.BODIPY- α -GalCer vs. OVA- α -GalCer	0.728	13	-12.27	1.402	5	5	12.37	26
Ff.FLAG.BODIPY- α -GalCer vs. PBS	0.728	0.2967	0.4313	1.619	5	3	0.3768	26
Ff.OVA + BODIPY- α -GalCer vs. OVA- α -GalCer	1.578	13	-11.42	1.402	5	5	11.52	26
Ff.OVA + BODIPY- α -GalCer vs. PBS	1.578	0.2967	1.281	1.619	5	3	1.119	26
OVA- α -GalCer vs. PBS	13	0.2967	12.7	1.619	5	3	11.09	26

OVA⁺ CD8⁺ T cells (without OVA- α -GalCer) - Figure 4.7

Number of families	1							
Number of comparisons per family	15							
Alpha	0.05							
Tukey's multiple comparisons test	Mean Diff.	95.00% CI of diff.	Significant?	Summary	Adjusted P Value			
Ff.FLAG vs. Ff.OVA	-0.114	-1.223 to 0.9947	No	ns	0.9995	A-B		
Ff.FLAG vs. Ff.OVA.BODIPY- α -GalCer	-0.206	-1.315 to 0.9027	No	ns	0.9915	A-C		
Ff.FLAG vs. Ff.FLAG.BODIPY- α -GalCer	-0.492	-1.601 to 0.6167	No	ns	0.7367	A-D		
Ff.FLAG vs. Ff.OVA + BODIPY- α -GalCer	-1.342	-2.451 to -0.2333	Yes	*	0.0118	A-E		
Ff.FLAG vs. PBS	-0.06067	-1.341 to 1.220	No	ns	>0.9999	A-G		
Ff.OVA vs. Ff.OVA.BODIPY- α -GalCer	-0.092	-1.201 to 1.017	No	ns	0.9998	B-C		
Ff.OVA vs. Ff.FLAG.BODIPY- α -GalCer	-0.378	-1.487 to 0.7307	No	ns	0.891	B-D		
Ff.OVA vs. Ff.OVA + BODIPY- α -GalCer	-1.228	-2.337 to -0.1193	Yes	*	0.0242	B-E		
Ff.OVA vs. PBS	0.05333	-1.227 to 1.334	No	ns	>0.9999	B-G		
Ff.OVA.BODIPY- α -GalCer vs. Ff.FLAG.BODIPY- α -GalCer	-0.286	-1.395 to 0.8227	No	ns	0.9638	C-D		
Ff.OVA.BODIPY- α -GalCer vs. Ff.OVA + BODIPY- α -GalCer	-1.136	-2.245 to -0.02732	Yes	*	0.0425	C-E		
Ff.OVA.BODIPY- α -GalCer vs. PBS	0.1453	-1.135 to 1.426	No	ns	0.9992	C-G		
Ff.FLAG.BODIPY- α -GalCer vs. Ff.OVA + BODIPY- α -GalCer	-0.85	-1.959 to 0.2587	No	ns	0.2032	D-E		
Ff.FLAG.BODIPY- α -GalCer vs. PBS	0.4313	-0.8489 to 1.712	No	ns	0.8956	D-G		
Ff.OVA + BODIPY- α -GalCer vs. PBS	1.281	0.001137 to 2.562	Yes	*	0.0497	E-G		
Test details	Mean 1	Mean 2	Mean Diff.	SE of diff.	n1	n2	q	DF
Ff.FLAG vs. Ff.OVA	0.236	0.35	-0.114	0.3559	5	5	0.453	22
Ff.FLAG vs. Ff.OVA.BODIPY- α -GalCer	0.236	0.442	-0.206	0.3559	5	5	0.8186	22
Ff.FLAG vs. Ff.FLAG.BODIPY- α -GalCer	0.236	0.728	-0.492	0.3559	5	5	1.955	22
Ff.FLAG vs. Ff.OVA + BODIPY- α -GalCer	0.236	1.578	-1.342	0.3559	5	5	5.333	22
Ff.FLAG vs. PBS	0.236	0.2967	-0.06067	0.411	5	3	0.2088	22
Ff.OVA vs. Ff.OVA.BODIPY- α -GalCer	0.35	0.442	-0.092	0.3559	5	5	0.3656	22
Ff.OVA vs. Ff.FLAG.BODIPY- α -GalCer	0.35	0.728	-0.378	0.3559	5	5	1.502	22

Ff.OVA vs. Ff.OVA + BODIPY- α -GalCer	0.35	1.578	-1.228	0.3559	5	5	4.88	22
Ff.OVA vs. PBS	0.35	0.2967	0.05333	0.411	5	3	0.1835	22
Ff.OVA.BODIPY- α - GalCer vs. Ff.FLAG.BODIPY- α - GalCer	0.442	0.728	-0.286	0.3559	5	5	1.136	22
Ff.OVA.BODIPY- α - GalCer vs. Ff.OVA + BODIPY- α -GalCer	0.442	1.578	-1.136	0.3559	5	5	4.514	22
Ff.OVA.BODIPY- α - GalCer vs. PBS	0.442	0.2967	0.1453	0.411	5	3	0.5001	22
Ff.FLAG.BODIPY- α - GalCer vs. Ff.OVA + BODIPY- α -GalCer	0.728	1.578	-0.85	0.3559	5	5	3.378	22
Ff.FLAG.BODIPY- α - GalCer vs. PBS	0.728	0.2967	0.4313	0.411	5	3	1.484	22
Ff.OVA + BODIPY- α - GalCer vs. PBS	1.578	0.2967	1.281	0.411	5	3	4.409	22

7.4.3 iNKT cell activation after nine days (Section 4.2.2)

Cell count per organ (spleen) - Figure 4.8A

Number of families	1								
Number of comparisons per family	21								
Alpha	0.05								
Tukey's multiple comparisons test	Mean Diff.	95.00% CI of diff.	Significant?	Summary	Adjusted P Value				
Ff.FLAG vs. Ff.OVA	10800000	-30879476 to 9279476	No	ns	0.6122	A-B			
Ff.FLAG vs. Ff.OVA.BODIPY- α -GalCer	47400000	-67479476 to -27320524	Yes	****	<0.0001	A-C			
Ff.FLAG vs. Ff.FLAG.BODIPY- α -GalCer	53200000	-73279476 to -33120524	Yes	****	<0.0001	A-D			
Ff.FLAG vs. Ff.OVA + BODIPY- α -GalCer	36600000	-56679476 to -16520524	Yes	****	<0.0001	A-E			
Ff.FLAG vs. OVA- α -GalCer	49400000	-69479476 to -29320524	Yes	****	<0.0001	A-F			
Ff.FLAG vs. PBS	19800000	-42985782 to 3385782	No	ns	0.1318	A-G			
Ff.OVA vs. Ff.OVA.BODIPY- α -GalCer	36600000	-56679476 to -16520524	Yes	****	<0.0001	B-C			
Ff.OVA vs. Ff.FLAG.BODIPY- α -GalCer	42400000	-62479476 to -22320524	Yes	****	<0.0001	B-D			
Ff.OVA vs. Ff.OVA + BODIPY- α -GalCer	25800000	-45879476 to -5720524	Yes	**	0.0058	B-E			
Ff.OVA vs. OVA- α -GalCer	38600000	-58679476 to -18520524	Yes	****	<0.0001	B-F			
Ff.OVA vs. PBS	-9000000	-32185782 to 14185782	No	ns	0.8726	B-G			
Ff.OVA.BODIPY- α -GalCer vs. Ff.FLAG.BODIPY- α -GalCer	-5800000	-25879476 to 14279476	No	ns	0.9656	C-D			
Ff.OVA.BODIPY- α -GalCer vs. Ff.OVA + BODIPY- α -GalCer	10800000	-9279476 to 30879476	No	ns	0.6122	C-E			
Ff.OVA.BODIPY- α -GalCer vs. OVA- α -GalCer	-2000000	-22079476 to 18079476	No	ns	0.9999	C-F			
Ff.OVA.BODIPY- α -GalCer vs. PBS	27600000	4414218 to 50785782	Yes	*	0.0122	C-G			
Ff.FLAG.BODIPY- α -GalCer vs. Ff.OVA + BODIPY- α -GalCer	16600000	-3479476 to 36679476	No	ns	0.1557	D-E			
Ff.FLAG.BODIPY- α -GalCer vs. OVA- α -GalCer	3800000	-16279476 to 23879476	No	ns	0.9961	D-F			
Ff.FLAG.BODIPY- α -GalCer vs. PBS	33400000	10214218 to 56585782	Yes	**	0.0017	D-G			
Ff.OVA + BODIPY- α -GalCer vs. OVA- α -GalCer	12800000	-32879476 to 7279476	No	ns	0.4189	E-F			
Ff.OVA + BODIPY- α -GalCer vs. PBS	16800000	-6385782 to 39985782	No	ns	0.2763	E-G			
OVA- α -GalCer vs. PBS	29600000	6414218 to 52785782	Yes	**	0.0062	F-G			
Test details	Mean 1	Mean 2	Mean Diff.	SE of diff.	n1	n2	q	DF	
Ff.FLAG vs. Ff.OVA	40200000	51000000	-10800000	6294320	5	5	2.427	26	
Ff.FLAG vs. Ff.OVA.BODIPY- α -GalCer	40200000	87600000	-47400000	6294320	5	5	10.65	26	

Ff.FLAG vs. Ff.FLAG.BODIPY- α -GalCer	40200000	93400000	-53200000	6294320	5	5	11.95	26
Ff.FLAG vs. Ff.OVA + BODIPY- α -GalCer	40200000	76800000	-36600000	6294320	5	5	8.223	26
Ff.FLAG vs. OVA- α -GalCer	40200000	89600000	-49400000	6294320	5	5	11.1	26
Ff.FLAG vs. PBS	40200000	60000000	-19800000	7268054	5	3	3.853	26
Ff.OVA vs. Ff.OVA.BODIPY- α -GalCer	51000000	87600000	-36600000	6294320	5	5	8.223	26
Ff.OVA vs. Ff.FLAG.BODIPY- α -GalCer	51000000	93400000	-42400000	6294320	5	5	9.526	26
Ff.OVA vs. Ff.OVA + BODIPY- α -GalCer	51000000	76800000	-25800000	6294320	5	5	5.797	26
Ff.OVA vs. OVA- α -GalCer	51000000	89600000	-38600000	6294320	5	5	8.673	26
Ff.OVA vs. PBS	51000000	60000000	-9000000	7268054	5	3	1.751	26
Ff.OVA.BODIPY- α -GalCer vs. Ff.FLAG.BODIPY- α -GalCer	87600000	93400000	-5800000	6294320	5	5	1.303	26
Ff.OVA.BODIPY- α -GalCer vs. Ff.OVA + BODIPY- α -GalCer	87600000	76800000	10800000	6294320	5	5	2.427	26
Ff.OVA.BODIPY- α -GalCer vs. OVA- α -GalCer	87600000	89600000	-2000000	6294320	5	5	0.4494	26
Ff.OVA.BODIPY- α -GalCer vs. PBS	87600000	60000000	27600000	7268054	5	3	5.37	26
Ff.FLAG.BODIPY- α -GalCer vs. Ff.OVA + BODIPY- α -GalCer	93400000	76800000	16600000	6294320	5	5	3.73	26
Ff.FLAG.BODIPY- α -GalCer vs. OVA- α -GalCer	93400000	89600000	3800000	6294320	5	5	0.8538	26
Ff.FLAG.BODIPY- α -GalCer vs. PBS	93400000	60000000	33400000	7268054	5	3	6.499	26
Ff.OVA + BODIPY- α -GalCer vs. OVA- α -GalCer	76800000	89600000	-12800000	6294320	5	5	2.876	26
Ff.OVA + BODIPY- α -GalCer vs. PBS	76800000	60000000	16800000	7268054	5	3	3.269	26
OVA- α -GalCer vs. PBS	89600000	60000000	29600000	7268054	5	3	5.76	26

% α -GalCer tetramer⁺ CD1d⁺ cells in spleen - Figure 4.8B

Number of families	1								
Number of comparisons per family	21								
Alpha	0.05								
Tukey's multiple comparisons test	Mean Diff.	95.00% CI of diff.	Significant?	Summary	Adjusted P Value				
Ff.FLAG vs. Ff.OVA	-1.46	-12.82 to 9.902	No	ns	0.9996	A-B			
Ff.FLAG vs. Ff.OVA.BODIPY- α -GalCer	42.52	31.16 to 53.88	Yes	****	<0.0001	A-C			
Ff.FLAG vs. Ff.FLAG.BODIPY- α -GalCer	41.09	29.73 to 52.45	Yes	****	<0.0001	A-D			
Ff.FLAG vs. Ff.OVA + BODIPY- α -GalCer	34.24	22.88 to 45.60	Yes	****	<0.0001	A-E			
Ff.FLAG vs. OVA- α -GalCer	38.52	27.16 to 49.88	Yes	****	<0.0001	A-F			
Ff.FLAG vs. PBS	4.947	-8.173 to 18.07	No	ns	0.8868	A-G			
Ff.OVA vs. Ff.OVA.BODIPY- α -GalCer	43.98	32.62 to 55.34	Yes	****	<0.0001	B-C			
Ff.OVA vs. Ff.FLAG.BODIPY- α -GalCer	42.55	31.19 to 53.91	Yes	****	<0.0001	B-D			
Ff.OVA vs. Ff.OVA + BODIPY- α -GalCer	35.7	24.34 to 47.06	Yes	****	<0.0001	B-E			
Ff.OVA vs. OVA- α -GalCer	39.98	28.62 to 51.34	Yes	****	<0.0001	B-F			
Ff.OVA vs. PBS	6.407	-6.713 to 19.53	No	ns	0.7087	B-G			
Ff.OVA.BODIPY- α -GalCer vs. Ff.FLAG.BODIPY- α -GalCer	-1.43	-12.79 to 9.932	No	ns	0.9996	C-D			
Ff.OVA.BODIPY- α -GalCer vs. Ff.OVA + BODIPY- α -GalCer	-8.28	-19.64 to 3.082	No	ns	0.2703	C-E			
Ff.OVA.BODIPY- α -GalCer vs. OVA- α -GalCer	-4	-15.36 to 7.362	No	ns	0.9151	C-F			
Ff.OVA.BODIPY- α -GalCer vs. PBS	-37.57	-50.69 to -24.45	Yes	****	<0.0001	C-G			
Ff.FLAG.BODIPY- α -GalCer vs. Ff.OVA + BODIPY- α -GalCer	-6.85	-18.21 to 4.512	No	ns	0.4838	D-E			
Ff.FLAG.BODIPY- α -GalCer vs. OVA- α -GalCer	-2.57	-13.93 to 8.792	No	ns	0.9899	D-F			
Ff.FLAG.BODIPY- α -GalCer vs. PBS	-36.14	-49.26 to -23.02	Yes	****	<0.0001	D-G			
Ff.OVA + BODIPY- α -GalCer vs. OVA- α -GalCer	4.28	-7.082 to 15.64	No	ns	0.8872	E-F			
Ff.OVA + BODIPY- α -GalCer vs. PBS	-29.29	-42.41 to -16.17	Yes	****	<0.0001	E-G			
OVA- α -GalCer vs. PBS	-33.57	-46.69 to -20.45	Yes	****	<0.0001	F-G			
Test details	Mean 1	Mean 2	Mean Diff.	SE of diff.	n1	n2	q	DF	
Ff.FLAG vs. Ff.OVA	58.58	60.04	-1.46	3.562	5	5	0.5797	26	
Ff.FLAG vs. Ff.OVA.BODIPY- α -GalCer	58.58	16.06	42.52	3.562	5	5	16.88	26	
Ff.FLAG vs. Ff.FLAG.BODIPY- α -GalCer	58.58	17.49	41.09	3.562	5	5	16.32	26	
Ff.FLAG vs. Ff.OVA + BODIPY- α -GalCer	58.58	24.34	34.24	3.562	5	5	13.6	26	
Ff.FLAG vs. OVA- α -GalCer	58.58	20.06	38.52	3.562	5	5	15.29	26	

Ff.FLAG vs. PBS	58.58	53.63	4.947	4.113	5	3	1.701	26
Ff.OVA vs. Ff.OVA.BODIPY- α - GalCer	60.04	16.06	43.98	3.562	5	5	17.46	26
Ff.OVA vs. Ff.FLAG.BODIPY- α - GalCer	60.04	17.49	42.55	3.562	5	5	16.9	26
Ff.OVA vs. Ff.OVA + BODIPY- α -GalCer	60.04	24.34	35.7	3.562	5	5	14.18	26
Ff.OVA vs. OVA- α - GalCer	60.04	20.06	39.98	3.562	5	5	15.87	26
Ff.OVA vs. PBS	60.04	53.63	6.407	4.113	5	3	2.203	26
Ff.OVA.BODIPY- α - GalCer vs. Ff.FLAG.BODIPY- α - GalCer	16.06	17.49	-1.43	3.562	5	5	0.5678	26
Ff.OVA.BODIPY- α - GalCer vs. Ff.OVA + BODIPY- α -GalCer	16.06	24.34	-8.28	3.562	5	5	3.288	26
Ff.OVA.BODIPY- α - GalCer vs. OVA- α - GalCer	16.06	20.06	-4	3.562	5	5	1.588	26
Ff.OVA.BODIPY- α - GalCer vs. PBS	16.06	53.63	-37.57	4.113	5	3	12.92	26
Ff.FLAG.BODIPY- α - GalCer vs. Ff.OVA + BODIPY- α -GalCer	17.49	24.34	-6.85	3.562	5	5	2.72	26
Ff.FLAG.BODIPY- α - GalCer vs. OVA- α - GalCer	17.49	20.06	-2.57	3.562	5	5	1.02	26
Ff.FLAG.BODIPY- α - GalCer vs. PBS	17.49	53.63	-36.14	4.113	5	3	12.43	26
Ff.OVA + BODIPY- α - GalCer vs. OVA- α - GalCer	24.34	20.06	4.28	3.562	5	5	1.699	26
Ff.OVA + BODIPY- α - GalCer vs. PBS	24.34	53.63	-29.29	4.113	5	3	10.07	26
OVA- α -GalCer vs. PBS	20.06	53.63	-33.57	4.113	5	3	11.54	26

Spleen #NKT - Figure 4.8C

Number of families	1							
Number of comparisons per family	21							
Alpha	0.05							
Tukey's multiple comparisons test	Mean Diff.	95.00% CI of diff.	Significant?	Summary	Adjusted P Value			
Ff.FLAG vs. Ff.OVA	-2E+05	-548565 to 202085	No	ns	0.7578	A-B		
Ff.FLAG vs. Ff.OVA.BODIPY- α -GalCer	-9E+05	-1255885 to -505235	Yes	****	<0.0001	A-C		
Ff.FLAG vs. Ff.FLAG.BODIPY- α -GalCer	-9E+05	-1258225 to -507575	Yes	****	<0.0001	A-D		
Ff.FLAG vs. Ff.OVA + BODIPY- α -GalCer	-1E+05	-510805 to 239845	No	ns	0.9056	A-E		
Ff.FLAG vs. OVA- α -GalCer	-8E+05	-1133925 to -383275	Yes	****	<0.0001	A-F		
Ff.FLAG vs. PBS	-1E+05	-542228 to 324548	No	ns	0.9828	A-G		
Ff.OVA vs. Ff.OVA.BODIPY- α -GalCer	-7E+05	-1082645 to -331995	Yes	****	<0.0001	B-C		
Ff.OVA vs. Ff.FLAG.BODIPY- α -GalCer	-7E+05	-1084985 to -334335	Yes	****	<0.0001	B-D		
Ff.OVA vs. Ff.OVA + BODIPY- α -GalCer	37760	-337565 to 413085	No	ns	0.9999	B-E		
Ff.OVA vs. OVA- α -GalCer	-6E+05	-960685 to -210035	Yes	***	0.0006	B-F		
Ff.OVA vs. PBS	64400	-368988 to 497788	No	ns	0.999	B-G		
Ff.OVA.BODIPY- α -GalCer vs. Ff.FLAG.BODIPY- α -GalCer	-2340	-377665 to 372985	No	ns	>0.9999	C-D		
Ff.OVA.BODIPY- α -GalCer vs. Ff.OVA + BODIPY- α -GalCer	745080	369755 to 1120405	Yes	****	<0.0001	C-E		
Ff.OVA.BODIPY- α -GalCer vs. OVA- α -GalCer	121960	-253365 to 497285	No	ns	0.9404	C-F		
Ff.OVA.BODIPY- α -GalCer vs. PBS	771720	338332 to 1205108	Yes	***	0.0001	C-G		
Ff.FLAG.BODIPY- α -GalCer vs. Ff.OVA + BODIPY- α -GalCer	747420	372095 to 1122745	Yes	****	<0.0001	D-E		
Ff.FLAG.BODIPY- α -GalCer vs. OVA- α -GalCer	124300	-251025 to 499625	No	ns	0.9351	D-F		
Ff.FLAG.BODIPY- α -GalCer vs. PBS	774060	340672 to 1207448	Yes	****	<0.0001	D-G		
Ff.OVA + BODIPY- α -GalCer vs. OVA- α -GalCer	-6E+05	-998445 to -247795	Yes	***	0.0003	E-F		
Ff.OVA + BODIPY- α -GalCer vs. PBS	26640	-406748 to 460028	No	ns	>0.9999	E-G		
OVA- α -GalCer vs. PBS	649760	216372 to 1083148	Yes	**	0.001	F-G		
Test details	Mean 1	Mean 2	Mean Diff.	SE of diff.	n1	n2	q	DF
Ff.FLAG vs. Ff.OVA	341160	514400	-2E+05	117653	5	5	2.082	26
Ff.FLAG vs. Ff.OVA.BODIPY- α -GalCer	341160	1E+06	-9E+05	117653	5	5	10.58	26
Ff.FLAG vs. Ff.FLAG.BODIPY- α -GalCer	341160	1E+06	-9E+05	117653	5	5	10.61	26
Ff.FLAG vs. Ff.OVA + BODIPY- α -GalCer	341160	476640	-1E+05	117653	5	5	1.628	26
Ff.FLAG vs. OVA- α -GalCer	341160	1E+06	-8E+05	117653	5	5	9.119	26
Ff.FLAG vs. PBS	341160	450000	-1E+05	135854	5	3	1.133	26

Ff.OVA vs. Ff.OVA.BODIPY- α - GalCer	514400	1E+06	-7E+05	117653	5	5	8.502	26
Ff.OVA vs. Ff.FLAG.BODIPY- α - GalCer	514400	1E+06	-7E+05	117653	5	5	8.53	26
Ff.OVA vs. Ff.OVA + BODIPY- α -GalCer	514400	476640	37760	117653	5	5	0.4539	26
Ff.OVA vs. OVA- α - GalCer	514400	1E+06	-6E+05	117653	5	5	7.036	26
Ff.OVA vs. PBS	514400	450000	64400	135854	5	3	0.6704	26
Ff.OVA.BODIPY- α - GalCer vs. Ff.FLAG.BODIPY- α - GalCer	1E+06	1E+06	-2340	117653	5	5	0.0281	26
Ff.OVA.BODIPY- α - GalCer vs. Ff.OVA + BODIPY- α -GalCer	1E+06	476640	745080	117653	5	5	8.956	26
Ff.OVA.BODIPY- α - GalCer vs. OVA- α - GalCer	1E+06	1E+06	121960	117653	5	5	1.466	26
Ff.OVA.BODIPY- α - GalCer vs. PBS	1E+06	450000	771720	135854	5	3	8.033	26
Ff.FLAG.BODIPY- α - GalCer vs. Ff.OVA + BODIPY- α -GalCer	1E+06	476640	747420	117653	5	5	8.984	26
Ff.FLAG.BODIPY- α - GalCer vs. OVA- α - GalCer	1E+06	1E+06	124300	117653	5	5	1.494	26
Ff.FLAG.BODIPY- α - GalCer vs. PBS	1E+06	450000	774060	135854	5	3	8.058	26
Ff.OVA + BODIPY- α - GalCer vs. OVA- α - GalCer	476640	1E+06	-6E+05	117653	5	5	7.49	26
Ff.OVA + BODIPY- α - GalCer vs. PBS	476640	450000	26640	135854	5	3	0.2773	26
OVA- α -GalCer vs. PBS	1E+06	450000	649760	135854	5	3	6.764	26

Spleen %NK1.1 - Figure 4.9A

Number of families	1								
Number of comparisons per family	21								
Alpha	0.05								
Tukey's multiple comparisons test	Mean Diff.	95.00% CI of diff.	Significant?	Summary	Adjusted P Value				
Ff.FLAG vs. Ff.OVA	-1.46	-12.82 to 9.902	No	ns	0.9996	A-B			
Ff.FLAG vs. Ff.OVA.BODIPY- α -GalCer	42.52	31.16 to 53.88	Yes	****	<0.0001	A-C			
Ff.FLAG vs. Ff.OVA.BODIPY- α -GalCer	41.09	29.73 to 52.45	Yes	****	<0.0001	A-D			
Ff.FLAG vs. Ff.OVA + BODIPY- α -GalCer	34.24	22.88 to 45.60	Yes	****	<0.0001	A-E			
Ff.FLAG vs. OVA- α -GalCer	38.52	27.16 to 49.88	Yes	****	<0.0001	A-F			
Ff.FLAG vs. PBS	4.947	-8.173 to 18.07	No	ns	0.8868	A-G			
Ff.OVA vs. Ff.OVA.BODIPY- α -GalCer	43.98	32.62 to 55.34	Yes	****	<0.0001	B-C			
Ff.OVA vs. Ff.FLAG.BODIPY- α -GalCer	42.55	31.19 to 53.91	Yes	****	<0.0001	B-D			
Ff.OVA vs. Ff.OVA + BODIPY- α -GalCer	35.7	24.34 to 47.06	Yes	****	<0.0001	B-E			
Ff.OVA vs. OVA- α -GalCer	39.98	28.62 to 51.34	Yes	****	<0.0001	B-F			
Ff.OVA vs. PBS	6.407	-6.713 to 19.53	No	ns	0.7087	B-G			
Ff.OVA.BODIPY- α -GalCer vs. Ff.FLAG.BODIPY- α -GalCer	-1.43	-12.79 to 9.932	No	ns	0.9996	C-D			
Ff.OVA.BODIPY- α -GalCer vs. Ff.OVA + BODIPY- α -GalCer	-8.28	-19.64 to 3.082	No	ns	0.2703	C-E			
Ff.OVA.BODIPY- α -GalCer vs. OVA- α -GalCer	-4	-15.36 to 7.362	No	ns	0.9151	C-F			
Ff.OVA.BODIPY- α -GalCer vs. PBS	-37.57	-50.69 to -24.45	Yes	****	<0.0001	C-G			
Ff.FLAG.BODIPY- α -GalCer vs. Ff.OVA + BODIPY- α -GalCer	-6.85	-18.21 to 4.512	No	ns	0.4838	D-E			
Ff.FLAG.BODIPY- α -GalCer vs. OVA- α -GalCer	-2.57	-13.93 to 8.792	No	ns	0.9899	D-F			
Ff.FLAG.BODIPY- α -GalCer vs. PBS	-36.14	-49.26 to -23.02	Yes	****	<0.0001	D-G			
Ff.OVA + BODIPY- α -GalCer vs. OVA- α -GalCer	4.28	-7.082 to 15.64	No	ns	0.8872	E-F			
Ff.OVA + BODIPY- α -GalCer vs. PBS	-29.29	-42.41 to -16.17	Yes	****	<0.0001	E-G			
OVA- α -GalCer vs. PBS	-33.57	-46.69 to -20.45	Yes	****	<0.0001	F-G			
Test details	Mean 1	Mean 2	Mean Diff.	SE of diff.	n1	n2	q	DF	
Ff.FLAG vs. Ff.OVA	58.58	60.04	-1.46	3.562	5	5	0.5797	26	
Ff.FLAG vs. Ff.OVA.BODIPY- α -GalCer	58.58	16.06	42.52	3.562	5	5	16.88	26	
Ff.FLAG vs. Ff.OVA.BODIPY- α -GalCer	58.58	17.49	41.09	3.562	5	5	16.32	26	
Ff.FLAG vs. Ff.OVA + BODIPY- α -GalCer	58.58	24.34	34.24	3.562	5	5	13.6	26	
Ff.FLAG vs. OVA- α -GalCer	58.58	20.06	38.52	3.562	5	5	15.29	26	

Ff.FLAG vs. PBS	58.58	53.63	4.947	4.113	5	3	1.701	26
Ff.OVA vs. Ff.OVA.BODIPY- α - GalCer	60.04	16.06	43.98	3.562	5	5	17.46	26
Ff.OVA vs. Ff.FLAG.BODIPY- α - GalCer	60.04	17.49	42.55	3.562	5	5	16.9	26
Ff.OVA vs. Ff.OVA + BODIPY- α -GalCer	60.04	24.34	35.7	3.562	5	5	14.18	26
Ff.OVA vs. OVA- α - GalCer	60.04	20.06	39.98	3.562	5	5	15.87	26
Ff.OVA vs. PBS	60.04	53.63	6.407	4.113	5	3	2.203	26
Ff.OVA.BODIPY- α - GalCer vs. Ff.FLAG.BODIPY- α - GalCer	16.06	17.49	-1.43	3.562	5	5	0.5678	26
Ff.OVA.BODIPY- α - GalCer vs. Ff.OVA + BODIPY- α -GalCer	16.06	24.34	-8.28	3.562	5	5	3.288	26
Ff.OVA.BODIPY- α - GalCer vs. OVA- α - GalCer	16.06	20.06	-4	3.562	5	5	1.588	26
Ff.OVA.BODIPY- α - GalCer vs. PBS	16.06	53.63	-37.57	4.113	5	3	12.92	26
Ff.FLAG.BODIPY- α - GalCer vs. Ff.OVA + BODIPY- α -GalCer	17.49	24.34	-6.85	3.562	5	5	2.72	26
Ff.FLAG.BODIPY- α - GalCer vs. OVA- α - GalCer	17.49	20.06	-2.57	3.562	5	5	1.02	26
Ff.FLAG.BODIPY- α - GalCer vs. PBS	17.49	53.63	-36.14	4.113	5	3	12.43	26
Ff.OVA + BODIPY- α - GalCer vs. OVA- α - GalCer	24.34	20.06	4.28	3.562	5	5	1.699	26
Ff.OVA + BODIPY- α - GalCer vs. PBS	24.34	53.63	-29.29	4.113	5	3	10.07	26
OVA- α -GalCer vs. PBS	20.06	53.63	-33.57	4.113	5	3	11.54	26

MFI CD69 - Figure 4.9B

Number of families	1								
Number of comparisons per family	21								
Alpha	0.05								
Tukey's multiple comparisons test	Mean Diff.	95.00% CI of diff.	Significant?	Summary	Adjusted P Value				
Ff.FLAG vs. Ff.OVA	-209	-428.5 to 10.47	No	ns	0.0695	A-B			
Ff.FLAG vs. Ff.OVA.BODIPY- α -GalCer	319.2	99.73 to 538.7	Yes	**	0.0015	A-C			
Ff.FLAG vs. Ff.FLAG.BODIPY- α -GalCer	145	-74.47 to 364.5	No	ns	0.3776	A-D			
Ff.FLAG vs. Ff.OVA + BODIPY- α -GalCer	441	221.5 to 660.5	Yes	****	<0.0001	A-E			
Ff.FLAG vs. OVA- α -GalCer	567.8	348.3 to 787.3	Yes	****	<0.0001	A-F			
Ff.FLAG vs. PBS	-230.9	-484.3 to 22.55	No	ns	0.0916	A-G			
Ff.OVA vs. Ff.OVA.BODIPY- α -GalCer	528.2	308.7 to 747.7	Yes	****	<0.0001	B-C			
Ff.OVA vs. Ff.FLAG.BODIPY- α -GalCer	354	134.5 to 573.5	Yes	***	0.0004	B-D			
Ff.OVA vs. Ff.OVA + BODIPY- α -GalCer	650	430.5 to 869.5	Yes	****	<0.0001	B-E			
Ff.OVA vs. OVA- α -GalCer	776.8	557.3 to 996.3	Yes	****	<0.0001	B-F			
Ff.OVA vs. PBS	-21.87	-275.3 to 231.6	No	ns	>0.9999	B-G			
Ff.OVA.BODIPY- α -GalCer vs. Ff.FLAG.BODIPY- α -GalCer	-174.2	-393.7 to 45.27	No	ns	0.1891	C-D			
Ff.OVA.BODIPY- α -GalCer vs. Ff.OVA + BODIPY- α -GalCer	121.8	-97.67 to 341.3	No	ns	0.5781	C-E			
Ff.OVA.BODIPY- α -GalCer vs. OVA- α -GalCer	248.6	29.13 to 468.1	Yes	*	0.019	C-F			
Ff.OVA.BODIPY- α -GalCer vs. PBS	-550.1	-803.5 to -296.6	Yes	****	<0.0001	C-G			
Ff.FLAG.BODIPY- α -GalCer vs. Ff.OVA + BODIPY- α -GalCer	296	76.53 to 515.5	Yes	**	0.0035	D-E			
Ff.FLAG.BODIPY- α -GalCer vs. OVA- α -GalCer	422.8	203.3 to 642.3	Yes	****	<0.0001	D-F			
Ff.FLAG.BODIPY- α -GalCer vs. PBS	-375.9	-629.3 to -122.4	Yes	**	0.0012	D-G			
Ff.OVA + BODIPY- α -GalCer vs. OVA- α -GalCer	126.8	-92.67 to 346.3	No	ns	0.5329	E-F			
Ff.OVA + BODIPY- α -GalCer vs. PBS	-671.9	-925.3 to -418.4	Yes	****	<0.0001	E-G			
OVA- α -GalCer vs. PBS	-798.7	-1052 to -545.2	Yes	****	<0.0001	F-G			
Test details	Mean 1	Mean 2	Mean Diff.	SE of diff.	n1	n2	q	DF	
Ff.FLAG vs. Ff.OVA	1089	1298	-209	68.8	5	5	4.296	26	
Ff.FLAG vs. Ff.OVA.BODIPY- α -GalCer	1089	769.6	319.2	68.8	5	5	6.562	26	
Ff.FLAG vs. Ff.FLAG.BODIPY- α -GalCer	1089	943.8	145	68.8	5	5	2.981	26	
Ff.FLAG vs. Ff.OVA + BODIPY- α -GalCer	1089	647.8	441	68.8	5	5	9.065	26	
Ff.FLAG vs. OVA- α -GalCer	1089	521	567.8	68.8	5	5	11.67	26	

Ff.FLAG vs. PBS	1089	1320	-230.9	79.44	5	3	4.11	26
Ff.OVA vs. Ff.OVA.BODIPY- α -GalCer	1298	769.6	528.2	68.8	5	5	10.86	26
Ff.OVA vs. Ff.FLAG.BODIPY- α -GalCer	1298	943.8	354	68.8	5	5	7.277	26
Ff.OVA vs. Ff.OVA + BODIPY- α -GalCer	1298	647.8	650	68.8	5	5	13.36	26
Ff.OVA vs. OVA- α -GalCer	1298	521	776.8	68.8	5	5	15.97	26
Ff.OVA vs. PBS	1298	1320	-21.87	79.44	5	3	0.3893	26
Ff.OVA.BODIPY- α -GalCer vs. Ff.FLAG.BODIPY- α -GalCer	769.6	943.8	-174.2	68.8	5	5	3.581	26
Ff.OVA.BODIPY- α -GalCer vs. Ff.OVA + BODIPY- α -GalCer	769.6	647.8	121.8	68.8	5	5	2.504	26
Ff.OVA.BODIPY- α -GalCer vs. OVA- α -GalCer	769.6	521	248.6	68.8	5	5	5.11	26
Ff.OVA.BODIPY- α -GalCer vs. PBS	769.6	1320	-550.1	79.44	5	3	9.793	26
Ff.FLAG.BODIPY- α -GalCer vs. Ff.OVA + BODIPY- α -GalCer	943.8	647.8	296	68.8	5	5	6.085	26
Ff.FLAG.BODIPY- α -GalCer vs. OVA- α -GalCer	943.8	521	422.8	68.8	5	5	8.691	26
Ff.FLAG.BODIPY- α -GalCer vs. PBS	943.8	1320	-375.9	79.44	5	3	6.691	26
Ff.OVA + BODIPY- α -GalCer vs. OVA- α -GalCer	647.8	521	126.8	68.8	5	5	2.607	26
Ff.OVA + BODIPY- α -GalCer vs. PBS	647.8	1320	-671.9	79.44	5	3	11.96	26
OVA- α -GalCer vs. PBS	521	1320	-798.7	79.44	5	3	14.22	26

7.4.4 OVA-specific T cell responses (Section 4.2.3)

CD8⁺ OVA⁺ T cells - Figure 4.10

Number of families	1					
Number of comparisons per family	28					
Alpha	0.05					
Tukey's multiple comparisons test	Mean Diff.	95.00% CI of diff.	Significant?	Summary	Adjusted P Value	
Ff.FLAG vs. Ff.OVA	0.0148	-0.8563 to 0.8859	No	ns	>0.9999	A-B
Ff.FLAG vs. Ff.OVA.BODIPY- α -GalCer	0.0132	-0.8579 to 0.8843	No	ns	>0.9999	A-C
Ff.FLAG vs. Ff.FLAG.BODIPY- α -GalCer	0.0058	-0.8653 to 0.8769	No	ns	>0.9999	A-D
Ff.FLAG vs. Ff.OVA + BODIPY- α -GalCer	-0.1326	-1.004 to 0.7385	No	ns	0.9996	A-E
Ff.FLAG vs. OVA- α -GalCer	-4.555	-5.426 to -3.683	Yes	****	<0.0001	A-F
Ff.FLAG vs. PBS	0.0026	-0.8685 to 0.8737	No	ns	>0.9999	A-G
Ff.FLAG vs. Column H	-0.0032	-0.8743 to 0.8679	No	ns	>0.9999	A-H
Ff.OVA vs. Ff.OVA.BODIPY- α -GalCer	-0.0016	-0.8727 to 0.8695	No	ns	>0.9999	B-C
Ff.OVA vs. Ff.FLAG.BODIPY- α -GalCer	-0.009	-0.8801 to 0.8621	No	ns	>0.9999	B-D
Ff.OVA vs. Ff.OVA + BODIPY- α -GalCer	-0.1474	-1.019 to 0.7237	No	ns	0.9992	B-E
Ff.OVA vs. OVA- α -GalCer	-4.569	-5.441 to -3.698	Yes	****	<0.0001	B-F
Ff.OVA vs. PBS	-0.0122	-0.8833 to 0.8589	No	ns	>0.9999	B-G
Ff.OVA vs. Column H	-0.018	-0.8891 to 0.8531	No	ns	>0.9999	B-H
Ff.OVA.BODIPY- α -GalCer vs. Ff.FLAG.BODIPY- α -GalCer	-0.0074	-0.8785 to 0.8637	No	ns	>0.9999	C-D
Ff.OVA.BODIPY- α -GalCer vs. Ff.OVA + BODIPY- α -GalCer	-0.1458	-1.017 to 0.7253	No	ns	0.9993	C-E
Ff.OVA.BODIPY- α -GalCer vs. OVA- α -GalCer	-4.568	-5.439 to -3.697	Yes	****	<0.0001	C-F
Ff.OVA.BODIPY- α -GalCer vs. PBS	-0.0106	-0.8817 to 0.8605	No	ns	>0.9999	C-G
Ff.OVA.BODIPY- α -GalCer vs. Column H	-0.0164	-0.8875 to 0.8547	No	ns	>0.9999	C-H
Ff.FLAG.BODIPY- α -GalCer vs. Ff.OVA + BODIPY- α -GalCer	-0.1384	-1.010 to 0.7327	No	ns	0.9995	D-E
Ff.FLAG.BODIPY- α -GalCer vs. OVA- α -GalCer	-4.56	-5.432 to -3.689	Yes	****	<0.0001	D-F
Ff.FLAG.BODIPY- α -GalCer vs. PBS	-0.0032	-0.8743 to 0.8679	No	ns	>0.9999	D-G
Ff.FLAG.BODIPY- α -GalCer vs. Column H	-0.009	-0.8801 to 0.8621	No	ns	>0.9999	D-H
Ff.OVA + BODIPY- α -GalCer vs. OVA- α -GalCer	-4.422	-5.293 to -3.551	Yes	****	<0.0001	E-F
Ff.OVA + BODIPY- α -GalCer vs. PBS	0.1352	-0.7359 to 1.006	No	ns	0.9996	E-G
Ff.OVA + BODIPY- α -GalCer vs. Column H	0.1294	-0.7417 to 1.001	No	ns	0.9997	E-H

OVA- α -GalCer vs. PBS	4.557	3.686 to 5.428	Yes	****	<0.0001	F-G		
OVA- α -GalCer vs. Column H	4.551	3.680 to 5.423	Yes	****	<0.0001	F-H		
PBS vs. Column H	-0.0058	-0.8769 to 0.8653	No	ns	>0.9999	G-H		
Test details	Mean 1	Mean 2	Mean Diff.	SE of diff.	n1	n2	q	DF
Ff.FLAG vs. Ff.OVA	0.0474	0.0326	0.0148	0.2689	5	5	0.07783	32
Ff.FLAG vs. Ff.OVA.BODIPY- α -GalCer	0.0474	0.0342	0.0132	0.2689	5	5	0.06941	32
Ff.FLAG vs. Ff.FLAG.BODIPY- α -GalCer	0.0474	0.0416	0.0058	0.2689	5	5	0.0305	32
Ff.FLAG vs. Ff.OVA + BODIPY- α -GalCer	0.0474	0.18	-0.1326	0.2689	5	5	0.6973	32
Ff.FLAG vs. OVA- α -GalCer	0.0474	4.602	-4.555	0.2689	5	5	23.95	32
Ff.FLAG vs. PBS	0.0474	0.0448	0.0026	0.2689	5	5	0.01367	32
Ff.FLAG vs. Column H	0.0474	0.0506	-0.0032	0.2689	5	5	0.01683	32
Ff.OVA vs. Ff.OVA.BODIPY- α -GalCer	0.0326	0.0342	-0.0016	0.2689	5	5	0.008414	32
Ff.OVA vs. Ff.FLAG.BODIPY- α -GalCer	0.0326	0.0416	-0.009	0.2689	5	5	0.04733	32
Ff.OVA vs. Ff.OVA + BODIPY- α -GalCer	0.0326	0.18	-0.1474	0.2689	5	5	0.7751	32
Ff.OVA vs. OVA- α -GalCer	0.0326	4.602	-4.569	0.2689	5	5	24.03	32
Ff.OVA vs. PBS	0.0326	0.0448	-0.0122	0.2689	5	5	0.06416	32
Ff.OVA vs. Column H	0.0326	0.0506	-0.018	0.2689	5	5	0.09466	32
Ff.OVA.BODIPY- α -GalCer vs. Ff.FLAG.BODIPY- α -GalCer	0.0342	0.0416	-0.0074	0.2689	5	5	0.03891	32
Ff.OVA.BODIPY- α -GalCer vs. Ff.OVA + BODIPY- α -GalCer	0.0342	0.18	-0.1458	0.2689	5	5	0.7667	32
Ff.OVA.BODIPY- α -GalCer vs. OVA- α -GalCer	0.0342	4.602	-4.568	0.2689	5	5	24.02	32
Ff.OVA.BODIPY- α -GalCer vs. PBS	0.0342	0.0448	-0.0106	0.2689	5	5	0.05574	32
Ff.OVA.BODIPY- α -GalCer vs. Column H	0.0342	0.0506	-0.0164	0.2689	5	5	0.08624	32
Ff.FLAG.BODIPY- α -GalCer vs. Ff.OVA + BODIPY- α -GalCer	0.0416	0.18	-0.1384	0.2689	5	5	0.7278	32
Ff.FLAG.BODIPY- α -GalCer vs. OVA- α -GalCer	0.0416	4.602	-4.56	0.2689	5	5	23.98	32
Ff.FLAG.BODIPY- α -GalCer vs. PBS	0.0416	0.0448	-0.0032	0.2689	5	5	0.01683	32
Ff.FLAG.BODIPY- α -GalCer vs. Column H	0.0416	0.0506	-0.009	0.2689	5	5	0.04733	32
Ff.OVA + BODIPY- α -GalCer vs. OVA- α -GalCer	0.18	4.602	-4.422	0.2689	5	5	23.25	32
Ff.OVA + BODIPY- α -GalCer vs. PBS	0.18	0.0448	0.1352	0.2689	5	5	0.711	32
Ff.OVA + BODIPY- α -GalCer vs. Column H	0.18	0.0506	0.1294	0.2689	5	5	0.6805	32
OVA- α -GalCer vs. PBS	4.602	0.0448	4.557	0.2689	5	5	23.96	32
OVA- α -GalCer vs. Column H	4.602	0.0506	4.551	0.2689	5	5	23.93	32
PBS vs. Column H	0.0448	0.0506	-0.0058	0.2689	5	5	0.0305	32

OVA⁺ CD8⁺ T cells without OVA- α -GalCer - Figure 4.10

Number of families	1								
Number of comparisons per family	21								
Alpha	0.05								
Tukey's multiple comparisons test	Mean Diff.	95.00% CI of diff.	Significant?	Summary	Adjusted P Value				
Ff.FLAG vs. Ff.OVA	0.0148	-0.04969 to 0.07929	No	ns	0.9896	A-B			
Ff.FLAG vs. Ff.OVA.BODIPY- α -GalCer	0.0132	-0.05129 to 0.07769	No	ns	0.9943	A-C			
Ff.FLAG vs. Ff.FLAG.BODIPY- α -GalCer	0.0058	-0.05869 to 0.07029	No	ns	>0.9999	A-D			
Ff.FLAG vs. Ff.OVA + BODIPY- α -GalCer	-0.1326	-0.1971 to -0.06811	Yes	****	<0.0001	A-E			
Ff.FLAG vs. PBS	0.0026	-0.06189 to 0.06709	No	ns	>0.9999	A-G			
Ff.FLAG vs. Column H	-0.0032	-0.06769 to 0.06129	No	ns	>0.9999	A-H			
Ff.OVA vs. Ff.OVA.BODIPY- α -GalCer	-0.0016	-0.06609 to 0.06289	No	ns	>0.9999	B-C			
Ff.OVA vs. Ff.FLAG.BODIPY- α -GalCer	-0.009	-0.07349 to 0.05549	No	ns	0.9993	B-D			
Ff.OVA vs. Ff.OVA + BODIPY- α -GalCer	-0.1474	-0.2119 to -0.08291	Yes	****	<0.0001	B-E			
Ff.OVA vs. PBS	-0.0122	-0.07669 to 0.05229	No	ns	0.9963	B-G			
Ff.OVA vs. Column H	-0.018	-0.08249 to 0.04649	No	ns	0.9719	B-H			
Ff.OVA.BODIPY- α -GalCer vs. Ff.FLAG.BODIPY- α -GalCer	-0.0074	-0.07189 to 0.05709	No	ns	0.9998	C-D			
Ff.OVA.BODIPY- α -GalCer vs. Ff.OVA + BODIPY- α -GalCer	-0.1458	-0.2103 to -0.08131	Yes	****	<0.0001	C-E			
Ff.OVA.BODIPY- α -GalCer vs. PBS	-0.0106	-0.07509 to 0.05389	No	ns	0.9983	C-G			
Ff.OVA.BODIPY- α -GalCer vs. Column H	-0.0164	-0.08089 to 0.04809	No	ns	0.9823	C-H			
Ff.FLAG.BODIPY- α -GalCer vs. Ff.OVA + BODIPY- α -GalCer	-0.1384	-0.2029 to -0.07391	Yes	****	<0.0001	D-E			
Ff.FLAG.BODIPY- α -GalCer vs. PBS	-0.0032	-0.06769 to 0.06129	No	ns	>0.9999	D-G			
Ff.FLAG.BODIPY- α -GalCer vs. Column H	-0.009	-0.07349 to 0.05549	No	ns	0.9993	D-H			
Ff.OVA + BODIPY- α -GalCer vs. PBS	0.1352	0.07071 to 0.1997	Yes	****	<0.0001	E-G			
Ff.OVA + BODIPY- α -GalCer vs. Column H	0.1294	0.06491 to 0.1939	Yes	****	<0.0001	E-H			
PBS vs. Column H	-0.0058	-0.07029 to 0.05869	No	ns	>0.9999	G-H			
Test details	Mean 1	Mean 2	Mean Diff.	SE of diff.	n1	n2	q	DF	
Ff.FLAG vs. Ff.OVA	0.0474	0.0326	0.0148	0.02033	5	5	1.029	28	
Ff.FLAG vs. Ff.OVA.BODIPY- α -GalCer	0.0474	0.0342	0.0132	0.02033	5	5	0.9182	28	
Ff.FLAG vs. Ff.FLAG.BODIPY- α -GalCer	0.0474	0.0416	0.0058	0.02033	5	5	0.4034	28	
Ff.FLAG vs. Ff.OVA + BODIPY- α -GalCer	0.0474	0.18	-0.1326	0.02033	5	5	9.224	28	
Ff.FLAG vs. PBS	0.0474	0.0448	0.0026	0.02033	5	5	0.1809	28	
Ff.FLAG vs. Column H	0.0474	0.0506	-0.0032	0.02033	5	5	0.2226	28	

Ff.OVA vs. Ff.OVA.BODIPY- α - GalCer	0.0326	0.0342	-0.0016	0.02033	5	5	0.1113	28
Ff.OVA vs. Ff.FLAG.BODIPY- α - GalCer	0.0326	0.0416	-0.009	0.02033	5	5	0.626	28
Ff.OVA vs. Ff.OVA + BODIPY- α -GalCer	0.0326	0.18	-0.1474	0.02033	5	5	10.25	28
Ff.OVA vs. PBS	0.0326	0.0448	-0.0122	0.02033	5	5	0.8486	28
Ff.OVA vs. Column H	0.0326	0.0506	-0.018	0.02033	5	5	1.252	28
Ff.OVA.BODIPY- α - GalCer vs. Ff.FLAG.BODIPY- α - GalCer	0.0342	0.0416	-0.0074	0.02033	5	5	0.5147	28
Ff.OVA.BODIPY- α - GalCer vs. Ff.OVA + BODIPY- α -GalCer	0.0342	0.18	-0.1458	0.02033	5	5	10.14	28
Ff.OVA.BODIPY- α - GalCer vs. PBS	0.0342	0.0448	-0.0106	0.02033	5	5	0.7373	28
Ff.OVA.BODIPY- α - GalCer vs. Column H	0.0342	0.0506	-0.0164	0.02033	5	5	1.141	28
Ff.FLAG.BODIPY- α - GalCer vs. Ff.OVA + BODIPY- α -GalCer	0.0416	0.18	-0.1384	0.02033	5	5	9.627	28
Ff.FLAG.BODIPY- α - GalCer vs. PBS	0.0416	0.0448	-0.0032	0.02033	5	5	0.2226	28
Ff.FLAG.BODIPY- α - GalCer vs. Column H	0.0416	0.0506	-0.009	0.02033	5	5	0.626	28
Ff.OVA + BODIPY- α - GalCer vs. PBS	0.18	0.0448	0.1352	0.02033	5	5	9.404	28
Ff.OVA + BODIPY- α - GalCer vs. Column H	0.18	0.0506	0.1294	0.02033	5	5	9.001	28
PBS vs. Column H	0.0448	0.0506	-0.0058	0.02033	5	5	0.4034	28

7.4.5 iNKT cell activation after eight days (Section 4.2.3)

Cell count per organ (spleen) - Figure 4.11A

Number of families	1					
Number of comparisons per family	28					
Alpha	0.05					
Tukey's multiple comparisons test	Mean Diff.	95.00% CI of diff.	Significant?	Summary	Adjusted P Value	
Ff.FLAG vs. Ff.OVA	-9600000	-46686218 to 27486218	No	ns	0.9893	A-B
Ff.FLAG vs. Ff.OVA.BODIPY- α -GalCer	-3.8E+07	-75366218 to -1193782	Yes	*	0.0391	A-C
Ff.FLAG vs. Ff.FLAG.BODIPY- α -GalCer	-3E+07	-66686218 to 7486218	No	ns	0.1983	A-D
Ff.FLAG vs. Ff.OVA + BODIPY- α -GalCer	-3.8E+07	-75166218 to -993782	Yes	*	0.0408	A-E
Ff.FLAG vs. OVA- α -GalCer	-2.2E+07	-59046218 to 15126218	No	ns	0.5492	A-F
Ff.FLAG vs. PBS	-4640000	-41726218 to 32446218	No	ns	0.9999	A-G
Ff.FLAG vs. Column H	-3.8E+07	-75486218 to -1313782	Yes	*	0.0382	A-H
Ff.OVA vs. Ff.OVA.BODIPY- α -GalCer	-2.9E+07	-65766218 to 8406218	No	ns	0.2296	B-C
Ff.OVA vs. Ff.FLAG.BODIPY- α -GalCer	-2E+07	-57086218 to 17086218	No	ns	0.6581	B-D
Ff.OVA vs. Ff.OVA + BODIPY- α -GalCer	-2.8E+07	-65566218 to 8606218	No	ns	0.2368	B-E
Ff.OVA vs. OVA- α -GalCer	-1.2E+07	-49446218 to 24726218	No	ns	0.9566	B-F
Ff.OVA vs. PBS	4960000	-32126218 to 42046218	No	ns	0.9998	B-G
Ff.OVA vs. Column H	-2.9E+07	-65886218 to 8286218	No	ns	0.2253	B-H
Ff.OVA.BODIPY- α -GalCer vs. Ff.FLAG.BODIPY- α -GalCer	8680000	-28406218 to 45766218	No	ns	0.9941	C-D
Ff.OVA.BODIPY- α -GalCer vs. Ff.OVA + BODIPY- α -GalCer	200000	-36886218 to 37286218	No	ns	>0.9999	C-E
Ff.OVA.BODIPY- α -GalCer vs. OVA- α -GalCer	16320000	-20766218 to 53406218	No	ns	0.8388	C-F
Ff.OVA.BODIPY- α -GalCer vs. PBS	33640000	-3446218 to 70726218	No	ns	0.0979	C-G
Ff.OVA.BODIPY- α -GalCer vs. Column H	-120000	-37206218 to 36966218	No	ns	>0.9999	C-H
Ff.FLAG.BODIPY- α -GalCer vs. Ff.OVA + BODIPY- α -GalCer	-8480000	-45566218 to 28606218	No	ns	0.9949	D-E
Ff.FLAG.BODIPY- α -GalCer vs. OVA- α -GalCer	7640000	-29446218 to 44726218	No	ns	0.9973	D-F
Ff.FLAG.BODIPY- α -GalCer vs. PBS	24960000	-12126218 to 62046218	No	ns	0.3895	D-G
Ff.FLAG.BODIPY- α -GalCer vs. Column H	-8800000	-45886218 to 28286218	No	ns	0.9936	D-H

Ff.OVA + BODIPY- α -GalCer vs. OVA- α -GalCer	16120000	-20966218 to 53206218	No	ns	0.8469	E-F		
Ff.OVA + BODIPY- α -GalCer vs. PBS	33440000	-3646218 to 70526218	No	ns	0.1016	E-G		
Ff.OVA + BODIPY- α -GalCer vs. Column H	-320000	-37406218 to 36766218	No	ns	>0.9999	E-H		
OVA- α -GalCer vs. PBS	17320000	-19766218 to 54406218	No	ns	0.795	F-G		
OVA- α -GalCer vs. Column H	-1.6E+07	-53526218 to 20646218	No	ns	0.8338	F-H		
PBS vs. Column H	-3.4E+07	-70846218 to 3326218	No	ns	0.0957	G-H		
Test details	Mean 1	Mean 2	Mean Diff.	SE of diff.	n1	n2	q	DF
Ff.FLAG vs. Ff.OVA	50200000	59800000	-9600000	11448843	5	5	1.186	32
Ff.FLAG vs. Ff.OVA.BODIPY- α -GalCer	50200000	88480000	-3.8E+07	11448843	5	5	4.729	32
Ff.FLAG vs. Ff.FLAG.BODIPY- α -GalCer	50200000	79800000	-3E+07	11448843	5	5	3.656	32
Ff.FLAG vs. Ff.OVA + BODIPY- α -GalCer	50200000	88280000	-3.8E+07	11448843	5	5	4.704	32
Ff.FLAG vs. OVA- α -GalCer	50200000	72160000	-2.2E+07	11448843	5	5	2.713	32
Ff.FLAG vs. PBS	50200000	54840000	-4640000	11448843	5	5	0.5732	32
Ff.FLAG vs. Column H	50200000	88600000	-3.8E+07	11448843	5	5	4.743	32
Ff.OVA vs. Ff.OVA.BODIPY- α -GalCer	59800000	88480000	-2.9E+07	11448843	5	5	3.543	32
Ff.OVA vs. Ff.FLAG.BODIPY- α -GalCer	59800000	79800000	-2E+07	11448843	5	5	2.47	32
Ff.OVA vs. Ff.OVA + BODIPY- α -GalCer	59800000	88280000	-2.8E+07	11448843	5	5	3.518	32
Ff.OVA vs. OVA- α -GalCer	59800000	72160000	-1.2E+07	11448843	5	5	1.527	32
Ff.OVA vs. PBS	59800000	54840000	4960000	11448843	5	5	0.6127	32
Ff.OVA vs. Column H	59800000	88600000	-2.9E+07	11448843	5	5	3.558	32
Ff.OVA.BODIPY- α -GalCer vs. Ff.FLAG.BODIPY- α -GalCer	88480000	79800000	8680000	11448843	5	5	1.072	32
Ff.OVA.BODIPY- α -GalCer vs. Ff.OVA + BODIPY- α -GalCer	88480000	88280000	200000	11448843	5	5	0.0247	32
Ff.OVA.BODIPY- α -GalCer vs. OVA- α -GalCer	88480000	72160000	16320000	11448843	5	5	2.016	32
Ff.OVA.BODIPY- α -GalCer vs. PBS	88480000	54840000	33640000	11448843	5	5	4.155	32
Ff.OVA.BODIPY- α -GalCer vs. Column H	88480000	88600000	-120000	11448843	5	5	0.01482	32
Ff.FLAG.BODIPY- α -GalCer vs. Ff.OVA + BODIPY- α -GalCer	79800000	88280000	-8480000	11448843	5	5	1.047	32
Ff.FLAG.BODIPY- α -GalCer vs. OVA- α -GalCer	79800000	72160000	7640000	11448843	5	5	0.9437	32
Ff.FLAG.BODIPY- α -GalCer vs. PBS	79800000	54840000	24960000	11448843	5	5	3.083	32
Ff.FLAG.BODIPY- α -GalCer vs. Column H	79800000	88600000	-8800000	11448843	5	5	1.087	32
Ff.OVA + BODIPY- α -GalCer vs. OVA- α -GalCer	88280000	72160000	16120000	11448843	5	5	1.991	32
Ff.OVA + BODIPY- α -GalCer vs. PBS	88280000	54840000	33440000	11448843	5	5	4.131	32
Ff.OVA + BODIPY- α -GalCer vs. Column H	88280000	88600000	-320000	11448843	5	5	0.03953	32

OVA- α -GalCer vs. PBS	72160000	54840000	17320000	11448843	5	5	2.139	32
OVA- α -GalCer vs. Column H	72160000	88600000	-1.6E+07	11448843	5	5	2.031	32
PBS vs. Column H	54840000	88600000	-3.4E+07	11448843	5	5	4.17	32

% α -GalCer tetramer⁺ CD1d⁺ cells in spleen - Figure 4.11B

Number of families	1					
Number of comparisons per family	28					
Alpha	0.05					
Tukey's multiple comparisons test	Mean Diff.	95.00% CI of diff.	Significant?	Summary	Adjusted P Value	
Ff.FLAG vs. Ff.OVA	0.222	-1.132 to 1.576	No	ns	0.9994	A-B
Ff.FLAG vs. Ff.OVA.BODIPY- α -GalCer	-0.578	-1.932 to 0.7761	No	ns	0.8583	A-C
Ff.FLAG vs. Ff.FLAG.BODIPY- α -GalCer	-0.586	-1.940 to 0.7681	No	ns	0.8498	A-D
Ff.FLAG vs. Ff.OVA + BODIPY- α -GalCer	-0.26	-1.614 to 1.094	No	ns	0.9983	A-E
Ff.FLAG vs. OVA- α -GalCer	-1.418	-2.772 to -0.06386	Yes	*	0.0348	A-F
Ff.FLAG vs. PBS	-0.458	-1.812 to 0.8961	No	ns	0.9531	A-G
Ff.FLAG vs. Column H	-1.066	-2.420 to 0.2881	No	ns	0.2117	A-H
Ff.OVA vs. Ff.OVA.BODIPY- α -GalCer	-0.8	-2.154 to 0.5541	No	ns	0.552	B-C
Ff.OVA vs. Ff.FLAG.BODIPY- α -GalCer	-0.808	-2.162 to 0.5461	No	ns	0.5398	B-D
Ff.OVA vs. Ff.OVA + BODIPY- α -GalCer	-0.482	-1.836 to 0.8721	No	ns	0.9392	B-E
Ff.OVA vs. OVA- α -GalCer	-1.64	-2.994 to -0.2859	Yes	**	0.0091	B-F
Ff.OVA vs. PBS	-0.68	-2.034 to 0.6741	No	ns	0.7313	B-G
Ff.OVA vs. Column H	-1.288	-2.642 to 0.06614	No	ns	0.0717	B-H
Ff.OVA.BODIPY- α -GalCer vs. Ff.FLAG.BODIPY- α -GalCer	-0.008	-1.362 to 1.346	No	ns	>0.9999	C-D
Ff.OVA.BODIPY- α -GalCer vs. Ff.OVA + BODIPY- α -GalCer	0.318	-1.036 to 1.672	No	ns	0.994	C-E
Ff.OVA.BODIPY- α -GalCer vs. OVA- α -GalCer	-0.84	-2.194 to 0.5141	No	ns	0.4916	C-F
Ff.OVA.BODIPY- α -GalCer vs. PBS	0.12	-1.234 to 1.474	No	ns	>0.9999	C-G
Ff.OVA.BODIPY- α -GalCer vs. Column H	-0.488	-1.842 to 0.8661	No	ns	0.9354	C-H
Ff.FLAG.BODIPY- α -GalCer vs. Ff.OVA + BODIPY- α -GalCer	0.326	-1.028 to 1.680	No	ns	0.9931	D-E
Ff.FLAG.BODIPY- α -GalCer vs. OVA- α -GalCer	-0.832	-2.186 to 0.5221	No	ns	0.5036	D-F
Ff.FLAG.BODIPY- α -GalCer vs. PBS	0.128	-1.226 to 1.482	No	ns	>0.9999	D-G
Ff.FLAG.BODIPY- α -GalCer vs. Column H	-0.48	-1.834 to 0.8741	No	ns	0.9405	D-H
Ff.OVA + BODIPY- α -GalCer vs. OVA- α -GalCer	-1.158	-2.512 to 0.1961	No	ns	0.1387	E-F

Ff.OVA + BODIPY- α -GalCer vs. PBS	-0.198	-1.552 to 1.156	No	ns	0.9997	E-G		
Ff.OVA + BODIPY- α -GalCer vs. Column H	-0.806	-2.160 to 0.5481	No	ns	0.5429	E-H		
OVA- α -GalCer vs. PBS	0.96	-0.3941 to 2.314	No	ns	0.3263	F-G		
OVA- α -GalCer vs. Column H	0.352	-1.002 to 1.706	No	ns	0.9891	F-H		
PBS vs. Column H	-0.608	-1.962 to 0.7461	No	ns	0.8248	G-H		
Test details	Mean 1	Mean 2	Mean Diff.	SE of diff.	n1	n2	q	DF
Ff.FLAG vs. Ff.OVA	2.848	2.626	0.222	0.418	5	5	0.751	32
Ff.FLAG vs. Ff.OVA.BODIPY- α -GalCer	2.848	3.426	-0.578	0.418	5	5	1.955	32
Ff.FLAG vs. Ff.FLAG.BODIPY- α -GalCer	2.848	3.434	-0.586	0.418	5	5	1.982	32
Ff.FLAG vs. Ff.OVA + BODIPY- α -GalCer	2.848	3.108	-0.26	0.418	5	5	0.8796	32
Ff.FLAG vs. OVA- α -GalCer	2.848	4.266	-1.418	0.418	5	5	4.797	32
Ff.FLAG vs. PBS	2.848	3.306	-0.458	0.418	5	5	1.549	32
Ff.FLAG vs. Column H	2.848	3.914	-1.066	0.418	5	5	3.606	32
Ff.OVA vs. Ff.OVA.BODIPY- α -GalCer	2.626	3.426	-0.8	0.418	5	5	2.706	32
Ff.OVA vs. Ff.FLAG.BODIPY- α -GalCer	2.626	3.434	-0.808	0.418	5	5	2.733	32
Ff.OVA vs. Ff.OVA + BODIPY- α -GalCer	2.626	3.108	-0.482	0.418	5	5	1.631	32
Ff.OVA vs. OVA- α -GalCer	2.626	4.266	-1.64	0.418	5	5	5.548	32
Ff.OVA vs. PBS	2.626	3.306	-0.68	0.418	5	5	2.3	32
Ff.OVA vs. Column H	2.626	3.914	-1.288	0.418	5	5	4.357	32
Ff.OVA.BODIPY- α -GalCer vs. Ff.FLAG.BODIPY- α -GalCer	3.426	3.434	-0.008	0.418	5	5	0.02706	32
Ff.OVA.BODIPY- α -GalCer vs. Ff.OVA + BODIPY- α -GalCer	3.426	3.108	0.318	0.418	5	5	1.076	32
Ff.OVA.BODIPY- α -GalCer vs. OVA- α -GalCer	3.426	4.266	-0.84	0.418	5	5	2.842	32
Ff.OVA.BODIPY- α -GalCer vs. PBS	3.426	3.306	0.12	0.418	5	5	0.406	32
Ff.OVA.BODIPY- α -GalCer vs. Column H	3.426	3.914	-0.488	0.418	5	5	1.651	32
Ff.FLAG.BODIPY- α -GalCer vs. Ff.OVA + BODIPY- α -GalCer	3.434	3.108	0.326	0.418	5	5	1.103	32
Ff.FLAG.BODIPY- α -GalCer vs. OVA- α -GalCer	3.434	4.266	-0.832	0.418	5	5	2.815	32
Ff.FLAG.BODIPY- α -GalCer vs. PBS	3.434	3.306	0.128	0.418	5	5	0.433	32
Ff.FLAG.BODIPY- α -GalCer vs. Column H	3.434	3.914	-0.48	0.418	5	5	1.624	32
Ff.OVA + BODIPY- α -GalCer vs. OVA- α -GalCer	3.108	4.266	-1.158	0.418	5	5	3.918	32
Ff.OVA + BODIPY- α -GalCer vs. PBS	3.108	3.306	-0.198	0.418	5	5	0.6698	32
Ff.OVA + BODIPY- α -GalCer vs. Column H	3.108	3.914	-0.806	0.418	5	5	2.727	32
OVA- α -GalCer vs. PBS	4.266	3.306	0.96	0.418	5	5	3.248	32
OVA- α -GalCer vs. Column H	4.266	3.914	0.352	0.418	5	5	1.191	32

PBS vs. Column H	3.306	3.914	-0.608	0.418	5	5	2.057	32
------------------	-------	-------	--------	-------	---	---	-------	----

Spleen #NKT - Figure 4.11C

Number of families	1						
Number of comparisons per family	28						
Alpha	0.05						
Tukey's multiple comparisons test	Mean Diff.	95.00% CI of diff.	Significant?	Summary	Adjusted P Value		
Ff.FLAG vs. Ff.OVA	-89200	-856535 to 678135	No	ns	>0.9999	A-B	
Ff.FLAG vs. Ff.OVA.BODIPY- α -GalCer	-694660	-1461995 to 72675	No	ns	0.0991	A-C	
Ff.FLAG vs. Ff.FLAG.BODIPY- α -GalCer	-743884	-1511219 to 23451	No	ns	0.0627	A-D	
Ff.FLAG vs. Ff.OVA + Ff.FLAG.BODIPY- α -GalCer	-	-1805715 to -271045	Yes	**	0.0027	A-E	
Ff.FLAG vs. Ff.OVA + BODIPY- α -GalCer	-664180	-1431515 to 103155	No	ns	0.1296	A-F	
Ff.FLAG vs. OVA- α -GalCer	-758456	-1525791 to 8879	No	ns	0.0545	A-G	
Ff.FLAG vs. PBS	-207364	-974699 to 559971	No	ns	0.9863	A-H	
Ff.OVA vs. Ff.OVA.BODIPY- α -GalCer	-605460	-1372795 to 161875	No	ns	0.2094	B-C	
Ff.OVA vs. Ff.FLAG.BODIPY- α -GalCer	-654684	-1422019 to 112651	No	ns	0.1405	B-D	
Ff.OVA vs. Ff.OVA + Ff.FLAG.BODIPY- α -GalCer	-949180	-1716515 to -181845	Yes	**	0.0073	B-E	
Ff.OVA vs. Ff.OVA + BODIPY- α -GalCer	-574980	-1342315 to 192355	No	ns	0.263	B-F	
Ff.OVA vs. OVA- α -GalCer	-669256	-1436591 to 98079	No	ns	0.124	B-G	
Ff.OVA vs. PBS	-118164	-885499 to 649171	No	ns	0.9996	B-H	
Ff.OVA.BODIPY- α -GalCer vs. Ff.FLAG.BODIPY- α -GalCer	-49224	-816559 to 718111	No	ns	>0.9999	C-D	
Ff.OVA.BODIPY- α -GalCer vs. Ff.OVA + Ff.FLAG.BODIPY- α -GalCer	-343720	-1111055 to 423615	No	ns	0.8265	C-E	
Ff.OVA.BODIPY- α -GalCer vs. Ff.OVA + BODIPY- α -GalCer	30480	-736855 to 797815	No	ns	>0.9999	C-F	
Ff.OVA.BODIPY- α -GalCer vs. OVA- α -GalCer	-63796	-831131 to 703539	No	ns	>0.9999	C-G	
Ff.OVA.BODIPY- α -GalCer vs. PBS	487296	-280039 to 1254631	No	ns	0.4622	C-H	
Ff.FLAG.BODIPY- α -GalCer vs. Ff.OVA + Ff.FLAG.BODIPY- α -GalCer	-294496	-1061831 to 472839	No	ns	0.9124	D-E	
Ff.FLAG.BODIPY- α -GalCer vs. Ff.OVA + BODIPY- α -GalCer	79704	-687631 to 847039	No	ns	>0.9999	D-F	
Ff.FLAG.BODIPY- α -GalCer vs. OVA- α -GalCer	-14572	-781907 to 752763	No	ns	>0.9999	D-G	
Ff.FLAG.BODIPY- α -GalCer vs. PBS	536520	-230815 to 1303855	No	ns	0.3428	D-H	

Ff.OVA + Ff.FLAG.BODIPY- α - GalCer vs. Ff.OVA + BODIPY- α -GalCer	374200	-393135 to 1141535	No	ns	0.7584	E-F		
Ff.OVA + Ff.FLAG.BODIPY- α - GalCer vs. OVA- α - GalCer	279924	-487411 to 1047259	No	ns	0.9314	E-G		
Ff.OVA + Ff.FLAG BODIPY- α -GalCer vs. PBS	831016	63681 to 1598351	Yes	*	0.0263	E-H		
Ff.OVA + BODIPY- α - GalCer vs. OVA- α - GalCer	-94276	-861611 to 673059	No	ns	>0.9999	F-G		
Ff.OVA + BODIPY- α - GalCer vs. PBS	456816	-310519 to 1224151	No	ns	0.5426	F-H		
OVA- α -GalCer vs. PBS	551092	-216243 to 1318427	No	ns	0.311	G-H		
Test details	Mean 1	Mean 2	Mean Diff.	SE of diff.	n1	n2	q	DF
Ff.FLAG vs. Ff.OVA	526380	615580	-89200	236883	5	5	0.5325	32
Ff.FLAG vs. Ff.OVA.BODIPY- α - GalCer	526380	1221040	-694660	236883	5	5	4.147	32
Ff.FLAG vs. Ff.FLAG.BODIPY- α - GalCer	526380	1270264	-743884	236883	5	5	4.441	32
Ff.FLAG vs. Ff.OVA + Ff.FLAG BODIPY- α - GalCer	526380	1564760	-1038380	236883	5	5	6.199	32
Ff.FLAG vs. Ff.OVA + BODIPY- α -GalCer	526380	1190560	-664180	236883	5	5	3.965	32
Ff.FLAG vs. OVA- α - GalCer	526380	1284836	-758456	236883	5	5	4.528	32
Ff.FLAG vs. PBS	526380	733744	-207364	236883	5	5	1.238	32
Ff.OVA vs. Ff.OVA.BODIPY- α - GalCer	615580	1221040	-605460	236883	5	5	3.615	32
Ff.OVA vs. Ff.FLAG.BODIPY- α - GalCer	615580	1270264	-654684	236883	5	5	3.909	32
Ff.OVA vs. Ff.OVA + Ff.FLAG.BODIPY- α - GalCer	615580	1564760	-949180	236883	5	5	5.667	32
Ff.OVA vs. Ff.OVA + BODIPY- α -GalCer	615580	1190560	-574980	236883	5	5	3.433	32
Ff.OVA vs. OVA- α - GalCer	615580	1284836	-669256	236883	5	5	3.996	32
Ff.OVA vs. PBS	615580	733744	-118164	236883	5	5	0.7054	32
Ff.OVA BODIPY- α - GalCer vs. Ff.FLAG BODIPY- α -GalCer	1221040	1270264	-49224	236883	5	5	0.2939	32
Ff.OVA.BODIPY- α - GalCer vs. Ff.OVA + Ff.FLAG BODIPY- α - GalCer	1221040	1564760	-343720	236883	5	5	2.052	32
Ff.OVA.BODIPY- α - GalCer vs. Ff.OVA + BODIPY- α -GalCer	1221040	1190560	30480	236883	5	5	0.182	32
Ff.OVA.BODIPY- α - GalCer vs. OVA- α - GalCer	1221040	1284836	-63796	236883	5	5	0.3809	32
Ff.OVA.BODIPY- α - GalCer vs. PBS	1221040	733744	487296	236883	5	5	2.909	32
Ff.FLAG.BODIPY- α - GalCer vs. Ff.OVA + Ff.FLAG BODIPY- α - GalCer	1270264	1564760	-294496	236883	5	5	1.758	32
Ff.FLAG.BODIPY- α - GalCer vs. Ff.OVA + BODIPY- α -GalCer	1270264	1190560	79704	236883	5	5	0.4758	32

Ff.FLAG.BODIPY- α -GalCer vs. OVA- α -GalCer	1270264	1284836	-14572	236883	5	5	0.087	32
Ff.FLAG.BODIPY- α -GalCer vs. PBS	1270264	733744	536520	236883	5	5	3.203	32
Ff.OVA + Ff.FLAG.BODIPY- α -GalCer vs. Ff.OVA + BODIPY- α -GalCer	1564760	1190560	374200	236883	5	5	2.234	32
Ff.OVA + Ff.FLAG.BODIPY- α -GalCer vs. OVA- α -GalCer	1564760	1284836	279924	236883	5	5	1.671	32
Ff.OVA + Ff.FLAG.BODIPY- α -GalCer vs. PBS	1564760	733744	831016	236883	5	5	4.961	32
Ff.OVA + BODIPY- α -GalCer vs OVA- α -GalCer	1190560	1284836	-94276	236883	5	5	0.5628	32
Ff.OVA + BODIPY- α -GalCer vs. PBS	1190560	733744	456816	236883	5	5	2.727	32
OVA- α -GalCer vs. PBS	1284836	733744	551092	236883	5	5	3.29	32

%NK1.1 - Figure 4.12A

Number of families	1					
Number of comparisons per family	28					
Alpha	0.05					
Tukey's multiple comparisons test	Mean Diff.	95.00% CI of diff.	Significant?	Summary	Adjusted P Value	
Ff.FLAG vs. Ff.OVA	-0.6	-11.54 to 10.34	No	ns	>0.9999	A-B
Ff.FLAG vs. Ff.OVA.BODIPY- α -GalCer	57.46	46.52 to 68.40	Yes	****	<0.0001	A-C
Ff.FLAG vs. Ff.FLAG.BODIPY- α -GalCer	56.26	45.32 to 67.20	Yes	****	<0.0001	A-D
Ff.FLAG vs. Ff.OVA + BODIPY- α -GalCer	46.64	35.70 to 57.58	Yes	****	<0.0001	A-E
Ff.FLAG vs. OVA- α -GalCer	47.96	37.02 to 58.90	Yes	****	<0.0001	A-F
Ff.FLAG vs. PBS	2.3	-8.640 to 13.24	No	ns	0.997	A-G
Ff.FLAG vs. Column H	53.42	42.48 to 64.36	Yes	****	<0.0001	A-H
Ff.OVA vs. Ff.OVA.BODIPY- α -GalCer	58.06	47.12 to 69.00	Yes	****	<0.0001	B-C
Ff.OVA vs. Ff.FLAG.BODIPY- α -GalCer	56.86	45.92 to 67.80	Yes	****	<0.0001	B-D
Ff.OVA vs. Ff.OVA + BODIPY- α -GalCer	47.24	36.30 to 58.18	Yes	****	<0.0001	B-E
Ff.OVA vs. OVA- α -GalCer	48.56	37.62 to 59.50	Yes	****	<0.0001	B-F
Ff.OVA vs. PBS	2.9	-8.040 to 13.84	No	ns	0.9877	B-G
Ff.OVA vs. Column H	54.02	43.08 to 64.96	Yes	****	<0.0001	B-H
Ff.OVA.BODIPY- α -GalCer vs. Ff.FLAG.BODIPY- α -GalCer	-1.2	-12.14 to 9.740	No	ns	>0.9999	C-D
Ff.OVA.BODIPY- α -GalCer vs. Ff.OVA + BODIPY- α -GalCer	-10.82	-21.76 to 0.1196	No	ns	0.0543	C-E
Ff.OVA.BODIPY- α -GalCer vs. OVA- α -GalCer	-9.5	-20.44 to 1.440	No	ns	0.1272	C-F
Ff.OVA.BODIPY- α -GalCer vs. PBS	-55.16	-66.10 to -44.22	Yes	****	<0.0001	C-G
Ff.OVA.BODIPY- α -GalCer vs. Column H	-4.04	-14.98 to 6.900	No	ns	0.9271	C-H
Ff.FLAG.BODIPY- α -GalCer vs. Ff.OVA + BODIPY- α -GalCer	-9.62	-20.56 to 1.320	No	ns	0.1182	D-E
Ff.FLAG.BODIPY- α -GalCer vs. OVA- α -GalCer	-8.3	-19.24 to 2.640	No	ns	0.2496	D-F
Ff.FLAG.BODIPY- α -GalCer vs. PBS	-53.96	-64.90 to -43.02	Yes	****	<0.0001	D-G
Ff.FLAG.BODIPY- α -GalCer vs. Column H	-2.84	-13.78 to 8.100	No	ns	0.9891	D-H
Ff.OVA + BODIPY- α -GalCer vs. OVA- α -GalCer	1.32	-9.620 to 12.26	No	ns	>0.9999	E-F
Ff.OVA + BODIPY- α -GalCer vs. PBS	-44.34	-55.28 to -33.40	Yes	****	<0.0001	E-G
Ff.OVA + BODIPY- α -GalCer vs. Column H	6.78	-4.160 to 17.72	No	ns	0.4927	E-H
OVA- α -GalCer vs. PBS	-45.66	-56.60 to -34.72	Yes	****	<0.0001	F-G
OVA- α -GalCer vs. Column H	5.46	-5.480 to 16.40	No	ns	0.7371	F-H

PBS vs. Column H	51.12	40.18 to 62.06	Yes	****	<0.0001	G-H		
Test details	Mean 1	Mean 2	Mean Diff.	SE of diff.	n1	n2	q	DF
Ff.FLAG vs. Ff.OVA	75.26	75.86	-0.6	3.377	5	5	0.2513	32
Ff.FLAG vs. Ff.OVA.BODIPY- α -GalCer	75.26	17.8	57.46	3.377	5	5	24.06	32
Ff.FLAG vs. Ff.FLAG.BODIPY- α -GalCer	75.26	19	56.26	3.377	5	5	23.56	32
Ff.FLAG vs. Ff.OVA + BODIPY- α -GalCer	75.26	28.62	46.64	3.377	5	5	19.53	32
Ff.FLAG vs. OVA- α -GalCer	75.26	27.3	47.96	3.377	5	5	20.08	32
Ff.FLAG vs. PBS	75.26	72.96	2.3	3.377	5	5	0.9631	32
Ff.FLAG vs. Column H	75.26	21.84	53.42	3.377	5	5	22.37	32
Ff.OVA vs. Ff.OVA.BODIPY- α -GalCer	75.86	17.8	58.06	3.377	5	5	24.31	32
Ff.OVA vs. Ff.FLAG.BODIPY- α -GalCer	75.86	19	56.86	3.377	5	5	23.81	32
Ff.OVA vs. Ff.OVA + BODIPY- α -GalCer	75.86	28.62	47.24	3.377	5	5	19.78	32
Ff.OVA vs. OVA- α -GalCer	75.86	27.3	48.56	3.377	5	5	20.33	32
Ff.OVA vs. PBS	75.86	72.96	2.9	3.377	5	5	1.214	32
Ff.OVA vs. Column H	75.86	21.84	54.02	3.377	5	5	22.62	32
Ff.OVA.BODIPY- α -GalCer vs. Ff.FLAG.BODIPY- α -GalCer	17.8	19	-1.2	3.377	5	5	0.5025	32
Ff.OVA.BODIPY- α -GalCer vs. Ff.OVA + BODIPY- α -GalCer	17.8	28.62	-10.82	3.377	5	5	4.531	32
Ff.OVA.BODIPY- α -GalCer vs. OVA- α -GalCer	17.8	27.3	-9.5	3.377	5	5	3.978	32
Ff.OVA.BODIPY- α -GalCer vs. PBS	17.8	72.96	-55.16	3.377	5	5	23.1	32
Ff.OVA.BODIPY- α -GalCer vs. Column H	17.8	21.84	-4.04	3.377	5	5	1.692	32
Ff.FLAG.BODIPY- α -GalCer vs. Ff.OVA + BODIPY- α -GalCer	19	28.62	-9.62	3.377	5	5	4.028	32
Ff.FLAG.BODIPY- α -GalCer vs. OVA- α -GalCer	19	27.3	-8.3	3.377	5	5	3.476	32
Ff.FLAG.BODIPY- α -GalCer vs. PBS	19	72.96	-53.96	3.377	5	5	22.6	32
Ff.FLAG.BODIPY- α -GalCer vs. Column H	19	21.84	-2.84	3.377	5	5	1.189	32
Ff.OVA + BODIPY- α -GalCer vs. OVA- α -GalCer	28.62	27.3	1.32	3.377	5	5	0.5528	32
Ff.OVA + BODIPY- α -GalCer vs. PBS	28.62	72.96	-44.34	3.377	5	5	18.57	32
Ff.OVA + BODIPY- α -GalCer vs. Column H	28.62	21.84	6.78	3.377	5	5	2.839	32
OVA- α -GalCer vs. PBS	27.3	72.96	-45.66	3.377	5	5	19.12	32
OVA- α -GalCer vs. Column H	27.3	21.84	5.46	3.377	5	5	2.286	32
PBS vs. Column H	72.96	21.84	51.12	3.377	5	5	21.41	32

MFI CD69 - Figure 4.12B

Number of families	1					
Number of comparisons per family	28					
Alpha	0.05					
Tukey's multiple comparisons test	Mean Diff.	95.00% CI of diff.	Significant?	Summary	Adjusted P Value	
Ff.FLAG vs. Ff.OVA	237.4	-141.3 to 616.1	No	ns	0.4785	A-B
Ff.FLAG vs. Ff.OVA.BODIPY- α -GalCer	1457	1078 to 1836	Yes	****	<0.0001	A-C
Ff.FLAG vs. Ff.FLAG.BODIPY- α -GalCer	1646	1268 to 2025	Yes	****	<0.0001	A-D
Ff.FLAG vs. Ff.OVA + BODIPY- α -GalCer	1525	1147 to 1904	Yes	****	<0.0001	A-E
Ff.FLAG vs. OVA- α -GalCer	1609	1230 to 1988	Yes	****	<0.0001	A-F
Ff.FLAG vs. PBS	1018	638.9 to 1396	Yes	****	<0.0001	A-G
Ff.FLAG vs. Column H	1584	1205 to 1962	Yes	****	<0.0001	A-H
Ff.OVA vs. Ff.OVA.BODIPY- α -GalCer	1220	840.9 to 1598	Yes	****	<0.0001	B-C
Ff.OVA vs. Ff.FLAG.BODIPY- α -GalCer	1409	1030 to 1788	Yes	****	<0.0001	B-D
Ff.OVA vs. Ff.OVA + BODIPY- α -GalCer	1288	909.3 to 1667	Yes	****	<0.0001	B-E
Ff.OVA vs. OVA- α -GalCer	1372	993.1 to 1751	Yes	****	<0.0001	B-F
Ff.OVA vs. PBS	780.2	401.5 to 1159	Yes	****	<0.0001	B-G
Ff.OVA vs. Column H	1346	967.5 to 1725	Yes	****	<0.0001	B-H
Ff.OVA.BODIPY- α -GalCer vs. Ff.FLAG.BODIPY- α -GalCer	189.4	-189.3 to 568.1	No	ns	0.7352	C-D
Ff.OVA.BODIPY- α -GalCer vs. Ff.OVA + BODIPY- α -GalCer	68.4	-310.3 to 447.1	No	ns	0.9988	C-E
Ff.OVA.BODIPY- α -GalCer vs. OVA- α -GalCer	152.2	-226.5 to 530.9	No	ns	0.8915	C-F
Ff.OVA.BODIPY- α -GalCer vs. PBS	-439.4	-818.1 to -60.69	Yes	*	0.014	C-G
Ff.OVA.BODIPY- α -GalCer vs. Column H	126.6	-252.1 to 505.3	No	ns	0.9559	C-H
Ff.FLAG.BODIPY- α -GalCer vs. Ff.OVA + BODIPY- α -GalCer	-121	-499.7 to 257.7	No	ns	0.9652	D-E
Ff.FLAG.BODIPY- α -GalCer vs. OVA- α -GalCer	-37.2	-415.9 to 341.5	No	ns	>0.9999	D-F
Ff.FLAG.BODIPY- α -GalCer vs. PBS	-628.8	-1008 to -250.1	Yes	***	0.0002	D-G
Ff.FLAG.BODIPY- α -GalCer vs. Column H	-62.8	-441.5 to 315.9	No	ns	0.9993	D-H
Ff.OVA + BODIPY- α -GalCer vs. OVA- α -GalCer	83.8	-294.9 to 462.5	No	ns	0.9958	E-F
Ff.OVA + BODIPY- α -GalCer vs. PBS	-507.8	-886.5 to -129.1	Yes	**	0.003	E-G
Ff.OVA + BODIPY- α -GalCer vs. Column H	58.2	-320.5 to 436.9	No	ns	0.9996	E-H
OVA- α -GalCer vs. PBS	-591.6	-970.3 to -212.9	Yes	***	0.0004	F-G
OVA- α -GalCer vs. Column H	-25.6	-404.3 to 353.1	No	ns	>0.9999	F-H
PBS vs. Column H	566	187.3 to 944.7	Yes	***	0.0007	G-H

Test details	Mean 1	Mean 2	Mean Diff.	SE of diff.	n1	n2	q	DF
Ff.FLAG vs. Ff.OVA	2272	2035	237.4	116.9	5	5	2.872	32
Ff.FLAG vs. Ff.OVA.BODIPY- α -GalCer	2272	815	1457	116.9	5	5	17.62	32
Ff.FLAG vs. Ff.FLAG.BODIPY- α -GalCer	2272	625.6	1646	116.9	5	5	19.92	32
Ff.FLAG vs. Ff.OVA + BODIPY- α -GalCer	2272	746.6	1525	116.9	5	5	18.45	32
Ff.FLAG vs. OVA- α -GalCer	2272	662.8	1609	116.9	5	5	19.47	32
Ff.FLAG vs. PBS	2272	1254	1018	116.9	5	5	12.31	32
Ff.FLAG vs. Column H	2272	688.4	1584	116.9	5	5	19.16	32
Ff.OVA vs. Ff.OVA.BODIPY- α -GalCer	2035	815	1220	116.9	5	5	14.75	32
Ff.OVA vs. Ff.FLAG.BODIPY- α -GalCer	2035	625.6	1409	116.9	5	5	17.04	32
Ff.OVA vs. Ff.OVA + BODIPY- α -GalCer	2035	746.6	1288	116.9	5	5	15.58	32
Ff.OVA vs. OVA- α -GalCer	2035	662.8	1372	116.9	5	5	16.59	32
Ff.OVA vs. PBS	2035	1254	780.2	116.9	5	5	9.438	32
Ff.OVA vs. Column H	2035	688.4	1346	116.9	5	5	16.28	32
Ff.OVA.BODIPY- α -GalCer vs. Ff.FLAG.BODIPY- α -GalCer	815	625.6	189.4	116.9	5	5	2.291	32
Ff.OVA.BODIPY- α -GalCer vs. Ff.OVA + BODIPY- α -GalCer	815	746.6	68.4	116.9	5	5	0.8274	32
Ff.OVA.BODIPY- α -GalCer vs. OVA- α -GalCer	815	662.8	152.2	116.9	5	5	1.841	32
Ff.OVA.BODIPY- α -GalCer vs. PBS	815	1254	-439.4	116.9	5	5	5.315	32
Ff.OVA.BODIPY- α -GalCer vs. Column H	815	688.4	126.6	116.9	5	5	1.531	32
Ff.FLAG.BODIPY- α -GalCer vs. Ff.OVA + BODIPY- α -GalCer	625.6	746.6	-121	116.9	5	5	1.464	32
Ff.FLAG.BODIPY- α -GalCer vs. OVA- α -GalCer	625.6	662.8	-37.2	116.9	5	5	0.45	32
Ff.FLAG.BODIPY- α -GalCer vs. PBS	625.6	1254	-628.8	116.9	5	5	7.606	32
Ff.FLAG.BODIPY- α -GalCer vs. Column H	625.6	688.4	-62.8	116.9	5	5	0.7597	32
Ff.OVA + BODIPY- α -GalCer vs. OVA- α -GalCer	746.6	662.8	83.8	116.9	5	5	1.014	32
Ff.OVA + BODIPY- α -GalCer vs. PBS	746.6	1254	-507.8	116.9	5	5	6.143	32
Ff.OVA + BODIPY- α -GalCer vs. Column H	746.6	688.4	58.2	116.9	5	5	0.704	32
OVA- α -GalCer vs. PBS	662.8	1254	-591.6	116.9	5	5	7.156	32
OVA- α -GalCer vs. Column H	662.8	688.4	-25.6	116.9	5	5	0.3097	32
PBS vs. Column H	1254	688.4	566	116.9	5	5	6.847	32

REFERENCES

- Abdolalizadeh, J., Nouri, M., Zolbanin, J.M., Barzegari, A., Baradaran, B., Barar, J., Coukos, G., and Omid, Y. (2013). Targeting cytokines: production and characterization of anti-TNF- α scFvs by phage display technology. *Curr Pharm Des* **19**, 2839-2847.
- Ackerman, A.L., Kyritsis, C., Tampé, R., and Cresswell, P. (2005). Access of soluble antigens to the endoplasmic reticulum can explain cross-presentation by dendritic cells. *Nature immunology* **6**, 107-113.
- Adams, M.H. (1959). Bacteriophages. Bacteriophages.
- Akhmetzyanova, I., Zelinsky, G., Schimmer, S., Brandau, S., Altenhoff, P., Sparwasser, T., and Dittmer, U. (2013). Tumor-specific CD4⁺ T cells develop cytotoxic activity and eliminate virus-induced tumor cells in the absence of regulatory T cells. *Cancer Immunol Immunother* **62**, 257-271.
- Albarran, B., Goncalves, L., Salmen, S., Borges, L., Fields, H., Soyano, A., Montes, H., and Berrueta, L. (2005). Profiles of NK, NKT cell activation and cytokine production following vaccination against hepatitis B. *APMIS* **113**, 526-535.
- Anderson, R.J., Compton, B.J., Tang, C.W., Authier-Hall, A., Hayman, C.M., Swinerd, G.W., Kowalczyk, R., Harris, P., Brimble, M.A., Larsen, D.S., *et al.* (2015). NKT cell-

References

dependent glycolipid-peptide vaccines with potent anti-tumour activity. *Chem Sci* **6**, 5120-5127.

Anderson, R.J., Tang, C.W., Daniels, N.J., Compton, B.J., Hayman, C.M., Johnston, K.A., Knight, D.A., Gasser, O., Poyntz, H.C., Ferguson, P.M., *et al.* (2014). A self-adjuvanting vaccine induces cytotoxic T lymphocytes that suppress allergy. *Nat Chem Biol* **10**, 943-949.

Ando, T., Ito, H., Ohtaki, H., and Seishima, M. (2013). Toll-like receptor agonists and alpha-galactosylceramide synergistically enhance the production of interferon-gamma in murine splenocytes. *Scientific reports* **3**, 2559.

Arase, H., Arase, N., Nakagawa, K., Good, R.A., and Onoe, K. (1993). NK1.1+ CD4+ CD8- thymocytes with specific lymphokine secretion. *Eur J Immunol* **23**, 307-310.

Arens, R., and Schoenberger, S.P. (2010). Plasticity in programming of effector and memory CD8 T-cell formation. *Immunological reviews* **235**, 190-205.

Aronow, R., Danon, D., Shahar, A., and Aronson, M. (1964). Electron Microscopy of in Vitro Endocytosis of T2 Phage by Cells from Rabbit Peritoneal Exudate. *J Exp Med* **120**, 943-954.

Attarwala, H. (2010). Role of antibodies in cancer targeting. *J Nat Sci Biol Med* **1**, 53-56.

Baba, T., Ara, T., Hasegawa, M., Takai, Y., Okumura, Y., Baba, M., Datsenko, K.A., Tomita, M., Wanner, B.L., and Mori, H. (2006a). Construction of *Escherichia coli* K-

- 12 in-frame, single-gene knockout mutants: the Keio collection. *Mol Syst Biol* **2**, 2006-2008.
- Baba, T., Ara, T., Hasegawa, M., Takai, Y., Okumura, Y., Baba, M., Datsenko, K.A., Tomita, M., Wanner, B.L., and Mori, H. (2006b). Construction of *Escherichia coli* K-12 in-frame, single-gene knockout mutants: the Keio collection. *Mol Syst Biol* **2**, 2006 0008.
- Bakhshinejad, B., Karimi, M., and Khalaj-Kondori, M. (2015). Phage display: development of nanocarriers for targeted drug delivery to the brain. *Neural Regen Res* **10**, 862-865.
- Balaji, K.N., Schaschke, N., Machleidt, W., Catalfamo, M., and Henkart, P.A. (2002). Surface cathepsin B protects cytotoxic lymphocytes from self-destruction after degranulation. *J Exp Med* **196**, 493-503.
- Bar, H., Yacoby, I., and Benhar, I. (2008). Killing cancer cells by targeted drug-carrying phage nanomedicines. *BMC Biotechnol* **8**, 37.
- Barbas, C.F., 3rd (1993). Recent advances in phage display. *Curr Opin Biotechnol* **4**, 526-530.
- Barbas, C.F., 3rd, Kang, A.S., Lerner, R.A., and Benkovic, S.J. (1991). Assembly of combinatorial antibody libraries on phage surfaces: the gene III site. *Proc Natl Acad Sci U S A* **88**, 7978-7982.
- Beck, E., Sommer, R., Auerswald, E.A., Kurz, C., Zink, B., Osterburg, G., Schaller, H., Sugimoto, K., Sugisaki,

References

- H., Okamoto, T., *et al.* (1978). Nucleotide sequence of bacteriophage fd DNA. *Nucleic Acids Res* **5**, 4495-4503.
- Belz, G.T., and Kallies, A. (2010). Effector and memory CD8+ T cell differentiation: toward a molecular understanding of fate determination. *Curr Opin Immunol* **22**, 279-285.
- Bendelac, A., Lantz, O., Quimby, M.E., Yewdell, J.W., Bennink, J.R., and Brutkiewicz, R.R. (1995). CD1 recognition by mouse NK1+ T lymphocytes. *Science* **268**, 863-865.
- Bendelac, A., Savage, P.B., and Teyton, L. (2007). The biology of NKT cells. *Annu Rev Immunol* **25**, 297-336.
- Benlagha, K., Weiss, A., Beavis, A., Teyton, L., and Bendelac, A. (2000). In vivo identification of glycolipid antigen-specific T cells using fluorescent CD1d tetramers. *J Exp Med* **191**, 1895-1903.
- Bennett, N.J., and Rakonjac, J. (2006). Unlocking of the filamentous bacteriophage virion during infection is mediated by the C domain of pIII. *J Mol Biol* **356**, 266-273.
- Bennett, S.R., Carbone, F.R., Karamalis, F., Miller, J.F., and Heath, W.R. (1997). Induction of a CD8+ cytotoxic T lymphocyte response by cross-priming requires cognate CD4+ T cell help. *The Journal of experimental medicine* **186**, 65-70.
- Bennstein, S.B. (2017). Unraveling Natural Killer T-Cells Development. *Front Immunol* **8**, 1950.

- Bernard, J.M., and Francis, M.B. (2014). Chemical strategies for the covalent modification of filamentous phage. *Front Microbiol* **5**, 734.
- Bertrand, N., Wu, J., Xu, X., Kamaly, N., and Farokhzad, O.C. (2014). Cancer nanotechnology: the impact of passive and active targeting in the era of modern cancer biology. *Adv Drug Deliv Rev* **66**, 2-25.
- Beurskens, F.J., Lindorfer, M.A., Farooqui, M., Beum, P.V., Engelberts, P., Mackus, W.J., Parren, P.W., Wiestner, A., and Taylor, R.P. (2012). Exhaustion of cytotoxic effector systems may limit monoclonal antibody-based immunotherapy in cancer patients. *J Immunol* **188**, 3532-3541.
- Bevan, M.J. (1976). Cross-priming for a secondary cytotoxic response to minor H antigens with H-2 congenic cells which do not cross-react in the cytotoxic assay. *J Exp Med* **143**, 1283-1288.
- Binnicker, M.J. (2020). Emergence of a Novel Coronavirus Disease (COVID-19) and the Importance of Diagnostic Testing: Why Partnership between Clinical Laboratories, Public Health Agencies, and Industry Is Essential to Control the Outbreak. *Clin Chem* **66**, 664-666.
- Blanco, J., Moore, R.A., Kabaleeswaran, V., and Viola, R.E. (2003). A structural basis for the mechanism of aspartate-beta-semialdehyde dehydrogenase from *Vibrio cholerae*. *Protein Sci* **12**, 27-33.

References

- Boeke, J.D., and Model, P. (1982). A prokaryotic membrane anchor sequence: carboxyl terminus of bacteriophage f1 gene III protein retains it in the membrane. *Proc Natl Acad Sci U S A* **79**, 5200-5204.
- Boeke, J.D., Model, P., and Zinder, N.D. (1982). Effects of bacteriophage f1 gene III protein on the host cell membrane. *Mol Gen Genet* **186**, 185-192.
- Boffey, S.A. (1985). Agarose gel electrophoresis of DNA. *Methods Mol Biol* **2**, 43-50.
- Boisen, M.L., Ottamasathien, D., Jones, A.B., Millett, M.M., Nelson, D.S., Bornholdt, Z.A., Fusco, M.L., Abelson, D.M., Oda, S., Hartnett, J.N., *et al.* (2015). Development of Prototype Filovirus Recombinant Antigen Immunoassays. *J Infect Dis* **212 Suppl 2**, S359-367.
- Bonner, W.A., Hulett, H.R., Sweet, R.G., and Herzenberg, L.A. (1972). Fluorescence activated cell sorting. *Rev Sci Instrum* **43**, 404-409.
- Borg, N.A., Wun, K.S., Kjer-Nielsen, L., Wilce, M.C., Pellicci, D.G., Koh, R., Besra, G.S., Bharadwaj, M., Godfrey, D.I., McCluskey, J., *et al.* (2007). CD1d-lipid-antigen recognition by the semi-invariant NKT T-cell receptor. *Nature* **448**, 44-49.
- Bradley, D.E., Coetzee, J.N., Bothma, T., and Hedges, R.W. (1981). Phage X: a plasmid-dependent, broad host range, filamentous bacterial virus. *J Gen Microbiol* **126**, 389-396.

- Brito, L.A., and Singh, M. (2011). Acceptable levels of endotoxin in vaccine formulations during preclinical research. *J Pharm Sci* **100**, 34-37.
- Bromberg, J.F., Horvath, C.M., Wen, Z., Schreiber, R.D., and Darnell, J.E., Jr. (1996). Transcriptionally active Stat1 is required for the antiproliferative effects of both interferon alpha and interferon gamma. *P Natl Acad Sci USA* **93**, 7673-7678.
- Brower, V. (2010). Approval of provenge seen as first step for cancer treatment vaccines. *J Natl Cancer Inst* **102**, 1108-1110.
- Brussow, H., Canchaya, C., and Hardt, W.D. (2004). Phages and the evolution of bacterial pathogens: from genomic rearrangements to lysogenic conversion. *Microbiol Mol Biol Rev* **68**, 560-602, table of contents.
- Bryant, P., and Ploegh, H. (2004). Class II MHC peptide loading by the professionals. *Curr Opin Immunol* **16**, 96-102.
- Caminschi, I., Maraskovsky, E., and Heath, W.R. (2012). Targeting Dendritic Cells in vivo for Cancer Therapy. *Front Immunol* **3**, 13.
- Carbone, F.R., Sterry, S.J., Butler, J., Rodda, S., and Moore, M.W. (1992). T cell receptor alpha-chain pairing determines the specificity of residue 262 within the Kb-restricted, ovalbumin257-264 determinant. *Int Immunol* **4**, 861-867.

References

- Carnaud, C., Lee, D., Donnars, O., Park, S.-H., Beavis, A., Koezuka, Y., and Bendelac, A. (1999). Cutting Edge: Cross-Talk Between Cells of the Innate Immune System: NKT Cells Rapidly Activate NK Cells. *The Journal of Immunology* **163**, 4647-4650.
- Carreno, B.M., Magrini, V., Becker-Hapak, M., Kaabinejadian, S., Hundal, J., Petti, A.A., Ly, A., Lie, W.R., Hildebrand, W.H., Mardis, E.R., *et al.* (2015). Cancer immunotherapy. A dendritic cell vaccine increases the breadth and diversity of melanoma neoantigen-specific T cells. *Science* **348**, 803-808.
- Carreno, L.J., Kharkwal, S.S., and Porcelli, S.A. (2014). Optimizing NKT cell ligands as vaccine adjuvants. *Immunotherapy* **6**, 309-320.
- Carrio, A., Sampedro, C., Sanchez-Lopez, J.L., Pimienta, M., and Campoy, P. (2015). Automated Low-Cost Smartphone-Based Lateral Flow Saliva Test Reader for Drugs-of-Abuse Detection. *Sensors (Basel)* **15**, 29569-29593.
- Carroll-Portillo, A., and Lin, H.C. (2019). Bacteriophage and the Innate Immune System: Access and Signaling. *Microorganisms* **7**.
- Caspi, R., Altman, T., Billington, R., Dreher, K., Foerster, H., Fulcher, C.A., Holland, T.A., Keseler, I.M., Kothari, A., Kubo, A., *et al.* (2014). The MetaCyc database of metabolic pathways and enzymes and the BioCyc collection of Pathway/Genome Databases. *Nucleic Acids Res* **42**, D459-471.

- Caux, C., Massacrier, C., Vanbervliet, B., Dubois, B., Van Kooten, C., Durand, I., and Banchereau, J. (1994). Activation of human dendritic cells through CD40 cross-linking. *J Exp Med* *180*, 1263-1272.
- Cazacu, A.C., Greer, J., Taherivand, M., and Demmler, G.J. (2003). Comparison of lateral-flow immunoassay and enzyme immunoassay with viral culture for rapid detection of influenza virus in nasal wash specimens from children. *J Clin Microbiol* *41*, 2132-2134.
- Cella, M., Scheidegger, D., Palmer-Lehmann, K., Lane, P., Lanzavecchia, A., and Alber, G. (1996). Ligation of CD40 on dendritic cells triggers production of high levels of interleukin-12 and enhances T cell stimulatory capacity: T-T help via APC activation. *J Exp Med* *184*, 747-752.
- Cerundolo, V., and Kronenberg, M. (2010). The role of invariant NKT cells at the interface of innate and adaptive immunity. *Semin Immunol* *22*, 59-60.
- Chang, C.H., Chen, Y.C., Zhang, W., Leung, P.S., Gershwin, M.E., and Chuang, Y.H. (2015). Innate immunity drives the initiation of a murine model of primary biliary cirrhosis. *PLoS One* *10*, e0121320.
- Chavez-Galan, L., Arenas-Del Angel, M.C., Zenteno, E., Chavez, R., and Lascurain, R. (2009). Cell death mechanisms induced by cytotoxic lymphocytes. *Cell Mol Immunol* *6*, 15-25.

References

- Chen, Y., Shen, Y., Guo, X., Zhang, C., Yang, W., Ma, M., Liu, S., Zhang, M., and Wen, L.P. (2006). Transdermal protein delivery by a coadministered peptide identified via phage display. *Nat Biotechnol* **24**, 455-460.
- Cheng, J.M.H. (2014). The Synthesis and Biological Evaluation of Glycolipids for Improved Cancer Immunotherapy (Wellington, New Zealand: Victoria University of Wellington).
- Cherepanov, P.P., and Wackernagel, W. (1995). Gene disruption in *Escherichia coli*: TcR and KmR cassettes with the option of Flp-catalyzed excision of the antibiotic-resistance determinant. *Gene* **158**, 9-14.
- Chiba, A., Dascher, C.C., Besra, G.S., and Brenner, M.B. (2008). Rapid NKT cell responses are self-terminating during the course of microbial infection. *J Immunol* **181**, 2292-2302.
- Chin, Y.E., Kitagawa, M., Su, W.-C.S., You, Z.-H., Iwamoto, Y., and Fu, X.-Y. (1996). Cell Growth Arrest and Induction of Cyclin-Dependent Kinase Inhibitor p21^{WAF1/CIP1} Mediated by STAT1. *Science* **272**, 719-722.
- Ching, K.H., He, X., Stanker, L.H., Lin, A.V., McGarvey, J.A., and Hnasko, R. (2015). Detection of shiga toxins by lateral flow assay. *Toxins (Basel)* **7**, 1163-1173.
- Chopin, M.C., Rouault, A., Ehrlich, S.D., and Gautier, M. (2002). Filamentous phage active on the gram-positive

- bacterium *Propionibacterium freudenreichii*. J Bacteriol *184*, 2030-2033.
- Chopra, I.J. (1972). A radioimmunoassay for measurement of thyroxine in unextracted serum. J Clin Endocrinol Metab *34*, 938-947.
- Chopra, I.J., Ho, R.S., and Lam, R. (1972). An improved radioimmunoassay of triiodothyronine in serum: its application to clinical and physiological studies. The Journal of laboratory and clinical medicine *80*, 729-739.
- Cinquanta, L., Fontana, D.E., and Bizzaro, N. (2017). Chemiluminescent immunoassay technology: what does it change in autoantibody detection? Auto Immun Highlights *8*, 9.
- Clackson, T., Hoogenboom, H.R., Griffiths, A.D., and Winter, G. (1991). Making antibody fragments using phage display libraries. Nature *352*, 624-628.
- Clarke, S.R., Barnden, M., Kurts, C., Carbone, F.R., Miller, J.F., and Heath, W.R. (2000). Characterization of the ovalbumin-specific TCR transgenic line OT-I: MHC elements for positive and negative selection. Immunol Cell Biol *78*, 110-117.
- Click, E.M., and Webster, R.E. (1998). The TolQRA proteins are required for membrane insertion of the major capsid protein of the filamentous phage f1 during infection. J Bacteriol *180*, 1723-1728.

References

- Compton, B.J., Tang, C.W., Johnston, K.A., Osmond, T.L., Hayman, C.M., Larsen, D.S., Hermans, I.F., and Painter, G.F. (2015). Synthesis and Activity of 6'''-Deoxy-6'''-thio-alpha-GalCer and Peptide Conjugates. *Org Lett* **17**, 5954-5957.
- Connelly, J.T., Nugen, S.R., Borejsza-Wysocki, W., Durst, R.A., Montagna, R.A., and Baeumner, A.J. (2008). Human pathogenic *Cryptosporidium* species bioanalytical detection method with single oocyst detection capability. *Anal Bioanal Chem* **391**, 487-495.
- Coquet, J.M., Chakravarti, S., Kyparissoudis, K., McNab, F.W., Pitt, L.A., McKenzie, B.S., Berzins, S.P., Smyth, M.J., and Godfrey, D.I. (2008). Diverse cytokine production by NKT cell subsets and identification of an IL-17-producing CD4-NK1.1- NKT cell population. *Proc Natl Acad Sci U S A* **105**, 11287-11292.
- Coquet, J.M., Kyparissoudis, K., Pellicci, D.G., Besra, G., Berzins, S.P., Smyth, M.J., and Godfrey, D.I. (2007). IL-21 is produced by NKT cells and modulates NKT cell activation and cytokine production. *J Immunol* **178**, 2827-2834.
- Couzin-Frankel, J. (2013). Breakthrough of the year 2013. Cancer immunotherapy. *Science* **342**, 1432-1433.
- Cwirla, S.E., Peters, E.A., Barrett, R.W., and Dower, W.J. (1990). Peptides on phage: a vast library of peptides for identifying ligands. *Proc Natl Acad Sci U S A* **87**, 6378-6382.

- Daeschlein, G., Langner, I., Wild, T., von Podewils, S., Sicher, C., Kiefer, T., and Junger, M. (2017). Hyperspectral imaging as a novel diagnostic tool in microcirculation of wounds. *Clin Hemorheol Microcirc* **67**, 467-474.
- Dan, N., Setua, S., Kashyap, V.K., Khan, S., Jaggi, M., Yallapu, M.M., and Chauhan, S.C. (2018). Antibody-Drug Conjugates for Cancer Therapy: Chemistry to Clinical Implications. *Pharmaceuticals (Basel)* **11**.
- Darwish, I.A. (2006). Immunoassay Methods and their Applications in Pharmaceutical Analysis: Basic Methodology and Recent Advances. *Int J Biomed Sci* **2**, 217-235.
- Datsenko, K.A., and Wanner, B.L. (2000). One-step inactivation of chromosomal genes in *Escherichia coli* K-12 using PCR products. *Proc Natl Acad Sci U S A* **97**, 6640-6645.
- Dawson, N. (2010). Immunotherapeutic approaches in prostate cancer: PROVENGE. *Clin Adv Hematol Oncol* **8**, 419-421.
- Day, L.A., Marzec, C.J., Reisberg, S.A., and Casadevall, A. (1988). DNA packing in filamentous bacteriophages. *Annu Rev Biophys Biophys Chem* **17**, 509-539.
- De Berardinis, P., Sartorius, R., Fanutti, C., Perham, R.N., Del Pozzo, G., and Guardiola, J. (2000). Phage display of peptide epitopes from HIV-1 elicits strong cytolytic responses. *Nat Biotechnol* **18**, 873-876.

References

- de Boer, H.A., Comstock, L.J., and Vasser, M. (1983). The tac promoter: a functional hybrid derived from the trp and lac promoters. *Proc Natl Acad Sci U S A* **80**, 21-25.
- De Boer, R.J., Oprea, M., Antia, R., Murali-Krishna, K., Ahmed, R., and Perelson, A.S. (2001). Recruitment times, proliferation, and apoptosis rates during the CD8(+) T-cell response to lymphocytic choriomeningitis virus. *J Virol* **75**, 10663-10669.
- Demotz, S., Grey, H.M., and Sette, A. (1990). The minimal number of class II MHC-antigen complexes needed for T cell activation. *Science* **249**, 1028-1030.
- Deutscher, S.L. (2010). Phage display in molecular imaging and diagnosis of cancer. *Chem Rev* **110**, 3196-3211.
- Devlin, J.J., Panganiban, L.C., and Devlin, P.E. (1990). Random peptide libraries: a source of specific protein binding molecules. *Science* **249**, 404-406.
- Dhodapkar, M.V., Steinman, R.M., Krasovsky, J., Munz, C., and Bhardwaj, N. (2001). Antigen-specific inhibition of effector T cell function in humans after injection of immature dendritic cells. *J Exp Med* **193**, 233-238.
- di Marzo Veronese, F., Willis, A.E., Boyer-Thompson, C., Appella, E., and Perham, R.N. (1994). Structural mimicry and enhanced immunogenicity of peptide epitopes displayed on filamentous bacteriophage. The V3 loop of HIV-1 gp120. *J Mol Biol* **243**, 167-172.
- Diaz-Perlas, C., Sanchez-Navarro, M., Oller-Salvia, B., Moreno, M., Teixido, M., and Giralt, E. (2017). Phage

- display as a tool to discover blood-brain barrier (BBB)-shuttle peptides: panning against a human BBB cellular model. *Biopolymers* **108**.
- Dieu, M.C., Vanbervliet, B., Vicari, A., Bridon, J.M., Oldham, E., Aït-Yahia, S., Brière, F., Zlotnik, A., Lebecque, S., and Caux, C. (1998). Selective recruitment of immature and mature dendritic cells by distinct chemokines expressed in different anatomic sites. *The Journal of experimental medicine* **188**, 373-386.
- Dor-On, E., and Solomon, B. (2015). Targeting glioblastoma via intranasal administration of Ff bacteriophages. *Front Microbiol* **6**, 530.
- Eagle, H. (1971). Buffer combinations for mammalian cell culture. *Science* **174**, 500-503.
- Endemann, H., and Model, P. (1995). Location of filamentous phage minor coat proteins in phage and in infected cells. *J Mol Biol* **250**, 496-506.
- Eriksson, F., Culp, W.D., Massey, R., Egevad, L., Garland, D., Persson, M.A., and Pisa, P. (2007). Tumor specific phage particles promote tumor regression in a mouse melanoma model. *Cancer Immunol Immunother* **56**, 677-687.
- Eriksson, F., Tsagozis, P., Lundberg, K., Parsa, R., Mangsbo, S.M., Persson, M.A., Harris, R.A., and Pisa, P. (2009). Tumor-specific bacteriophages induce tumor destruction through activation of tumor-associated macrophages. *J Immunol* **182**, 3105-3111.

References

- Fagbohun, O.A., Kazmierczak, R.A., Petrenko, V.A., and Eisenstark, A. (2013). Metastatic prostate cancer cell-specific phage-like particles as a targeted gene-delivery system. *J Nanobiotechnology* *11*, 31.
- Fan, Y., and Moon, J.J. (2015). Nanoparticle Drug Delivery Systems Designed to Improve Cancer Vaccines and Immunotherapy. *Vaccines (Basel)* *3*, 662-685.
- Feau, S., Arens, R., Togher, S., and Schoenberger, S.P. (2011). Autocrine IL-2 is required for secondary population expansion of CD8(+) memory T cells. *Nature immunology* *12*, 908-913.
- Finbloom, J.A., Aanei, I.L., Bernard, J.M., Klass, S.H., Elledge, S.K., Han, K., Ozawa, T., Nicolaides, T.P., Berger, M.S., and Francis, M.B. (2018). Evaluation of Three Morphologically Distinct Virus-Like Particles as Nanocarriers for Convection-Enhanced Drug Delivery to Glioblastoma. *Nanomaterials (Basel)* *8*.
- Frenkel, D., and Solomon, B. (2002). Filamentous phage as vector-mediated antibody delivery to the brain. *Proc Natl Acad Sci U S A* *99*, 5675-5679.
- Fujii, S., Liu, K., Smith, C., Bonito, A.J., and Steinman, R.M. (2004). The linkage of innate to adaptive immunity via maturing dendritic cells in vivo requires CD40 ligation in addition to antigen presentation and CD80/86 costimulation. *J Exp Med* *199*, 1607-1618.
- Fujii, S., Shimizu, K., Hemmi, H., and Steinman, R.M. (2007). Innate Valpha14(+) natural killer T cells

- mature dendritic cells, leading to strong adaptive immunity. *Immunol Rev* **220**, 183-198.
- Fujii, S., Shimizu, K., Smith, C., Bonifaz, L., and Steinman, R.M. (2003). Activation of natural killer T cells by alpha-galactosylceramide rapidly induces the full maturation of dendritic cells in vivo and thereby acts as an adjuvant for combined CD4 and CD8 T cell immunity to a coadministered protein. *Journal of Experimental Medicine* **198**, 267-279.
- Garg, P. (2019). Filamentous bacteriophage: A prospective platform for targeting drugs in phage-mediated cancer therapy. *J Cancer Res Ther* **15**, S1-S10.
- Gibbins, J.D. (2014). The Role of Langerin+ CD8a+ Dendritic Cells in Tumour Immunotherapy (Wellington, New Zealand: Victoria University of Wellington).
- Girardi, E., and Zajonc, D.M. (2012). Molecular basis of lipid antigen presentation by CD1d and recognition by natural killer T cells. *Immunol Rev* **250**, 167-179.
- Goldberg, A.L., Cascio, P., Saric, T., and Rock, K.L. (2002). The importance of the proteasome and subsequent proteolytic steps in the generation of antigenic peptides. *Mol Immunol* **39**, 147-164.
- Gorski, A., Kniotek, M., Perkowska-Ptasinska, A., Mroz, A., Przerwa, A., Gorczyca, W., Dabrowska, K., Weber-Dabrowska, B., and Nowaczyk, M. (2006). Bacteriophages and transplantation tolerance. *Transplant Proc* **38**, 331-333.

References

- Gottschalk, C., Mettke, E., and Kurts, C. (2015). The Role of Invariant Natural Killer T Cells in Dendritic Cell Licensing, Cross-Priming, and Memory CD8(+) T Cell Generation. *Front Immunol* **6**, 379.
- Grant, R., Lin, T., Webster, R., and Konigsberg, W. (1980). Structure of filamentous bacteriophage: isolation, characterization, and localization of the minor coat proteins and orientation of the DNA. In *Bacteriophage assembly*, M. DuBow, ed. (New York: Alan. R. Liss, Inc.), pp. 413-428.
- Guermonprez, P., Saveanu, L., Kleijmeer, M., Davoust, J., van Endert, P., and Amigorena, S. (2003). ER-phagosome fusion defines an MHC class I cross-presentation compartment in dendritic cells. *Nature* **425**, 397-402.
- Guo, A.J., and Cai, X.P. (2006). [Application of filamentous phage display technology in parasitology]. *Zhongguo Ji Sheng Chong Xue Yu Ji Sheng Chong Bing Za Zhi* **24**, 304-308.
- Hairul Bahara, N.H., Tye, G.J., Choong, Y.S., Ong, E.B., Ismail, A., and Lim, T.S. (2013). Phage display antibodies for diagnostic applications. *Biologicals* **41**, 209-216.
- Harlow, E., and Lane, D. (1999). *Using antibodies : a laboratory manual* (Cold Spring Harbor, N.Y.: Cold Spring Harbor Laboratory Press).
- Harris, N.S., and Feinstein, R. (1979). The LAL-bead assay for endotoxin. *Prog Clin Biol Res* **29**, 265-274.

- Heilpern, A.J., and Waldor, M.K. (2000). CTX ϕ infection of *Vibrio cholerae* requires the tolQRA gene products. *J Bacteriol* **182**, 1739-1747.
- Hein, C.D., Liu, X.-M., and Wang, D. (2008). Click chemistry, a powerful tool for pharmaceutical sciences. *Pharmaceutical research* **25**, 2216-2230.
- Henry, K.A., Arbabi-Ghahroudi, M., and Scott, J.K. (2015). Beyond phage display: non-traditional applications of the filamentous bacteriophage as a vaccine carrier, therapeutic biologic, and bioconjugation scaffold. *Front Microbiol* **6**, 755.
- Hermans, I.F., Silk, J.D., Gileadi, U., Masri, S.H., Shepherd, D., Farrand, K.J., Salio, M., and Cerundolo, V. (2007). Dendritic cell function can be modulated through cooperative actions of TLR ligands and invariant NKT cells. *J Immunol* **178**, 2721-2729.
- Hermans, I.F., Silk, J.D., Gileadi, U., Salio, M., Mathew, B., Ritter, G., Schmidt, R., Harris, A.L., Old, L., and Cerundolo, V. (2003). NKT cells enhance CD4+ and CD8+ T cell responses to soluble antigen in vivo through direct interaction with dendritic cells. *J Immunol* **171**, 5140-5147.
- Hernandez, J., Aung, S., Redmond, W.L., and Sherman, L.A. (2001). Phenotypic and functional analysis of CD8(+) T cells undergoing peripheral deletion in response to cross-presentation of self-antigen. *J Exp Med* **194**, 707-717.

References

- Hess, G.T., Cragnolini, J.J., Popp, M.W., Allen, M.A., Dougan, S.K., Spooner, E., Ploegh, H.L., Belcher, A.M., and Guimaraes, C.P. (2012). M13 bacteriophage display framework that allows sortase-mediated modification of surface-accessible phage proteins. *Bioconjug Chem* **23**, 1478-1487.
- Hirschhorn-Cymerman, D., Budhu, S., Kitano, S., Liu, C., Zhao, F., Zhong, H., Lesokhin, A.M., Avogadri-Connors, F., Yuan, J., Li, Y., *et al.* (2012). Induction of tumoricidal function in CD4+ T cells is associated with concomitant memory and terminally differentiated phenotype. *J Exp Med* **209**, 2113-2126.
- Hodyra-Stefaniak, K., Miernikiewicz, P., Drapala, J., Drab, M., Jonczyk-Matysiak, E., Lecion, D., Kazmierczak, Z., Beta, W., Majewska, J., Harhala, M., *et al.* (2015). Mammalian Host-Versus-Phage immune response determines phage fate in vivo. *Scientific reports* **5**, 14802.
- Hoffman, E.P., and Wilhelm, R.C. (1970). Genetic mapping and dominance of the amber suppressor, Su1 (supD), in *Escherichia coli* K-12. *J Bacteriol* **103**, 32-36.
- Hofmeister, L.H., Lee, S.H., Norlander, A.E., Montaniel, K.R., Chen, W., Harrison, D.G., and Sung, H.J. (2015). Phage-display-guided nanocarrier targeting to atheroprone vasculature. *ACS Nano* **9**, 4435-4446.
- Hogquist, K.A., Jameson, S.C., Heath, W.R., Howard, J.L., Bevan, M.J., and Carbone, F.R. (1994). T cell receptor antagonist peptides induce positive selection. *Cell* **76**, 17-27.

- Holz, L.E., Chua, Y.C., de Menezes, M.N., Anderson, R.J., Draper, S.L., Compton, B.J., Chan, S.T.S., Mathew, J., Li, J., Kedzierski, L., *et al.* (2020). Glycolipid-peptide vaccination induces liver-resident memory CD8(+) T cells that protect against rodent malaria. *Sci Immunol* **5**.
- Honey, K., and Rudensky, A.Y. (2003). Lysosomal cysteine proteases regulate antigen presentation. *Nat Rev Immunol* **3**, 472-482.
- Hoogenboom, H.R., de Bruine, A.P., Hufton, S.E., Hoet, R.M., Arends, J.W., and Roovers, R.C. (1998). Antibody phage display technology and its applications. *Immunotechnology* **4**, 1-20.
- Iannolo, G., Minenkova, O., Gonfloni, S., Castagnoli, L., and Cesareni, G. (1997). Construction, exploitation and evolution of a new peptide library displayed at high density by fusion to the major coat protein of filamentous phage. *Biol Chem* **378**, 517-521.
- Imai, J., Hasegawa, H., Maruya, M., Koyasu, S., and Yahara, I. (2005). Exogenous antigens are processed through the endoplasmic reticulum-associated degradation (ERAD) in cross-presentation by dendritic cells. *Int Immunol* **17**, 45-53.
- Inaba, K., Turley, S., Iyoda, T., Yamaide, F., Shimoyama, S., Reis e Sousa, C., Germain, R.N., Mellman, I., and Steinman, R.M. (2000). The formation of immunogenic major histocompatibility complex class II-peptide ligands in lysosomal compartments of dendritic cells

References

- is regulated by inflammatory stimuli. *The Journal of experimental medicine* **191**, 927-936.
- Ingulli, E., Mondino, A., Khoruts, A., and Jenkins, M.K. (1997). In vivo detection of dendritic cell antigen presentation to CD4(+) T cells. *The Journal of experimental medicine* **185**, 2133-2141.
- Jain, A., and Cheng, K. (2017). The principles and applications of avidin-based nanoparticles in drug delivery and diagnosis. *Journal of controlled release : official journal of the Controlled Release Society* **245**, 27-40.
- Joung, H.A., Oh, Y.K., and Kim, M.G. (2014). An automatic enzyme immunoassay based on a chemiluminescent lateral flow immunosensor. *Biosens Bioelectron* **53**, 330-335.
- Ju, Z., and Sun, W. (2017). Drug delivery vectors based on filamentous bacteriophages and phage-mimetic nanoparticles. *Drug Deliv* **24**, 1898-1908.
- Jung, S., Unutmaz, D., Wong, P., Sano, G., De los Santos, K., Sparwasser, T., Wu, S., Vuthoori, S., Ko, K., Zavala, F., *et al.* (2002). In vivo depletion of CD11c+ dendritic cells abrogates priming of CD8+ T cells by exogenous cell-associated antigens. *Immunity* **17**, 211-220.
- Kalkanidis, M., Pietersz, G.A., Xiang, S.D., Mottram, P.L., Crimeen-Irwin, B., Ardipradja, K., and Plebanski, M. (2006). Methods for nano-particle based vaccine

- formulation and evaluation of their immunogenicity. *Methods* **40**, 20-29.
- Kandalaft, L.E., Powell, D.J., Jr., Chiang, C.L., Tanyi, J., Kim, S., Bosch, M., Montone, K., Mick, R., Levine, B.L., Torigian, D.A., *et al.* (2013). Autologous lysate-pulsed dendritic cell vaccination followed by adoptive transfer of vaccine-primed ex vivo co-stimulated T cells in recurrent ovarian cancer. *Oncoimmunology* **2**, e22664.
- Karimi, M., Mirshekari, H., Moosavi Basri, S.M., Bahrami, S., Moghoofei, M., and Hamblin, M.R. (2016). Bacteriophages and phage-inspired nanocarriers for targeted delivery of therapeutic cargos. *Adv Drug Deliv Rev* **106**, 45-62.
- Kawano, T., Cui, J., Koezuka, Y., Toura, I., Kaneko, Y., Motoki, K., Ueno, H., Nakagawa, R., Sato, H., Kondo, E., *et al.* (1997). CD1d-restricted and TCR-mediated activation of valpha14 NKT cells by glycosylceramides. *Science* **278**, 1626-1629.
- Kazmierczak, Z., Piotrowicz, A., Owczarek, B., Hodyra, K., Miernikiewicz, P., Lecion, D., Harhala, M., Gorski, A., and Dabrowska, K. (2014). Molecular imaging of T4 phage in mammalian tissues and cells. *Bacteriophage* **4**, e28364.
- Kelly, K.A., Waterman, P., and Weissleder, R. (2006). In vivo imaging of molecularly targeted phage. *Neoplasia* **8**, 1011-1018.

References

- Kiick, K.L., Saxon, E., Tirrell, D.A., and Bertozzi, C.R. (2002). Incorporation of azides into recombinant proteins for chemoselective modification by the Staudinger ligation. *Proc Natl Acad Sci U S A* **99**, 19-24.
- Kim, A.Y., and Blaschek, H.P. (1991). Isolation and characterization of a filamentous viruslike particle from *Clostridium acetobutylicum* NCIB 6444. *J Bacteriol* **173**, 530-535.
- Kim, Y.K., Lim, S.I., Cho, I.S., Cheong, K.M., Lee, E.J., Lee, S.O., Kim, J.B., Kim, J.H., Jeong, D.S., An, B.H., *et al.* (2015). A novel diagnostic approach to detecting porcine epidemic diarrhea virus: The lateral immunochromatography assay. *J Virol Methods* **225**, 4-8.
- Kneissel, S., Queitsch, I., Petersen, G., Behrsing, O., Micheel, B., and Dubel, S. (1999). Epitope structures recognised by antibodies against the major coat protein (g8p) of filamentous bacteriophage fd (Inoviridae). *J Mol Biol* **288**, 21-28.
- Koch, F., Stanzl, U., Jennewein, P., Janke, K., Heufler, C., Kämpgen, E., Romani, N., and Schuler, G. (1996). High level IL-12 production by murine dendritic cells: upregulation via MHC class II and CD40 molecules and downregulation by IL-4 and IL-10. *The Journal of experimental medicine* **184**, 741-746.
- Koczula, K.M., and Gallotta, A. (2016). Lateral flow assays. *Essays Biochem* **60**, 111-120.

- Kolb, H.C., Finn, M.G., and Sharpless, K.B. (2001). Click Chemistry: Diverse Chemical Function from a Few Good Reactions. *Angew Chem Int Ed Engl* **40**, 2004-2021.
- Koniev, O., and Wagner, A. (2015). Developments and recent advancements in the field of endogenous amino acid selective bond forming reactions for bioconjugation. *Chem Soc Rev* **44**, 5743.
- Kremser, A., and Rasched, I. (1994). The adsorption protein of filamentous phage fd: assignment of its disulfide bridges and identification of the domain incorporated in the coat. *Biochemistry* **33**, 13954-13958.
- Kropinski, A.M., Mazzocco, A., Waddell, T.E., Lingohr, E., and Johnson, R.P. (2009). Enumeration of bacteriophages by double agar overlay plaque assay. *Methods Mol Biol* **501**, 69-76.
- Kurschus, F.C., Fellows, E., Stegmann, E., and Jenne, D.E. (2008). Granzyme B delivery via perforin is restricted by size, but not by heparan sulfate-dependent endocytosis. *Proceedings of the National Academy of Sciences* **105**, 13799-13804.
- Kurts, C., Kosaka, H., Carbone, F.R., Miller, J.F., and Heath, W.R. (1997). Class I-restricted cross-presentation of exogenous self-antigens leads to deletion of autoreactive CD8(+) T cells. *J Exp Med* **186**, 239-245.
- Kuzmicheva, G.A., Jayanna, P.K., Eroshkin, A.M., Grishina, M.A., Pereyaslavskaya, E.S., Potemkin, V.A., and

References

- Petrenko, V.A. (2009). Mutations in fd phage major coat protein modulate affinity of the displayed peptide. *Protein Eng Des Sel* **22**, 631-639.
- Laemmli, U.K. (1970). Cleavage of structural proteins during the assembly of the head of bacteriophage T4. *Nature* **227**, 680-685.
- Lahoud, M.H., Ahmet, F., Kitsoulis, S., Wan, S.S., Vremec, D., Lee, C.N., Phipson, B., Shi, W., Smyth, G.K., Lew, A.M., *et al.* (2011). Targeting antigen to mouse dendritic cells via Clec9A induces potent CD4 T cell responses biased toward a follicular helper phenotype. *J Immunol* **187**, 842-850.
- Lantz, O., and Bendelac, A. (1994). An invariant T cell receptor alpha chain is used by a unique subset of major histocompatibility complex class I-specific CD4+ and CD4-8- T cells in mice and humans. *J Exp Med* **180**, 1097-1106.
- Lanzavecchia, A. (1998). Immunology. Licence to kill. *Nature* **393**, 413-414.
- Larsen, C.P., Ritchie, S.C., Pearson, T.C., Linsley, P.S., and Lowry, R.P. (1992). Functional expression of the costimulatory molecule, B7/BB1, on murine dendritic cell populations. *J Exp Med* **176**, 1215-1220.
- Lawn, A.M., Meynell, G.G., Meynell, E., and Datta, N. (1967). Sex pili and the classification of sex factors in the enterobacteriaceae. *Nature* **216**, 343-346.

- Lee, A., Sun, S., Sandler, A., and Hoang, T. (2018). Recent progress in therapeutic antibodies for cancer immunotherapy. *Current opinion in chemical biology* **44**, 56-65.
- Lee, J.W., Song, J., Hwang, M.P., and Lee, K.H. (2013). Nanoscale bacteriophage biosensors beyond phage display. *Int J Nanomedicine* **8**, 3917-3925.
- Lessl, M., Balzer, D., Lurz, R., Waters, V.L., Guiney, D.G., and Lanka, E. (1992). Dissection of IncP conjugative plasmid transfer: definition of the transfer region Tra2 by mobilization of the Tra1 region in trans. *J Bacteriol* **174**, 2493-2500.
- Li, K., Chen, Y., Li, S., Nguyen, H.G., Niu, Z., You, S., Mello, C.M., Lu, X., and Wang, Q. (2010a). Chemical modification of M13 bacteriophage and its application in cancer cell imaging. *Bioconjug Chem* **21**, 1369-1377.
- Li, Z., Koch, H., and Dubel, S. (2003). Mutations in the N-terminus of the major coat protein (pVIII, gp8) of filamentous bacteriophage affect infectivity. *J Mol Microbiol Biotechnol* **6**, 57-66.
- Li, Z., Wang, Y., Wang, J., Tang, Z., Pounds, J.G., and Lin, Y. (2010b). Rapid and Sensitive Detection of Protein Biomarker Using a Portable Fluorescence Biosensor Based on Quantum Dots and a Lateral Flow Test Strip. *Analytical Chemistry* **82**, 7008-7014.
- Liang, Z., Yu, C., and Huang, A.H. (1982). Isolation of spinach leaf peroxisomes in 0.25 molar sucrose solution

References

- by percoll density gradient centrifugation. *Plant Physiol* **70**, 1210-1212.
- Lin, A., Jimenez, J., Derr, J., Vera, P., Manapat, M.L., Esvelt, K.M., Villanueva, L., Liu, D.R., and Chen, I.A. (2011). Inhibition of bacterial conjugation by phage M13 and its protein g3p: quantitative analysis and model. *PLoS ONE* **6**, e19991.
- Lin, M.L., Zhan, Y., Proietto, A.I., Prato, S., Wu, L., Heath, W.R., Villadangos, J.A., and Lew, A.M. (2008a). Selective suicide of cross-presenting CD8⁺ dendritic cells by cytochrome *c* injection shows functional heterogeneity within this subset. *Proceedings of the National Academy of Sciences* **105**, 3029-3034.
- Lin, Y.Y., Wang, J., Liu, G., Wu, H., Wai, C.M., and Lin, Y. (2008b). A nanoparticle label/immunochromatographic electrochemical biosensor for rapid and sensitive detection of prostate-specific antigen. *Biosens Bioelectron* **23**, 1659-1665.
- Liu, C., Jia, Q., Yang, C., Qiao, R., Jing, L., Wang, L., Xu, C., and Gao, M. (2011). Lateral flow immunochromatographic assay for sensitive pesticide detection by using Fe₃O₄ nanoparticle aggregates as color reagents. *Anal Chem* **83**, 6778-6784.
- Liu, J., Cao, S., Kim, S., Chung, E.Y., Homma, Y., Guan, X., Jimenez, V., and Ma, X. (2005a). Interleukin-12: an update on its immunological activities, signaling and

- regulation of gene expression. *Curr Immunol Rev* **1**, 119-137.
- Liu, K., Idoyaga, J., Charalambous, A., Fujii, S., Bonito, A., Mordoh, J., Wainstok, R., Bai, X.F., Liu, Y., and Steinman, R.M. (2005b). Innate NKT lymphocytes confer superior adaptive immunity via tumor-capturing dendritic cells. *J Exp Med* **202**, 1507-1516.
- Liu, P., Han, L., Wang, F., Petrenko, V.A., and Liu, A. (2016a). Gold nanoprobe functionalized with specific fusion protein selection from phage display and its application in rapid, selective and sensitive colorimetric biosensing of *Staphylococcus aureus*. *Biosens Bioelectron* **82**, 195-203.
- Liu, Y., Jiang, D., Lu, X., Wang, W., Xu, Y., and He, Q. (2016b). Phage-Mediated Immuno-PCR for Ultrasensitive Detection of Cry1Ac Protein Based on Nanobody. *J Agric Food Chem* **64**, 7882-7889.
- Lopez Marzo, A.M., Pons, J., Blake, D.A., and Merkoci, A. (2013). High sensitive gold-nanoparticle based lateral flow Immunodevice for Cd²⁺ detection in drinking waters. *Biosens Bioelectron* **47**, 190-198.
- MacDonald, H.R. (1995). NK1.1+ T cell receptor-alpha/beta+ cells: new clues to their origin, specificity, and function. *J Exp Med* **182**, 633-638.
- Magambo, K.A., Kalluvya, S.E., Kapoor, S.W., Seni, J., Chofle, A.A., Fitzgerald, D.W., and Downs, J.A. (2014). Utility of urine and serum lateral flow assays to

References

- determine the prevalence and predictors of cryptococcal antigenemia in HIV-positive outpatients beginning antiretroviral therapy in Mwanza, Tanzania. *J Int AIDS Soc* **17**, 19040.
- Mai-Prochnow, A., Hui, J.G., Kjelleberg, S., Rakonjac, J., McDougald, D., and Rice, S.A. (2015). Big things in small packages: the genetics of filamentous phage and effects on fitness of their host. *FEMS Microbiol Rev* **39**, 465-487.
- Maniatis, T., and Efstratiadis, A. (1980). Fractionation of low molecular weight DNA or RNA in polyacrylamide gels containing 98% formamide or 7 M urea. *Methods Enzymol* **65**, 299-305.
- Mardani, R., Ahmadi Vasmehjani, A., Zali, F., Gholami, A., Mousavi Nasab, S.D., Kaghazian, H., Kaviani, M., and Ahmadi, N. (2020). Laboratory Parameters in Detection of COVID-19 Patients with Positive RT-PCR; a Diagnostic Accuracy Study. *Arch Acad Emerg Med* **8**, e43.
- Marhelava, K., Pilch, Z., Bajor, M., Graczyk-Jarzynka, A., and Zagozdzon, R. (2019). Targeting Negative and Positive Immune Checkpoints with Monoclonal Antibodies in Therapy of Cancer. *Cancers (Basel)* **11**.
- Marks, J.D., Hoogenboom, H.R., Bonnert, T.P., McCafferty, J., Griffiths, A.D., and Winter, G. (1991). By-passing immunization. Human antibodies from V-gene libraries displayed on phage. *J Mol Biol* **222**, 581-597.

- Marvin, D.A., Hale, R.D., Nave, C., and Helmer-Citterich, M. (1994). Molecular models and structural comparisons of native and mutant class I filamentous bacteriophages Ff (fd, f1, M13), If1 and IKe. *J Mol Biol* **235**, 260-286.
- Marvin, D.A., and Hohn, B. (1969). Filamentous bacterial viruses. *Bacteriol Rev* **33**, 172-209.
- Marvin, D.A., Welsh, L.C., Symmons, M.F., Scott, W.R., and Straus, S.K. (2006). Molecular structure of fd (f1, M13) filamentous bacteriophage refined with respect to X-ray fibre diffraction and solid-state NMR data supports specific models of phage assembly at the bacterial membrane. *J Mol Biol* **355**, 294-309.
- Masuda, K., Makino, Y., Cui, J., Ito, T., Tokuhisa, T., Takahama, Y., Koseki, H., Tsuchida, K., Koike, T., Moriya, H., *et al.* (1997). Phenotypes and invariant alpha beta TCR expression of peripheral V alpha 14+ NK T cells. *J Immunol* **158**, 2076-2082.
- Matthews, R., and Hondorp, E. (2013). Methionine. *EcoSal Plus* **1**.
- Mattner, J., Debord, K.L., Ismail, N., Goff, R.D., Cantu, C., 3rd, Zhou, D., Saint-Mezard, P., Wang, V., Gao, Y., Yin, N., *et al.* (2005). Exogenous and endogenous glycolipid antigens activate NKT cells during microbial infections. *Nature* **434**, 525-529.
- Maurizi, M.R. (1992). Proteases and protein degradation in *Escherichia coli*. *Experientia* **48**, 178-201.

References

- McDonnell, A.M., Robinson, B.W., and Currie, A.J. (2010). Tumor antigen cross-presentation and the dendritic cell: where it all begins? *Clin Dev Immunol* **2010**, 539519.
- McKee, S.J., Young, V.L., Clow, F., Hayman, C.M., Baird, M.A., Hermans, I.F., Young, S.L., and Ward, V.K. (2012). Virus-like particles and alpha-galactosylceramide form a self-adjuvanting composite particle that elicits anti-tumor responses. *Journal of controlled release : official journal of the Controlled Release Society* **159**, 338-345.
- McLellan, A.D., Bröcker, E.B., and Kämpgen, E. (2000). Dendritic cell activation by danger and antigen-specific T-cell signalling. *Exp Dermatol* **9**, 313-322.
- Meaden, S., and Koskella, B. (2013). Exploring the risks of phage application in the environment. *Front Microbiol* **4**, 358.
- Mei, Z., Qu, W., Deng, Y., Chu, H., Cao, J., Xue, F., Zheng, L., El-Nezamic, H.S., Wu, Y., and Chen, W. (2013). One-step signal amplified lateral flow strip biosensor for ultrasensitive and on-site detection of bisphenol A (BPA) in aqueous samples. *Biosens Bioelectron* **49**, 457-461.
- Melief, C.J., van Hall, T., Arens, R., Ossendorp, F., and van der Burg, S.H. (2015). Therapeutic cancer vaccines. *J Clin Invest* **125**, 3401-3412.

- Mescher, M.F., Curtsinger, J.M., Agarwal, P., Casey, K.A., Gerner, M., Hammerbeck, C.D., Popescu, F., and Xiao, Z. (2006). Signals required for programming effector and memory development by CD8⁺ T cells. *Immunol Rev* **211**, 81-92.
- Metkar, S.S., Wang, B., Ebbs, M.L., Kim, J.H., Lee, Y.J., Raja, S.M., and Froelich, C.J. (2003). Granzyme B activates procaspase-3 which signals a mitochondrial amplification loop for maximal apoptosis. *The Journal of cell biology* **160**, 875-885.
- Miernikiewicz, P., Dabrowska, K., Piotrowicz, A., Owczarek, B., Wojas-Turek, J., Kicielinska, J., Rossowska, J., Pajtasz-Piasecka, E., Hodyra, K., Macegoniuk, K., *et al.* (2013). T4 phage and its head surface proteins do not stimulate inflammatory mediator production. *PLoS One* **8**, e71036.
- Minenkova, O.O., Ilyichev, A.A., Kishchenko, G.P., and Petrenko, V.A. (1993). Design of specific immunogens using filamentous phage as the carrier. *Gene* **128**, 85-88.
- Minot, S., Sinha, R., Chen, J., Li, H., Keilbaugh, S.A., Wu, G.D., Lewis, J.D., and Bushman, F.D. (2011). The human gut virome: inter-individual variation and dynamic response to diet. *Genome Res* **21**, 1616-1625.
- Mirasoli, M., Buragina, A., Dolci, L.S., Guardigli, M., Simoni, P., Montoya, A., Maiolini, E., Girotti, S., and Roda, A. (2012). Development of a chemiluminescence-based quantitative lateral flow immunoassay for on-

References

- field detection of 2,4,6-trinitrotoluene. *Anal Chim Acta* **721**, 167-172.
- Model, P., and Russel, M. (1988). Filamentous bacteriophage. In *The Bacteriophages*, R. Calendar, ed. (New York: Plenum Publishing), pp. 375-456.
- Morales-Narvaez, E., Naghdi, T., Zor, E., and Merkoci, A. (2015). Photoluminescent lateral-flow immunoassay revealed by graphene oxide: highly sensitive paper-based pathogen detection. *Anal Chem* **87**, 8573-8577.
- Moran, A.E., Holzapfel, K.L., Xing, Y., Cunningham, N.R., Maltzman, J.S., Punt, J., and Hogquist, K.A. (2011). T cell receptor signal strength in Treg and iNKT cell development demonstrated by a novel fluorescent reporter mouse. *J Exp Med* **208**, 1279-1289.
- Morein, B., Hu, K.F., and Abusugra, I. (2004). Current status and potential application of ISCOMs in veterinary medicine. *Adv Drug Deliv Rev* **56**, 1367-1382.
- Moreland, N.J., Susanto, P., Lim, E., Tay, M.Y., Rajamanonmani, R., Hanson, B.J., and Vasudevan, S.G. (2012). Phage display approaches for the isolation of monoclonal antibodies against dengue virus envelope domain III from human and mouse derived libraries. *Int J Mol Sci* **13**, 2618-2635.
- Moreno, M.L., Cebolla, A., Munoz-Suano, A., Carrillo-Carrion, C., Comino, I., Pizarro, A., Leon, F., Rodriguez-Herrera, A., and Sousa, C. (2017). Detection of gluten immunogenic peptides in the urine of patients

- with coeliac disease reveals transgressions in the gluten-free diet and incomplete mucosal healing. *Gut* **66**, 250-257.
- Nagano, K., and Tsutsumi, Y. (2016). Development of novel drug delivery systems using phage display technology for clinical application of protein drugs. *Proc Jpn Acad Ser B Phys Biol Sci* **92**, 156-166.
- Nakamura, T., Kimura, H., Kato, M., Kurashige, S., and Wakamatsu, K. (2007). A sensitive and reliable quantification method for mouse interleukin-12 p70 based on fluorometric sandwich ELISA (FS-ELISA). *Cell Biol Int* **31**, 173-179.
- Neltner, B., Peddie, B., Xu, A., Doenlen, W., Durand, K., Yun, D.S., Speakman, S., Peterson, A., and Belcher, A. (2010). Production of hydrogen using nanocrystalline protein-templated catalysts on m13 phage. *ACS Nano* **4**, 3227-3235.
- Neumann, S., Young, K., Compton, B., Anderson, R., Painter, G., and Hook, S. (2015). Synthetic TRP2 long-peptide and alpha-galactosylceramide formulated into cationic liposomes elicit CD8+ T-cell responses and prevent tumour progression. *Vaccine* **33**, 5838-5844.
- Newman, J., Swinney, H.L., and Day, L.A. (1977). Hydrodynamic properties and structure of fd virus. *J Mol Biol* **116**, 593-603.
- Nielsen, K., Yu, W.L., Kelly, L., Bermudez, R., Renteria, T., Dajer, A., Gutierrez, E., Williams, J., Algire, J.,

References

- and de Eschaide, S.T. (2008). Development of a lateral flow assay for rapid detection of bovine antibody to *Anaplasma marginale*. *J Immunoassay Immunochem* **29**, 10-18.
- Nielsen, K., Yu, W.L., Kelly, L., Williams, J., Dajer, A., Gutierrez, E., Ramirez Cruz, G., Renteria, T., Bermudez, R., and Algire, J. (2009). Validation and field assessment of a rapid lateral flow assay for detection of bovine antibody to *Anaplasma marginale*. *J Immunoassay Immunochem* **30**, 313-321.
- Nishimura, T., Kitamura, H., Iwakabe, K., Yahata, T., Ohta, A., Sato, M., Takeda, K., Okumura, K., Van Kaer, L., Kawano, T., *et al.* (2000). The interface between innate and acquired immunity: glycolipid antigen presentation by CD1d-expressing dendritic cells to NKT cells induces the differentiation of antigen-specific cytotoxic T lymphocytes. *Int Immunol* **12**, 987-994.
- Nowak, A.K., Lake, R.A., Marzo, A.L., Scott, B., Heath, W.R., Collins, E.J., Frelinger, J.A., and Robinson, B.W. (2003). Induction of tumor cell apoptosis in vivo increases tumor antigen cross-presentation, cross-priming rather than cross-tolerizing host tumor-specific CD8 T cells. *J Immunol* **170**, 4905-4913.
- Nungester, W., and Watrous, R. (1934). Accumulation of bacteriophage in spleen and liver following its intravenous inoculation. *Proceedings of the Society for Experimental Biology and Medicine* **31**, 901-905.

- Oehen, S., and Brduscha-Riem, K. (1998). Differentiation of naive CTL to effector and memory CTL: correlation of effector function with phenotype and cell division. *J Immunol* **161**, 5338-5346.
- Oh, J.W., Chung, W.J., Heo, K., Jin, H.E., Lee, B.Y., Wang, E., Zueger, C., Wong, W., Meyer, J., Kim, C., *et al.* (2014). Biomimetic virus-based colourimetric sensors. *Nat Commun* **5**, 3043.
- Olsen, E.V., Sorokulova, I.B., Petrenko, V.A., Chen, I.H., Barbaree, J.M., and Vodyanoy, V.J. (2006). Affinity-selected filamentous bacteriophage as a probe for acoustic wave biodetectors of *Salmonella typhimurium*. *Biosens Bioelectron* **21**, 1434-1442.
- Olucha, F., Martinez-Garcia, F., and Lopez-Garcia, C. (1985). A new stabilizing agent for the tetramethyl benzidine (TMB) reaction product in the histochemical detection of horseradish peroxidase (HRP). *J Neurosci Methods* **13**, 131-138.
- Ornstein, L. (1964). Disc Electrophoresis. I. Background and Theory. *Ann N Y Acad Sci* **121**, 321-349.
- Palucka, K., and Banchereau, J. (2012). Cancer immunotherapy via dendritic cells. *Nat Rev Cancer* **12**, 265-277.
- Pardoll, D.M. (2012). The blockade of immune checkpoints in cancer immunotherapy. *Nat Rev Cancer* **12**, 252-264.
- Parekh, V.V., Wilson, M.T., Olivares-Villagomez, D., Singh, A.K., Wu, L., Wang, C.R., Joyce, S., and Van Kaer, L. (2005). Glycolipid antigen induces long-term natural

References

- killer T cell anergy in mice. *J Clin Invest* **115**, 2572-2583.
- Park, H.-Y., Tan, P.S., Kavishna, R., Ker, A., Lu, J., Chan, C.E.Z., Hanson, B.J., MacAry, P.A., Caminschi, I., Shortman, K., *et al.* (2017). Enhancing vaccine antibody responses by targeting Clec9A on dendritic cells. *npj Vaccines* **2**, 31.
- Park, H., Heldman, N., Rebentrost, P., Abbondanza, L., Iagatti, A., Alessi, A., Patrizi, B., Salvalaggio, M., Bussotti, L., Mohseni, M., *et al.* (2016). Enhanced energy transport in genetically engineered excitonic networks. *Nat Mater* **15**, 211-216.
- Parker, N. (1998). Lectin/Antibody "sandwich" ELISA for quantification of circulating mucin as a diagnostic test for pancreatic cancer. *Methods Mol Med* **9**, 249-253.
- Petersen, T.R., Dickgreber, N., and Hermans, I.F. (2010). Tumor antigen presentation by dendritic cells. *Critical reviews in immunology* **30**, 345-386.
- Petrenko, V.A. (2018). Landscape Phage: Evolution from Phage Display to Nanobiotechnology. *Viruses* **10**.
- Petrie, A. (2015). Expanding the bionanotechnology toolbox using an engineered bacteriophage M13 platform (UWSpace).
- Pilka, E.S., Werner, J.M., Schwarz-Linek, U., Pickford, A.R., Meenan, N.A., Campbell, I.D., and Potts, J.R. (2006). Structural insight into binding of

- Staphylococcus aureus to human fibronectin. FEBS Lett **580**, 273-277.
- Pinkoski, M.J., Waterhouse, N.J., Heibei, J.A., Wolf, B.B., Kuwana, T., Goldstein, J.C., Newmeyer, D.D., Bleackley, R.C., and Green, D.R. (2001). Granzyme B-mediated apoptosis proceeds predominantly through a Bcl-2-inhibitable mitochondrial pathway. J Biol Chem **276**, 12060-12067.
- Prendergast, K., Daniels, N., Petersen, T., Hermans, I., and Kirman, J. (2018). Langerin+ CD8 α + Dendritic Cells Drive Early CD8+ T Cell Activation and IL-12 Production During Systemic Bacterial Infection. Frontiers in Immunology **9**.
- Prisco, A., and De Berardinis, P. (2012). Filamentous bacteriophage fd as an antigen delivery system in vaccination. Int J Mol Sci **13**, 5179-5194.
- Prlic, M., and Bevan, M.J. (2008). Exploring regulatory mechanisms of CD8+ T cell contraction. Proc Natl Acad Sci U S A **105**, 16689-16694.
- Propper, D.J., Chao, D., Braybrooke, J.P., Bahl, P., Thavasu, P., Balkwill, F., Turley, H., Dobbs, N., Gatter, K., Talbot, D.C., et al. (2003). Low-dose IFN- γ induces tumor MHC expression in metastatic malignant melanoma. Clin Cancer Res **9**, 84-92.
- Qin, Z., Schwartzkopff, J., Pradera, F., Kammertöns, T., Seliger, B., Pircher, H., and Blankenstein, T. (2003). A Critical Requirement of Interferon γ -mediated

References

- Angiostasis for Tumor Rejection by CD8⁺ T Cells. *Cancer Res* **63**, 4095-4100.
- Qiu, W., Xu, H., Takalkar, S., Gurung, A.S., Liu, B., Zheng, Y., Guo, Z., Baloda, M., Baryeh, K., and Liu, G. (2015). Carbon nanotube-based lateral flow biosensor for sensitive and rapid detection of DNA sequence. *Biosens Bioelectron* **64**, 367-372.
- Quezada, S.A., Simpson, T.R., Peggs, K.S., Merghoub, T., Vider, J., Fan, X., Blasberg, R., Yagita, H., Muranski, P., Antony, P.A., *et al.* (2010). Tumor-reactive CD4(+) T cells develop cytotoxic activity and eradicate large established melanoma after transfer into lymphopenic hosts. *J Exp Med* **207**, 637-650.
- Rakonjac, J., Bennett, N.J., Spagnuolo, J., Gagic, D., and Russel, M. (2011). Filamentous Bacteriophage: Biology, Phage Display and Nanotechnology Applications. *Curr Issues Mol Biol* **13**, 51-76.
- Rakonjac, J., Feng, J., and Model, P. (1999). Filamentous phage are released from the bacterial membrane by a two-step mechanism involving a short C-terminal fragment of pIII. *J Mol Biol* **289**, 1253-1265.
- Rakonjac, J., and Model, P. (1998). Roles of pIII in filamentous phage assembly. *J Mol Biol* **282**, 25-41.
- Rakonjac, J.V., Robbins, J.C., and Fischetti, V.A. (1995). DNA sequence of the serum opacity factor of group A streptococci: identification of a fibronectin-binding repeat domain. *Infect Immun* **63**, 622-631.

- Rapoport, S. (1947). Dimensional, osmotic, and chemical changes of erythrocytes in stored blood evaluation of several acid and neutral preservation mixtures; effect of storage at 25 degrees C. in Alsever's solution. *J Clin Invest* **26**, 616-621.
- Raynes, J.M., Tay, M.L., By, S.H., Steemson, J.D., and Moreland, N.J. (2020). Isolation of Monoclonal Antibodies to Group A Streptococcus Antigens Using Phage Display. *Methods Mol Biol* **2136**, 255-268.
- Razdan, S., Wang, J.C., and Barua, S. (2019). PolyBall: A new adsorbent for the efficient removal of endotoxin from biopharmaceuticals. *Scientific reports* **9**, 8867.
- Ridge, J.P., Di Rosa, F., and Matzinger, P. (1998). A conditioned dendritic cell can be a temporal bridge between a CD4+ T-helper and a T-killer cell. *Nature* **393**, 474-478.
- Rock, K.L., York, I.A., Saric, T., and Goldberg, A.L. (2002). Protein degradation and the generation of MHC class I-presented peptides. *Adv Immunol* **80**, 1-70.
- Rodriguez, A., Regnault, A., Kleijmeer, M., Ricciardi-Castagnoli, P., and Amigorena, S. (1999). Selective transport of internalized antigens to the cytosol for MHC class I presentation in dendritic cells. *Nature cell biology* **1**, 362-368.
- Ross, G.M.S., Salentijn, G.I., and Nielen, M.W.F. (2019). A Critical Comparison between Flow-through and Lateral

References

- Flow Immunoassay Formats for Visual and Smartphone-Based Multiplex Allergen Detection. *Biosensors* **9**, 143.
- Rossomando, E.F., and Zinder, N.D. (1968). Studies on the bacteriophage fl. I. Alkali-induced disassembly of the phage into DNA and protein. *J Mol Biol* **36**, 387-399.
- Russel, M., and Model, P. (2006). Filamentous phage. In *The bacteriophages* R.C. Calendar, ed. (New York: Oxford University Press, Inc.), pp. 146-160.
- Sallusto, F., Schaerli, P., Loetscher, P., Schaniel, C., Lenig, D., Mackay, C.R., Qin, S., and Lanzavecchia, A. (1998). Rapid and coordinated switch in chemokine receptor expression during dendritic cell maturation. *Eur J Immunol* **28**, 2760-2769.
- Sambrook, J., and Russell, D.W. (2001). *Molecular cloning: a laboratory manual* (3rd. Edn.), 3rd edn (Cold Spring Harbor: Cold Spring Harbor).
- Sambrook, J., and Russell, D.W. (2006). Preparation of Single-stranded Bacteriophage M13 DNA. *CSH Protoc* **2006**.
- Sartorius, R., Bettua, C., D'Apice, L., Caivano, A., Trovato, M., Russo, D., Zanoni, I., Granucci, F., Mascolo, D., Barba, P., *et al.* (2011). Vaccination with filamentous bacteriophages targeting DEC-205 induces DC maturation and potent anti-tumor T-cell responses in the absence of adjuvants. *Eur J Immunol* **41**, 2573-2584.
- Sartorius, R., D'Apice, L., Barba, P., Cipria, D., Grauso, L., Cutignano, A., and De Berardinis, P. (2018).

- Vectorized Delivery of Alpha-GalactosylCeramide and Tumor Antigen on Filamentous Bacteriophage fd Induces Protective Immunity by Enhancing Tumor-Specific T Cell Response. *Front Immunol* **9**, 1496.
- Sartorius, R., D'Apice, L., Trovato, M., Cuccaro, F., Costa, V., De Leo, M.G., Marzullo, V.M., Biondo, C., D'Auria, S., De Matteis, M.A., *et al.* (2015). Antigen delivery by filamentous bacteriophage fd displaying an anti-DEC-205 single-chain variable fragment confers adjuvanticity by triggering a TLR9-mediated immune response. *EMBO Mol Med* **7**, 973-988.
- Sattar, S. (2013). Filamentous phage-derived nano-rods for applications in diagnostics and vaccines. In Institute of Fundamental Sciences (Palmerston North, New Zealand: Massey University).
- Sattar, S., Bennett, N.J., Wen, W.X., Guthrie, J.M., Blackwell, L.F., Conway, J.F., and Rakonjac, J. (2015). Ff-nano, short functionalized nanorods derived from Ff (f1, fd, or M13) filamentous bacteriophage. *Front Microbiol* **6**, Article 316.
- Schirrmann, T., Meyer, T., Schutte, M., Frenzel, A., and Hust, M. (2011). Phage display for the generation of antibodies for proteome research, diagnostics and therapy. *Molecules* **16**, 412-426.
- Schmittl, A., Keilholz, U., Bauer, S., Kuhne, U., Stevanovic, S., Thiel, E., and Scheibenbogen, C. (2001). Application of the IFN-gamma ELISPOT assay to

References

- quantify T cell responses against proteins. *J Immunol Methods* **247**, 17-24.
- Schulz, O., Edwards, A.D., Schito, M., Aliberti, J., Manickasingham, S., Sher, A., and Reis e Sousa, C. (2000). CD40 Triggering of Heterodimeric IL-12 p70 Production by Dendritic Cells In Vivo Requires a Microbial Priming Signal. *Immunity* **13**, 453-462.
- Scott, J.K., and Smith, G.P. (1990). Searching for peptide ligands with an epitope library. *Science* **249**, 386-390.
- Seder, R.A., Gazzinelli, R., Sher, A., and Paul, W.E. (1993). Interleukin 12 acts directly on CD4+ T cells to enhance priming for interferon gamma production and diminishes interleukin 4 inhibition of such priming. *Proc Natl Acad Sci U S A* **90**, 10188-10192.
- Service, R.F. (2020). Coronavirus antigen tests: quick and cheap, but too often wrong? In *Science Magazine (AAAS)*.
- Shen, L., Sigal, L.J., Boes, M., and Rock, K.L. (2004). Important role of cathepsin S in generating peptides for TAP-independent MHC class I crosspresentation in vivo. *Immunity* **21**, 155-165.
- Shyu, R.H., Shyu, H.F., Liu, H.W., and Tang, S.S. (2002). Colloidal gold-based immunochromatographic assay for detection of ricin. *Toxicon* **40**, 255-258.
- Silk, J.D., Hermans, I.F., Gileadi, U., Chong, T.W., Shepherd, D., Salio, M., Mathew, B., Schmidt, R.R., Lunt, S.J., Williams, K.J., *et al.* (2004). Utilizing the adjuvant properties of CD1d-dependent NK T cells

- in T cell-mediated immunotherapy. *J Clin Invest* **114**, 1800-1811.
- Sioud, M. (2019). Phage Display Libraries: From Binders to Targeted Drug Delivery and Human Therapeutics. *Mol Biotechnol* **61**, 286-303.
- Slifka, M.K., and Whitton, J.L. (2000). Activated and Memory CD8⁺ T Cells Can Be Distinguished by Their Cytokine Profiles and Phenotypic Markers. *The Journal of Immunology* **164**, 208-216.
- Smith, C.M., Wilson, N.S., Waithman, J., Villadangos, J.A., Carbone, F.R., Heath, W.R., and Belz, G.T. (2004). Cognate CD4⁺ T cell licensing of dendritic cells in CD8⁺ T cell immunity. *Nature immunology* **5**, 1143-1148.
- Smith, G.P. (1985). Filamentous fusion phage: novel expression vectors that display cloned antigens on the virion surface. *Science* **228**, 1315-1317.
- Song, L.W., Wang, Y.B., Fang, L.L., Wu, Y., Yang, L., Chen, J.Y., Ge, S.X., Zhang, J., Xiong, Y.Z., Deng, X.M., *et al.* (2015). Rapid fluorescent lateral-flow immunoassay for hepatitis B virus genotyping. *Anal Chem* **87**, 5173-5180.
- Staats, J., Divekar, A., McCoy, J.P., Jr., and Maecker, H.T. (2019). Guidelines for Gating Flow Cytometry Data for Immunological Assays. *Methods Mol Biol* **2032**, 81-104.
- Sternberg, N.L., and Maurer, R. (1991). Bacteriophage-mediated generalized transduction in *Escherichia coli*

References

- and *Salmonella typhimurium*. *Methods Enzymol* **204**, 18-43.
- Sullivan, B.A., and Kronenberg, M. (2005). Activation or anergy: NKT cells are stunned by α -galactosylceramide. *J Clin Invest* **115**, 2328-2329.
- Szaloki, G., and Goda, K. (2015). Compensation in multicolor flow cytometry. *Cytometry A* **87**, 982-985.
- Takayama, Y., Kusamori, K., and Nishikawa, M. (2019). Click Chemistry as a Tool for Cell Engineering and Drug Delivery. *Molecules* **24**.
- Tan, E.M., Smolen, J.S., McDougal, J.S., Butcher, B.T., Conn, D., Dawkins, R., Fritzler, M.J., Gordon, T., Hardin, J.A., Kalden, J.R., *et al.* (1999). A critical evaluation of enzyme immunoassays for detection of antinuclear autoantibodies of defined specificities. I. Precision, sensitivity, and specificity. *Arthritis Rheum* **42**, 455-464.
- Tan, J.K., and O'Neill, H.C. (2005). Maturation requirements for dendritic cells in T cell stimulation leading to tolerance versus immunity. *J Leukoc Biol* **78**, 319-324.
- Tay, R.E., Richardson, E.K., and Toh, H.C. (2020). Revisiting the role of CD4⁺ T cells in cancer immunotherapy—new insights into old paradigms. *Cancer Gene Therapy*.
- Teodorowicz, M., Perdijk, O., Verhoek, I., Govers, C., Savelkoul, H.F., Tang, Y., Wichers, H., and Broersen, K. (2017). Optimized Triton X-114 assisted

- lipopolysaccharide (LPS) removal method reveals the immunomodulatory effect of food proteins. *PLoS One* **12**, e0173778.
- Thompson, J.M., Gralow, J.R., Levy, R., and Miller, R.A. (1985). The optimal application of forward and ninety-degree light scatter in flow cytometry for the gating of mononuclear cells. *Cytometry* **6**, 401-406.
- Thorntwaite, J.T., and Leif, R.C. (1978). A permanent cell viability assay using alcian blue. *Stain Technol* **53**, 199-204.
- Tikunova, N.V., and Morozova, V.V. (2009). Phage display on the base of filamentous bacteriophages: application for recombinant antibodies selection. *Acta Naturae* **1**, 20-28.
- Tulchin, N., Ornstein, L., and Davis, B.J. (1976). A microgel system for disc electrophoresis. *Anal Biochem* **72**, 485-490.
- Tummatorn, J., Batsomboon, P., Clark, R.J., Alabugin, I.V., and Dudley, G.B. (2012). Strain-promoted azide-alkyne cycloadditions of benzocyclononynes. *J Org Chem* **77**, 2093-2097.
- Van Belleghem, J.D., Clement, F., Merabishvili, M., Lavigne, R., and Vaneechoutte, M. (2017). Pro- and anti-inflammatory responses of peripheral blood mononuclear cells induced by *Staphylococcus aureus* and *Pseudomonas aeruginosa* phages. *Scientific reports* **7**, 8004.

References

- Van Belleghem, J.D., Dąbrowska, K., Vaneechoutte, M., Barr, J.J., and Bollyky, P.L. (2018). Interactions between Bacteriophage, Bacteria, and the Mammalian Immune System. *Viruses* **11**.
- van Dam, G.J., de Dood, C.J., Lewis, M., Deelder, A.M., van Lieshout, L., Tanke, H.J., van Rooyen, L.H., and Corstjens, P.L. (2013). A robust dry reagent lateral flow assay for diagnosis of active schistosomiasis by detection of *Schistosoma* circulating anodic antigen. *Exp Parasitol* **135**, 274-282.
- van Houten, N.E., Henry, K.A., Smith, G.P., and Scott, J.K. (2010). Engineering filamentous phage carriers to improve focusing of antibody responses against peptides. *Vaccine* **28**, 2174-2185.
- van Houten, N.E., Zwick, M.B., Menendez, A., and Scott, J.K. (2006). Filamentous phage as an immunogenic carrier to elicit focused antibody responses against a synthetic peptide. *Vaccine* **24**, 4188-4200.
- Van Kaer, L., Parekh, V.V., and Wu, L. (2015). The Response of CD1d-Restricted Invariant NKT Cells to Microbial Pathogens and Their Products. *Front Immunol* **6**, 226.
- van Kasteren, P.B., van der Veer, B., van den Brink, S., Wijsman, L., de Jonge, J., van den Brandt, A., Molenkamp, R., Reusken, C., and Meijer, A. (2020). Comparison of seven commercial RT-PCR diagnostic kits for COVID-19. *J Clin Virol* **128**, 104412.

- van Stipdonk, M.J., Lemmens, E.E., and Schoenberger, S.P. (2001). Naïve CTLs require a single brief period of antigenic stimulation for clonal expansion and differentiation. *Nature immunology* *2*, 423-429.
- Vashist, S.K. (2020). In Vitro Diagnostic Assays for COVID-19: Recent Advances and Emerging Trends. *Diagnostics (Basel)* *10*.
- Vermaelen, K. (2019). Vaccine Strategies to Improve Anti-cancer Cellular Immune Responses. *Front Immunol* *10*, 8.
- Vresak, M., Olesen, M.H., Gislum, R., Bavec, F., and Ravn Jorgensen, J. (2016). The Use of Image-Spectroscopy Technology as a Diagnostic Method for Seed Health Testing and Variety Identification. *PLoS One* *11*, e0152011.
- Wang, D.B., Tian, B., Zhang, Z.P., Wang, X.Y., Fleming, J., Bi, L.J., Yang, R.F., and Zhang, X.E. (2015). Detection of *Bacillus anthracis* spores by super-paramagnetic lateral-flow immunoassays based on "Road Closure". *Biosens Bioelectron* *67*, 608-614.
- Warnken, T., Huber, K., and Feige, K. (2016). Comparison of three different methods for the quantification of equine insulin. *BMC Veterinary Research* *12*, 196.
- Watts, C. (2001). Antigen processing in the endocytic compartment. *Curr Opin Immunol* *13*, 26-31.
- Weber-Dabrowska, B., Zimecki, M., and Mulczyk, M. (2000). Effective phage therapy is associated with

References

- normalization of cytokine production by blood cell cultures. *Arch Immunol Ther Exp (Warsz)* **48**, 31-37.
- Webster, R.E. (2001). Filamentous phage biology. In *Phage display: a laboratory manual*, C.F.I. Barbas, D.R. Burton, J.K. Scott, and G.J. Silverman, eds. (Cold Spring Harbor, New York: Cold Spring Harbor Laboratory Press), pp. 1.1-1.37.
- Weiner, L.M., Murray, J.C., and Shuptrine, C.W. (2012). Antibody-based immunotherapy of cancer. *Cell* **148**, 1081-1084.
- Weissbach, H., and Brot, N. (1991). Regulation of methionine synthesis in *Escherichia coli*. *Mol Microbiol* **5**, 1593-1597.
- Wenger, S.L., Turner, J.H., and Petricciani, J.C. (1978). The cytogenetic, proliferative and viability effects of four bacteriophages on human lymphocytes. *In Vitro* **14**, 543-549.
- Weninger, W., Crowley, M.A., Manjunath, N., and von Andrian, U.H. (2001). Migratory properties of naive, effector, and memory CD8(+) T cells. *J Exp Med* **194**, 953-966.
- Willats, W.G. (2002). Phage display: practicalities and prospects. *Plant Mol Biol* **50**, 837-854.
- Williams, M.A., Tyznik, A.J., and Bevan, M.J. (2006). Interleukin-2 signals during priming are required for secondary expansion of CD8+ memory T cells. *Nature* **441**, 890-893.

- Wilson, E.B., and Livingstone, A.M. (2008). Cutting edge: CD4⁺ T cell-derived IL-2 is essential for help-dependent primary CD8⁺ T cell responses. *J Immunol* **181**, 7445-7448.
- Winter, G., Griffiths, A.D., Hawkins, R.E., and Hoogenboom, H.R. (1994). Making antibodies by phage display technology. *Annu Rev Immunol* **12**, 433-455.
- Wu, D., Xing, G.-W., Poles, M.A., Horowitz, A., Kinjo, Y., Sullivan, B., Bodmer-Narkevitch, V., Plettenburg, O., Kronenberg, M., Tsuji, M., *et al.* (2005). Bacterial glycolipids and analogs as antigens for CD1d-restricted NKT cells. *P Natl Acad Sci USA* **102**, 1351-1356.
- Wu, J., Zeng, X.Q., Zhang, H.B., Ni, H.Z., Pei, L., Zou, L.R., Liang, L.J., Zhang, X., Lin, J.Y., and Ke, C.W. (2014). Novel phage display-derived H5N1-specific scFvs with potential use in rapid avian flu diagnosis. *J Microbiol Biotechnol* **24**, 704-713.
- Xu, H., Mao, X., Zeng, Q., Wang, S., Kawde, A.N., and Liu, G. (2009). Aptamer-functionalized gold nanoparticles as probes in a dry-reagent strip biosensor for protein analysis. *Anal Chem* **81**, 669-675.
- Yalow, R.S., and Berson, S.A. (1959). Assay of plasma insulin in human subjects by immunological methods. *Nature* **184 (Suppl 21)**, 1648-1649.
- Yao, Q., Bu, Z., Vzorov, A., Yang, C., and Compans, R.W. (2003). Virus-like particle and DNA-based candidate AIDS vaccines. *Vaccine* **21**, 638-643.

References

- Zenkin, N., Naryshkina, T., Kuznedelov, K., and Severinov, K. (2006). The mechanism of DNA replication primer synthesis by RNA polymerase. *Nature* **439**, 617-620.
- Zhang, L., Hou, X., Sun, L., He, T., Wei, R., Pang, M., and Wang, R. (2018a). Corrigendum: Staphylococcus aureus Bacteriophage Suppresses LPS-Induced Inflammation in MAC-T Bovine Mammary Epithelial Cells. *Front Microbiol* **9**, 2511.
- Zhang, L., Hou, X., Sun, L., He, T., Wei, R., Pang, M., and Wang, R. (2018b). Staphylococcus aureus Bacteriophage Suppresses LPS-Induced Inflammation in MAC-T Bovine Mammary Epithelial Cells. *Front Microbiol* **9**, 1614.
- Zhang, L., Yang, X., Sun, Z., Li, J., Zhu, H., Li, J., and Pang, Y. (2016a). Dendritic cell vaccine and cytokine-induced killer cell therapy for the treatment of advanced non-small cell lung cancer. *Oncol Lett* **11**, 2605-2610.
- Zhang, L., Zhu, W., Li, J., Yang, X., Ren, Y., Niu, J., and Pang, Y. (2016b). Clinical outcome of immunotherapy with dendritic cell vaccine and cytokine-induced killer cell therapy in hepatobiliary and pancreatic cancer. *Mol Clin Oncol* **4**, 129-133.
- Zhang, P., Wang, J., Wang, D., Wang, H., Shan, F., Chen, L., Hou, Y., Wang, E., and Lu, C.L. (2012). Dendritic cell vaccine modified by Ag85A gene enhances anti-tumor immunity against bladder cancer. *Int Immunopharmacol* **14**, 252-260.

- Zhang, S., Garcia-D'Angeli, A., Brennan, J.P., and Huo, Q. (2014). Predicting detection limits of enzyme-linked immunosorbent assay (ELISA) and bioanalytical techniques in general. *Analyst* **139**, 439-445.
- Zhou, L., Chong, M.M., and Littman, D.R. (2009). Plasticity of CD4+ T cell lineage differentiation. *Immunity* **30**, 646-655.
- Zhu, H., White, I.M., Suter, J.D., and Fan, X. (2008). Phage-based label-free biomolecule detection in an optofluidic ring resonator. *Biosens Bioelectron* **24**, 461-466.
- Zong, Y., Bice, T.W., Ton-That, H., Schneewind, O., and Narayana, S.V. (2004). Crystal structures of *Staphylococcus aureus* sortase A and its substrate complex. *J Biol Chem* **279**, 31383-31389.